Molecularly Imprinted Chromogenic and Fluorogenic Receptors as Optical Sensor Matrix

Dissertation

zur Erlangung des akademischen Grades
d o c t o r r e r u m n a t u r a l i u m
(Dr. rer. nat.)
im Fach Chemie

eigereicht an der
Mathematisch-Naturwissenschaftlichen Fakultät I

der Humboldt-Universität zu Berlin

Vorgelegt von
(Dipl.-Chem., Wei, Wan)

Präsidentin/Präsident der Humboldt-Universität zu Berlin
Prof. Dr. Jan-Hendrik Olbertz

Dekanin/Dekan der Mathematisch-Naturwissenschaftlichen Fakultät I
Prof. Dr. Elmar Kulke

Gutachter/innen: 1. Prof. Stefan Hecht, PhD

2. Prof. Dr. Michael G. Weller

Tag der Verteidigung: 28.11.2014

Die vorliegende Arbeit wurde in Zeit von June 2010 bis Aug 2014 am Institut für Chemie der Humboldt-Universität zu Berlin und an der BAM Bundesanstalt für Materialforschung und –prüfung im Fachbereich 1.9 Sensormaterialien unter der Leitung von Dr. Knut Rurack angefertigt

Acknowledgements

Foremost, I would like to express my sincere gratitude to my supervisor, Dr. Knut Rurack, not only for introducing me to the attractive research field, but because his knowledge and patience have guided and supported me throughout my Ph.D. studies and research. Also, his trust offered me the room to work in my own way. Next is my doctor father, Prof. Stefan Hecht, thank you for taking responsibility for my Ph.D. study and serving as my university supervisor. I would also thank Prof. Dr. Börje Sellergren for immense help and advice in the field of molecular imprinting. What I learned in this period will be a great fortune in my life. I would also thank Prof. Michael G. Weller for reviewing my thesis.

During the past 4 years, I have received plenty of aids. I would like to thank Dr. Mustafa Biyikal, Dr. Ana Descalzo and Dr. Ricarda Wagner for the synthesis of some of the functional monomers employed in this work, Dr. Dietmar Pfeifer and Dr. Hardy Weißhoff for help with the NMR titrations, Dr. Sören Selve for TEM measurements, Dr. Andreas Lehmann for HPLC validation, Dr. Stefan Reinsch for TGA measurements, Sigrid Benemman for T-SEM measurements, Dr Shinde Arjun Sudhirkumar, Dr. Mustafa Biyikal and Dr. Ricarda Wagner for the intensive discussions. Last but not least, I would like to thank the members of Dr. Rurack´s research group, Delia Gröninger, Dominik Sarma, Dr. Estela Climent Terol, Dr. Jérémy Bell, Karin Keil, Dr. Mustafa Biyikal, Mandy Hecht, Dr. Pichandi Ashokkumar, Sabine Wagner, Shengchao Zhu and Tobias Fischer for the nice working atmosphere which has helped me to finish this research.

In particular, I would like to thank my parents, Wan Guogeng and Wang Shuying, for giving me the opportunity to see, to feel and to study the world. Of course, my very special thanks go to my wife, Zhou Ying, who always supported me with my research. It is so nice to be together with you.

Abstract

Research in the field of molecularly imprinted polymers (MIPs) has grown rapidly in the past two decades. Their areas of application cover a broad range including chiral separation, enzyme mimics, drug delivery and chemical sensing. This dissertation aimed at the preparation of optical sensor materials for anionic targets through combing the outstanding recognition properties of MIPs with sensitive fluorescence detection techniques.

A single-step direct sensing strategy was adopted to prepare the sensor material in this thesis. In particular, a fluorescence probe was covalently embedded into the cavities of the MIP matrix for signal transduction. Fluorophores from different classes (indole, naphthalimide, BODIPY, benzoxadiazole, phenoxazinone and phenazine) were used to prepare the functional monomers. Their performance was evaluated from spectroscopic properties and binding affinities, mostly by optical spectroscopic methods. Those monomers which showed outstanding optical properties (optimal excitation/emission wavelengths, prominent change in brightness) and interaction with the anionic targets in molecular solution studies were further used for preparation of the MIP sensor materials in the form of bulk monoliths, thin films and core/shell particles. The prepared materials were characterized with various techniques. The performance of the sensor materials was also assessed in terms of sensitivity, selectivity as well as response time. Both the signaling through a switching “on” or “off” of the fluorescence were tested in this thesis.

The prepared materials achieved many of the goals of the project. Both the prepared thin films as well as core/shell particles showed prominent selectivity for imprinted amino acids, even strong enantioselective discrimination. These sensing materials were also characterized by low limits of detection down to 60 μM and fast sensing responses of 20 seconds. Especially the core/shell sensing particles can be coupled with various detection techniques and are potentially applicable for developing miniaturized sensing devices for on-line detection as well as point-of-care diagnostics.

Kurzzusammenfassung

Das Forschungsgebiet der molekular geprägten Polymere (molecularly imprinted polymers, MIPs) ist in den vergangenen zwei Jahrzehnten enorm gewachsen. Die Anwendungsbereiche umfassen dabei ein breites Spektrum, von der chiralen Trennung über Enzym-Mimetika und Wirkstofffreisetzung bis zur chemischen Sensorik. Diese Dissertation befasste sich mit der Entwicklung von optischen Sensormaterialien für anionische Zielmoleküle durch die Kopplung der herausragenden Erkennungsfähigkeiten von MIPs mit der Empfindlichkeit fluorometrischer Nachweisverfahren.

In dieser Arbeit wurde dabei der direkte Einschritt-Nachweis für das Design der Sensormaterialien adaptiert. Hierbei wird eine Fluoreszenzsonde für die Signalübertragung kovalent in die Hohlräume der MIP-Matrix eingebaut. Fluorophore unterschiedlicher Klassen (Indol, Naphthalimid, BODIPY, Benzoxadiazol, Phenoxazinon und Phenazin) wurden zur Synthese der funktionellen Monomere eingesetzt. Ihre Performanz wurde aufgrund ihrer spektroskopischen Eigenschaften und Bindungsaffinitäten bewertet, vor allem mittels optisch-spektroskopischer Messungen. Monomere, die hervorragende optische Eigenschaften (optimale Anregungs-/Emissionswellenlänge, prominente Änderung der Helligkeit) und Wechselwirkungen mit den anionischen Zielmolekülen in molekularen Studien in Lösung zeigten, wurden für die weitere Herstellung der MIP-Sensormaterialien in monolithischen, Dünnfilm- und Kern/Schale-Partikel-Formaten verwendet. Die hergestellten Materialien wurden unter Verwendung unterschiedlicher Techniken charakterisiert. Die Performanz der Sensormaterialien wurde auch in Bezug auf die Sensitivität, Selektivität sowie Ansprechzeit bewertet. In dieser Arbeit wurden dabei Systeme untersucht, bei denen die Signalerzeugung sowohl auf dem „Einschalten“ als auch auf dem „Ausschalten“ der Fluoreszenz beruhte.

Mit den hergestellten Materialien wurden dabei viele Ziele des Projekts erreicht. Sowohl die synthetisierten dünnen Filme als auch die Kern/Schale-Partikel zeigten eine hohe Selektivität für die geprägten Aminosäuren, auch in Bezug auf die Unterscheidung von Enantiomeren. Diese Sensormaterialien waren ebenfalls durch eine niedrige Nachweisgrenze bis 60 µM und eine schnelle Ansprechzeit von 20 Sekunden gekennzeichnet. Insbesondere die Kern/Schale-Partikel können mit verschiedenen Detektionstechniken gekoppelt werden und sind potentiell für die Entwicklung von miniaturisierten Messinstrumenten für die on-line-Detektion sowie Point-of-Care-Diagnostik (patientennahe Labordiagnostik) einsetzbar.

Table of Contents

If I have seen further it is by standing on the shoulders of giants.

Isaac Newton, *Letter to Robert Hooke, February 5, 1675*

1 The History of Molecular Imprinting

Already as early as the 5th century B.C., the Chinese used the lost-wax process to produce bronze instruments and Figures in large scale. A template which has the same shape as the desired product was made of wax. They buried this wax template into sand, hardened it, and then burned it to make a mould. The wax template was then removed by melting and a cavity which has the shape of the template was left. When the melted iron and bronze were poured into this mould, a bronze or iron figure was thus made. This method enabled large scale manufacture (**Fig. 1.1**).

After two millennia, the technique developed along the history. In the 20th century A.C., the wax template was replaced by a small template molecule and the sand was replaced by polymerizable molecules (**Fig. 1.1**). People later called this technique *molecular imprinting*.

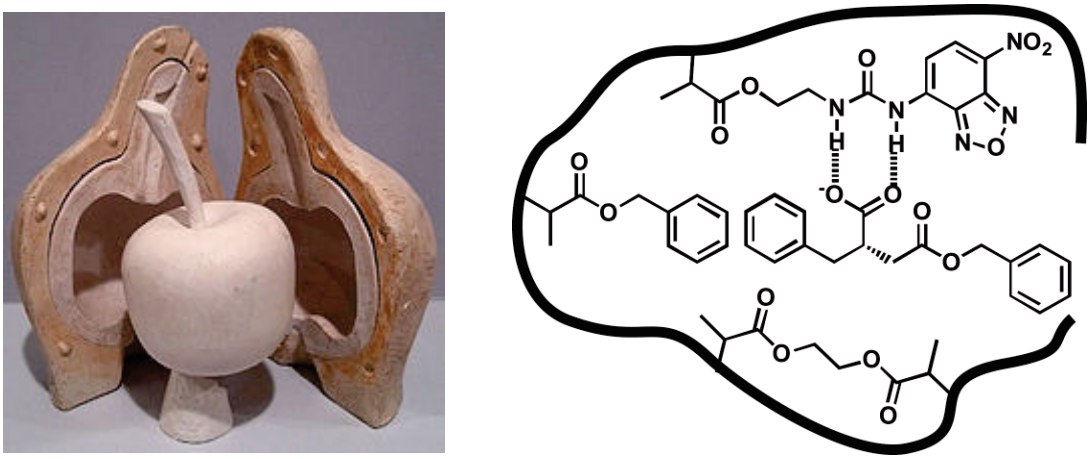

Fig. 1.1 Lost wax process[1](left) and molecular imprinting process (right)

The history of molecular imprinting can be traced back to the 1930s. Polyakov firstly observed the selective adsorption of small molecules in a silica matrix.[2] Another report came from Dickey, student of Linus Pauling. Pauling was studying the formation principle of antibodies at that time. He proposed an "instruction theory" that the antigen instructs the antibody to form a structure complementary to its own.[3] Although his theory was finally discarded, his idea was developed further by his student Dickey who prepared a silica matrix which can selectively adsorb dyes (methyl orange).[4] Dickey's experiments can be regarded as the birth of the molecular imprinting technique. However, the problems that arose due to the lack of specific binding of the monomers to the analyte (only hydrogen bonding through silanol, i.e., Si-OH groups) made a systematic modification of the cavity difficult and limited the development of molecularly imprinted silica.

In the next 20 years, alkaloids and aromatic hydrocarbons were also reported to be specifically adsorbed in silica matrices. However, the real breakthrough came only in 1972 when Wulff reported a racemate-discriminating polymer in *Angewandte Chemie*, opening a new era for molecularly imprinted polymers or MIPs.[5] The next ten years can be named the "golden time" for Wulff, whose group published many papers especially on a series of enzyme-like built polymers. The term *molecular imprinting* however did not appear until 1984, when Wulff proposed this name in an article in the *Annals of the New York Academy of Sciences*.[6]

Mosbach had studied enzyme engineering in earlier times and is known for his contributions in the field of affinity chromatography. As a biochemist, it became natural for him to utilize non-covalent interactions to prepare MIPs. The first paper of a molecularly imprinted polymer prepared with noncovalent interactions was published by Mosbach in 1981.[7] In that paper, it was still termed *host-guest polymerization* instead of molecular imprinting. This noncovalent approach made Mosbach the most famous scientist in the molecular imprinting community. Nowadays, most MIPs are prepared by noncovalent approaches.[8]

Since the end of the 1990s, MIPs attracted more and more the interest of scientists. The number of publications increased rapidly in the past ten years. According to the MIP database, 1082 papers were published in 2013. A literature exploration of the ISI knowledge database shows an increasing trend of MIP papers among the total chemistry papers of 1.55% in 1993, 2.86% in 2006 and 3.5% in 2013.

Very interesting is the fact that the birth of molecular imprinting has a close relationship with the study of the mechanisms of operation of enzymes and with the purpose to mimic the function of natural enzymes.[6] However, today much more other applications have been derived from this attractive material.[9,10] In the following, except where indicated, when referring to MIPs, only such polymers prepared by noncovalent imprinting are meant.

2 Synthesis Strategies of MIPs

As shown in **Scheme 2.1**, the preparation of MIPs always begins from a pre-polymerization step where the template forms a stable complex with the monomer(s) and crosslinker in the presence of solvent and an initiator.[11,12] Although in principle all polymerization methods can be applied for the synthesis of MIPs, most MIPs are prepared through free radical polymerization.[13] The polymerization can be initiated through either thermo- or photo-dissociation of the initiator. The radical adds to the monomer to form a new radical and hence gradually extends the polymer length to form a long polymer chain. When a crosslinker which has more than two polymerizable groups is present, a rigid 2D or 3D polymer network is formed. The rigidity of the matrix is related to the crosslinking level.[14] The higher the crosslinking level is, the more rigid is the matrix. After polymerization, the template is removed and an empty cavity is left. This cavity has a complementary shape and size to the template molecule and the interaction to the template is also preserved. Thus, MIPs can be used for target rebinding. The crosslinked network ensures the stability of the matrix, besides, it can provide additional interactions to the template molecule to increase the selectivity. The solvent is responsible for building porous channels which enable the template molecule to diffuse into the network and to those binding sites; thus the solvent is often termed *porogen*.[15]

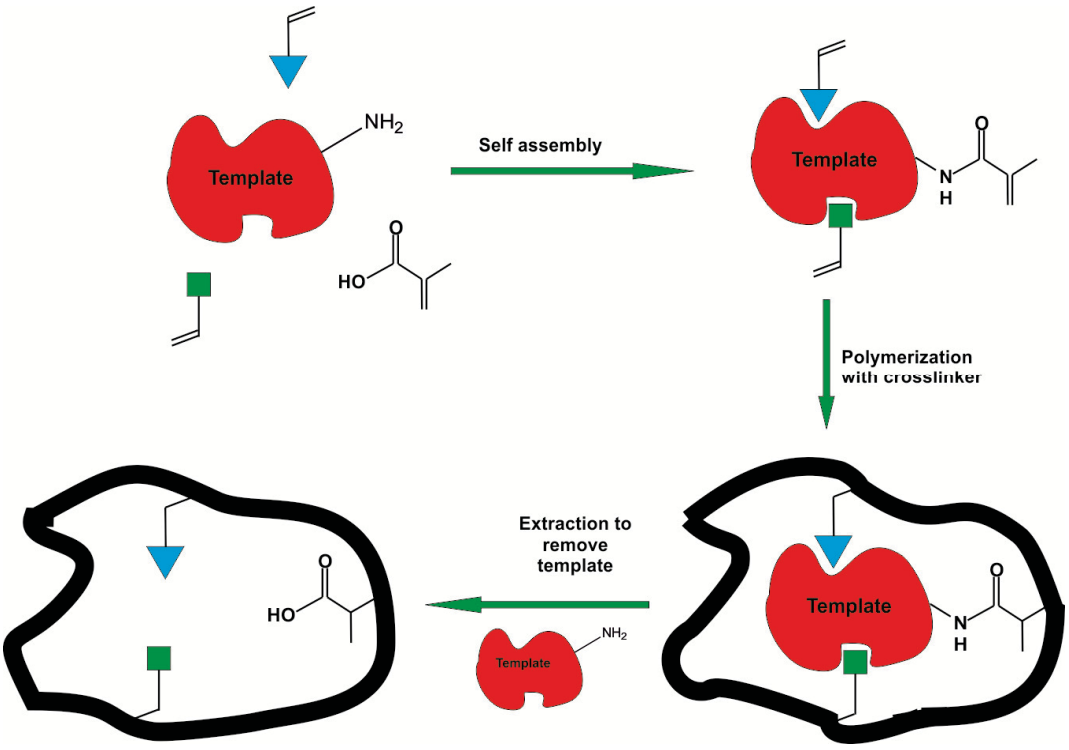

Scheme 2.1 Principle of molecularly imprinted polymer synthesis process

2.1 Covalent imprinting

Two main strategies based on the type of prepolymerization complex formation are used in molecular imprinting as shown in **Fig. 2.1**. In covalent imprinting, the template is fused to monomers through covalent bonds.[16] Thus, these conjugates are quite stable during the whole polymerization process and can be look on as real stoichiometric imprinting. These covalent bonds should be fully cleavable under mild conditions to recover the binding cavity without influencing its structure. However, only limited chemistry is available, such as boron-diols, Schiff bases and amides.[17] The latter is the main shortcoming of this strategy. The other drawback lies in the slow rebinding rate of a MIP prepared by the covalent strategy.[13,18,19] An alternative is to use a semi-covalent strategy where MIP is prepared by covalent strategy and the rebinding is based on non-covalent interactions. However, the small distance between the template and functional group when covalently attached during imprinting provides very limited buffer space and makes lots of cavities difficult or unavailable for rebinding.[20] A better variation is to introduce a spacer, such as a carbonyl group, between the template and the monomer.[21] Nevertheless, despite the covalent imprinting strategy can provide more homogeneous binding cavities, it is more and more substituted by the more convenient noncovalent methods.

2.2 Noncovalent imprinting

In the early 1980s, Mosbach's group introduced the noncovalent imprinting method.[7, 22] In this strategy, the template firstly forms a prepolymerization complex through various noncovalent interactions with the monomers. These interactions include hydrogen bonding, hydrophobic interactions, van der Waals forces, π-π stacking and electrostatic interactions.[13] Thus, a much broader spectrum of analytes can be imprinted. Due to the avoidance of synthesis and cleavage of the prepolymerization complex, noncovalent imprinting is much more relevant and became the major method for molecular imprinting. Nowadays, most MIPs are prepared by noncovalent imprinting.[23] Compared to the covalent imprinting, many more types of monomer can be used. This provides us with a larger possibility to fine tune the polymer character to enhance the imprinting performance. One limitation usually is the considerably low affinity of the monomer(s) (M) to the template (T) molecule. To achieve complete M-T complexation with respect to the template, often a large excess of monomer is

needed. This introduces a lot of unspecific binding sites due to excessive monomers and amends the selectivity performance.

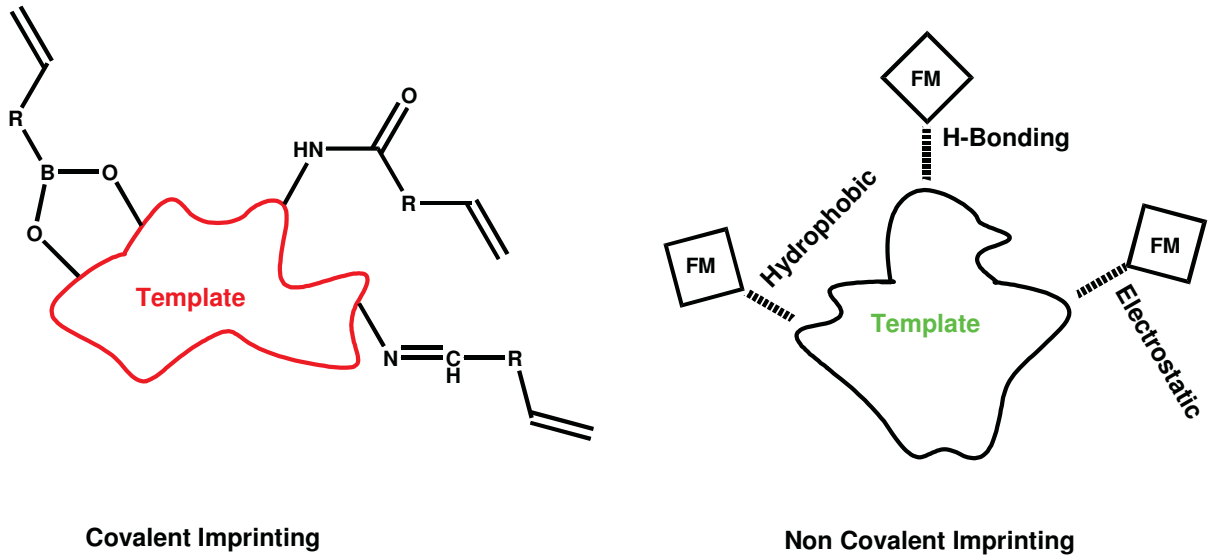

Fig. 2.1 Covalent molecular imprinting (left) and noncovalent molecular imprinting (right), FM = functional monomer

Recently a lot of custom-designed monomers which have higher binding affinities to the analyte were developed in many research groups.[24] The binding constants log*K* can be higher than 4 which can ensure 99.9% complexation and renders noncovalent stoichiometric imprinting possible.[25]

3 Components in MIP Synthesis

In conventional MIP synthesis, four components play an essential role, functional monomers, crosslinkers, the initiator and the solvent. These building blocks and auxiliary agents will be introduced in the next Sections.

3.1 Functional monomer

The functional monomers are the basic components in MIP preparation. They interact with the template to form a stables complex during the synthesis. After template removal, they provide interaction sites to rebind the target in the cavity. Besides, they also form the polymer matrix together with the crosslinkers. A convenient classification of monomers is to divide them into basic, acidic and neutral ones.

Methacrylic acid, acrylic acid and (2-trifluoromethyl) acrylic acid are the most often used acidic monomers (**Fig. 3.1**). They can provide high affinity to basic and neutral analytes including amino acids, alkaloids and steroids.[26]

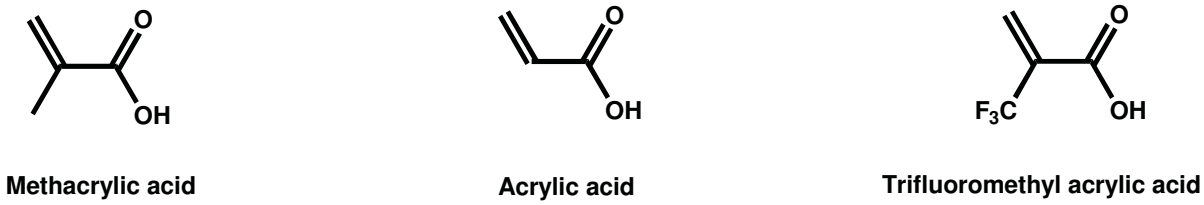

Fig. 3.1 Examples of acidic functional monomers

Vinylpyridine, vinylimidazole and methacrylamide are important basic monomers (**Fig. 3.2**). They can form strong interactions with acidic and neutral templates, also they can act as H-bonding acceptor to provide additional interactions.[27, 28]

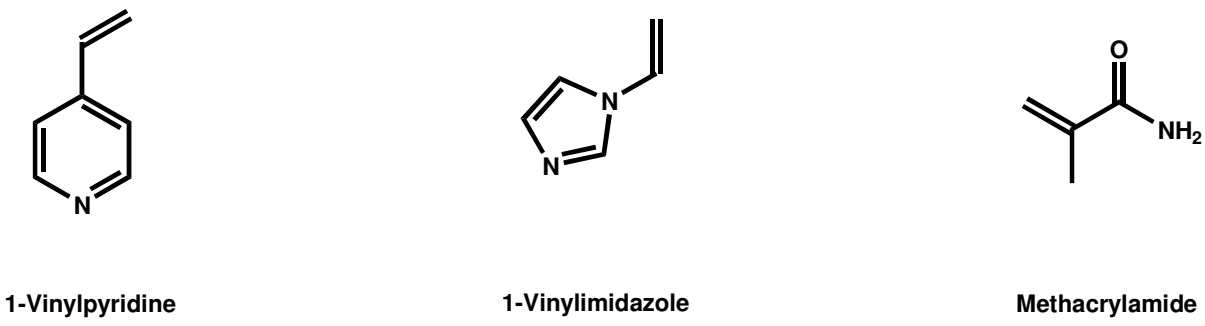

Fig. 3.2 Examples of basic functional monomers

Styrene, methyl methacrylate and 2-hydroxyethyl methacrylate are representative neutral monomers and are also widely used (**Fig. 3.3**).[29, 30]

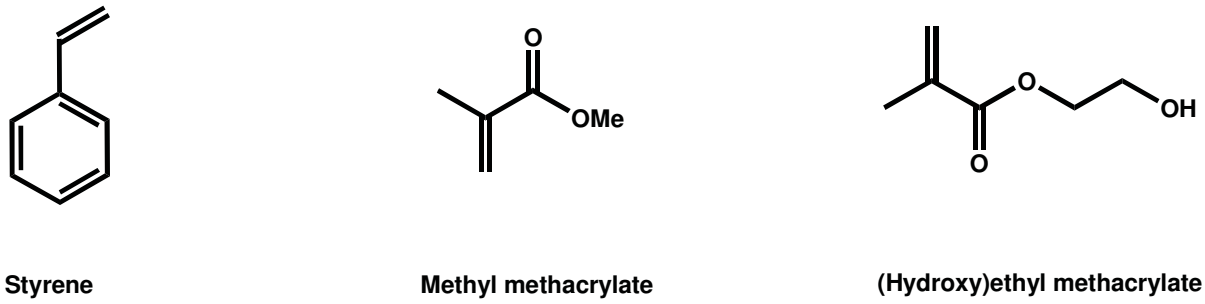

Styrene **Methyl methacrylate** **(Hydroxy)ethyl methacrylate**

Fig. 3.3 Examples of neutral functional monomers

However, these traditional monomers have an only limited affinity to many templates. In order to achieve higher affinity, more and more custom-designed monomers have been developed, facilitating noncovalent stoichiometric imprinting. For stoichiometric noncovalent imprinting, binding constants log*K* higher than 3 are required.[31] Thus, 99.9% of the template is engaged in the prepolymerization complex at a 1:1 ratio. Tanabe et al. have introduced a custom-designed receptor monomer to build more sensitive and selective MIP cavities for barbital.[25] From Sellergren's group, monomers with binding constants log*K* above 4 have been reported.[32] In this thesis, we also developed functional monomers with very high binding constants. The binding constant is determined by the geometric structure and electronic features of the binding site however can be influenced also by other factors such as the solvent and counter-ion of the target molecule. These issues will be discussed in later Sections.

The introduction of custom-designed monomers constitutes a further step in the process of mimicking natural receptors, since it separates the function of the monomer into matrix building and target recognition. This makes it more similar to natural receptors and greatly increases the performance of the MIPs.

3.2 Crosslinker

The main function of a crosslinker is to fix the polymer matrix rigidly to provide a stable binding cavity. In nature, only small portions of disulfide bonds play the role as crosslinker, so that a protein can easily denature irreversibly at higher temperature, lower pH or even at high concentrations of dissolved salts. In MIPs, a much higher crosslinking level is usually reached which makes the MIP more stable than the natural receptors (**Fig. 3.4**).[33]

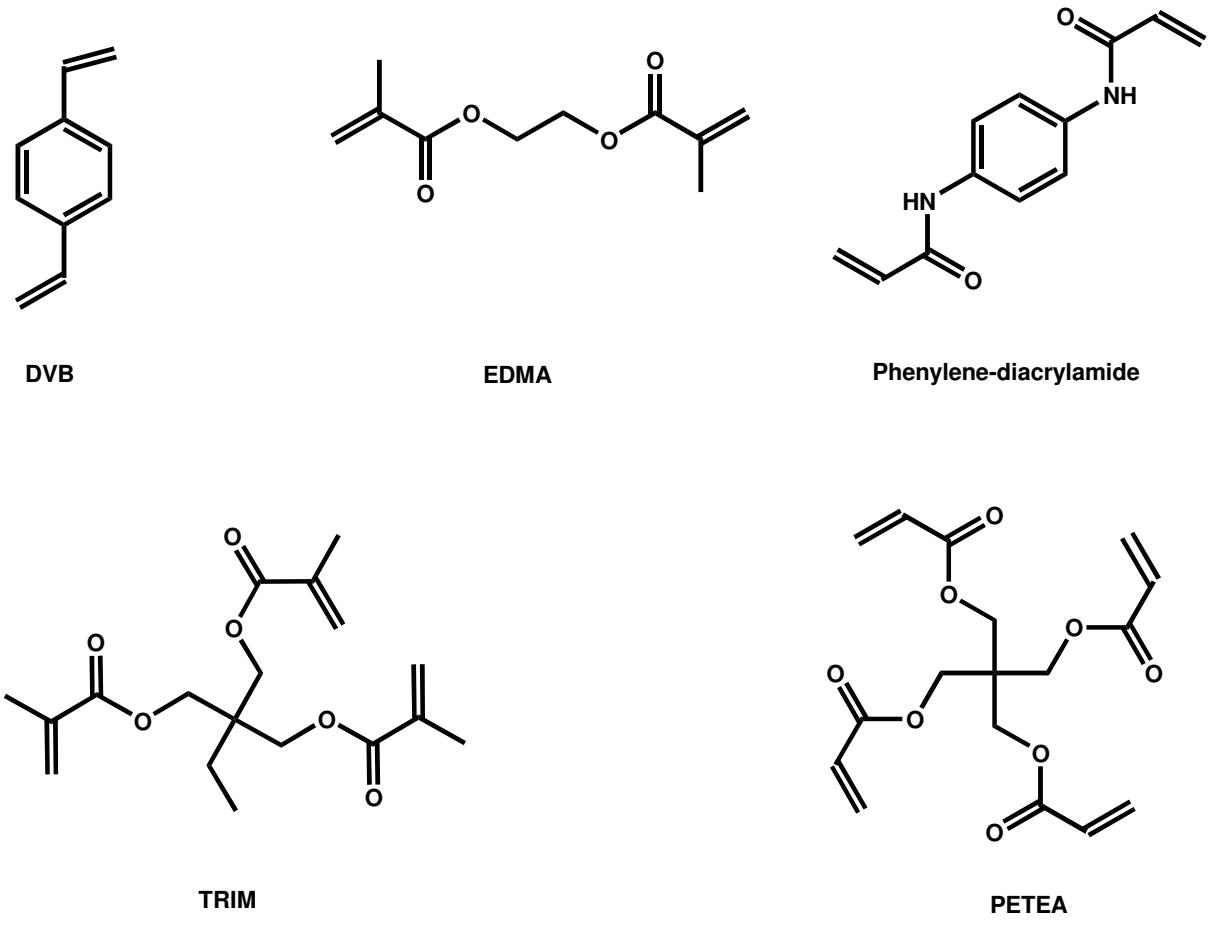

Fig. 3.4 Examples of crosslinkers used for molecular imprinting

Commonly, a large excess of over 70% crosslinker is used in MIP preparation. Thus, the properties of the crosslinker can greatly influence the character of the polymer matrix, including the refractive index, polarity and hydrophobicity. Wulff's group has compared the performance of MIPs prepared by DVB and EDMA and found that MIPs prepared with EDMA have much better performance in terms of stability, wettability and recognition ability in most rebinding scenarios.[34]

The crosslinking level can also rise with increasing numbers of functional groups on the crosslinker. Trifunctional trimethylolpropane trimethacrylate (TRIM), pentaerythritol triacrylate (PETRA) and tetrafunctional pentaerythritol tetraacrylate (PETEA) show outstanding performance in some cases.[14, 35] Crosslinkers can also provide additional interaction sites for the template. It is known that multipoint recognition can provide much better selectivity. These additional interactions contributed by the crosslinker can sometimes become a critical parameter for an improved selectivity.[36]

Recently, for instance, Spivak's group developed novel crosslinkers which act as both functional monomer and crosslinker. They called the MIPs prepared with these crosslinkers *one monomer molecularly imprinted polymers* (OMNiMIPs), as shown in **Fig. 3.5**.[37] These functional crosslinkers showed good separation for the chiral substrate used by these researchers. However, only few examples have been presented until now. According to a private communication by Spivak, the selectivity decreased with addition of other co-monomers.[38] In this thesis we also used this crosslinker for MIP preparation, which will be discussed in a later chapter.

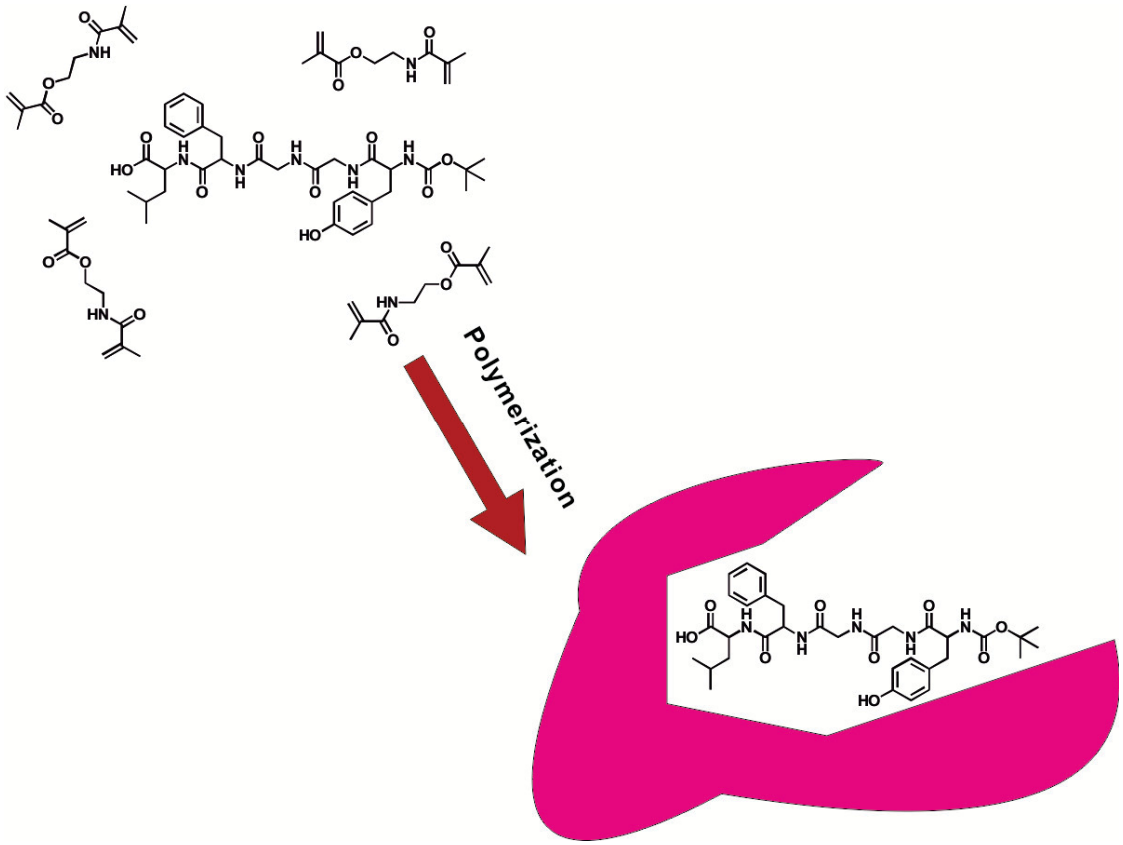

Fig. 3.5 N, O - bismethacryloyl ethanolamine (NOBE) used in one monomer molecularly imprinted polymers

3.3 Initiator

For a radical polymerization process, everything begins with the birth of the free radical. The initiator is the source of the radical. According to the method of radical generation, they can be roughly divided into photo- and thermally initiating types (**Fig. 3.6**).[39] Benzophenones and benzylketals are oft used as photo-initiators. They can be cleaved through irradiation with UV or visible light to form the free radicals. The use of photo-initiators can enable low-temperature polymerization, often at 0 ^{o}C.[40,41] This low-temperature polymerization can provide much more stable M-T complexes as well as reduced vibration and rotation of the complex during the polymerization and hence better imprinting performance. O'Shannessy et al. have compared the MIP prepared by UV initiation at 0 ^{o}C and thermal initiation at 60 ^{o}C using AIBN as initiator and claimed that the polymerization at low temperature has improved the separation factor, especially at low column temperature, that is, the factor describing the discrimination of the desired template against potential competitors by the MIP.[41] Fuchs et al. also showed the feasibility to assemble MIP thin films with a photo-polymerization method.[40] However, as can be easily deduced from the title of this thesis, it is not suitable in our case. It will potentially bleach the fluorogenic functional monomers through the rather high-energy UV-light that has to be used for photo-polymerization.

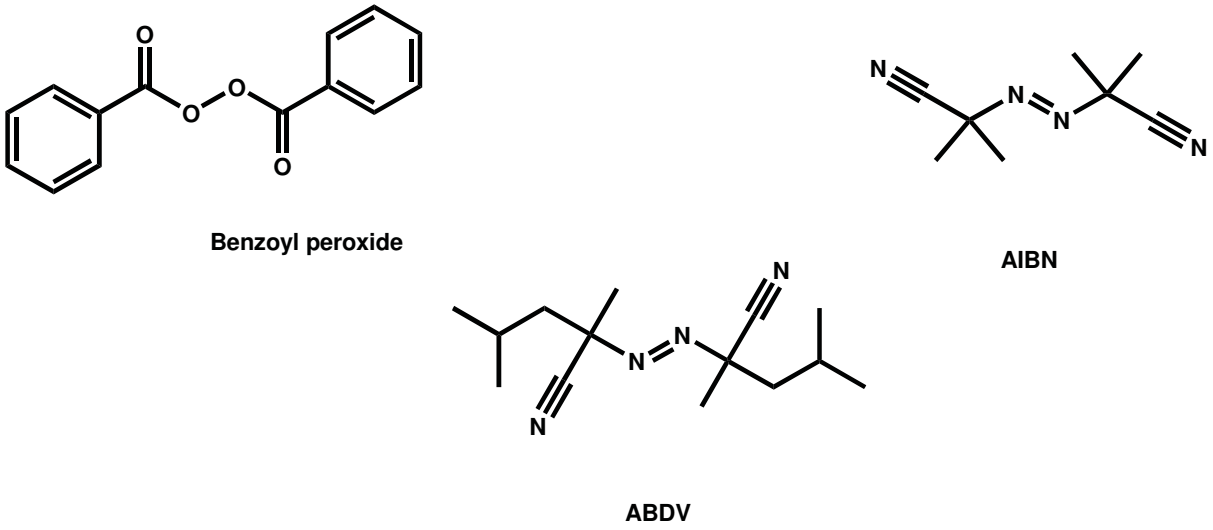

Fig. 3.6 Examples of radical initiators

AIBN and ABDV can be used as either thermo- or photo-initiator. The dissociation temperatures are 60 ^{o}C and 40 ^{o}C, respectively. To ensure the stability of the complex, ABDV was used throughout this study.

3.4 Solvent or porogen

The solvent is another critical parameter in MIP synthesis. In this process, the solvent has functions other than simply dissolving all the components. The solvent usually is involved in pore formation inside the polymer; thus it is also termed *porogen* in the MIP synthesis.[42] It can also strengthen the T-M interactions, enabling stoichiometric imprinting. In applications of MIPs such as in optical sensors, it also influences the microenvironmental polarity in the MIP cavity and hence the spectroscopic response.

3.4.1 Role of solvent in molecular imprinting

In noncovalent imprinting, the stability of the M-T complex during the whole synthesis process is decisive. The binding strength of the complex is decided by the cumulative interactions between the monomer and template and it can be influenced by the solvent. In this sense, a solvent with poor solubility to the template but good solubility to the complex is preferred. For instance, polar aprotic solvents such as DMF tend to solvate the polar and ionic species and hence to interfere with the stability of the M-T complex. Protic solvents like methanol on the other hand can interfere with hydrogen bonding within the M-T complex. Thus, aprotic non-polar solvents are more preferred in MIP synthesis when solubility permits their use.[42, 43]

Pore formation is a very important function of the solvent in MIP synthesis. It is widely reported that the MIP structure is influenced by the solvent. This includes the pore structure, pore size distribution, swelling ability, toughness and morphology.[44] For example, a poor solvent promotes the aggregation of the polymer and hence the formation of densely crosslinked matrices. Thus, the polymer has a low swelling ability. In a good solvent on the other hand, the material prepared has high swelling ability and behaves more similar to gels.[45] To control the structure solvent combinations are also frequently used for MIP preparation.[46]

3.4.2 Solubility parameter

There are several parameters to evaluate solvent properties. The first is the dielectric constant, which is roughly used as a measure of solvent polarity. It is especially important for the electrostatic forces between analyte and receptor. The force is strengthened by solvents with a low dielectric constant. However, it is generally accepted that the solvent polarity cannot be described using this single parameter. Thus, a second parameter, the hydrogen bonding parameter (HBP) is introduced. HBP includes both hydrogen bond accepting (HBA) and hydrogen bond donating (HBD) abilities. A solvent with a high HBP will easily dissolve polar molecules through hydrogen bonds. But it will also become the primary interference when the hydrogen bonding interactions are the main driving force for M-T complex formation.

Sellergren has suggested to take even more parameters into account when choosing a solvent for MIP preparation (**Table 3.1**). In this table the solubility parameter is divided into a dispersive term δ_d, a polar term δ_p and a hydrogen bonding term δ_h. *H-bond* here is a measure of the hydrogen bonding capacity in terms of both H-bond donor and acceptor. They are classified as poor (P), moderate (M) and strong (S).

Table 3.1 Solubility parameters (δ_d as dispersion, δ_p as polarity and δ_h as hydrogen bonding, hydrogen bond capacity (P as poor, M as moderate and S as strong) and refractive indices (n_D) of solvents used for preparing MIPs [47]

Solvent	δ_d	δ_p	δ_h	H-bond	n_D
MeCN	15.3	18.0	6.1	P	1.34
THF	16.8	5.7	8.0	M	1.41
$CHCl_3$	17.8	3.1	5.7	P	1.45
C_6H_6	18.4	0.0	2.0	P	1.5
DMF	17.4	13.7	11.3	M	1.43
CH_2Cl_2	18.2	6.3	6.1	P	1.42
i-Propanol	15.8	6.1	16.4	S	1.38
HOAc	14.5	8.0	13.5	S	1.37
MeOH	15.1	12.3	29.3	S	1.36
Toluene	18.0	1.4	2.0	P	1.50
H_2O	15.5	16.0	42.4	S	1.33
Cyclohexane	16.8	0.0	0.2	P	1.43

The solvent influences not only the synthesis processes, but also the later assay procedure in a MIP application.[48] A change of the solvent will change the analyte distribution between the surrounding bulk and the MIP, which means the affinity. Sellergren has reported that the addition of small portions of water can increase the recognition effect especially for hydrophobic templates.[49] Another effect can arise from the different swelling ability of the solvent. This swelling effect can influence the structure of the formed MIP cavity and hence the binding. It should be taken into account when synthesis and rebinding application are carried out in different solvents. However, there are cases where the MIPs are prepared in nonpolar solvents yet still work well in aqueous solution and polar solvents with a high dielectric constant such as water/methanol mixtures.[50]

3.5 Template

As discussed in the previous Sections, template is the used as a mould to form the binding cavity of our target molecule. Except for some applications, e.g., using MIPs to mimic enzymatic functions, for which a dummy of a similar structure as the molecular transition state is used as a template, the target molecule itself is most often used as the template. They vary from small ions, organic molecules, short peptides to macromolecular proteins. The template decides the selection of the monomers and crosslinker since the formed polymer matrix should provide strong and specific interaction towards the target molecule.

Oxyanions, like carboxylate, phosphate and sulfate, are of significant relevance to everyday life. These anions play an important role in our biological system, for example acting as metabolic intermediates which can be used as diagonostic indicator. A prominent example is phenylpyruvate which excessive presence in the urin suggests phenylketouria, a genetic disease.[51] Oxyanions are also important products in pharmaceutical industry such as aspirin and ibuprofen which belong to the family of carboxylic acids.[52] In environmental monitoring, phosphates in aqueous systems are an important parameter of eutrophication.[53] Yet, the selective supramolecular detection of anions is difficult due to their complicated structure and low charge density. The preparation of molecular receptors such as molecular tweezers,[54] large molecules as aptamers[55] or biological antibodies[56] often needs a long time and a considerable budget. Molecular imprinting, due to its analyte-instructed preparation, becomes a more competitive solution to address the problem of anion sensing. Since these oxyanions always carry a high electron density at the oxygen atom, they can form strong

interaction with H-bonding donors such as urea and guanidine groups. By using a monomer carrying such groups, the anion can be imprinted into the polymer, where the selectivity is achieved through the MIP cavity, just like the enzyme cavity fits to its substrate.

In this thesis, Z-D/L-Phe are firstly selected as templates. They have been studied in enantiomeric imprinting by several groups and are a good model system for our studies.[57, 58] Besides, the single amino acid imprinting will be helpful for us to figure out a map of imprinting effects of monomers towards different amino acids, the building block of peptides and proteins. This will further help us to quickly select suitable monomers aiming towards peptide/protein imprinting.

Penicillin G (PenG) was discovered by Fleming and has been widely used as antibiotic against bacteria. It is thus an important analytical species and has been imprinted by several groups and is also used in this thesis.[59, 60,61]

At last, we also target the phosphate anion, since the phosphorylation is an important protein post modification process and is a regulatory factor in many diseases.[62,63] The detection of protein phosphorylation will also contribute to the proteome. Phosphorylated tyrosine is selected as template in this thesis. The templates used in this thesis are listed in **Fig. 3.7**.

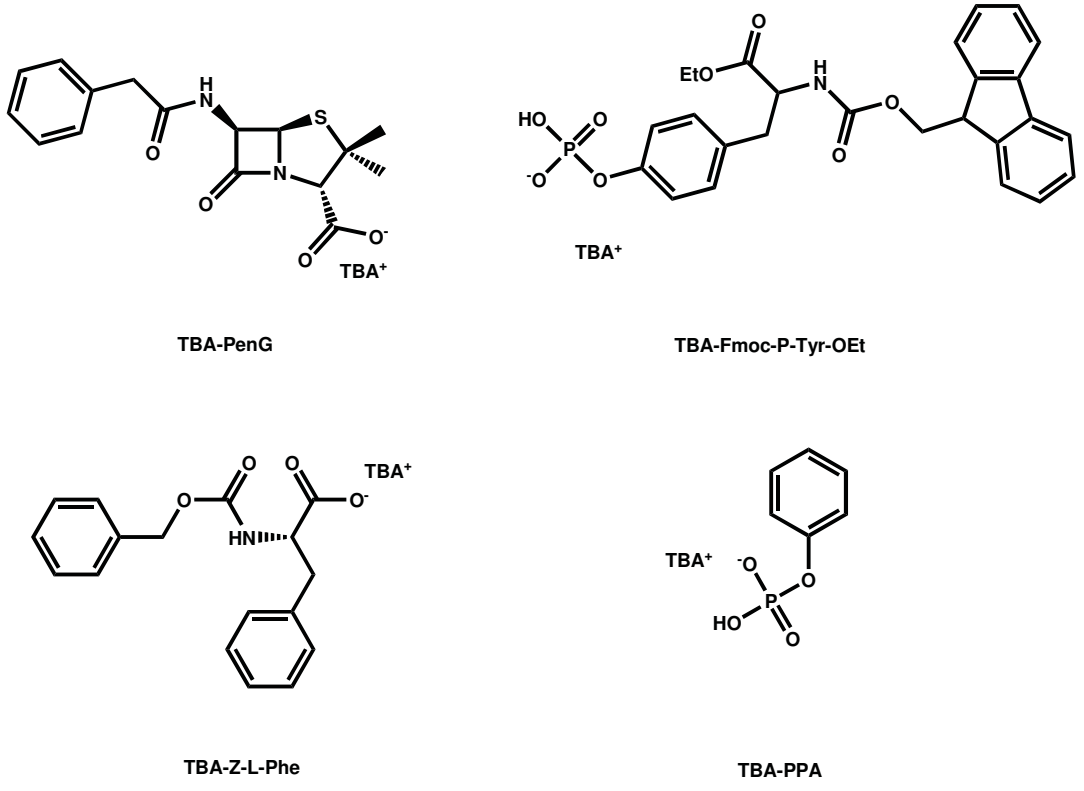

Fig. 3.7 Templates used in the Thesis

4 Polymerization Methods

The process of polymerization is to form a macroscopic matrix through interconnecting the small monomers with covalent bonds. Various methods can be used, including polycondensation, polyaddition, radical polymerization and electropolymerization (**Scheme 4.1**). The most versatile method is free radical polymerization using vinyl monomers.[31] It includes four different reactions: radical generation from the initiator, polymer chain propagation, chain transfer and termination by disproportionation or radical recombination. Since only radical polymerization techniques have been used in this thesis, the other types of procedures will not be discussed in detail here.[64, 65, 66]

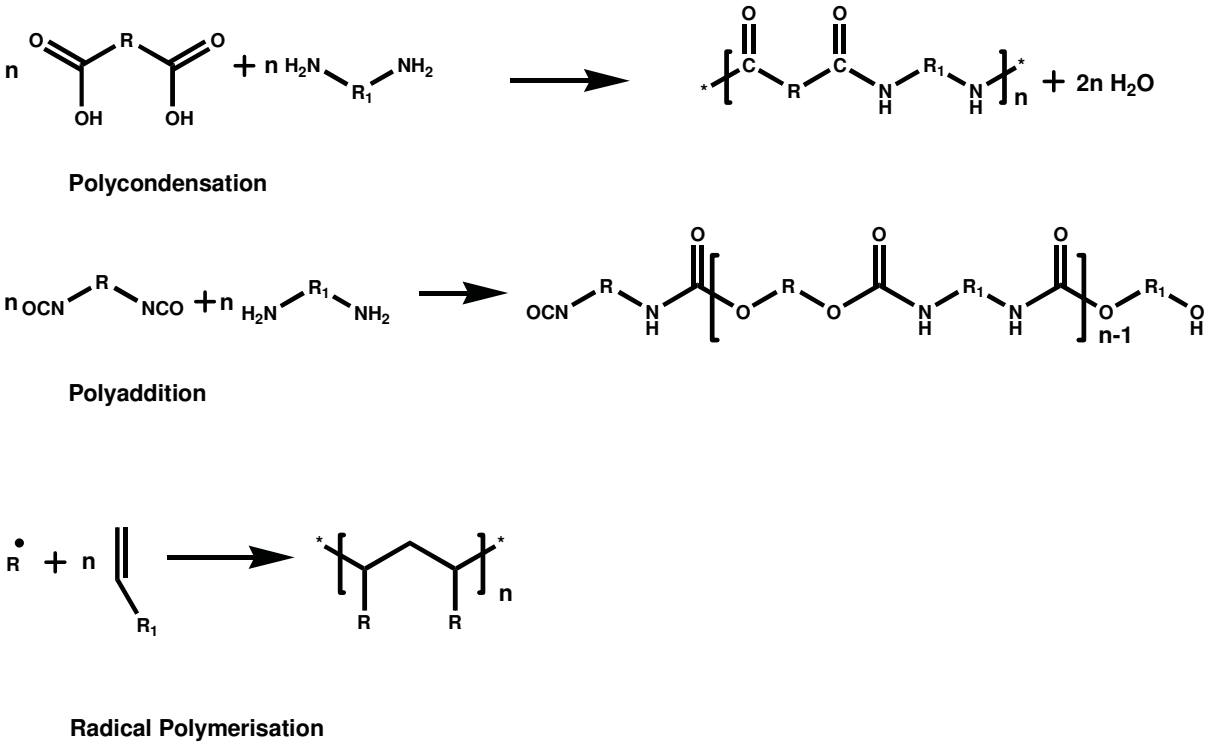

Scheme 4.1 Examples of polymerization methods

4.1 RAFT polymerization

The reversible addition-fragmentation chain transfer (RAFT) process together with nitroxide-mediated polymerization (NMP) and atom transfer radical polymerization (ATRP) are important variants of radical polymerization to achieve controlled radical polymerization (CRP).[67] RAFT can control the length of the synthesized polymer chain through a kinetic strategy.[68]

Most RAFT agents are dithioester derivatives. They have an activating group (Z) linked to the thioester carbon and a leaving group (R) linked to sulphur. In the first step, the propagating radical adds to the thiocarbonyl centre to form a radical intermediate. This radical can undergo a β-scission to liberate a new radical (the leaving group). This leaving group can reinitiate polymerization to form a more active, propagating radical to substitute the first propagating radical and eventually to a equilibrium (**Scheme 4.2**).

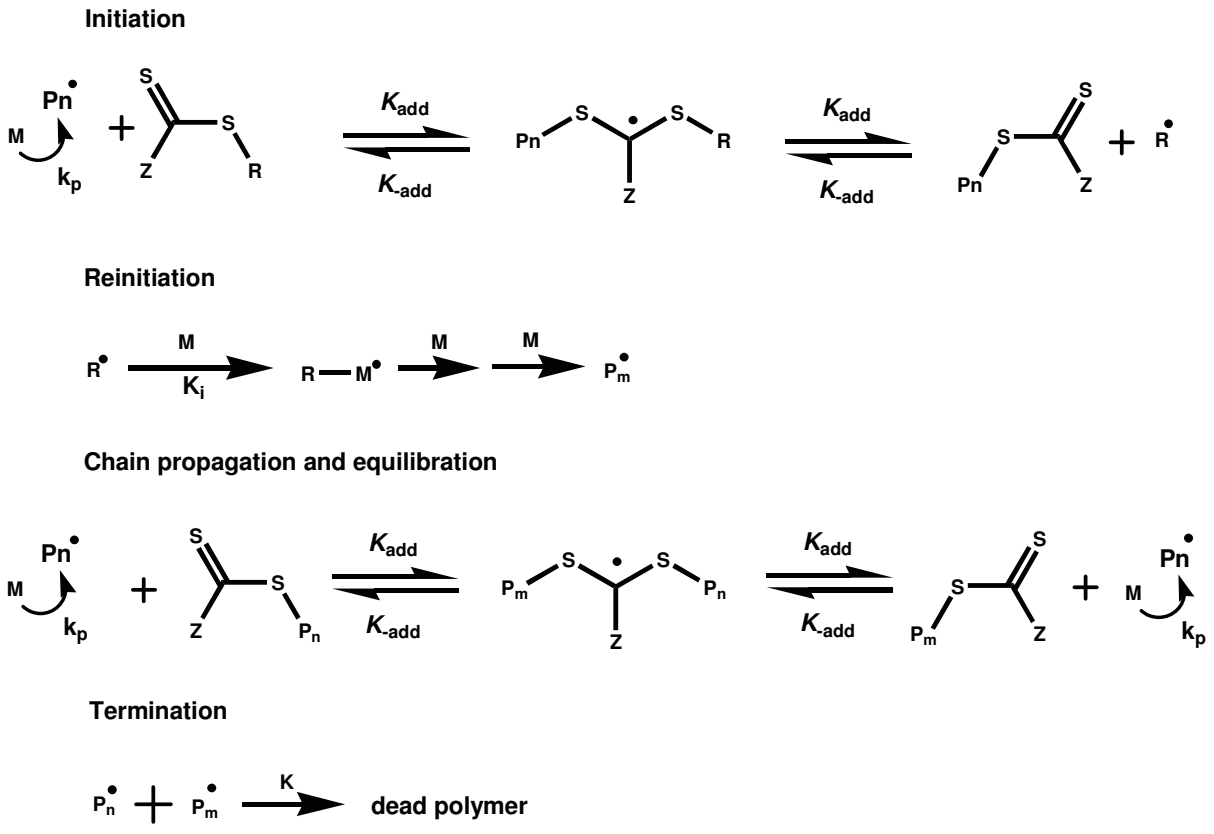

Scheme 4.2 Mechanism of RAFT polymerization process

5 MIP Formats

MIPs can be prepared in various formats including bulks, films and particles. This greatly facilitate the assembly of MIPs into sensing layers.

5.1 Monoliths

The simplest format of MIPs is a monolithic polymer. They have been widely prepared in earlier studies.[69, 70, 71] A universal preparation protocol is to mix all the components inside a glass tube, which is polymerized through thermal or UV irradiation. After that, the glass tube is broken and the solid polymer is grinded into small particles and sieved into different sizes for various applications. However, the uncontrollable particle size and shape during grinding leads not only to a certain loss of material but often also to rather poor separation performance. All these facts limit the application of MIPs in bulk or monolithic format for other than chromatographic applications.

5.2 Thin Films

Films and membranes are an attractive format. They are commonly thin layers ranging from several nm to several hundred μm. These thin polymer layers can be implemented in separation techniques for analyte concentration. For instance, Renkecz et al. have reported the concentration of propranolol using a MIP membrane prepared from MAA and EDMA.[72] MIP thin films can also be directly applied in the assembly of sensors. The transduction mechanisms then involve a change of the membrane profile after selective adsorption of an analyte and include parameters such as the frequency in quartz crystal microbalances (QCMs), the conductivity in electronic sensors or absorption/fluorescence profiles in optical sensors.[73]

However, the stability of this quasi-2D matrix seems to be still a problem at present, preventing a much more frequent use in many applications. This is especially critical in very thin films of several nm. According to a private conversation with Dechtritat, often such thin films lose their selectivity after the first cycle of target rebinding and are not suitable for reversible applications.[74]

5.3 Particles

Polymer particles are a widely used format. Particles can be prepared by emulsion, precipitation and dispersion polymerization and cover a wide size range from 100 nm to several tens of μm with narrow size distribution.[75, 76, 77] This morphological homogeneity ensures a narrow distribution of binding sites. Compared with monoliths or thin-films, MIP particles thus resemble better monoclonal antibodies in a biological sense. Particles also allow for large scale (industrial) production and potentially reduce the production costs significantly.

5.3.1 Core-Shell Particles

Core-shell particles have been intensively studied recently, especially for applications as sensor particles.[78, 79, 80] The advantage compared to bulk (or core-only) particles lies in the combination of a thin, effective MIP layer with a core part as support. Only a very thin, several nanometer thick polymer shell forms the sensing part. Thus less material is required, which is especially important in case of imprinting expensive templates. More importantly, the reproducibility of the thin layer can be greatly increased. The thin shell also reduces greatly the diffusion paths, enabling a fast sensing response. It also strongly reduces the background noise which stems from non-accessible binding cavities buried deeply inside bulk particles which are imprinted throughout their core. Besides, the core part can be modified with different functionalities such as small magnetic particles to facilitate separation and handling procedures. The particles can be easily coupled with various miniaturized analytical techniques such as microfluidic chips to assemble portable sensors. This is especially important for point-of-care diagnostics as well as health self-monitoring.

5.3.2 Particles with ordered pore systems

Besides bulk particle materials with a disordered pore system created by the solvent or porogen used during the MIP synthesis process, see e.g. Section 5.3, particles with an intrinsic, ordered pore system have also been used as substrate for MIP preparation. This porous structure endows the particles with a much larger surface and hence can provide much more effective binding sites. For this purpose, mesoporous silica particles of MCM-41 or SBA-15 type are commonly employed. For instance, Mehdinia et al. have reported the preparation of MIPs using ascorbic acid as template in the pores of SBA-15. They showed the possibility to

carry out the polymerization in aqueous environment.[81] Mesoporous structures are especially interesting to assemble ion-imprinted materials. For example, Kang and Guo have imprinted Cu(II) and Co(II) ions with MCM-41 and SBA-15, respectively.[82, 83] Nematollahzadeh has also reported the preparation of thin MIP layers on the surface of porous silica particles for separation of proteins in HPLC.[84]

5.4 Other formats

MIP gels are also an attractive format. They are mostly polymers with low crosslinking level, which are thus more flexible. They can behave more like natural proteins do and bind the analyte through an induced fit mechanism. Such MIPs are especially developed as artificial enzymes to catalyse chemical reactions.[85, 86, 87]

Other formats involve hybrid structures where the MIP is coated onto various materials including cellulose,[88] nanofilaments [89] and carbon nanotubes (CNTs)[90] to assemble for instance electronic sensors. Such hybrid materials can greatly expand the application of MIPs in various areas in the future.

6 Fields of Application of MIPs

MIPs are basically considered as plastic receptors. Thus, in principle, all functions derived from receptors can be mimicked.

6.1 Separation and extraction

Although MIPs were developed during the research on enzymes, separation and purification however are today still the most popular applications.[91] Solid phase extraction (SPE) is an important pre-treatment step in sample preparation. It concentrates a target and avoids interference from a sample's matrix. MIPs for this purpose are frequently termed molecularly imprinted SPEs (MISPEs).[92] Such MIPs can also recover targets from complex matrices. For instance, Gu has recovered chlorogenic acid from complex mixtures of traditional Chinese medicine. [93] MIPs can also promote the enantiomer separation performance of chiral chromatography techniques. This is especially interesting in drug production since often only one enantiomer can be used in a medicine. Balamurugan has reported the chiral separation of ephedrine with reasonable separation factors.[94] Separation and extraction may be the most successful applications for MIPs and various MIP phases are already available as commercial products.

6.2 Enzyme mimics

Mimicking enzymes is another important field of application. The function of a natural enzyme is to change the activation energy of a reaction so that the reaction rate is altered toward the desired product. A MIP cavity designed as an artificial enzyme can also preferentially stabilize the transition state and function as a catalyst. Different from other routes of MIP preparation, for which the target itself is used as the template, a dummy molecule, termed *transition state analogue* (TSA) which mimics the transition state of the substrate is used as template for catalytic MIPs. Up to now, a number of reactions such as Kemp elimination[95] or aldol addition[86] using MIPs as artificial enzyme have been reported.

6.3 MIPs in the context of drugs

MIPs employed in the area of drug applications have been developed along two directions. The first one is the use of MIPs as carriers in drug delivery. A main benefit here comes from an otherwise unwanted effect of many bulk MIPs, the long retention time of the target molecule in the MIP cavity.[96, 97] Asadi has shown that a cyproterone-imprinted polymer has a controlled release in physiological medium over a suitably long period of time.[98] In the second approach, MIPs are directly used as receptor inhibitor, which have promising prospects in the drug market. Here, MIPs are supposed to substitute the function of natural antibodies due to the simplified preparation and lower production costs.[99] The robust structure and tolerance to organic solvents also extends their application. Recently, for example MIPs have been reported as enzyme inhibitors for protease a-chymotrypsin (ChT).[100]

6.4 Sensors

MIPs as sensor matrices are perhaps the most attractive application.[101] A sensor is an instrument for us to recognize changes all around us, just like the eye recognizes a change of light, the nose recognizes a change in concentration of a gaseous chemicals and the tongue recognizes the change of an aqueous chemical concentration. In nature, some animals have developed organs for a much better recognition of such environmental changes such as the dog's nose, the bat's ear, the dragonfly's eye etc. Compared with many animals, the human senses are inferior and we thus strive to develop artificial sensors to enhance our ability of environmental recognition, such as electronic noses and tongues.[102] These sensors can greatly expand the human ability to recognize our world. At the same time, this enhancement is safer in a way that a sensor is much easier repaired or exchanged than our own natural organs. Especially today, accompanied by the tremendous development of electronic instruments such as smartphones, smartwatches or smartglasses, portable sensors are becoming more and more appealing. In future, sensors will not only be developed for industrial processes but also for our daily life.

Regarding MIPs in sensor applications, piezoelectric systems including the QCM are perhaps the ones most often studied.[103, 104, 105] QCMs measure the change of mass through a shift in the resonance frequency of a quartz crystal. A MIP layer is usually coated onto the crystal surface. After selective binding of the target, the change of the resonance frequency can be used to evaluate the target concentration. For instance, Stanley et al. have reported a

sensitive QCM sensor for enantioselective detection of L-Serine with a low limit of detection (LOD) of 2 ppb.[106]

Electrical MIP sensors have also been intensively studied. In an electrical sensor, only a single transducer is needed since the output is already an electronic signal. This can simplify the device. The binding of a target can change the conductivity and hence be measured. In combination with electropolymerization techniques, special monomers can be used for such MIPs.[74, 107, 108]

Optical sensors finally measure changes of optical properties including fluorescence, infrared transitions, surface plasmon resonances (SPR) or reflectrometric interferences. For instance, Bompart et al. have reported a MIP sensor that uses confocal microscopy.[109] Especially due to the high sensitivity of fluorescence techniques, MIPs are becoming a very promising recognition phase for optical sensor designs.[110, 111, 112]

7 MIPs with Advanced Functions

In earlier times, MIPs were prepared using simple commercially available functional monomers and crosslinkers. Thousands of publications are based on simple recipes with MMA and EDMA to imprint different targets. This non-oriented synthesis has damaged the reputation of MIPs to some extent. If we look at our natural models, enzymes and antibodies, we will find that the monomers (i.e., amino acids) usually serve two functions, namely to form the (global or super-) structure and to provide the adequate (local, commonly adaptable) surrounding for the active sites. This functional separation using a library of monomers greatly increases the specificity and performance of such natural receptors. Thus recently, to achieve better performance and increase the functionality of the MIP matrix, MIPs with advanced function have been approached.

7.1 Thermoresponsive MIPs

Pan et al. have prepared poly-NIPAAm brush-coated MIP particles for controlled recognition and release of target through temperature changes.[113] Li et al. have used 1-vinylimidazole to prepare a thermosensitive MIP for switching on and off the catalytic activity.[114] Li et al. have also reported a zipper-like on/off switchable MIP prepared by poly(acrylamide) (PAAm) and poly(2-acrylamide-2-methyl propanesulfonic acid) (PAMPS),[115] where the recognition ability is switched on at relatively high temperature (40 ^{o}C).

7.2 pH-responsive MIP

Kanekiyo et al. have imprinted bisphenol-A (BPA) using acryloylamylose and the resulting MIP shows enhanced analyte uptake under acidic condition but lower rebinding in a basic environment. This pH-responsive effect can be regenerated for several cycles.[116] Zhao et al. have prepared a MIP for selective absorption of BPA using N,N´-methylenebisacrylamide. After filling the pores with a pH-responsive PAA gel, the MIP exhibits a chemical valve effect between pH 3-6.[117]

7.3 Fluorescent and phosphorescent MIPs

Turkewitsch et al. were the first to introduce a polymerizable fluorescent dye, *trans*-4-[*p*-(*N*,*N*-dimethylamino)styryl]-*N*-vinylbenzylpyridinium chloride, into a MIP matrix for detecting cAMP.[118] However, the weak target response and high measurement uncertainty limited any real application. They used a bis-amidopyridine motif which possesses a H-bonding Donor-Acceptor-Donor (DAD) structure to bind barbiturates. Jordan et al. have reported the use of fluorescent pyridyl ureas as monomers for the imprinting of the CF_3COO^- anion with fluorescence responses in the UV range.[119] Sellergren also prepared 1,3-disubstituted monourea monomers with UV-fluorescence for imprinting oxoanions, achieving considerable separation factors.[32] Besides fluorescent MIPs, Sánchez-Barragán et al. have prepared a urethane MIP using tetraiodobisphenol and diphenylmethane diisocyanate for imprinting fluoranthene. The rigid iodide-enriched cavity enables the detection of the template molecule with room temperature phosphorescence (RTP) technique.[120] Further aspects of MIPs in the context of fluorescence signalling will be discussed in the following Sections.

8 Fluorescence Sensors and Fluorescent Probes

A sensor is a device that transforms the changes of a signal such as light (intensity or colour, i.e., wavelength), temperature or viscosity into an analytically useful, mostly electronic output. It is normally a rather elaborate device including a recognition element, a signal transducer and a detector with subsequent periphery as shown in **Scheme 8.1**. A chemical sensor can transform the chemical information, the concentration of a specific sample component and/or the total chemical composition in a research or sample medium, into an analytically useful output.[121] If the transduction mode is an optical signal, the recognition element of a chemical sensor usually incorporates a chromogenic or fluorescent probe (or indicator) molecule (or micro-/ nanoparticle) immobilized either sterically or covalently in the responsive matrix.[122]

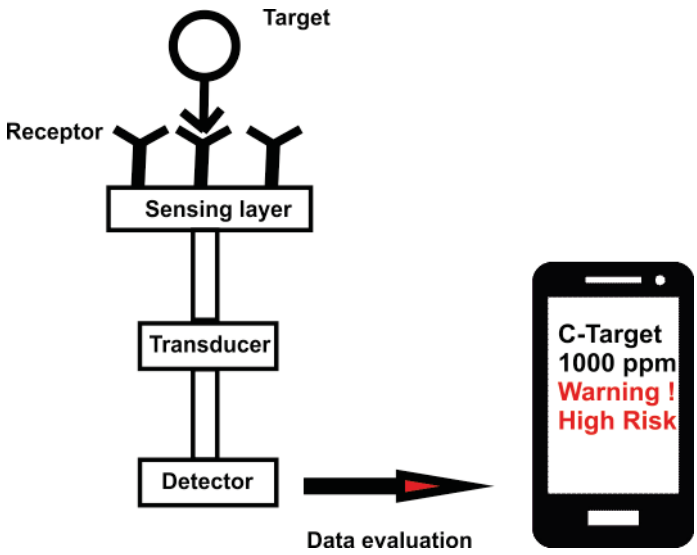

Scheme 8.1 Principle of chemical sensor

8.1 Receptor

The chemically most important component of a sensor as well as a probe is the recognition element, at the molecular scale, the receptor. Receptor units can be small molecules as crown ethers, cyclodextrins or calixarenes. They can also be larger biological components as antibodies, enzymes, nucleotide oligomers, which are termed aptamers, or synthetic peptides (**Fig. 8.1**). MIPs are a considerably novel recognition element, often referred to as plastic antibodies as mentioned above. Compared to the other natural or artificial receptors, MIPs are relatively simple to prepare and production can be up-scaled for industrial purposes. As a polymer, they are also more robust and stable than their natural competitors. Thus they are in

principle a very promising recognition element for chemical sensors. The adjustment of their properties is also straightforward due to the availability of many commercial as well as custom-designed monomers. However, because the underlying binding mechanisms are often still unclear and it is difficult to study them systematically at present due to the amorphous structure of the MIP, rational development of MIP recognition elements for chemical sensors is still rather tedious and it is still a long way before MIPs will equal natural receptors in the majority of sensor applications.

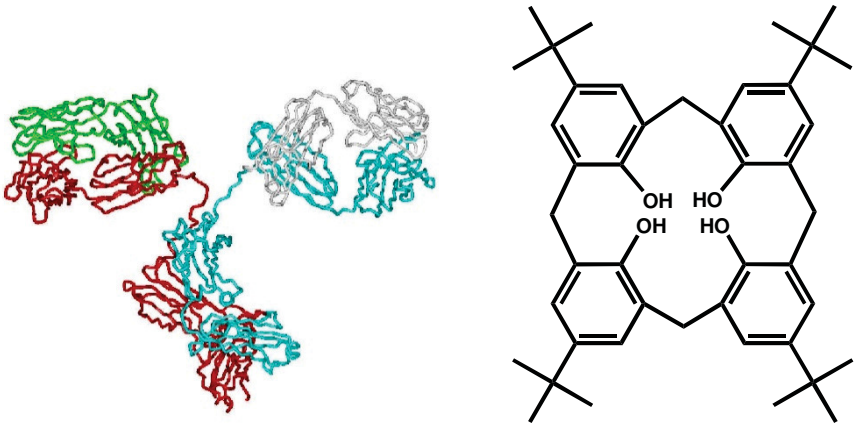

Fig. 8.1 Structures of a natural receptor (antibody, left) and an artificial receptor (calixarene, right)

Recognition is commonly achieved through selective binding of a target component from the bulk medium, in either kinetically and/or thermodynamically controlled fashion. It is a distribution-equilibrium of the target between the sample medium and the receptor surface. Such a binding profile can be usually described through a binding curve as shown in **Fig. 8.2**, where a certain physical parameter is plotted against the target concentration. Two parameters are used for describing the recognition ability of a receptor, the strength of the binding (affinity) and the specificity (selectivity).

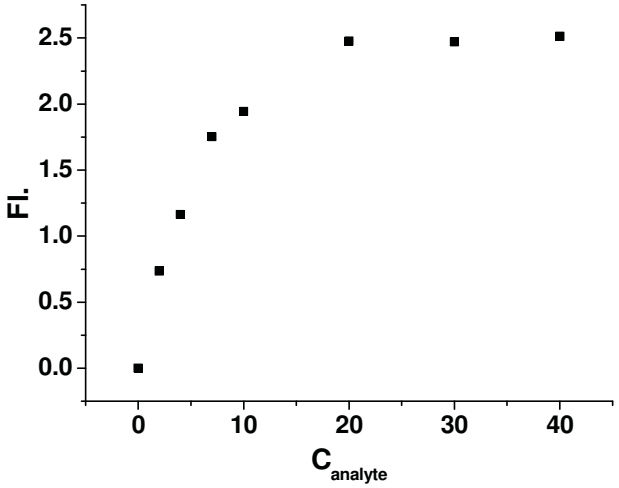

Fig. 8.2 Example of binding curve

A high affinity means strong binding which is reflected in the binding curve through a steep rise at low concentrations. It can be quantitatively described by the binding constant. This parameter relates to the sensitivity of a probe or sensor. A receptor with higher affinity shifts the distribution equilibrium of the target from the sample medium to the sensor surface and hence can provide a higher sensitivity (ability to detect the analyte at low concentration).

The selectivity arises from different binding preferences of the receptor towards various species. The larger the difference is the better is the selectivity of a sensor or probe. The discrimination can be reached through various mechanisms. The matching of the shape of binding site and target, for example, is often the most obvious approach and typically used for, for instance, alkaline-earth metal ion sensing with crown ether receptors. Selectivity can also arise from the interaction between the target and the receptor through non-covalent forces including ion pairing (electrostatic forces), H-bonding and solvatophobic interactions. It is especially interesting to assemble a multifunctional receptor with several hot recognition points toward a desired target. In any case, multipoint recognition can greatly increase the selectivity of a receptor since these non-covalent forces are accumulative.

8.2 Transducer

Whether in a chemical sensor or probe, the function of a transducer or transduction unit is to transfer the binding event into a measurable signal. This can be achieved through different mechanisms, including the change of mass, electric conductivity or optical properties.

In fluorescence sensors or fluorescent probes, this transduction mechanism arises from different fluorescence properties of the probe containing the receptor unit or from the responsive matrix in the bound and unbound state. These differences include the fluorescence intensity, the emission band's position and shape, the lifetime and the anisotropy and will be discussed in detail in Section 8.4.3. For a chemical fluorescence sensor, signal transduction is performed by probe molecules embedded in the recognition matrix, except for example when fluorescent analytes are targeted. For a molecular probe itself, the fluorophore unit usually accomplishes this task, as will be discussed in the later Sections.

8.3 Detector

A detector registers the change of the signal revealed by the transducer for further data processing and evaluation. In some sense, it is also a transducer, converting the change of a physical parameter into an electrical signal. Together with the affinity of the receptor, the detector often determines the sensor's sensitivity. Moreover, the detector is a true element of a sensor only since there is no equivalent at the molecular scale.

In optical fluorescence sensors, the detector collects the emitted photons of different energy (which means at different wavelength) from the fluorescent entities in the sensor matrix either globally, spectrally selected through a filter or spectrally resolved by a spectrograph or monochromator. The physical format of a detector is commonly a conventional photodiode (PD), an avalanche photodiode (APD) or, less frequently in miniaturized sensors, a photomultiplier tube (PMT).

8.4 Fluorescent probes

Since this thesis deals with the development of optical sensing matrices and not with the development of entire sensor devices, the focus will be laid on the former in the subsequent part of the thesis. An optical probe couples the receptor unit with an optically transducing unit,

the chromophore.[122] The latter transfers the target binding event into an optical signal change. These changes can happen for instance with regard to light absorption or fluorescence. A well-known example of a colorimetric probe based on changes in light absorption is the acid/base induced colour change of phenolphthalein. Fluorescence changes are however more attractive for the assembly of an optical sensor, because it is a potentially ultra-sensitive and fast technique which is also non-destructive and non-invasive.

8.4.1 Choice of chromophore and wavelength range

The spectroscopically active moiety to be incorporated into a sensor matrix is the chromophore. For developing a relevant sensor matrix, especially for developing miniaturized hand held sensor devices, the excitation wavelength is preferred to lie in the long wavelength region of the visible spectrum due to the availability of economical light sources. Furthermore, it can greatly reduce the background fluorescence which is mostly excited below 350 nm. This is especially the case in biological matrices where amino acids as phenyalanine, tryptophane and tyrosine are excited with UV light and introduce fluorescence interferences (auto fluorescence). Besides, some monomer building blocks, such as aromatic styrene, 4-vinypyridine and 1-vinylimidazole can absorb light in the UV range and interfere with the optical performance of the sensor matrix. Another reason is the often non-negligible scattering in a sensor matrix, which decreases according to a λ^{-4} law. Scattering can be non-elastic Rayleigh scattering and more critical, the elastic Raman scattering which is often difficult to be filtered out of the fluorescence signal through a simple filter.

A typical chromophore absorbing in the visible range always has an extended conjugated π electron system, as shown in **Fig. 8.3**, which can be either linear such as in a cyanine or stilbene dye or cyclic as in a boron–dipyrromethene (BODIPY) dye.[123] In principle and if we leave aside the intrinsic differences between aromatic, polyenic and polymethinic dyes,[124] the larger the conjugation is the smaller is the energy gap between ground and excited state of a dye, which means the longer is the wavelength of light absorption. In case of cyanine dyes, expansion of the conjugation system with a single vinyl group shifts the absorption (and emission) band about 100 nm to the red.

The cross-conjugated cyanine such as BODIPYs, [125] the merocyanine such as phenoxazinones[126] and the intramolecular charge transfer (ICT) dyes such as benzoxadiazoles or naphthalimides always provide a promising excitation and emission window, thus are

optimal chromophore candidates to be integrated into sensor matrices. Especially phenoxazinones, naphthalimides and benzoxadiazoles, they can, despite their small size, still be excited above 400 nm and emit with a large Stokes shift. Furthermore, these dyes can often yield strong analyte-induced spectral modulation.

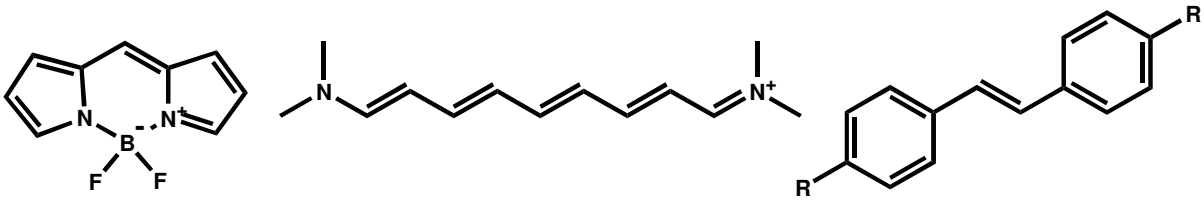

Fig. 8.3 Examples of chromophores, BODIPY (left), cyanine (middle) and stilbene (right)

8.4.2 Requirements on the fluorophore

For an optical sensor matrix to be interrogated by fluorescence, it is not only important that the chromophore unit of the probe molecule to be integrated into the matrix absorbs in the visible spectral range, but that at least one state of the probe, free or bound, shows a strong fluorescence output (ON mode) (regarding the possible modes of analyte signalling, see Section 9) and the other has low fluorescence (OFF mode) or also a high fluorescence yet in a different spectral range.

The brightness of a fluorophore is a combined result of the molar absorption coefficient and fluorescence quantum yield. The absorption coefficient reflects the light absorption ability of a dye, the higher the absorption coefficient is the higher is the probability that a photon is absorbed and the dye is excited. These excited molecules can relax by giving off the energy thermally, through energy transfer to nearby molecules and light emission (fluorescence). The quantum yield of fluorescence defines the efficiency of relaxing the excited molecule through fluorescence. An important criterion is the structural rigidity of the dye molecule. Intramolecular rotation and vibration can relax the excited molecule by thermal dissipation of energy. A rigid structure however can block these non-radiative processes and thus increase the fluorescence quantum yield. Representative examples are malachite green and rhodamine (**Fig. 8.4**). Malachite green is a non-fluorescent dye. After rigidifying the free rotating structure with an oxygen bridge, the fluorescence is greatly enhanced. From this point of view, the linear cyanines or stilbene are not promising, since their OFF mode mostly involves free rotation which is intrinsically hampered in the rigid polymer matrix. Besides the

above listed criteria, small dyes are preferred in building MIP sensor cavities. A small dye yields smaller binding cavities which can enhance the selectivity of the sensor matrix. It commonly provides also simple interaction with target molecules and increases cavity homogeneity during the polymerization process. ICT dyes as benzoxadiazoles and naphthalimides are good examples. They can be excited in the visible range despite their small size. Due to the ICT properties, these dyes show always large Stokes shifts. Besides, the switch between ON/OFF mode is direct related to the formation of the probe-template complex.

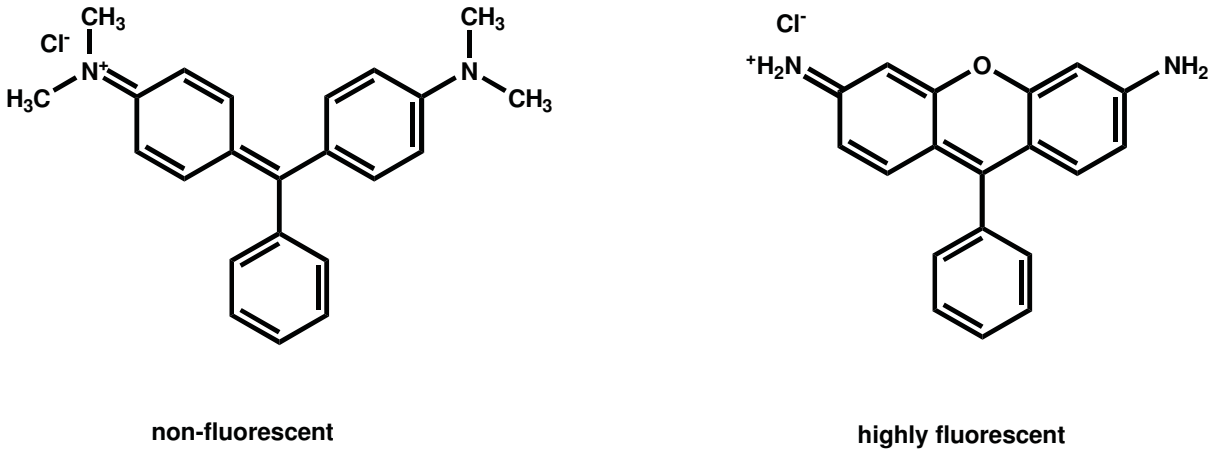

Fig. 8.4 Structure of malachite green (left) and rhodamine (right)

8.4.3 Fluorescence techniques for analysing binding interactions

Fluorescence spectroscopy has become an attractive technique in analytical chemistry. It is not only due to its high sensitivity but also due to the abundant methods and many parameters including the wavelength, intensity, lifetime and anisotropy of fluorescence which can be used for probing an analyte.

Tracking the change of fluorescence intensity is by far the most straightforward technique to estimate intermolecular binding strengths. Here the analyte bound state can be either the ON (high fluorescence) or OFF (low fluorescence) mode; the non-bound state should then be the contrary. It can be quickly measured with miniaturized instrumentation. However, only simple fluorescence intensity changes are less quantitative since they can be

influenced by many instrumental and matrix factors. Thus a reference dye is often needed for a reliable measurement. More promising mode in this regard is the spectral shift, where the fluorophore in the bound state has a shifted spectrum compared to the free fluorescence probe. Thus potential ratiometric assessment can be applied and the probe itself can act as an internal reference to simplify the instrumentation. These two techniques are based on the quantum yield change of the fluorescence probe at free and bound state measured at one or more wavelengths. Lifetime measurements are another important technique for estimating the molecular interaction. It corresponds to the time that the fluorophore resides on average in the excited state. In absence of an excited state reaction, the lifetime is independent to the emission wavelength and can be measured from the whole spectrum. The lifetime depends on its binding state, free and bound state have different lifetimes. The presence of a quencher molecule near the fluorophore can also change its lifetime. At relevant dilutions, the lifetime is independent of the fluorophore concentration but in a complicated medium where the fluorophore can be present in several different states, the liftetime is described as the sum of individual lifetimes normalized by their amplitudes according to **equation 8.1**, the amplitude relating to the relative concentration of the fluorophore in the mixture. Lifetime and intensity are not independent parameters. For example, a good shielding of the fluorophore from a quencher can greatly increase the fluorescence lifetime. Thus the increase of lifetime often accompanies an increase of fluorescence quantum yield. Due to the concentration independent property, lifetime is a more reliable technique. However, the measurement of lifetimes is relatively difficult and often needs expensive instrumentation compared to steady state measurement. The deconvolution of the decay curve also needs mathematic support, and it becomes more complicated when more components are present. Anisotropy is related to the free rotation speed of the fluorophore and is thus only suitable for large molecules and non-confined fluorophores and was not further investigated in this thesis.

$$I(t) = I(0) \sum_i \alpha_i e^{-t/\tau_i}$$ **equation 8.1**

8.4.4 Fluorescence quenching vs. enhancement

Fluorescence quenching is a universal phenomenon that decreases the fluorescence quantum yield of a fluorophore.[127] It includes dynamic quenching through molecular collisions in the excited state and static quenching, for example, when a fluorophore forms a weakly or non-fluorescent complex with another species in the ground state. O_2 is the most common dynamic fluorescence quencher via energy transfer from the excited molecule to O_2, to excite the electron from the $^1\Sigma$ to the $^1\Delta$ molecular orbital during collision.[128] Besides non-emissive complex formation, static quenching can also occur by formation of an effective quenching sphere around the fluorophore.[129] However, unspecific quenching can always interfere with the sensing performance, and to amend the interference of non-specific quenching, a reference fluorophore should be integrated into the sensing system. Fluorescence enhancement thus is more attractive. This enhancement can be due to the change of the electronic state after forming the complex such as a charge transfer state. It can be determined through the change in absorption spectra. It can also block a non-radiative process, such as photoinduced electron transfer (PET). In the latter case, the absorption spectrum does not change.

8.5 Analyte-dependent requirements

Before we begin to design a fluorescence sensor, besides chemical host-guest interactions, it is important to consider the electronic and spectroscopic properties of the target species, that is, whether these species themselves are fluorophores, quenchers or do not possess any specific optical properties.

8.5.1 Targeting fluorescent analytes

In case of fluorescent analytes, such as dyes, fluorescent aromatic amino acids or fluorescent compounds of anthropogenic or natural origin, the main task of the sensor remains the specific binding through the recognition elements.[130, 131, 132] The concentration can then be directly quantified through measuring the fluorescence intensity of the bound analytes after completion of the analytical reaction.

8.5.2 Targeting quenchers

Some important species such as O_2, SO_2, Cl^- and NO,[133, 134, 135] but also heavy and transition metal ions as well as small molecules like nitroaromatics,[136, 137] are themselves non-fluorescent yet can act as effective quenchers. In this case, either a fluorescent dye, for species which do not require dedicated chemical receptors such as O_2 or NO, or a fluorescent probe, for metal ions and small molecules, is commonly introduced into the sensing element. Few analytes such as Cl^- can act at the same time as collisional and static quenchers, depending on the choice of the fluorophore incorporated into the sensor,[138] leave the freedom to choose a desired format. In the quenching analytical reaction, the emission intensity is decreased in the presence of the target species and can be quantified through comparing the intensity of the two states in the absence and presence of the analyte. For example, in case of the dynamic quenching, the Stern-Volmer plot is usually used for the determination of the quencher concentration.

8.5.3 Targeting non-fluorescent and non-quenching analytes

Most challenging is the targeting of non-fluorescent and non-quenching analytes. However, it is also the most important task, since the majority of the analytes belong to this class. In this case, a specifically designed fluorescent probe is commonly required. The binding of these analytes must then trigger some change of the fluorescence properties of the probe. These changes can include intensity, both enhancement or quenching, spectral shifts or more advanced features such as two-band systems coupled by an energy transfer like Förster resonance energy transfer (FRET) probes.[139]

8.6 Fluorescence signalling modes

The fluorescence signal can be either directly (on site) or indirectly (off site) registered. The on-site mode, where a fluorescent indicator is embedded in the separation matrix, combines the analyte separation and detection process into a single step. In the off-site mode such as tandem or displacement approach, these two processes are separated.

8.6.1 Indirect detection (tandem approach, displacement approach, analyte labeling)

As shown in **Scheme 8.1**, a tandem approach separates the separation step from the indication step. The target is firstly enriched by the receptors in the enrichment phase. After extensive extraction, the bound target is washed out and transferred to the detection part such as a mass spectrometer or fluorescent detection matrix for quantification.[140] For sensing however, this approach has several drawbacks. First, the target, in the ideal case, should be strongly bound by the receptor to survive the washing step which serves to remove all the non-specifically bound species. Second, these bound targets should then be easily and quantitatively liberated from the matrix to give the correct concentration information. When using MIPs as separation phases especially the latter, the complete extraction of the target is sometimes difficult and can induce signal falsifications.[140] Third, after remobilization of the target it has to be quantitatively transferred to the detection unit, which is for instance difficult to realize for less volatile compounds in gas sensing applications or hydrophobic compounds in certain environments. Moreover, due to the two-step nature, this process cannot be used in continuous monitoring. Due to these factors, the tandem approach is not the ideal strategy for building a MIP sensor.

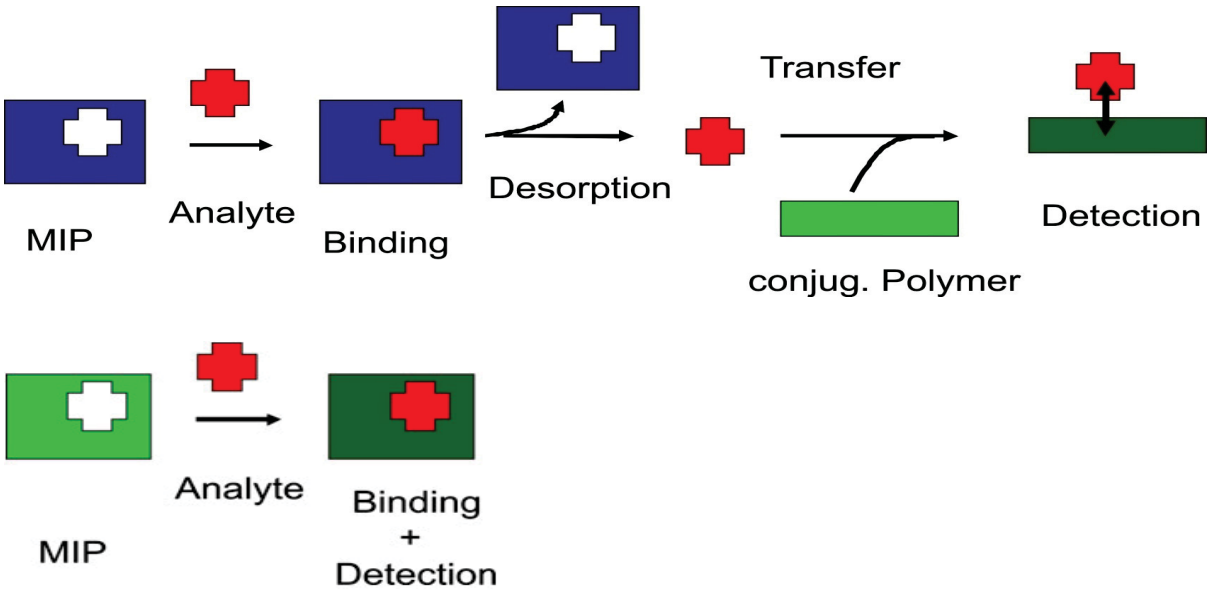

Scheme 8.1 Fluorescence signalling through tandem (top) and direct approach (bottom)

The second indirect approach is the displacement approach shown in **Scheme 8.2**, where the receptor is first saturated with fluorophore labelled analytes. The non-labelled analyte as real target can then compete with these labelled analytes, displacing them from the matrix and thus changing the optical properties of the matrix.[141, 142] However, the labelling of the analyte requires the often cumbersome synthesis of a conjugatable analyte derivative, the saturation of the receptor sites with these fluorescent analytes and the separation of the removed tracers from the recognition matrix after displacement.[143] If MIPs are used as recognition matrices another problem becomes important: space. For the tracer to be efficiently loaded into the cavities, the conjugate of analyte and label has to be rather small, which is especially problematic for many small-molecule analytes which are smaller in size than for instance a fluorescent label.

The third indirect approach is very similar to pre-column derivatization in chromatography, i. e., the analyte is labelled prior to detection. This requires that the labelled analyte is imprinted.[59]

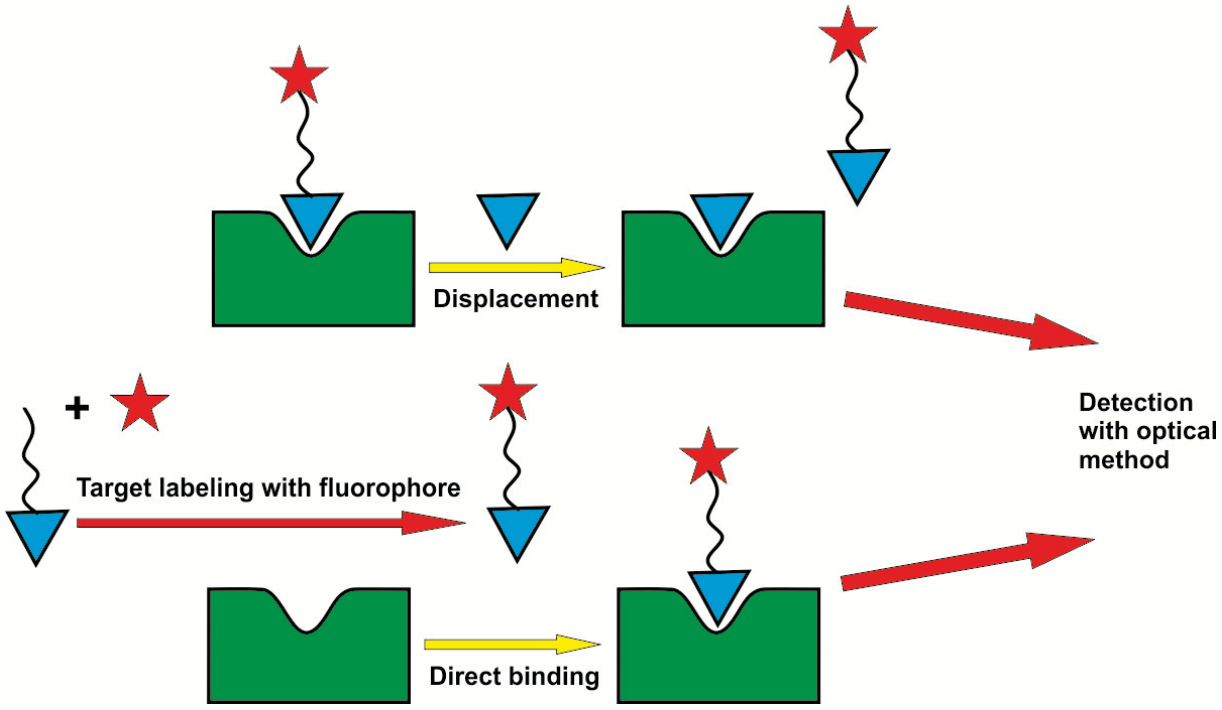

Scheme 8.2 Displacement assay (top) and a direct assay (bottom) with analyte pre-labelled with fluorescent probe

8.6.2 Direct detection (fluorescent analytes, embedding of indicators)

The analytes can also be directly measured without tedious washing or derivatization steps. In this case, the receptor is coupled with the fluorescent transducer so that the presence of analyte can be directly measured. While for fluorescent analytes, the strategy is rather simple – the recognition matrix has to be transparent in the wavelength range in which the fluorescent analyte absorbs and emits (**Scheme 8.2** bottom),[132] – for non-fluorescent analytes a suitable fluorescent probe has to be embedded into the matrix.[61] Binding of the analyte to the embedded probe than has to induce optical changes. The probe can be a solvatochromic fluorophore that simply probes the microenviromental polarity inside the MIP cavity and its change upon analyte binding.[144] Quantum dots (QDs) can also be used as fluorescence probe in MIPs. More attractive is using a dye linked receptor as monomer, so that the signal change is directly related to the binding event.[145]

9 Functional fluorescent monomers

Fluorescence probes can be looked on as an optical transducer, it fuses the recognition part with a fluorophore with or without a conjugation linker.[146] To achieve a better selectivity, the probe needs to be carefully designed according to the target molecule. This needs skilful synthesis technique and is time consuming. After modification of the fluorescence probe with a polymerizable group, it can be integrated into MIP matrix. The selectivity is then determined by the formed MIP cavity, the covalently integrated probe acts more as a reporter. Following this principle, one fluorescent probe can be used for targeting more species in a same group, carboxylate e.g., without much modification. The selectivity relies on the specificity of the formed cavities; with correctly selected crosslinker, comonomer and porogen, even promising enantiomeric discrimination can be reached.

9.1 Signalling mechanisms

Many fluorescence parameters including the lifetime, anisotropy, intensity and spectral properties can be used for signal generation. In this Section, we will only concentrate on changes of intensity and spectral properties. A spectral shift can be treated as the change of the energy gap between ground and excited state, for the most common probes involving the highest occupied and lowest unoccupied molecular orbitals HOMO and LUMO, and an intensity change is often connected with accelerated or decelerated depopulation of the excited fluorophores, whether because of the formation of a non-, weakly or more strongly fluorescent complex between probe and analyte in the ground state.

In terms of the photophysical properties of a fluorophore, the major difference between the free probe and a non-, weakly or strongly fluorescent, complexed probe usually is a change in the non-radiative rate constant k_{nr}, which is generally expressed as $k_{nr} = (1-\Phi_f)\,\tau_f^{-1}$, since the analytical reaction either opens up or suppresses a non-radiative (quenching) deactivation channel.[147] Only in the case of indicators that actually react with the analyte and form an entirely new chromophore, changes in fluorescence can also be due to changes in the radiative rate or $k_r = \Phi_f\,\tau_f^{-1}$ (if phosphorescence can be neglected, $k_r = k_f$, the rate constant for fluorescence deactivation).

9.1.1 Photoinduced electron transfer

The first class of signal transduction mechanism is photoinduced electron transfer (PET). A classic PET probe is formed by a chromophore and an oxidative/reductive group (**Fig. 9.1** top), linked through a short alkyl linkage so that both active subunits are not π-conjugated.[148] After localized excitation of the fluorophore unit, the analyte responsive group can be oxidized or reduced through the transfer of an electron to the chromophore's HOMO or the receipt of an electron from the chromophore's LUMO (**Fig. 9.2**). Thus the fluorescence is quenched. The spectroscopic properties of a PET probe are intensity changes of the fluorescence band without pronounced changes in the absorption spectra (**Fig. 9.1** bottom).[149]

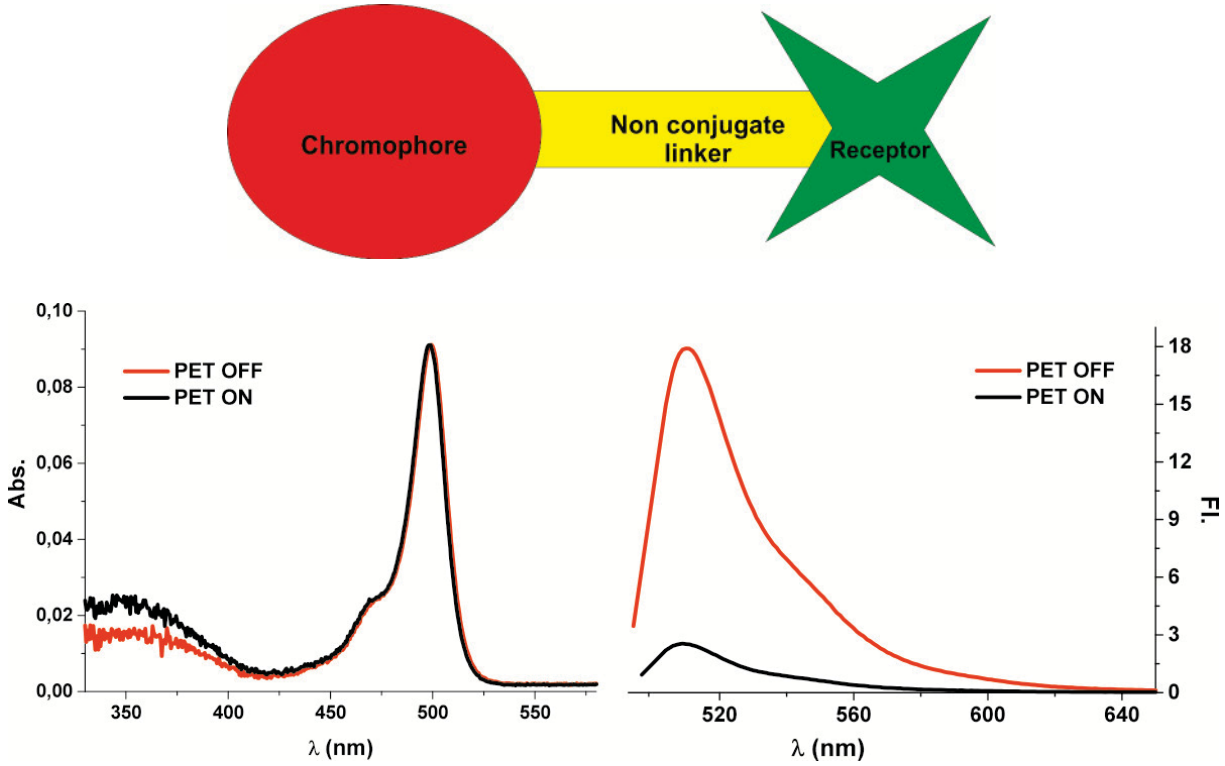

Fig. 9.1 Design principle of PET probe (top) and spectroscopic manifestation (bottom)

If the redox active group is used as binding site, the target molecule can for example either activate or block the electron transfer route and induce changes of fluorescence intensity which can be used to evaluate the target binding and hence the target concentration.[150]

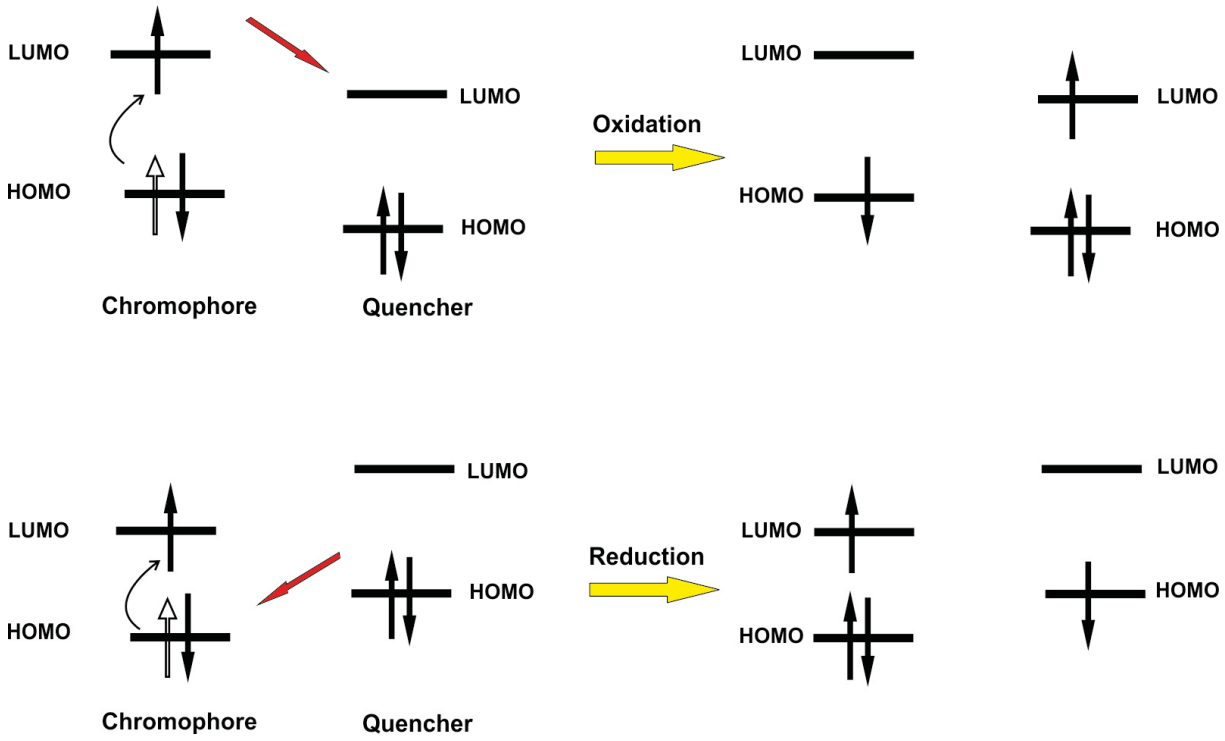

Fig. 9.2 Electron transfer in an oxidative PET (top) and reductive PET (bottom) sensor

9.1.2 Charge transfer

The second signalling mechanism is through charge transfer (CT). Different to the PET probe, in a CT probe, fluorophore and binding unit are not separated by a non-conjugating linker (**Fig. 9.3** top). Instead, electron pulling and electron pushing groups are placed on the opposite ends of a chromophore's delocalized π system.[151] This push-pull pair or donor-acceptor architecture increases the polarizability and is usually characterized by broad and non-structured absorption and emission bands with large Stokes shifts in polar media generally found in sensing applications (**Fig. 9.3** bottom).[152] A change of the push-pull ability can then influence the energy levels involved in absorption and emission. In a CT probe, the receptor is directly integrated in either the push or the pull group. If the receptor is coupled to the push or electron rich donor side, binding with an electron rich analyte such as an anion can strengthen the charge transfer and induce bathochromic shifts.[153] On the other hand, if the receptor is coupled to the pull side, the binding with an electron rich group of an analyte species will alleviate the charge transfer and induce hypsochromic shifts.[154] Since for CT fluorophores the CT process in the excited state entails often more pronounced dipole moment changes than the CT-type (Franck-Condon) absorption process, the shifts in emission are generally much

more pronounced than the shifts in absorption.[155] Thus different from a PET probe, the binding of the target will induce changes in both absorption and emission spectra.[146]

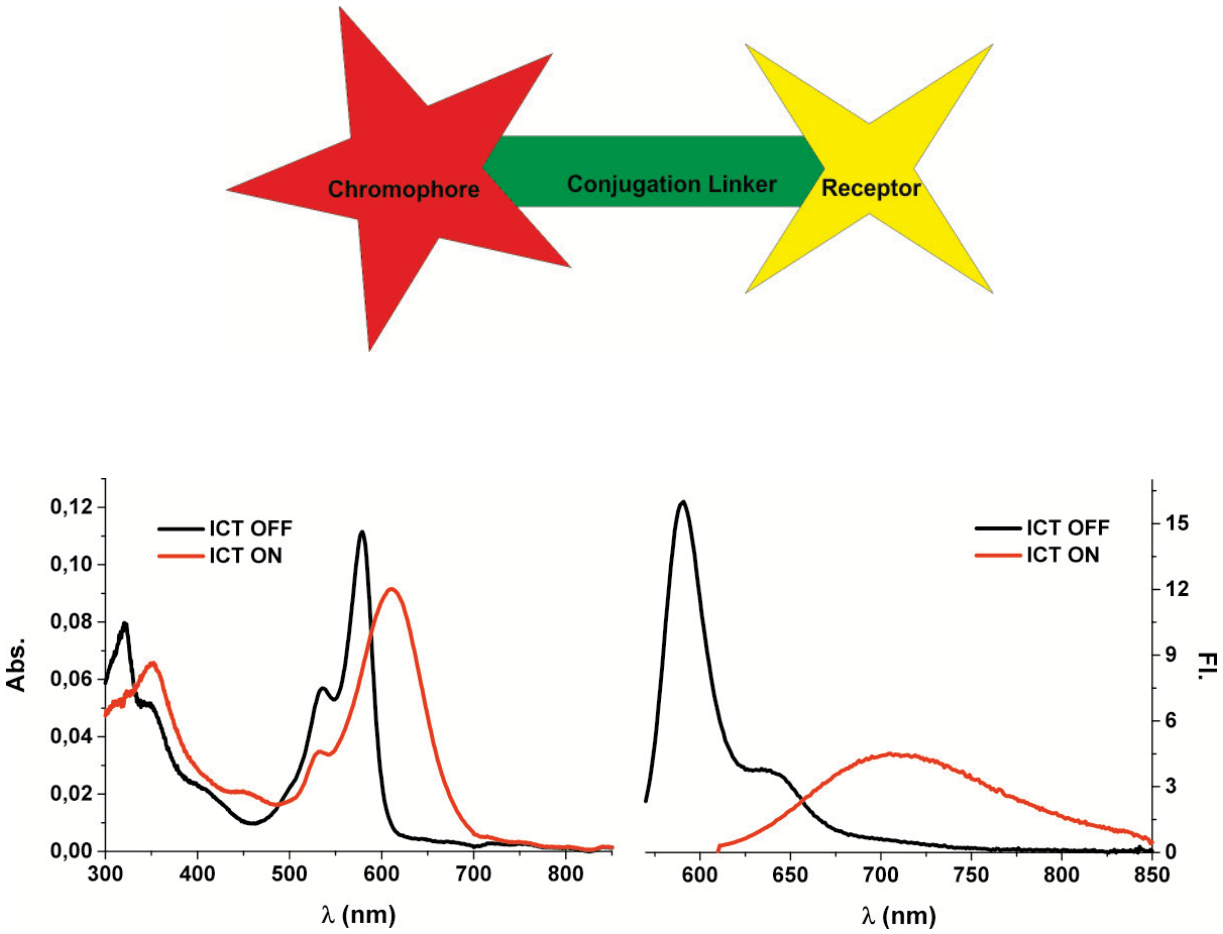

Fig. 9.3 Design principle of a CT probe (top) and spectroscopic manifestation

9.1.3 Energy transfer

Förster (or frequently also called fluorescence) resonance energy transfer (FRET) is a through-space energy transfer process.[156] In this case, the energy of the excited molecule is dissipated rapidly through an energy transfer to its nearby neighbour. To enable this energy transfer, several criteria must be fulfilled. Two fluorophores or a fluorophore and a quencher are involved in this process and have to show matching spectral properties. The energy donor has to absorb at shorter wavelengths than the acceptor. The emission band of the donor then has to overlap sufficiently with the absorption band of the acceptor, to ensure resonance energy transfer. Moreover, the distance between the donor and acceptor pair has to be short

enough, commonly between 1-10 nm.[139] The energy transfer efficiency is sensitive to the distance and can for example be used as a molecular ruler in biological studies.[157] Since this energy transfer is supposed to involve dipole-dipole interactions, the spatial orientation of the donor and acceptor pair is also important; in the random orientation case, an orientation factor of 2/3 is effective.

Probe design using FRET can involve the coupling of the donor and acceptor through a flexible chain that incorporates the binding sites.[158] At the free state when donor and acceptor are far apart, the excitation of the donor only results in emission of the donor. Upon target binding, folding of the flexible chain occurs and brings this pair into closer contact and hence the emission of the donor is decreased with a concomitant intensity increase of the acceptor's emission band.[159]

FRET is a very sensitive signalling method. It provides a much larger (pseudo) Stokes shift (donor absorption and acceptor emission are often separated by > 100 nm) so that the interference of scattering is strongly suppressed.[139] Moreover, the change in two spectral channels (donor and acceptor emission) also provides the possibility to use ratiometric measurements which is an internally referenced methods and avoids the introduction of a second dye as an internal reference. Although in this thesis we did not include this signalling strategy, it is still an attracting strategy and is worth of further studying.

9.2 Suitable classes of dyes

To assemble an optical MIP based sensor using the direct strategy, one possibility is to embed an optical probe into the MIP cavity, see above. This can be done through incorporation of a solvatochromic dye into the matrix that measures the microenvironmental polarity changes in the MIP cavity. Another possibility is to embed a target responsive dye into the cavity. The binding event then directly influences the electronic state of the dye according to one of the mechanisms outlined in Section 9.1 and hence the fluorescence response.

In our studies, a chromogenic monomer is firstly prepared by fusing the polymerizable group, the binding site and the fluorophore in a single molecule as shown in **Fig. 9.4**. We selected the urea group as the binding motif towards our model templates, oxoanions. Urea has two NH groups to form two stable H-bonds with oxoanions in an arrangement of two facing "Ys". The additional electrostatistic force of the charged species involved also

enhances the complex stability. Thus very high affinities can be reached. Additionally, the urea group is small and the two NH arms enable the fusing of a polymerizable group and a chromophore unit into a single molecule. In addition to the considerations mentioned in Section 8.4.1, the choice of the functional fluorescent monomers employed in this work will be detailed in the following.

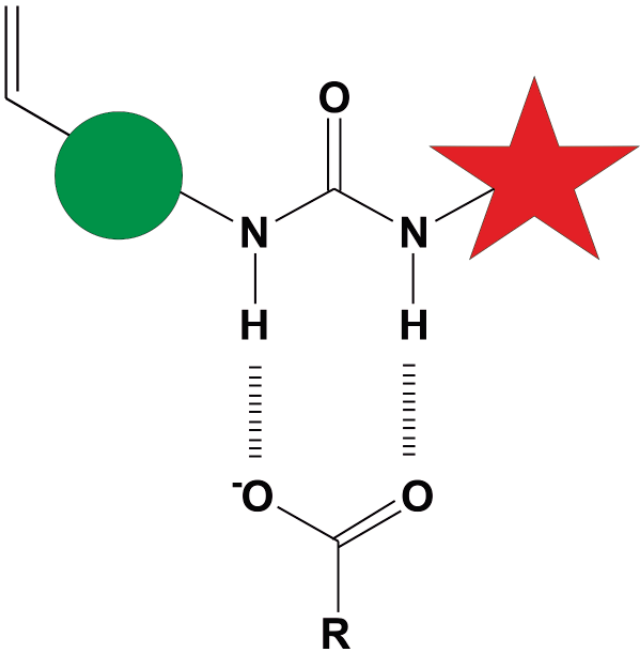

Fig. 9.4 Architecture of a fluorogenic monomer, circle = spacer, star = fluorophore

9.2.1 Rigid CT chromophores

Benzoxadiazoles and naphthalimides are small and rigid charge transfer chromophores which have an electron push and pull pair sitting at opposite positions of the π system and which absorb and emit at considerably long wavelengths. The intensity and position of the absorption and especially the emission bands is thus sensitive to the electron donating and accepting ability. Since we are targeting electron rich anions, we fused the urea binding motif to the electron donating side. After binding with an oxoanion, the charge transfer is therefore enhanced and a red shift of the emission band should be observed. In case of the benzoxadiazole based monomer, enhancement of the CT process is expected to lead to fluorescence enhancement.[160] In contrast, the fluorescence is expected to be quenched in case of the naphthalimide based monomer.[161]

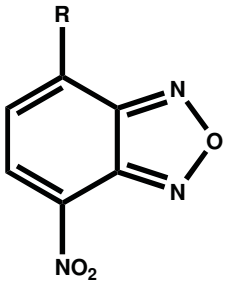

Benzoxadiazole

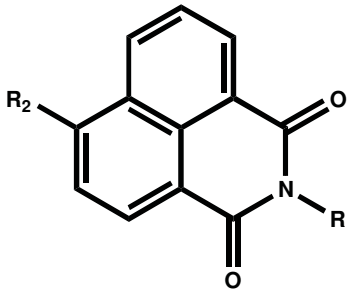

Naphthalimide

9.2.2 Rigid polymethines

BODIPYs (boron-dipyrromethenes) are structural analogues of cyanine dyes. BODIPYs have a structure related to porphyrines. They are usually nonpolar and net uncharged (formally zwitterionic).[162] Due to the rigid structure BODIPYs have commonly an intrinsically high QY and stability and usually possess high molar absorption coefficients.[163] The spectral properties can also be adjusted through extending the conjugation system for example at the 3- and 5-position. The meso position has relatively weak influence on the spectral features. Thus, bio-conjugation groups as well as PET active residues can be introduced at this position.

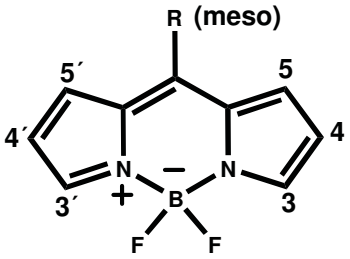

BODIPY

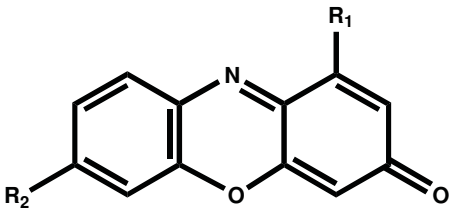

Phenoxazinone

Phenoxazinones are a long known class of dyes that are characterized by a heteroaromatic triple ring structure.[164] Since they are not charged, they are no classic cyanine dyes but belong to the class of merocyanine dyes. For instance, the famous pH indicator litmus includes orcein which also belongs to this group. The carbonyl group is an electron acceptor and an electron donor is fused at the opposite position. The latter can for instance be equipped with a receptor unit. The result is a fluorescent probe that shows features of a CT probe as well as of a polymethine probe.[165]

9.2.3 Other chromophores

The palette of other chromophores suitable for fluorescent MIP design is not very large when it comes to criteria such as small size and rigidity. Indole is perhaps a suitable candidate because it has a hetero-bicyclic ring structure, able to assist a receptor in directly forming hydrogen bonds through its NH group.[166] Indole is famous for its natural derivative, tryptophan, which is a fluorogenic amino acid. When adequately substituted, indole behaves as a solvatochromic dye; tryptophan for example was used for assessing the local polarity of proteins.[167] In our studies, we thus tested a fluorogenic monomer which was developed based on this dye. Phenazines are also classic chromophores with a triple ring structure. The important dye toluylene red, which is used to dye silk with fine scarlet, is a derivate of phenazine. Chauhan et al. have used phenazine to prepare a chromogenic probe for the detection anions.[168] In this thesis, we also developed one chromogenic monomer based on the phenazine structure for preparation of fluorogenic MIP sensor.

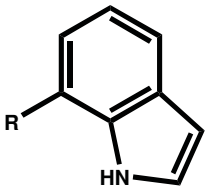

Indole

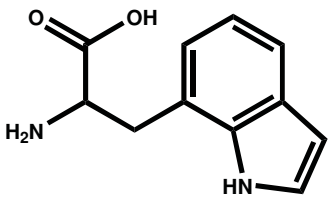

Tryptophan

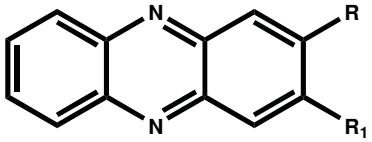

Phenazine

9.2.4 General performance assessment

The designed probe molecules should always have a high affinity to the template molecule to provide us with the possibility for stoichiometric imprinting. This high affinity should also ensure a high sensitivity of the attempted sensor matrix. For the fundamental research studies undertaken in this thesis, two classes of oxoanions were used as templates, carboxylates and phosphates. Urea is thus selected as the binding site in all of the functional monomers. Urea has a high affinity towards both types of oxoanions through the above mentioned, two directional hydrogen bonds and the negative charge of the anion contributes additional electrostatistic interactions to improve the affinity. Regarding the ease of synthesis of the functional probe monomers, the urea binding site can be formed through the condensation of an isocyanate carrying a polymerizable group to a fluorophore with an amino group. This requirement thus also had to be met by the chromophores selected.

Once the chromophores of various dye classes such as indole, BODIPY, phenoxazine, naphthalimide and benzoxodiazole were used to synthesize the functional monomers, the response behaviour of these monomers was studied in neat solvent in the presence of the target analytes. Those monomers which showed a good sensing response were evaluated in specific spectroscopic prepolymerization tests. Finally, in case of positive outcomes in phase two, the probe monomers were used to prepare MIP sensor matrices for actual MIP rebinding studies. The fluorogenic monomers and prepared MIP matrices were examined according to their spectral properties, binding constants in different solvents, and their absorption and fluorescence response towards the target analyte.

10 Indole-based Monomers

Indole is a well-known aromatic heterocyclic fluorophore. It is also the core part of the fluorescent amino acid tryptophan. Although indole dyes absorb and emit in the UV spectral range, the facts that indoles are dimensionally rather small and can undergo hydrogen-bonding through their NH group have led us to test a monomer based on this dye class. A polymerizable indole monomer was developed according to **Scheme 10.1** by Sellergren et al. The synthesis succeeds in 2 steps with a high yield of 94%.

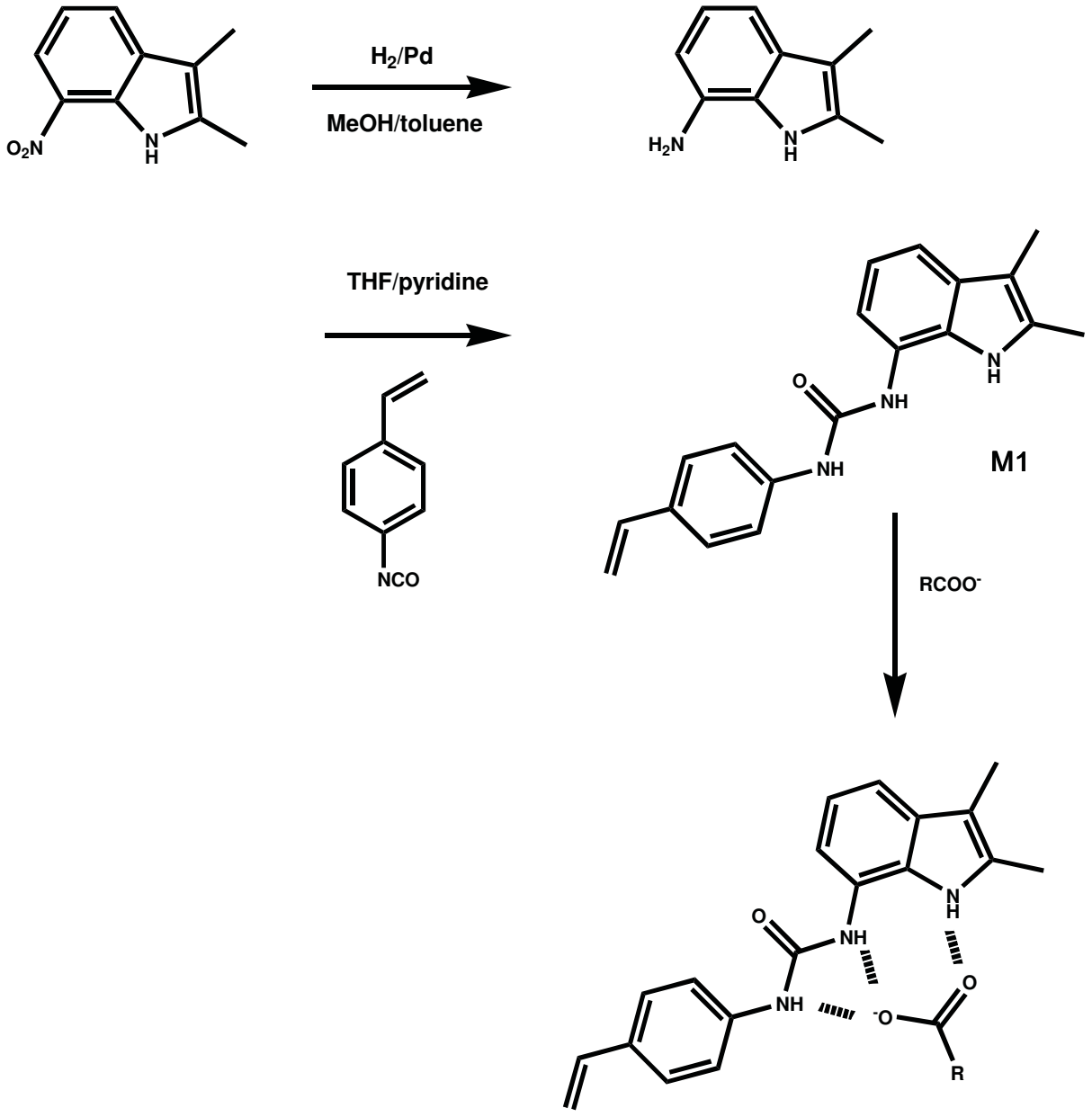

Scheme 10.1 Synthesis route and binding reaction of indole-based chromogenic monomer

10.1 Spectroscopic properties

Indole has a 6+5 heteroaromatic ring structure, it absorbs in the UV range and shows moderate blue fluorescence.[169] The indole-based monomer **M1** has an absorption maximum in the UV range near 310 nm and an emission maximum at around 460 nm. As written above, this is not an ideal excitation window since miniaturized light sources in this range are relatively expensive. Moreover, a lot of fluorescent impurities such as aromatic amino acid will be co-excited and can lead to background noise. Besides, compared to other fluorophores, the fluorescence quantum yield is only moderate. If the sensing response would be transduced by fluorescence quenching upon target recognition, this considerably low quantum yield would also limit its sensing performance. However, as is shown in **Scheme 11.1**, the architecture of the monomer with the possibility of forming three directed H bonds promises to yield high complexation constants which might account for the spectroscopic shortcomings.

10.2 Binding studies

Indole has been used to build anion receptor and most of these receptors can form multiple H-bonding to oxoanion and provide high affinity.[166,170] The binding study was firstly done by NMR titration in Sellergren's group. The affinity was determined to log$K$=4.17 by NMR titration in DMSO-d_6 using tetrabutylammonium benzoate (TBAB) as anion source. We reassessed the data by UV/Vis as well as fluorescence titrations here. The absorption maximum of **M1** lies at 302 nm in DMSO, as a flat maximum of a more shoulder-like band (**Fig. 10.1**). Complexation with TBAB shifted the absorption band to slightly longer wavelengths accompanied with a slight increase of the absorption coefficient.

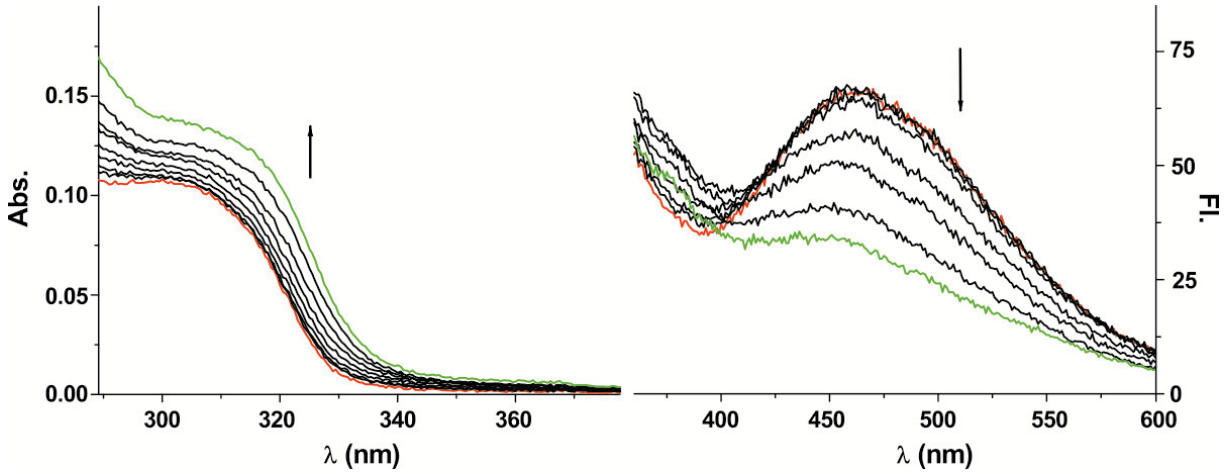

Fig. 10.1 Absorption (left) and fluorescence (right) titration spectra of **M1** (5 µM) with TBAB in DMSO (C_{TBAB}=2-500 µM, starting point spectra in red, end point spectra in green), fluorescence spectra registered by excitation at 310 nm.

The fluorescence of the monomer appears at 450 nm in DMSO with a relatively low quantum yield of fluorescence. The fluorescence is, as expected, further quenched upon addition of the model template TBAB (**Fig. 10.1**). Moreover, at this 100-fold lower concentration compared to the NMR titration, the binding constant calculated from this titration data amounts to only log*K*=3.88±0.08, smaller than that calculated from NMR titration. Because the fluorescence features are not promising and the exceptionally high complexation constant found by NMR could not be reached at the low concentrations which are relevant for an application, no further studies were carried out with this monomer towards the preparation of MIP sensors.

11 BODIPY-based Monomers

Two BODIPY-based fluorogenic monomers **M2** and **M3** have been developed according to **Scheme 11.1** in our group employing a urea binding motif. The BODIPY core is prepared by condensation of an aromatic aldehyde with pyrrole. The two monomers use different linkages to fuse the urea recognition part to the fluorophore's BODIPY core. In **M2**, the analyte binding site is coupled to the BODIPY core with a NH bridge through a S_N2 reaction. In **M3**, the binding site is coupled to the BODIPY core with a vinyl bridge through a Heck reaction with Pd as the catalyst.

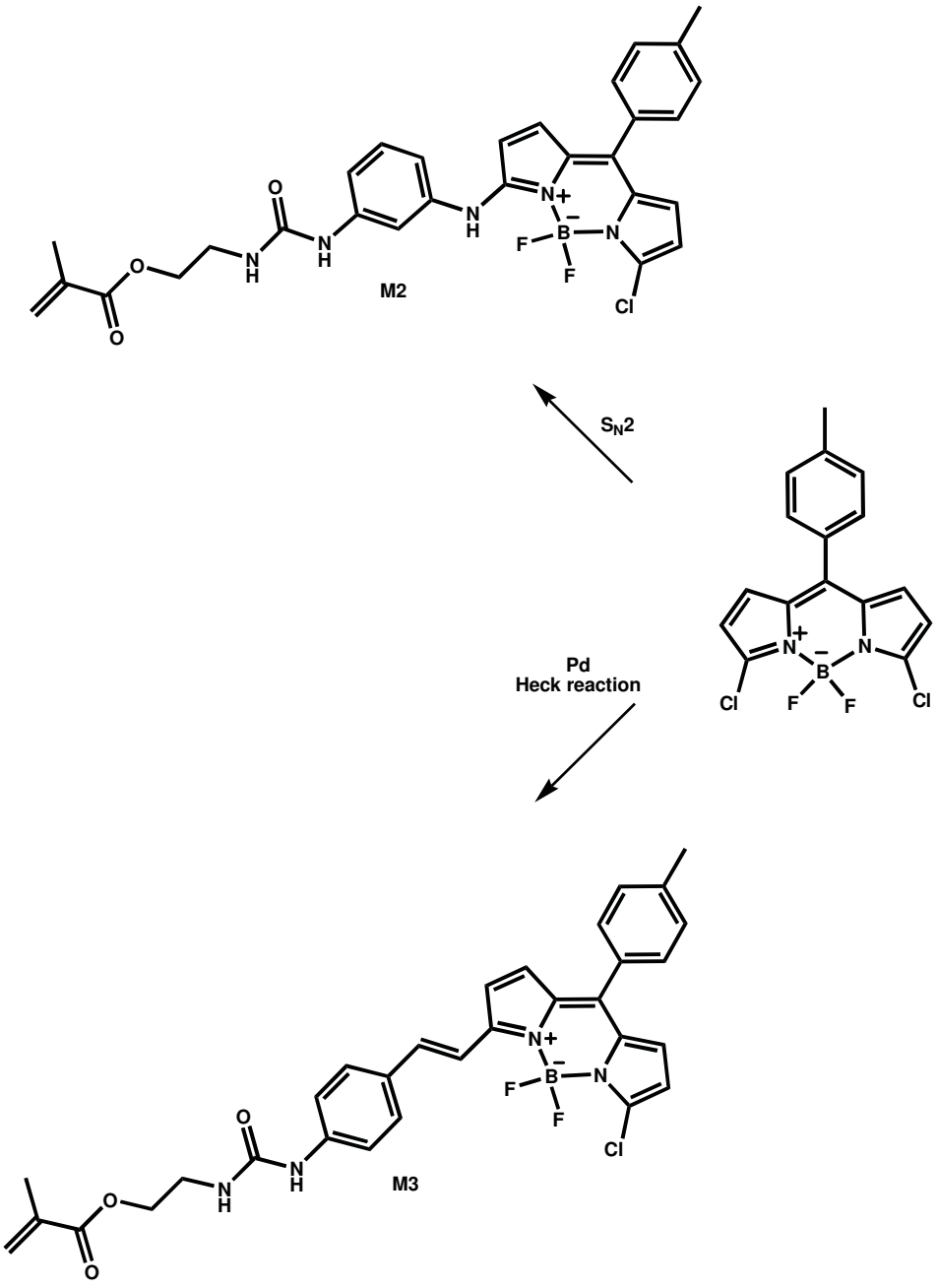

Scheme 11.1 Synthesis route of BODIPY-based fluorogenic monomers **M2** and **M3**

The modification of the affinity is achieved through the change of the substitution on the urea arm. In case of vinyl-bridged group, **M3** has an ethyl-methacrylate group, **C4** has a butyl group and **C3** has a bis-trifluorophenyl group (**Scheme 11.2**). In the group of NH-bridged group, **M2** has an ethyl-methacrylate group, **C1** and **C3** have a bis-trifluorophenyl group and for **C1**, instead of urea, thiourea is used as H-bonding donor in the sensor molecule in order to further improve the affinity.

A further modification lies in tuning the spectral property, the quantum yield. Because it is known that meso-phenyl BODIPYs lacking bulky substituents in the 1- and 7-position show reduced quantum yields compared with for example their 1,7-dimethyl counterparts,[171] a mesityl instead of the phenyl group was introduced to the meso-position in another series of model probes in case of **C5**, **C6** and **C7** (**Scheme. 11.2**). The urea moiety is linked through the ortho, meta and para position to the BODIPY core for spectral as well affinity tuning, respectively.

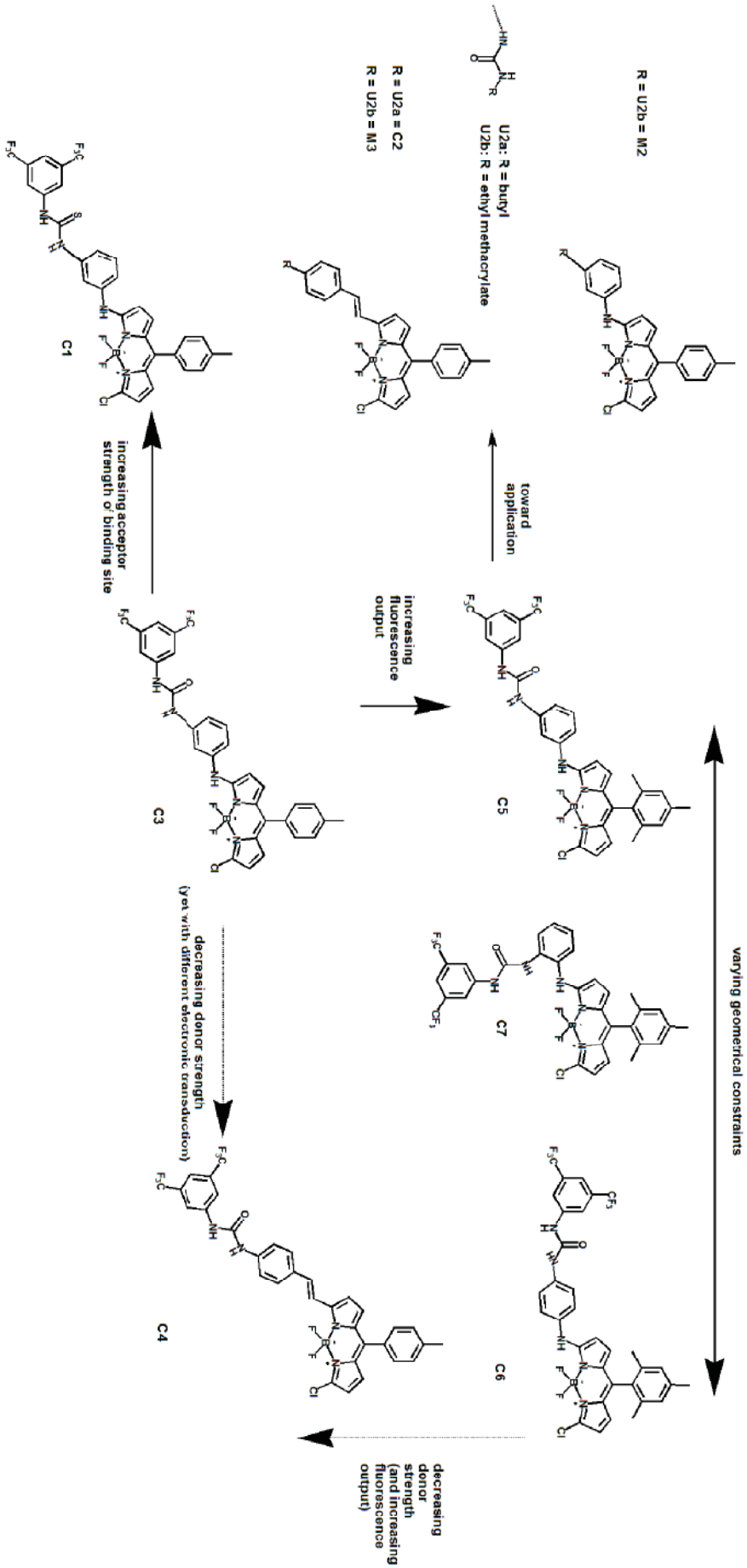

Scheme 11.2 Structure of BODIPY derivatives

11.1 Spectroscopic properties

M2 has broader absorption and emission bands than typical BODIPY dyes,[162] lying at around 504 nm and 578 nm respectively in $CHCl_3$. The absorption spectrum of **M2** is influenced by the solvent; with increased solvent polarity as well as HBD/HBA ability the absorption maximum shows a hypsochromic shift. The emission is less influenced. **C1**, **C3**, **C5**, **C6**, **C7** which have a similar structure show similar spectral features as shown for **M2** in **Fig. 11.1**. The quantum yield of the dyes in this class is low, especially in polar solvents. The data are listed in **Table 11.1**.

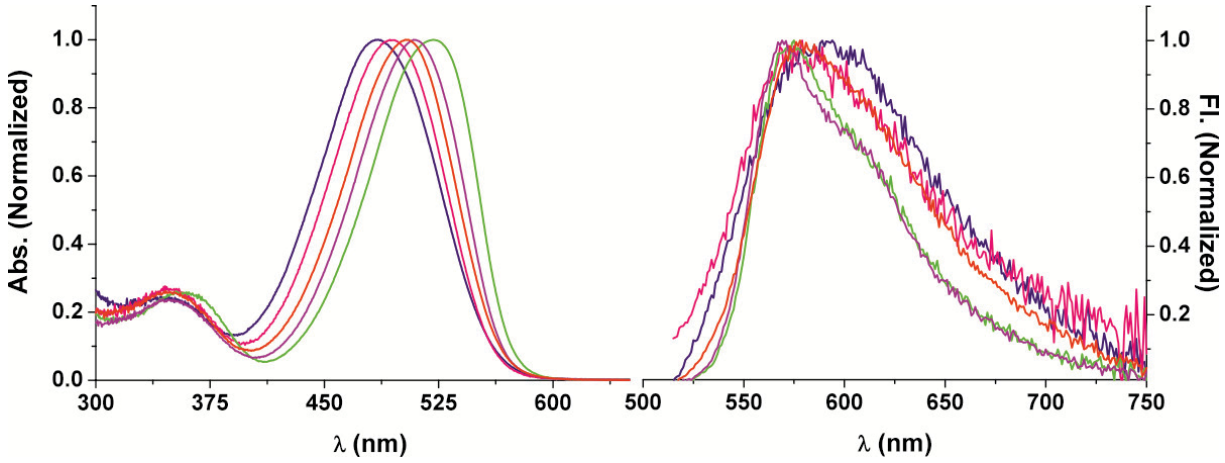

Fig. 11.1 Normalized absorption (left) and fluorescence (right) spectra of **M2** in selected solvents, DMSO (blue), MeCN (pink), Hexane (magenta), $CHCl_3$ (green) and THF (red)

The absorption band of **M3** is narrower than that of **M2** and lies at 584 nm with a shoulder at 550 nm in $CHCl_3$. It is thus red-shifted compared to **M2** which indicates that the conjugated system is extended. **M3** emits at 605 nm with a shoulder at 647 nm in $CHCl_3$. **M3** exhibits slightly bathochromic shifts when the solvent polarity is increased and also when the H-bonding ability is enhanced and the emission band is also red-shifted and broadened as shown in **Fig. 11.2**. **C4** and **C2** have a similar structure and show a similar spectroscopic profile.

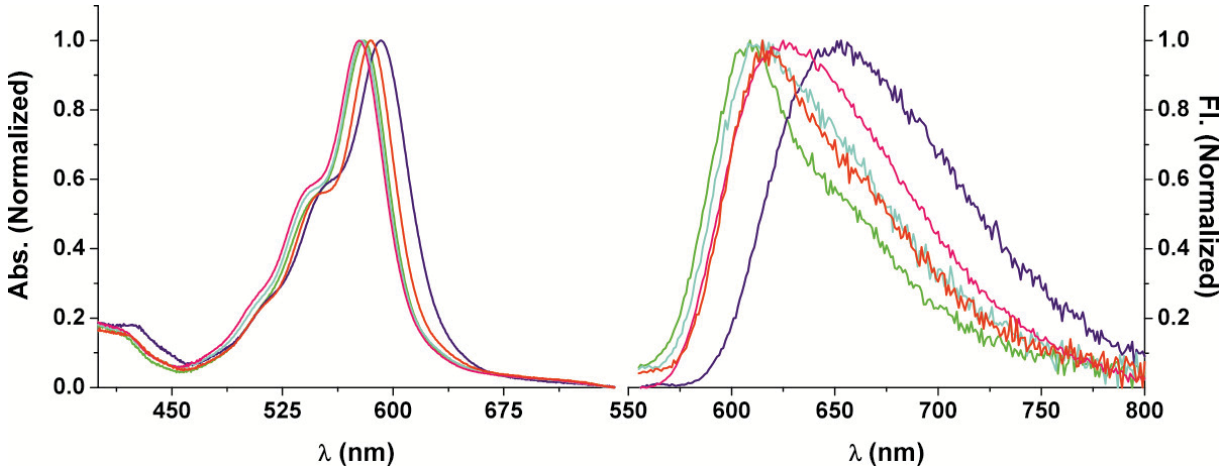

Fig. 11.2 Normalized absorption (left) and emission (right) spectra of **M3** in selected solvents, DMSO (blue), MeCN (pink), Ethanol (cyan), $CHCl_3$ (green) and THF (red)

The fluorescence quantum yields of **M3** and its derivatives are higher than those of **M2** and its derivatives. This can be due to both, the more pronounced distortion of the symmetric cyanine-like π system when the strongly electron donating nitrogen atom is attached to the 3-position and the intramolecular H-bonding between the NH proton and the fluoride atoms of the BF_2 group which might be enhanced by the quasi 6-membered ring structure that can form in **M2** and derivatives. The intramolecular H-bonding can also be the reason of the spectral broadening. We also found that the restricting mesityl group on the meso-position in **C5, C6** and **C7** has an enhancing effect on the quantum yield.

C4 has a higher QY as **C2** and **M3** (**Table 11.1**), this indicates the ethyl-methacrylate group is flexible where the fluorescence is quenched through vibration and rotation.

Table 11.1 Fluorescence quantum yield data of BODIPY dyes in selected solvent,

* The measured QY is smaller than 0.01

Φ_f	$CHCl_3$	Dioxane	DMSO	Ether	MeCN	MeOH	THF	Toluene	Hex
C2	**0.64**	**0.59**	**0.23**	**0.67**	**0.55**	**0.50**	**0.59**	**0.82**	**0.22**
C1	**0.22**	**0.02**	*	**0.02**	*	*	**0.01**	**0.21**	**0.24**
C4	**1.00**	**1.00**	**0.99**	**1.00**	**1.00**	**1.00**	**1.00**	**1.00**	**0.53**
M2	**0.19**	**0.01**	*	**0.02**	*	*	*	**0.20**	**0.24**
M3	**0.49**	**0.53**	**0.31**	**0.44**	**0.45**	**0.38**	**0.47**	**0.57**	**0.39**
C5	**0.56**	**0.07**	**0.01**	**0.08**	*	*	**0.01**	**0.54**	**0.65**
C6	**0.02**	*	*	*	*	*	*	**0.01**	**0.09**
C3	**0.07**	**0.03**	*	**0.03**	*	*	**0.01**	**0.03**	**0.33**
C7	**0.07**	**0.03**	*	**0.03**	**0.01**	**0.02**	**0.01**	**0.03**	**0.08**

The absorption coefficient ε_λ is also an important parameter to evaluate the chromophore performance. It reflects the ability of photon absorption by a chromophore and is a measure for the degree of π conjugation in it. Together with the QY, it determines the brightness of a fluorophore, which is an important application-oriented parameter when working with thin optical sensor layers. For two exemplary BODIPY dyes of the **M2** and **M3** series investigated here, the absorption coefficient was registered in $CHCl_3$. All dyes with NH bridge show prominent absorption coefficients of over $3*10^4$.

Table 11.2 Absorption coefficient of selected BODIPY monomers in $CHCl_3$

	$\varepsilon_{\lambda,max}$ in $CHCl_3$ (L $mol^{-1}cm^{-1}$)
M2	**41590±820**
C2	**34550±310**
C3	**43650±780**
C5	**46260±570**

11.2 Binding studies

The binding constants were evaluated by UV/Vis absorption as well as fluorescence titration of the monomers with tetrabutylammonium acetate (TBAA) in $CHCl_3$ and MeCN.

When the TBAA is added into a solution of **M3**, a red-shift was observed in the absorption spectra. A clear isosbestic point was observed at 590 nm. The spectrum became also broader after addition of TBAA. The binding constant for a 1:1 complex calculated with non-linear fitting (1:1 stöchiometry) is log*K*=4.25±0.02 (**Fig. 11.3**).

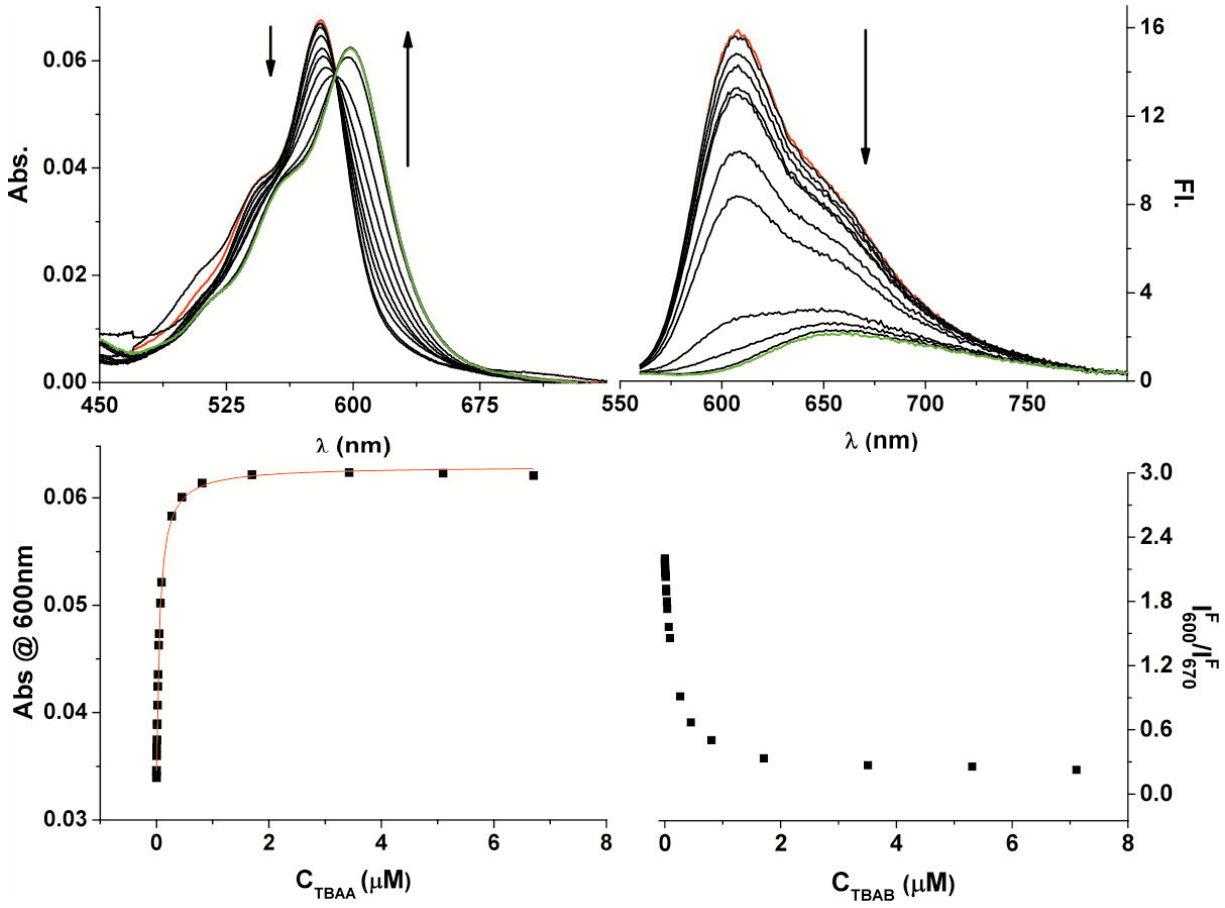

Fig. 11.3 Absorption (top left) and fluorescence (top right) titration spectra of **M3** (5 μM) with TBAA in $CHCl_3$ (C_{TBAA}=2-500 μM, starting point spectra in red, end point spectra in green), the binding curve (bottom left) fitted by absorption at 600 nm and by internal signal rationing at 600 and 670 nm in the fluorescence spectra (bottom right).

The fluorescence of **M3** at 605 nm shows a steady quenching upon addition of TBAA in $CHCl_3$. The binding constant calculated from this titration data is log*K*=4.16±0.02, which is in good agreement with the data obtained in absorption. At saturation concentration, the fluorescence quenching at 605 nm reaches over 95%. In agreement with the red-shifted absorption spectrum, the fluorescence spectrum of the complex shows also a maximum at longer wavelengths than free **M3**, at 660 nm. At the same time, the endpoint spectrum in **Fig. 11.5** suggests that the complex is weaker emissive than the free **M3**. This was verified by analyzing the fluorescence intensity of free **M3** and the complex after correction of the absorption intensity, which yields a 460-fold weaker fluorescence of the complex.

On the other hand, as can be seen directly in **Fig. 11.3**, this system is suitable for internal signal rationing when one registers the fluorescence intensity at 600 and 670 nm. Accompanied with the high brightness, **M3** shows its high potential as a promising sensor monomer to design MIP sensors with quenching response.

The structural analogue **C2** shows similar but a little bit bathochromically shifted absorption and emission spectra than **M3**. It also shows a similar binding response towards TBAA. However, the binding constant is even significantly higher with log*K*=5.22±0.05 in $CHCl_3$. An even larger binding constant of log*K*=5.68±0.07 was obtained for **C4** which carries a 3,5-bis-trifluorophenyl moiety as electron withdrawing group (EWG) on the other side of the urea. This confirms the observations made for other dialkyl, alkyl-aryl and diaryl ureas that the affinity is dependent on both substituents of the urea arm.[32] An enhanced affinity is achieved by better EWGs because the H-acidity of the NH groups is increased.

In contrast to the styryl-type BODIPYs such as **M3**, the binding of TBAA with **M2** shows a slight hypsochromic shift in the absorption spectrum (**Fig. 11.4**). The binding constant was calculated as log*K*=4.81±0.02 in $CHCl_3$ using non-linear fitting, which is significantly larger compared with **M3**. In the fluorescence channel, again fluorescence quenching is observed by addition of the anion. The quenching efficiency also reaches over 90% at saturation. In addition, the complex **M2**:AcO^- does not seem to emit sizeable fluorescence. **M2** can thus also be seen as a potent sensor monomer for fluorescence turn-off sensing.

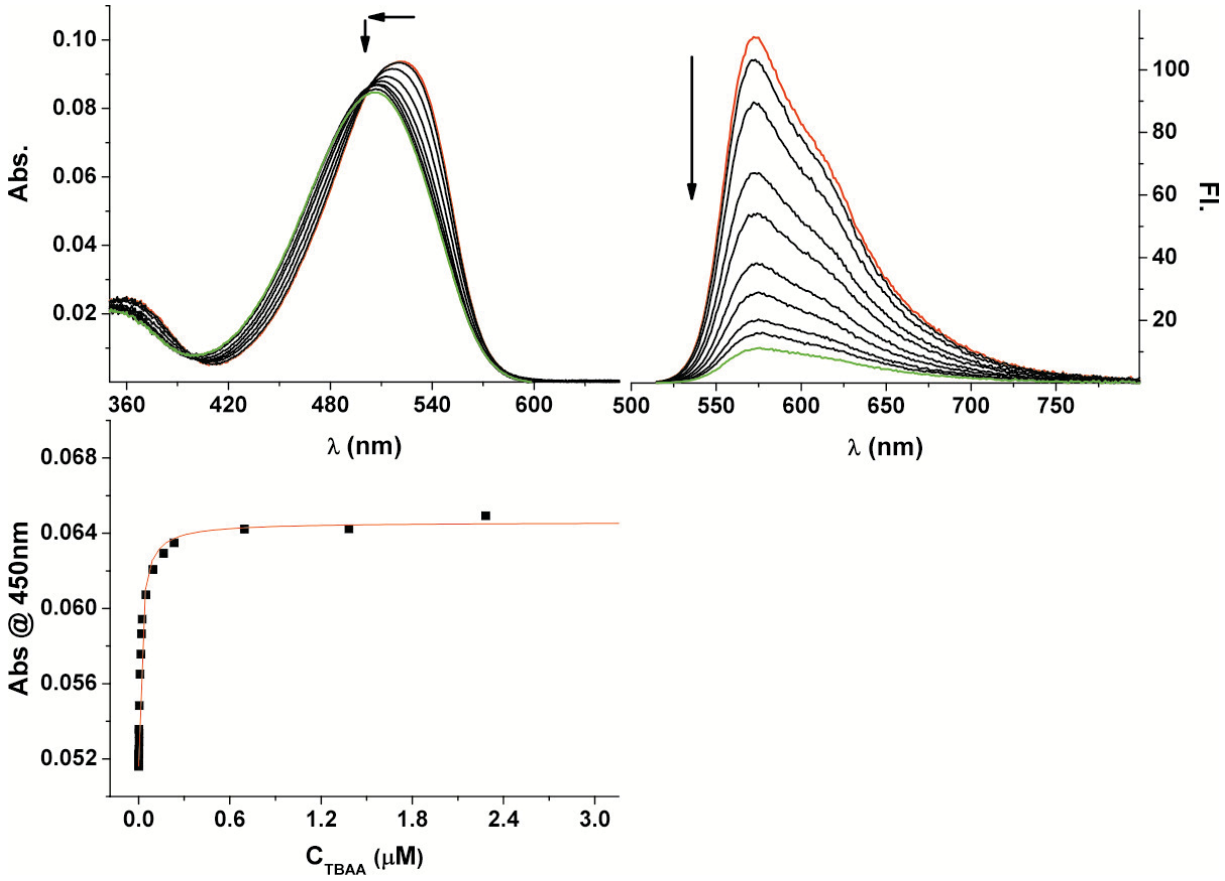

Fig. 11.4 Absorption (top left) and fluorescence (top right) titration spectra of 5 μM **M2** with TBAA in $CHCl_3$ (C_{TBAA}=2.5-600 μM, starting point spectra in red, end point spectra in green) and the binding curve (bottom) fitted by absorption at 450 nm

The structural analogue **C5** shows similar spectral responses but also larger binding constant of log*K*=6.08±0.05 in $CHCl_3$. This result further supports the fact that the affinity is a contribution of the EWG character of both substituents on the urea NH.

The comparison of urea at different substitution positions, (**C7** for ortho, **C5** for meta and **C6** for para) shows that the meta position has the highest binding constant. This is due to the fact that phenylene-diamine nitrogen in ortho- and para-position can donate electrons better across the phenyl ring into the urea, which greatly reduces the acidity of the urea proton and hence reduces the affinity towards oxoanions.

Being aware of the influence of the solvent on H bond complexation, the binding studies were carried out in different solvents (**Table 11.3**). Two trends are observed. For **M2**, **M3**, **C2** and **C6** the affinity is enhanced in less polar $CHCl_3$, however for **C1**, **C3** and **C4**, the affinity is enhanced in MeCN, for **C5**, it is not influenced. The thiourea derivative **C1**

however did not show stronger affinity than the urea derivative **C3,** which is opposite to Gomez's report.[172] Since this is only the case for the larger acetate but not for the fluoride ion, the reason seems to involve steric factors; a further investigation was not attempted here.

Table 11.3 Binding constants (log*K*) of BODIPY monomers and probes with TBAA in $CHCl_3$ and MeCN

log*K*	TBAA ($CHCl_3$)	TBAA (MeCN)
M3	4.25±0.02	3.96±0.04
C2	5.22±0.05	4.84±0.03
C4	5.68±0.07	5.79±0.06
M2	4.81±0.02	4.23±0.02
C3	5.65±0.04	6.09±0.04
C5	6.08±0.05	6.07±0.06
C6	5.91±0.04	5.24±0.03
C1	4.78±0.02	4.90±0.03

11.3 Polymerization attempts

Both **M2** and **M3** work under a quenching mode after binding the analyte, **M2** shows a lower QY, smaller than 0.01 in most selected solvents, the spectroscopic response towards target binding is fluorescence quenching which is not suitable for sensing applications. **M3** has a higher QY, over 0.4 in most solvents. However, a pilot polymerization study revealed that the vinyl bridge in **M3** is not stable under the radical polymerization conditions employed. The polymer prepared with this monomer shows a strongly blue shifted spectrum compared to the monomer. The absorption and emission resemble very much those of simple dipyrrin BODIPYs[162] which indicates the disruption of the conjugated system from the BODIPY core structure by cleavage of the double bond. To resolve this problem, another dye **M4** was developed.

11.4 Refined monomer M4

The preparation of **M4** succeeded from our newly designed BODIPY parent structure in 2 steps with acceptable yields (**Scheme 11.3**). The dye has very bright green fluorescence with an absorption coefficient ε_λ of 28280 (L $mol^{-1}cm^{-1}$) at 515 nm and QY of 0.86 in $CHCl_3$. As shown in **Picture 11.1**, the complexation with carboxylate anions shows over 90% quenching which is very promising for an application in an optical sensor. The green fluorescence is also suitable for a number of types of commercial instruments developed for use with fluorescein labels or dyes such as readers, scanners or cytometers.

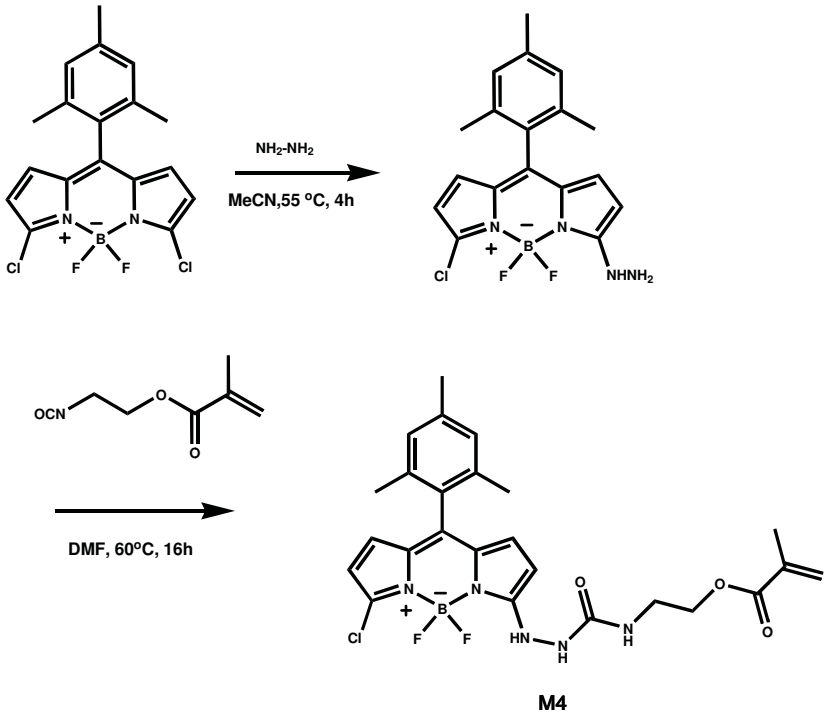

Scheme 11.3 Synthesis route of **M4**

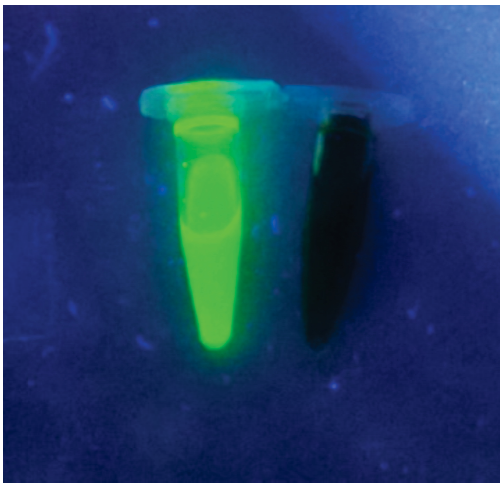

Picture11.1 M4 (left) and 1:1 complex of **M4** and TBA-Z-L-Phe (right)

The chromogenic monomer **M4** has an absorption maximum at 517 nm with a shoulder at 487 nm in $CHCl_3$. After addition of a carboxylate anion (Z-L-phenylalanine in form of the tetrabutylammonium salt), the main absorption band is decreased with an increase of a new band at 451 nm with blue- and red-shifted shoulders at ca. 400, 425, 540 and 570 nm. A clear isosbestic point is observed at 465 nm (**Fig. 11.5**).

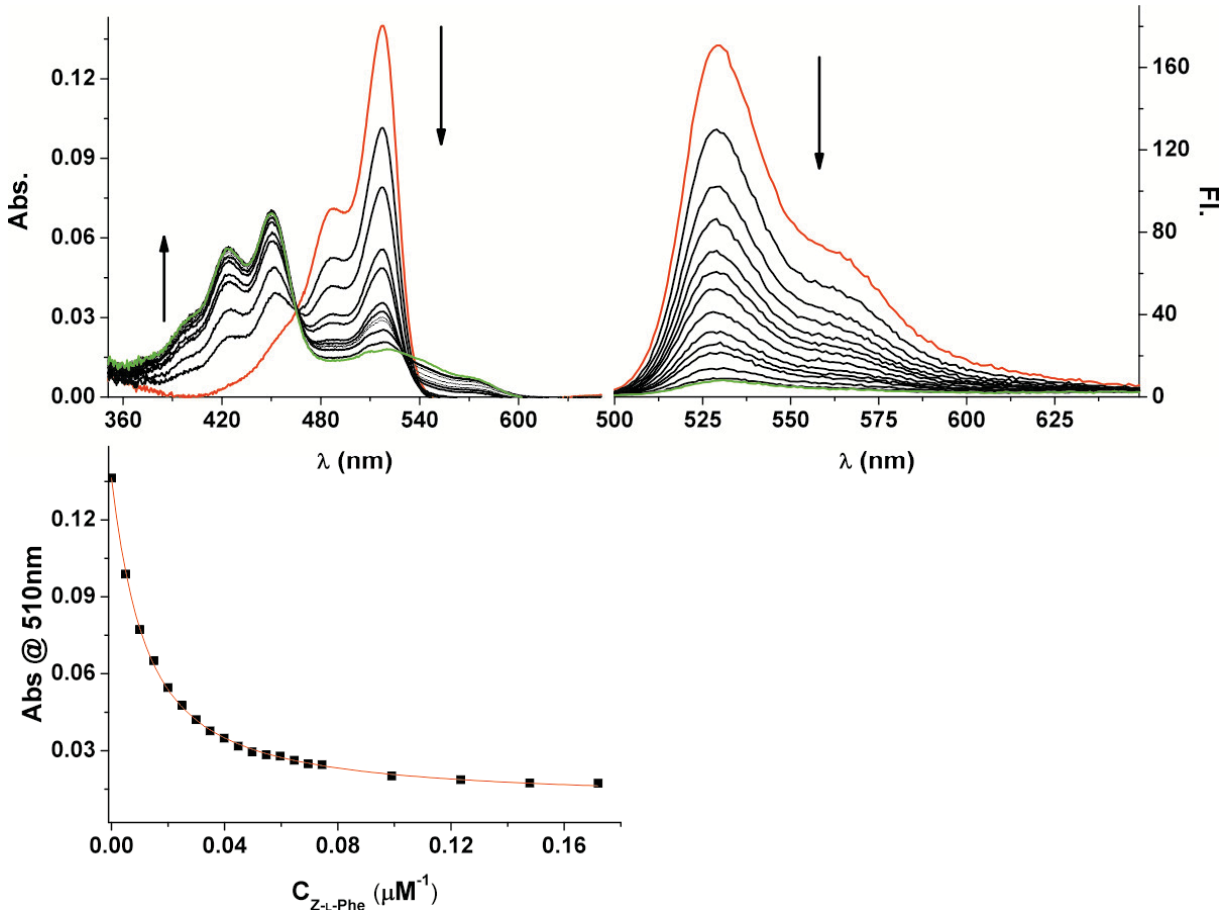

Fig. 11.5 Absorption (top-left) and fluorescence (top-right) titration spectra of **M4** (5μM) with TBA-Z-L-Phe in $CHCl_3$ ($C_{TBA\text{-}Z\text{-}L\text{-}Phe}$=2.5-1400 μM, starting point spectra in red, end point spectra in green) and binding curve (bottom) fitted by absorption at 510 nm

The emission maximum of this chromogenic monomer lies at 530 nm. This is in accordance with the green channel of many commercial fluorescence readers. After addition of the anion, the fluorescence is dramatically quenched (**Fig. 11.5**). The binding constant calculated using the titration spectra amounts to log*K*=5.05±0.17.

In conclusion, **M4** shows very promising sensing response as a chromogenic monomer. It possesses a strong emission and an intense absorption. The excitation as well as emission wavelengths are compatible to commercial fluorescence instruments equipped for fluorescein isothiocyanate (FITC)-based assays. It has also a high affinity to oxo-anions, which ensures stoichiometric noncovalent imprinting. The strong analyte-induced quenching response characterizes it as a sensitive probe. Accordingly, **M4** was further employed for the development of silica core-MIP shell particles, see Section 18.6.

12 Phenoxazinone-based Monomers

Phenoxazinones belong to the oxazine dyes and are another class of fluorophores with advantageous spectroscopic properties and promising sensing response.[126] Such dyes have a planar triple ring structure which is formed by fusing two benzene rings through a nitrogen and an oxygen bridge. As mentioned above, phenoxazinones are merocyanines which possess a certain CT character so that they are suitable for further functionalization close to or at the electron donating amino group and the electron accepting carbonyl group.[164] A representative example of this dye class is Nile Blue. Monomer **M5** was prepared in the group according to **Scheme 12.1** in 3 steps with acceptable yield.

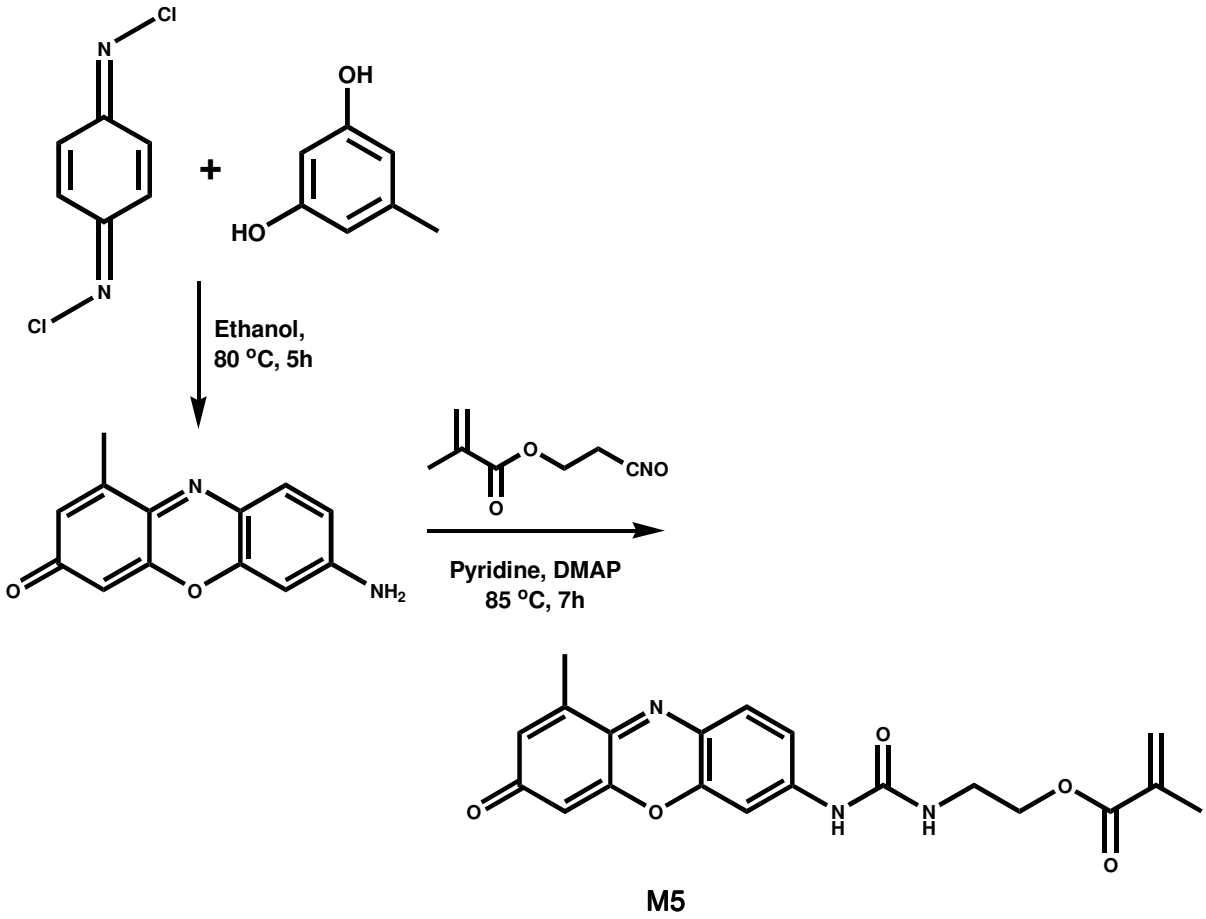

Scheme 12.1 Synthesis route of **M5**

12.1 Spectroscopic properties

Similar to other phenoxazine dyes,[126] **M5** shows a broad absorption band which is centred at 467 nm in MeCN with an absorption coefficient of 21140 (L $mol^{-1}cm^{-1}$). It has a rather low solubility in less polar solvents. In DMSO, the solubility is increased accompanied by a

bathochromic and hyperchromic shift of the absorption band to 483 nm. **M5** emits at 584 nm in MeCN; in DMSO the emission band is shifted to 598 nm (**Fig. 12.1**). The fluorescence is less influenced by the solvent polarity.

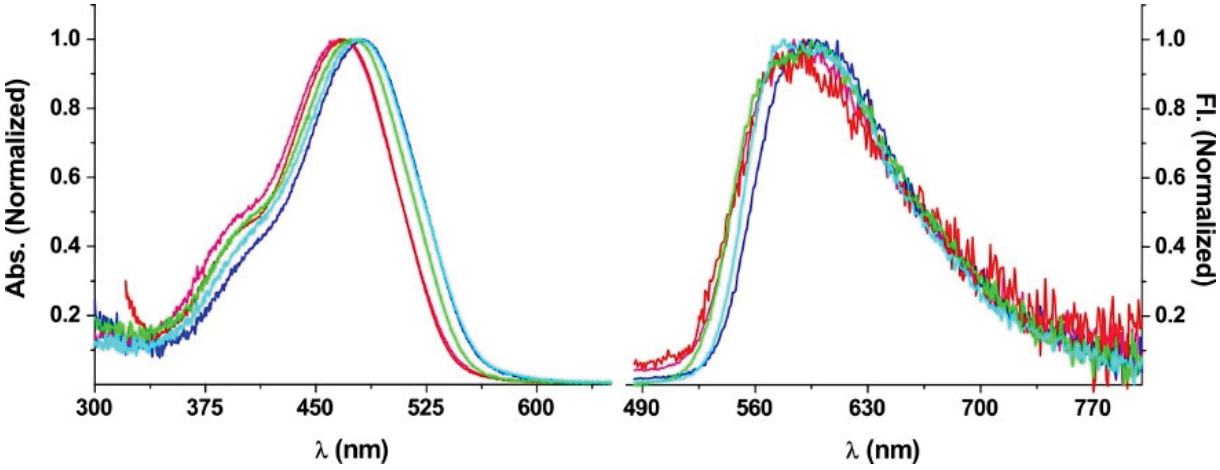

Fig. 12.1 Normalized absorption (left) and fluorescence (right) spectra of **M5** in selected solvents, DMSO (blue), MeCN (pink), Ethanol (cyan), $CHCl_3$ (green) and THF (red)

Additional spectroscopic data are listed in **Table 12.1**. This monomer has a relatively low quantum yield in all the selected solvents. The maximum appears in a moderately hydrogen-bonding solvent of high polarity, ethanol, with QY of 0.054. However, complexation with an anion (e.g., TBA-Z-L-Phe) shifts the absorption spectrum to longer wavelengths, e.g., 505 nm in $CHCl_3$, accompanied by a strong increase in fluorescence QY to 0.481. This fact makes **M5** a prominent sensor monomer.

Table 12.1 Spectroscopic properties of **M5** in different solvents

Compound	Solvent	λ_{abs} /nm	λ_{em} /nm	Φ_f
M5	DMSO	483	598	0.026
M5	MeCN	467	584	0.018
M5	THF	470	590	0.008
M5	$CHCl_3$	478	595	0.031
M5	MeOH	478	586	0.042
M5	Toluene	463	590	0.005
M5	Ethanol	481	578	0.054
M5+Z-L-Phe	$CHCl_3$	505	586	0.481

12.2 Binding studies with TBA-Z-L-Phe

M5 shows a broad and non-structured absorption band at 478 nm in $CHCl_3$. After addition of a carboxylate anion such as Z-L-Phe, the absorption band is shifted by 30 nm to 505 nm and the absorption coefficient is slightly increased (**Fig. 12.2**). This is in accordance with the previous report of our group.[164] A clear isosbestic point is observed at 485 nm. The binding constant is determined to log*K*=4.60±0.05. **M5** emits at 578 nm with a quantum yield of 0.031 in $CHCl_3$. After formation of a complex with the carboxylate anion, the fluorescence is obviously enhanced by a factor of 22, to a QY of 0.481. A slight red shift of 17 nm is also observed for the fluorescence maximum.

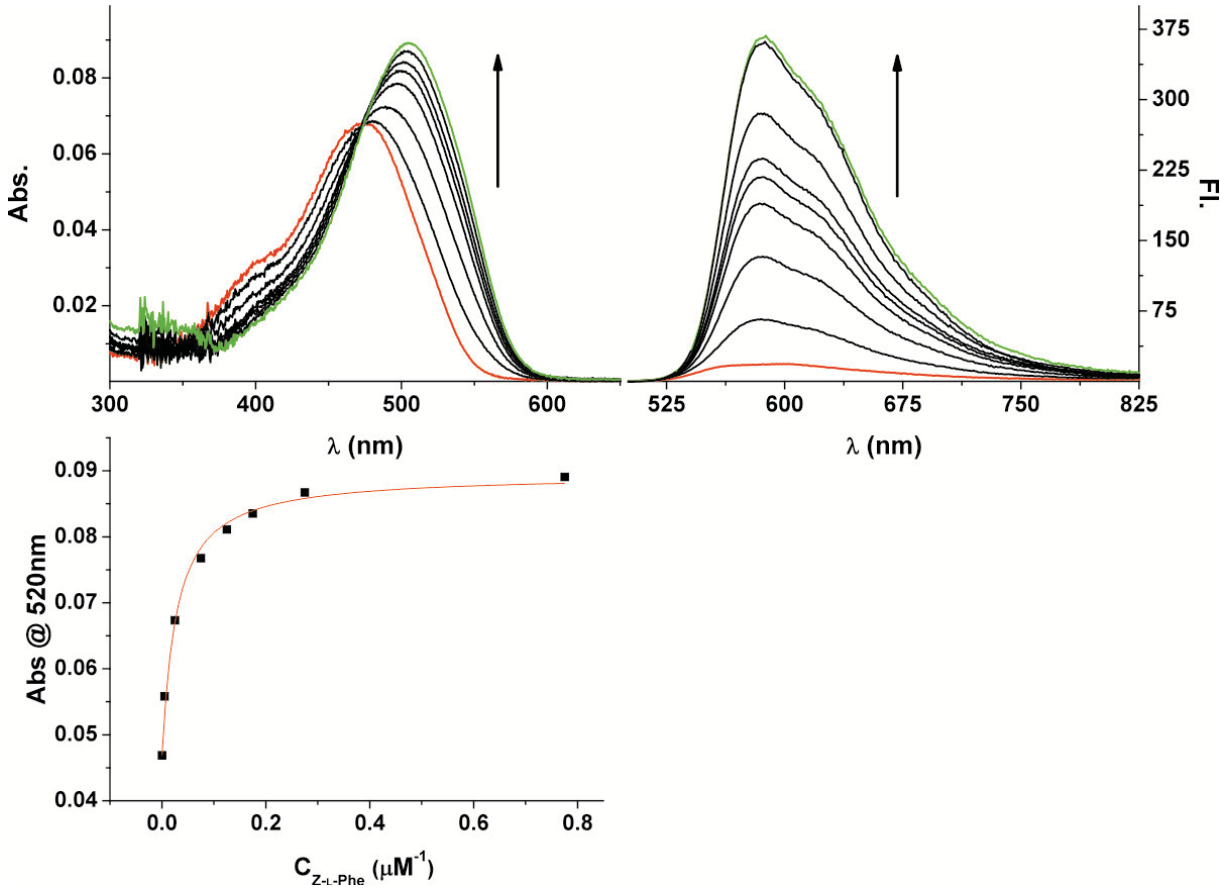

Fig. 12.2 Absorption (top left) and fluorescence (top right) titration spectra of **M5** (5μM) with TBA-Z-L-Phe in $CHCl_3$ ($C_{TBA\text{-}Z\text{-}L\text{-}Phe}$ =2.5-600μM, starting point spectra in red, end point spectra in green), binding curve (bottom) fitted by absorption at 520 nm.

The titration response is rather similar in MeCN and THF. In MeCN, due to the relatively higher QY of **M5** in this solvent compared with $CHCl_3$, a smaller fluorescence enhancement factor of 10 is achieved. However due to the lower QY of free **M5** in THF, the fluorescence enhancement factor increased to 31 after formation of the complex (**Fig. 12.3**).

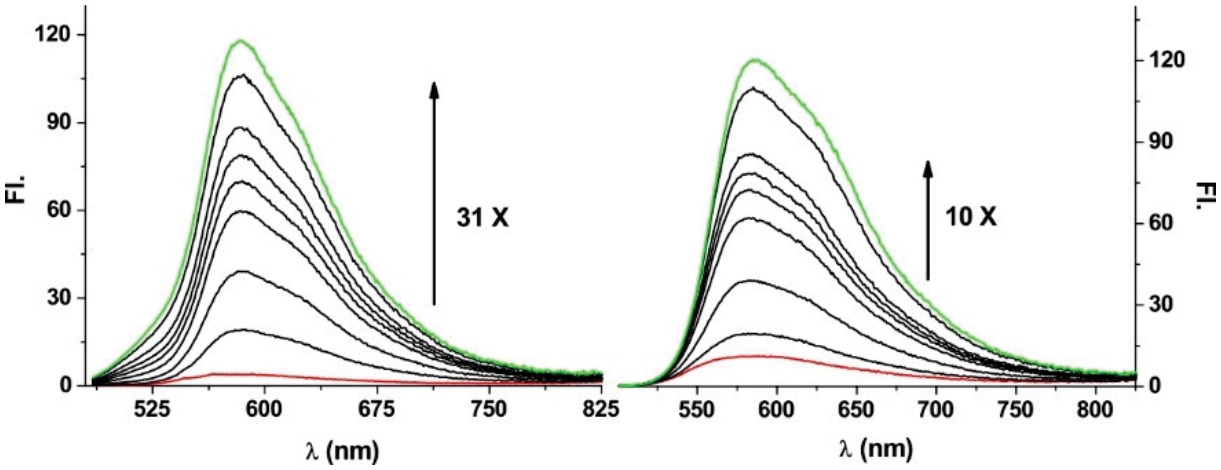

Fig. 12.3 Fluorescence titration spectra of **M5** (5μM) with TBA-Z-L-Phe in THF (left) and in MeCN (right) ($C_{\text{TBA-Z-L-Phe}}$ 2-500 μM, starting point spectra in red, end point spectra in green).

12.3 Binding studies with phenylphosphate

Besides carboxylates, phosphates are also an important class of oxoanions. They are important insecticides in agriculture. In addition, the phosphorylation of proteins for example is an important post modification pathway in biochemistry, the determination of amino acid phosphorylation (mostly tyrosine, serine and threonine) becomes an interesting topic.[173] Since urea has also a high affinity to the phosphate anion,[62] we firstly choose phenylphosphate (PPA) as a model template to assess the possibility of **M5** serving as a binder for phosphates.

Results that are similar to carboxylate case are obtained in titrations of **M5** with the phenylphosphate anion (PPA). The absorption band is red-shifted with a slight increase in the absorption coefficient. The fluorescence is also strongly enhanced by a factor of over 20 (**Fig. 12.4**). The binding constant is also higher of log*K*=4.21±0.01.

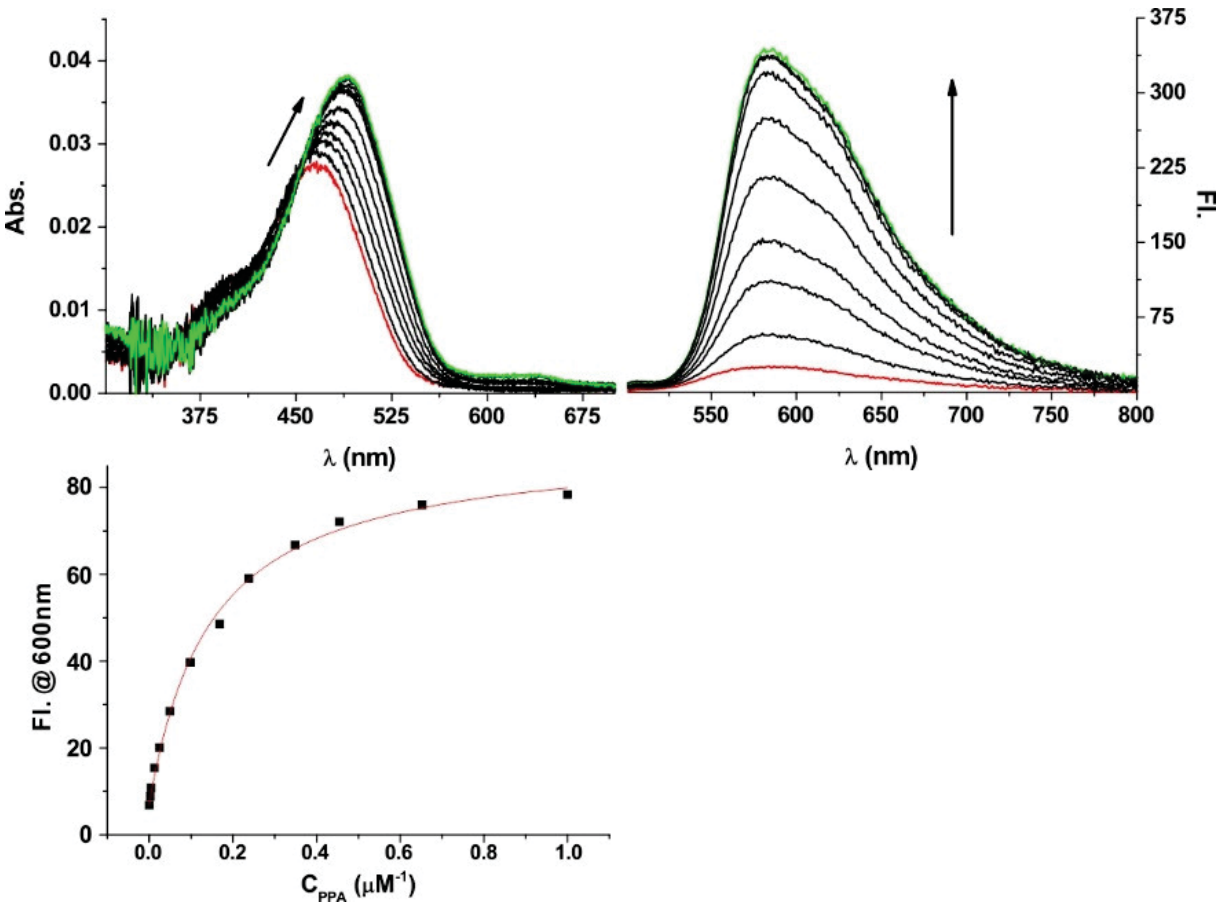

Fig. 12.4 Absorption (top left) and fluorescence (top right) titration spectra of **M5** (5 μM) with TBA-PPA in MeCN ($C_{TBA\text{-}PPA}$=2-700 μM, starting point spectra in red, end point spectra in green) and binding curve fitted by fluorescence at 600 nm (excitation at 485 nm)

12.4 Pre-polymerization studies

Unlike some of the early BODIPY monomers (see Section 11), the phenoxazinone monomer does not contain any radical-labile double bond and thus a polymerization test yielded satisfactory results. However, it is known that phenoxazinone-urea probes can be deprotonated.[164] The deprotonation is a proton transfer process which depends on the basicity of the anion and the acidicity of the urea monomer, it is also influenced by the component concentration due to the formation of anion-H-anion complexes. [174, 175, 176] Deprotonation is however undesired, since the electrostatistic interaction is non-directional which can introduce heterogeneity in the binding cavity and aggravate the selectivity of the binding cavity. In a pre-polymerization mixture, the fluorogenic monomer concentration is much higher than in a normal UV-Vis titration experiment (micromolar). This might be the reason that the different binding constants are obtained at different concentration as we showed in Section 10.

However, it is valuable to study the binding event in the pre-polymerization mixture since the results reflect directly the real interaction in the solution from which the MIP is obtained. For instance, Svensen et al. have also studied the interaction of template with monomer in a pre-polymerization mixture by spectroscopic titration, yet due to the lack of a chromophore in the monomer employed by those researchers, the response is only very small hampering a straightforward interpretation of the results.[177]

Commonly, a UV-Vis and/or fluorescence titration is carried out at micromolar concentration in a 1 cm quartz cell to ensure a thoroughly isolated system. The real pre-polymerization mixture, on the contrary, has a high, millimolar concentration. The high concentration always causes non-linear effects such as too weak transmission signals or inhomogeneous illumination in a fluorescence experiment. To solve this problem, a very thin micro-cell with a path length below 100 μm is used (**Picture 12.1**). This short optical path allows both absorption and fluorescence measurements at a much higher concentration.

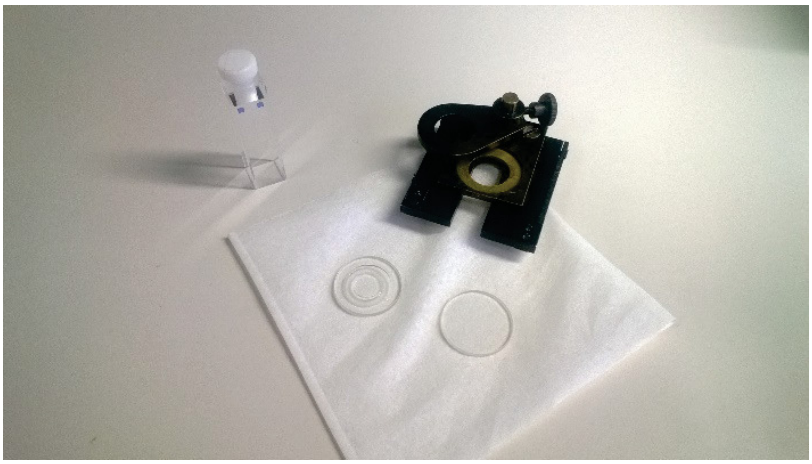

Picture 12.1 A normal 10 mm quartz cell (left) and a 100 μm micro-cell and the cell holder (right)

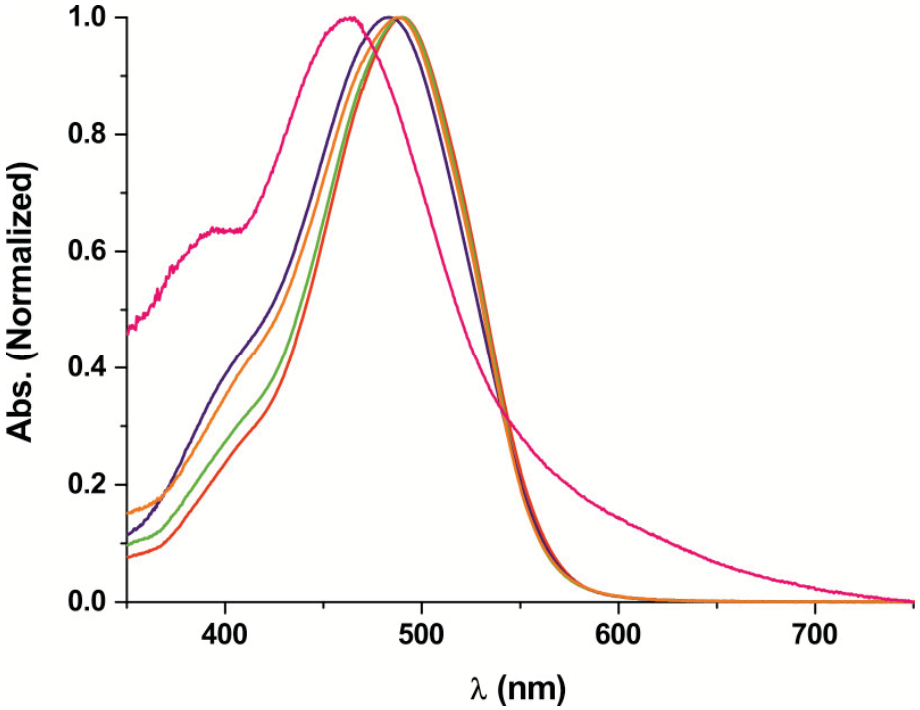

Fig. 12.5 Absorption spectra of 1mM **M5** in toluene (pink), **M5** with TBA-Z-L-Phe in toluene (red) and in the presence of various co-monomers and crosslinkers at pre-polymerization conditions, MMA/EDMA (green), HEMA/EDMA (blue) and Styrene/DVB (orange)

M5 has a low solubility in most solvents, the anionic complex however has a higher solubility. This is a common phenomenon in this thesis, the reason might be attributed to the self aggregation of the urea through H-bonding;[178] ureas have been thus used as organic gelators (**Fig. 12.6**). For comparison of the spectroscopic properties of the free and complex mode of **M5**, the spectra are registered in toluene. The absorption shifted from 463 to 489 nm after **M5** complexation with Z-L-Phe. After further addition of MMA and EDMA, virtually no additional shift was observed. The addition of styrene and DVB shifted the spectra also only slightly to 487 nm, whereas the addition of HEMA and EDMA shifted the spectra somewhat more to 482 nm (**Fig. 12.5**). This shows that OH groups in co-monomer and crosslinker can compete to a certain degree with the urea and thus alleviate the complex stability.

M5 operates in a prominent spectral window, i.e., it is excitable beyond 400 nm and emits above 500 nm. This makes the use of cheap instrumentation possible. This monomer has also a considerably high affinity towards the tested anion, ensuring the stability of the pre-polymerization complex under stoichiometric noncovalent imprinting conditions. In principle, these features promise sensitive sensing behaviour. The notable fluorescence response by enhancement towards the oxo-anion enables the use of the monomer for a turn-on intensity

sensor. **M5** was thus further used for preparation of MIP sensing matrices, see e.g. Section 18.7.

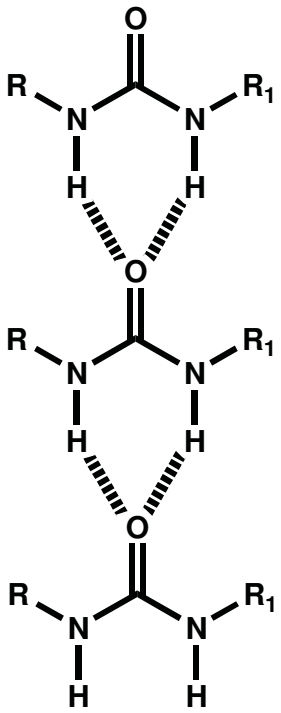

Fig. 12.6 Chain like self aggregation of urea through inter-molecular H-bonding

13 Naphthalimide-based Monomers

Naphthalimide dyes have been intensively studied as molecular probes and labels. Napthalimides display an ICT band involving an intra molecular donor-acceptor pair usually consisting of the 4-amino- or –urea-type electron donor and the imide-type acceptor motif. The functional monomer **M6** employed in this thesis was prepared according to **Scheme 13.1** in the Sellergren group from commercially available 4-bromo-1,8-naphthalic anhydride in 3 steps with an acceptable yield.[61]

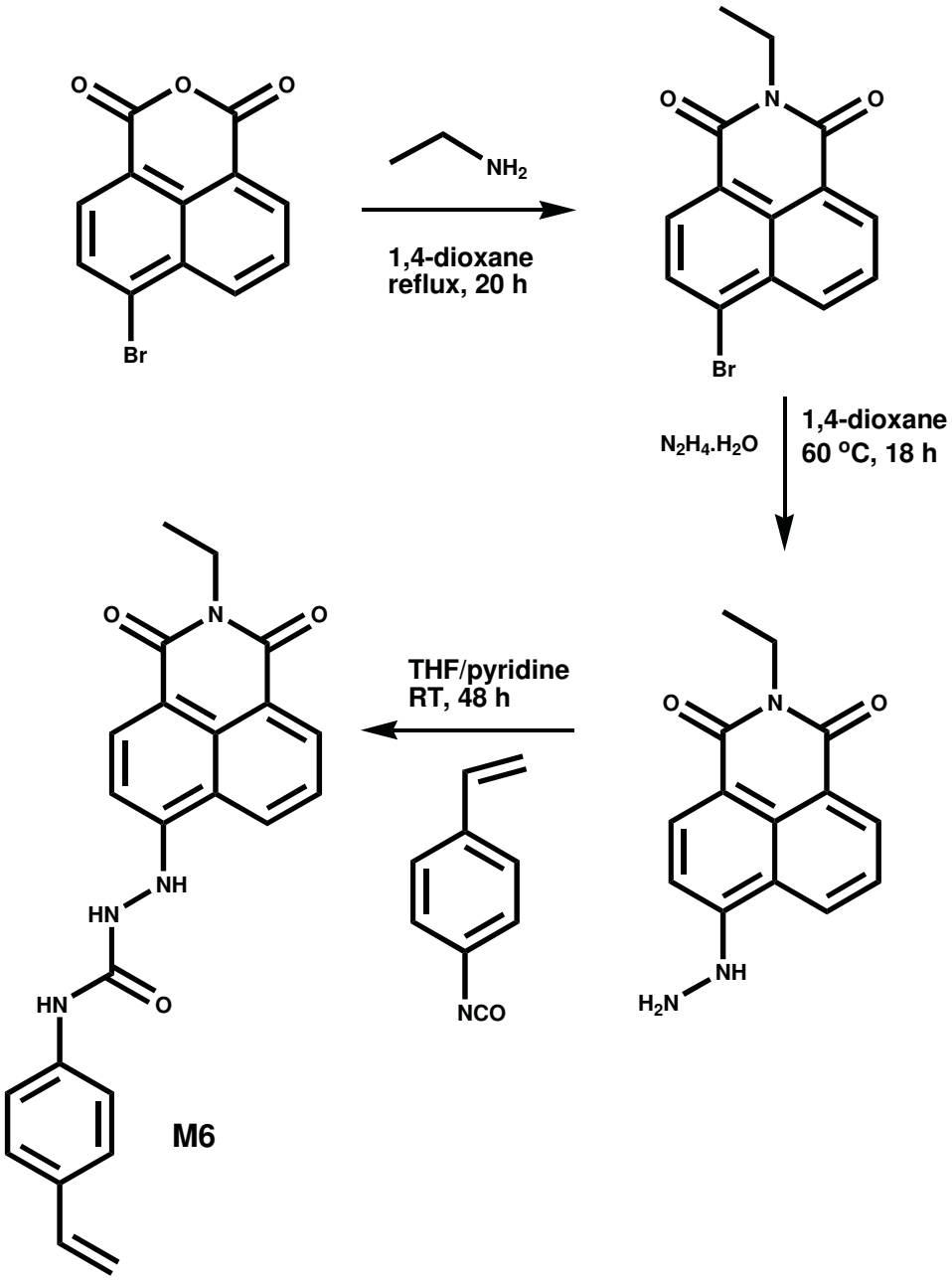

Scheme 13.1 Synthesis route for **M6**

13.1 Spectroscopic properties

1,8-Naphthalimide has been used for developing fluorescence probes due to the favorable intramolecular charge transfer properties. [179] , [180] The monomer **M6** prepared from naphthalimide has a non-structured absorption band at 400 nm and an emission band at 500 nm due to the charge transfer process between the hydrazine urea donor and the imido acceptor group (**Fig. 13.1**). It also has a considerable absorption coefficient of 18200 (L mol^{-1}cm^{-1}) at 404 nm in MeCN. Compared to the parent 1,8-naphthalimide, the monomer possesses red-shifted spectra and a larger Stokes shift because of the push-pull substitution at the opposite ends of the naphthalene system.

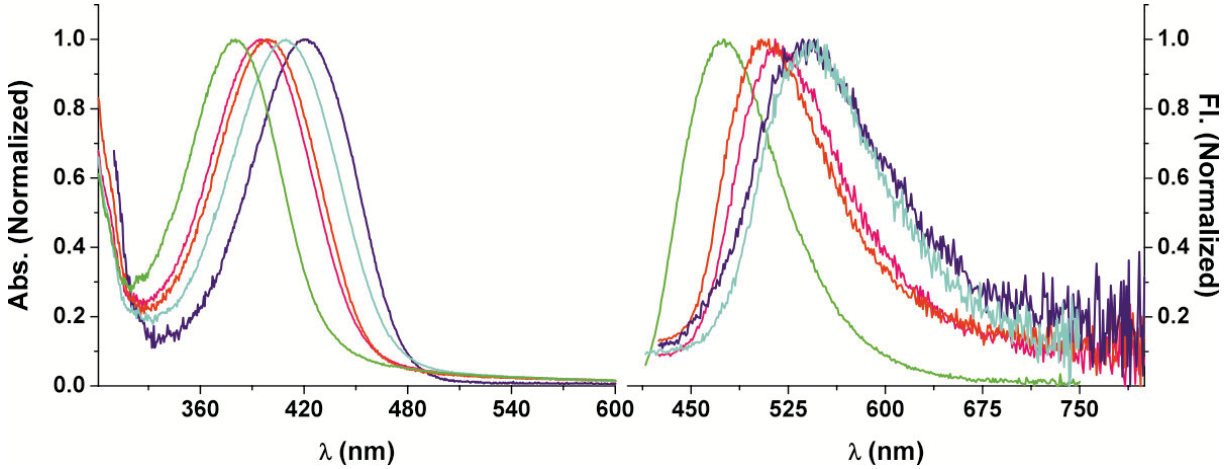

Fig. 13.1 Normalized Absorption (left) and fluorescence (right) spectra of **M6** in selected solvents, DMSO (blue), MeCN (pink), methanol (cyan), $CHCl_3$ (green) and THF (red)

Table 13.1 Spectroscopic properties of **M6** in selected solvents

Compound	Solvent	λ_{abs} /nm	λ_{em} /nm	Φ_f	τ_f /ns
M6	DMSO	420	542	0.018	0.14
M6	EtOH	412	535	0.013	0.04
M6	MeCN	404	517	0.015	0.12
M6	THF	402	512	0.020	0.14
M6	Dioxane	392	500	0.040	0.46
4-Hydrazine-1,8-napthalimide	MeCN	425	516	0.008	0.01

The monomer **M6** is also a solvatochromic dye. The absorption and emission spectra show a red shift when increasing the solvent polarity. The quantum yield (**Table 13.1**) decreases with increasing polarity and the formation of H-bonding complexes.

13.2 Binding studies

In the polar solvent DMSO, the monomer is deprotonated by an anion as basic as benzoate. This is confirmend by the large shift (120 nm) in the absorption spectra, in accordance with reports by Gunnlaugsson´s group.[161,179] In less polar solvents as THF and MeCN, the deprotonation is alleviated, and a new species with a smaller spectral shift of 30 nm is observed. This species is attributed to the hydrogen bonding complex.

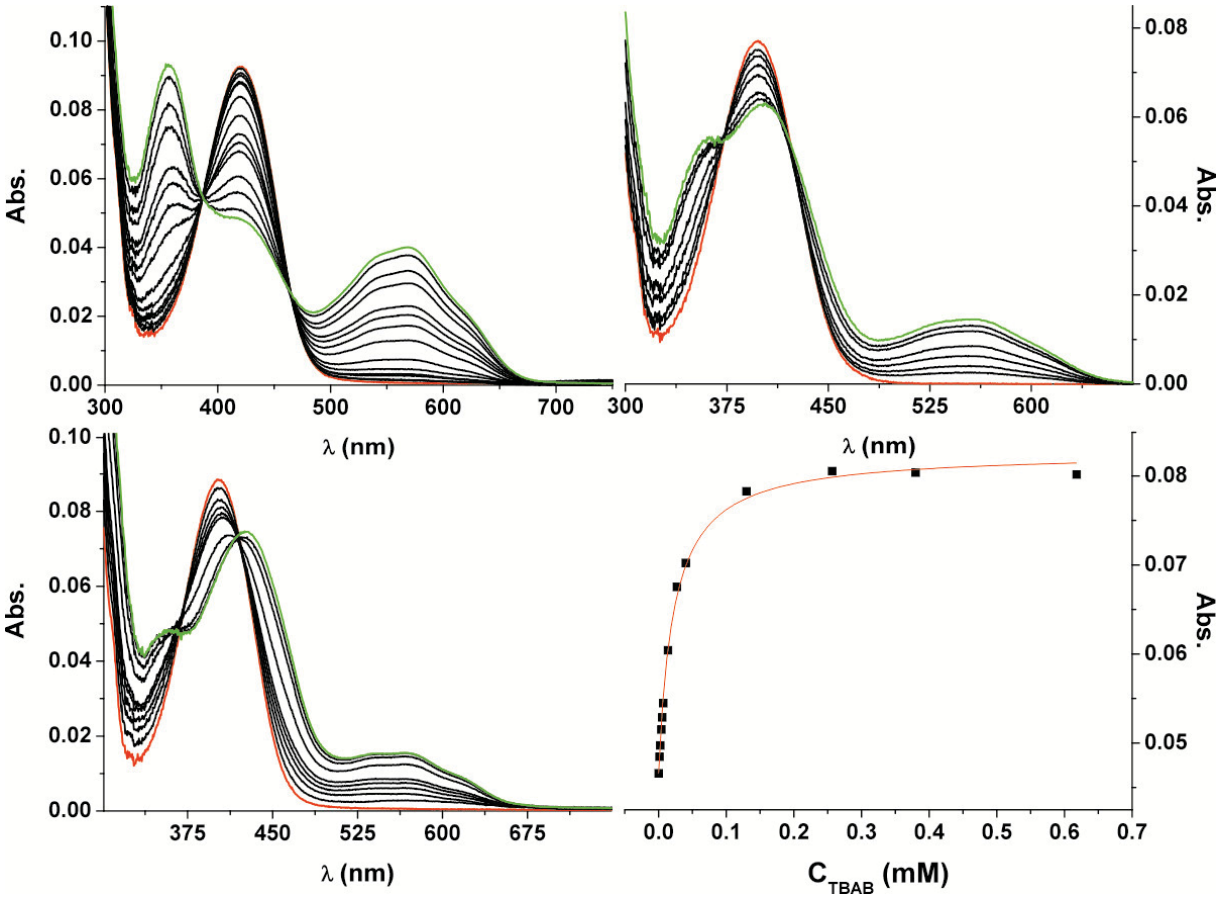

Fig. 13.2 Absorption titration spectra of **M6** (7 µM) with TBAB in DMSO (top left), MeCN (top right) and THF (bottom left) (C_{TBAB} = 1.5–600 µM, starting point spectra in red, end point spectra in green) and representative titration curve obtained from a plot of A_{435}vs. c_{TBAB} in THF (bottom right)

The binding constants measured in different solvents are listed in **Table 13.2**. These data were analysed by nonlinear regression fitting. From these data it is apparent that the affinity strongly depends on the solvent used. In a less competitive solvent as THF, the affinity is increased. We also found that the apparent binding constant differs when analysing different wavelengths of the THF and MeCN titration spectra. Since also the isosbestic points in these two solvents are not as sharp as that in DMSO, these features strongly suggest that more than two species are present in these two solvents.

Table 13.2 Binding constants of **M6** with TBAB in different solvents

	λ_{abs}/nm	log *K*
THF	403	6.17±0.13
	435	6.74±0.12
	565	6.47±0. 09
MeCN	400	5.04±0.05
	555	5.20±0.03
DMSO	430	4.04±0.02
	560	4.00±0.02

When further analysing these titration data according to multi-equilibria models employing the software Hyp Spec, it becomes evident that in DMSO, a single deprotonation process is taking place and that only two species are present in the solution. The deprotonation constant that can be derived from the fit is log*K*=3.93±0.01 which is in good agreement with the data in **Table 13.2**. However in THF and MeCN a mixture of H-bonding complex and deprotonated monomer seems to be present (**Fig. 13.2**). The constants for the H-bond process thus determined amount to log*K*=4.79±0.02 and log*K*=4.26±0.02, respectively.

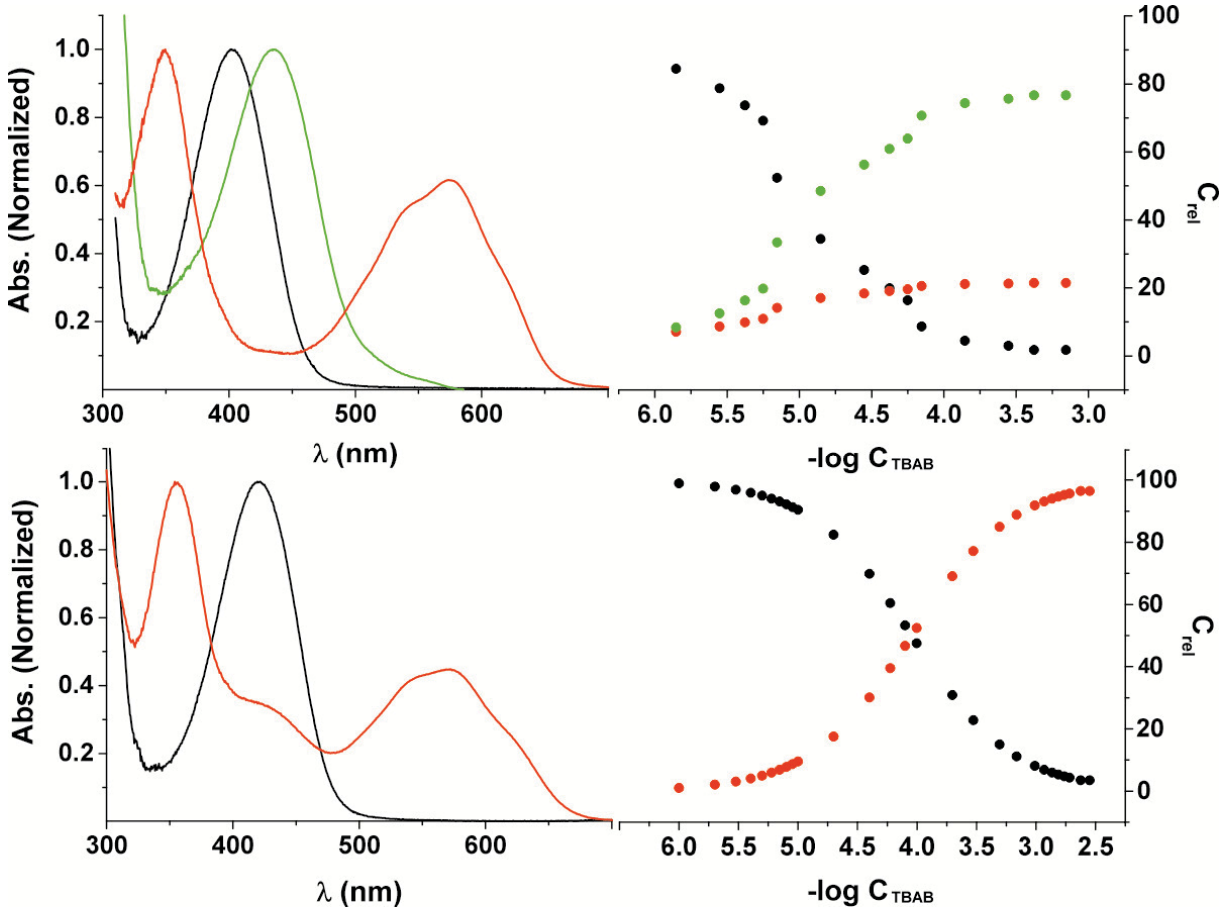

Fig. 13.3 The fitted results for the titration in Fig. 13.2 in THF (top) and DMSO (bottom) Species spectra (left) and relative concentrations (right) during the course of the titration of **M6** (black), **M6**$^-$ (red) and **M6**⊂Bz$^-$ (blue)

After having assessed the binding behaviour towards benzoate, a more realistic template model was considered: Z-L-Phe. It is a weaker base than benzoate and thus promises to be a suitable template while avoiding too many complications due to competition by deprotonation. Indeed, no deprotonated species were detected during the titration of **M6** with Z-L-Phe when it is in-situ deprotonated with 1,2,2,6,6-pentamethylpiperidine (PMP) in polar MeCN, and a steady fluorescence quenching was observed. The binding constant was calculated as log$K$=3.35±0.02 using non-linear curve fitting (**Fig. 13.4**).

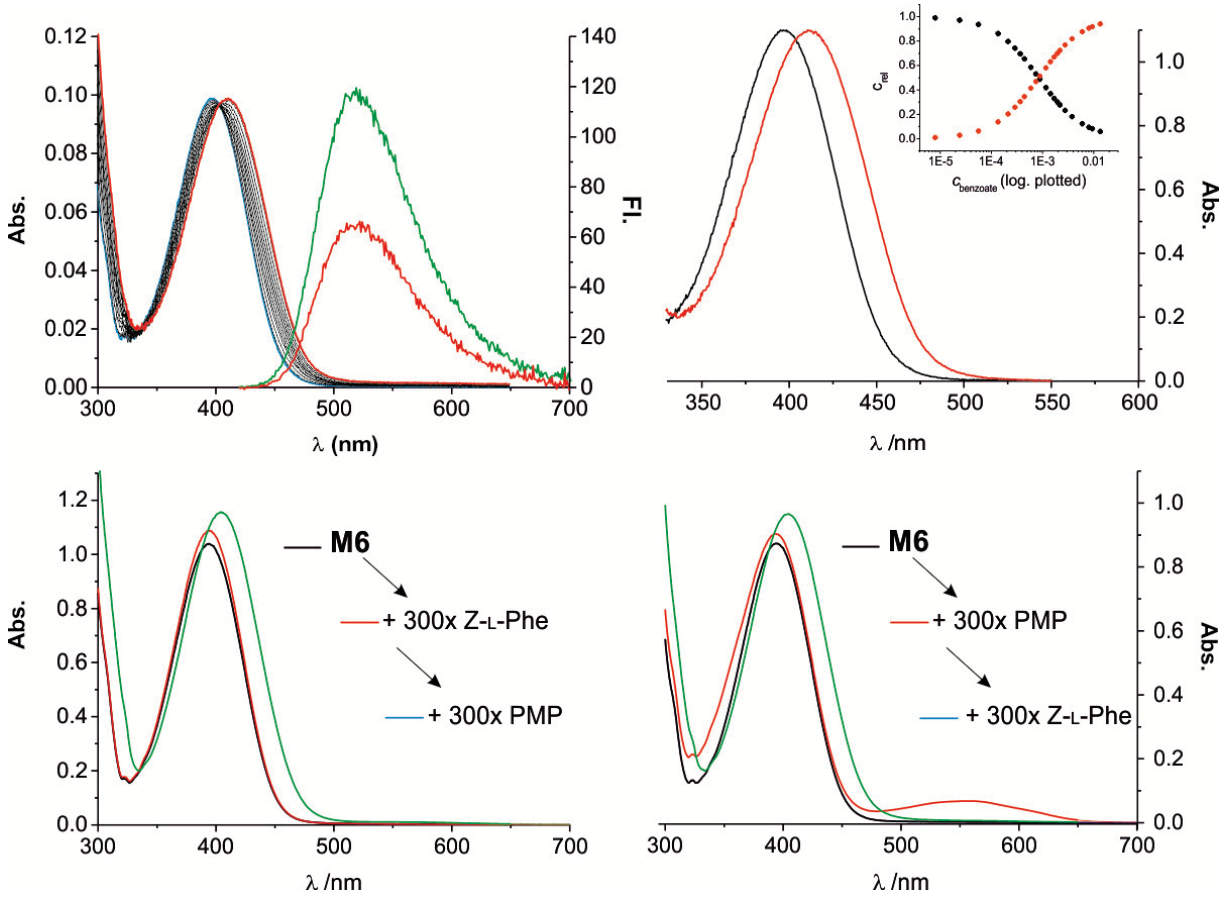

Fig. 13.4 Spectrophotometric titration spectra of **M6** (7 µM) upon addition of increasing amounts of a 1:1 mixture of Z-L-Phe and PMP (1–3300 eq.) in MeCN (top left); starting (blue) and end point (red) fluorescence spectra are also included. Species spectra of the fitted results (1:1 model) for the corresponding spectrophotometric titration (top right). Spectroscopic changes as a function of addition sequence: **M6** followed by an excess Z-L-Phe and the same excess PMP (bottom left) and **M6** followed by an excess PMP and the same excess Z-L-Phe (bottom right); excitation at isosbestic point (404 nm).

13.3 Pre-polymerization studies

As shown in **Fig. 13.5**, from the absorption spectra, an obvious red-shift of 50 nm is observed when **M6** forms a complex with TBA-Z-L-Phe. When we examine the absorption above 500 nm, no significant indication of deprotonation is noticed. The successive addition of MMA/EDMA and styrene/EDMA shows a minor blue shift, revealing that the co-monomer and crosslinker have only a minor influence on the complex stability. However, the addition of HEMA shows an obvious blue shift, which means that HEMA competes with Z-L-Phe for the urea binding sites, leading to decomplexation.

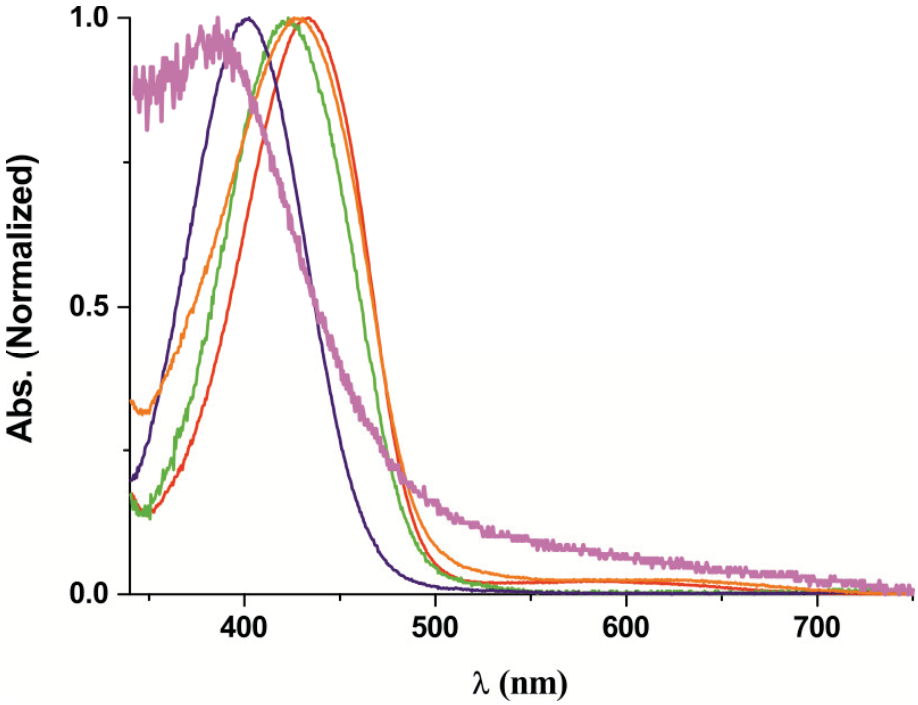

Fig. 13.5 Normalized absorption spectra of 1mM **M6** (pink), **M6** with TBA-Z-L-Phe (red) in toluene and in the presence of various co-monomers and crosslinkers at pre-polymerization conditions, MMA/EDMA (green), HEMA/EDMA (blue) and Styrene/DVB (orange)

The naphthalimide-based monomer **M6** can form a stable complex with the relatively weak base TBA-Z-L-Phe. However, a mixture of deprotonated species and H-bonding complex was observed when using a stronger base such as TBAB. The deprotonation is even enhanced in polar solvents like DMSO. The complexation with anions is accompanied by fluorescence quenching. The study of the pre-polymerization mixtures showed that MMA, styrene, EDMA and DVB have little influence on the **M6**-anion complex stability while HEMA interferes significantly. In essence, **M6** is a promising candidate and was used to prepare MIPs of different format discussed in Sections 16.1 and 17.1.

14 Nitrobenzoxadiazole-based Monomers

14.1 Synthesis

Nitrobenzo-2-oxa-1,3-diazole (NBD) dyes have been widely applied as fluorogenic reagents for amines. NBD dyes possess a 4,7-donor-acceptor-substituted benzofurazan ring. The synthesis is accomplished in two steps following **Scheme 14.1** with an overall yield of 70%. Three monomers with different polymerizable groups were prepared. A further analogue was prepared for model studies.

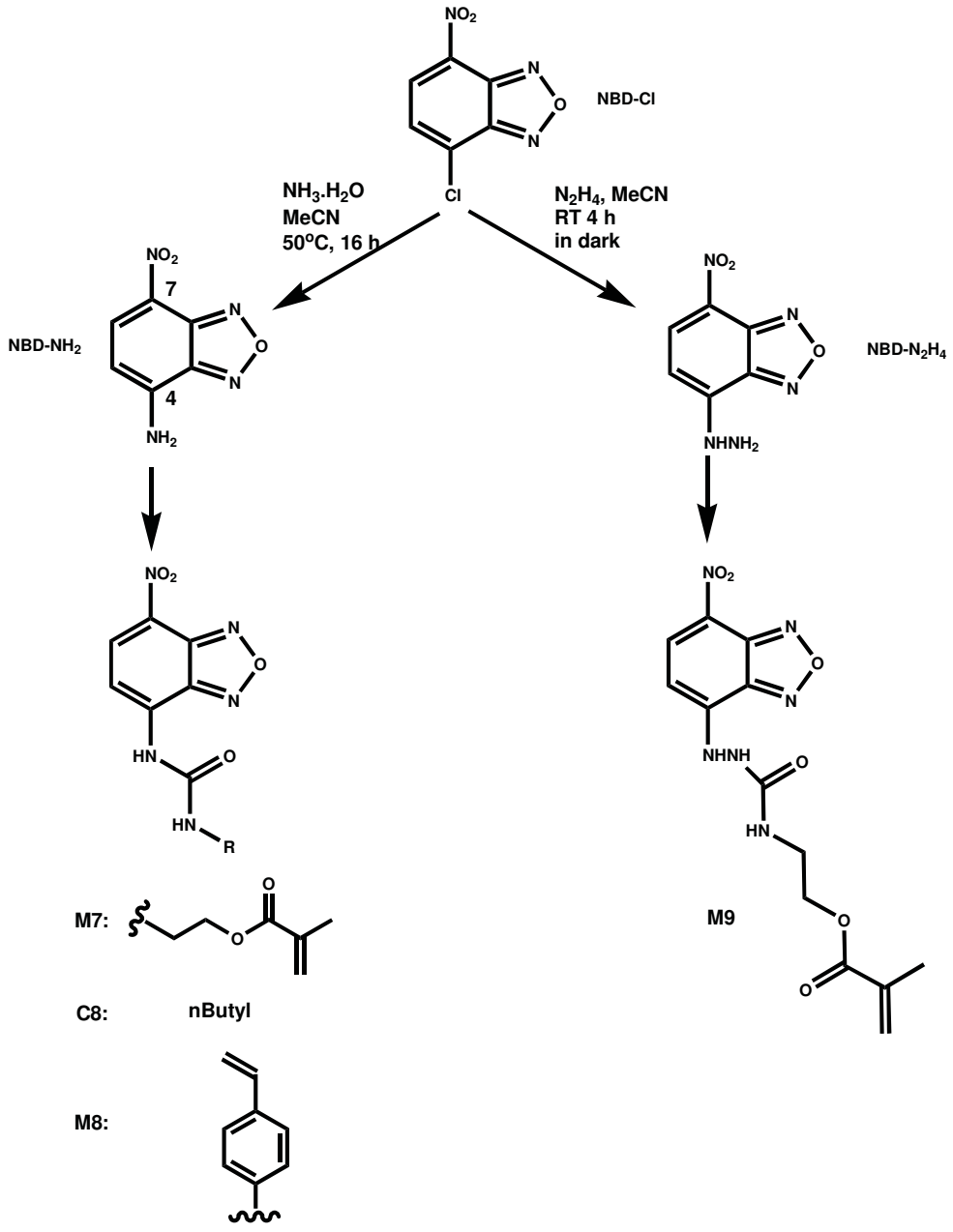

Scheme 14.1 Preparation of NBD-based chromogenic monomers **M7** with ethyl-methacrylate group, **M8** with vinylbenzyl group, **C8** with nButyl group

14.2 Spectroscopic properties

NBD dyes carry an electron donating and electron accepting pair at the opposite positions on the benzene ring. This substitution pattern gives rise to a typical non-structured charge transfer absorption band. It has also a considerable absorption coefficient of 15500 (L mol^{-1}cm^{-1}) at 403 nm in $CHCl_3$. The CT band is sensitive to any change taking place at these terminal ends of the push-pull system on the 4 and 7 positions (**Scheme 14.1**).[181]

As shown in **Fig. 14.1**, due to the weak donating ability of chlorine, the ICT band of **NBD-Cl** lies at 400 nm. After substitution with a stronger donor like an amino nitrogen, the absorption band is shifted to 467 nm as in **NBD-NH_2**. This principle has been widely applied for detection of biological amines.[182, 183] Moreover, in parallel to the red-shift in absorption, the fluorescence bands are displayed to longer wavelengths and the fluorescence quantum yield increases.[183] The latter has been ascribed to the fact that for NBD dyes, the CT state is much more strongly emissive than the excited state localized on the benzofurazan ring.[184]

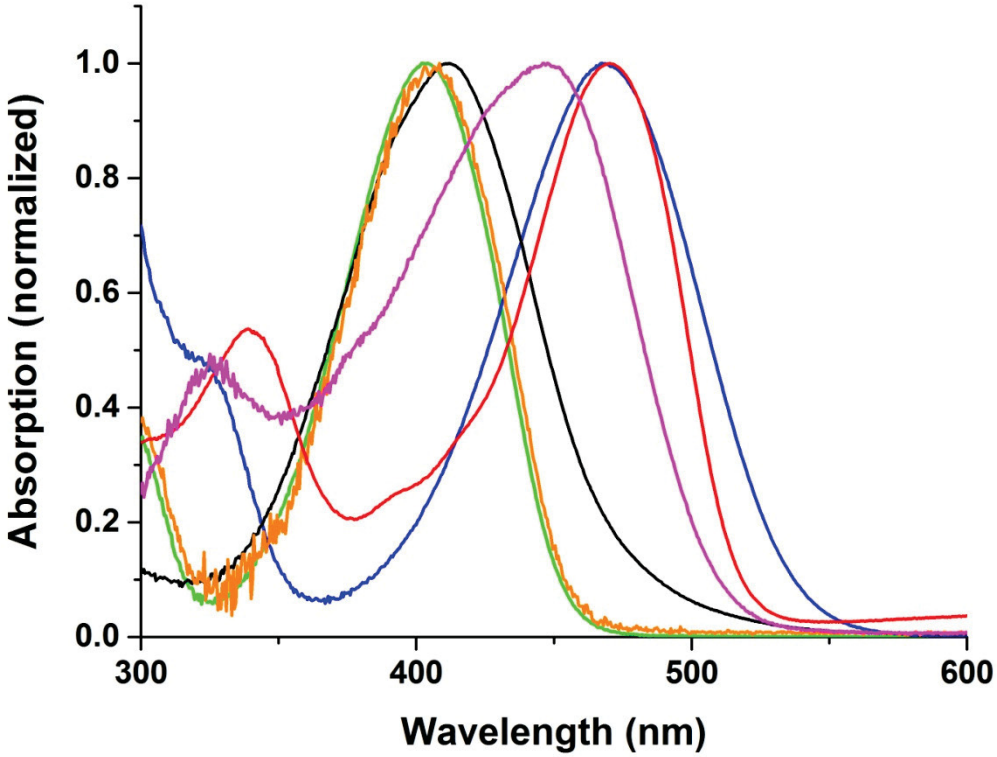

Fig. 14.1 Normalized absorption spectra of NBD derivatives, **M7** (green), **M8** (blue), **C8** (orange), **M9** (black), **NBD-NH_2** (red) and **NBD-N_2H_4** (magenta)

According to **Table 14.1**, the fluorescence quantum yield of **NBD-NH_2** exceeds that of **NBD-Cl** significantly, especially in moderately and highly polar solvents. **NBD-N_2H_4** with a hydrazine as the donor shows an intermediate absorption band at 447 nm. The fluorescence QY is also lower than that of **NBD-NH_2**. After transfer of the amine to a urea group, the electron density is decreased and thus the absorption band of **M7** is again blue-shifted to 403 nm in $CHCl_3$, accompanied by a decreased quantum yield. **C8** which has a butyl group on the other side of the urea arm has slightly red-shifted absorption and emission spectra and an increased QY compared to **M7**. However, in a related way to the BODIPY dyes discussed above, the change to a styrene substitution greatly changes the spectra. Absorption and emission spectra of **M8** show a more than 70 nm red shift, yet with a strongly decreased fluorescence QY. The latter is a rather unexpected finding, the origin of which is unclear at present.

Table 14.1 Spectroscopic data of selected NBD derivatives. * (Φ_f smaller as 0.001)

	M7			**C8**			**M8**			**M9**		
	λ_{abs}/nm	λ_{em}/nm	Φ_f	λ_{abs}/nm	λ_{em}/nm	Φ_f	λ_{abs}/nm	λ_{em}/nm	Φ_f	λ_{abs}/nm	λ_{em}/nm	Φ_f
$CHCl_3$	403	500	0.002	407	500	0.007	470	550	*	407	512	*
MeCN	410	501	0.024	414	503	0.057	478	542	*	433	534	*
THF	413	500	0.01	418	503	0.018	475	539	*	415	535	*
MeOH	411	507	0.043	414	508	0.074	481	553	*	410	633	*

Monomer **M7** is a solvatochromic dye which shows a red shift of the spectra with increasing solvent polarity. It has a low QY of 0.002 in low polarity solvents like $CHCl_3$. The QY is slightly enhanced to 0.03 in THF. Important for a use in MIP matrices however is the fact that upon H-bond driven binding of an electron rich (e.g., oxo-anion) species at the urea moiety, a fluorescence enhancement is to be expected. **Table 14.2** reveals that this is indeed the case. Compared to the case of fluorescence enhancement induced by solvent polarity, a pronounced increase of the fluorescence lifetime is observed for the complex which verifies that a distinct new species is formed.

Table 14.2 Spectroscopic properties of **M7** and related species in selected solvents

*: Φ_f <0.001

	λ_{abs} /nm	λ_{em} /nm	Φ_f	τ_f /ps
$CHCl_3$	404	519	0.002	610
Dioxane	406	502	0.003	40
DMSO	494	564	0.005	150
ether	408	489	0.021	/
H_2O	418	511	*	780
MeCN	410	501	0.024	320
MeOH	410	507	0.030	640
THF	413	494	0.033	120
toluene	394	509	0.002	/
Z-L-Phe/PMP	430	505	0.080	1350
Deprotonated in $CHCl_3$	520	650	*	40

14.3 Binding studies

According to Boiocchi's study, NBD-Urea has a high acidity and can be deprotonated by anions with higher negative charge on oxygen.[174] **M7** is relatively acidic, for it forms H-bonding complexes with anions that are relatively weak bases. These complexes are indicated through a fluorescence enhancement with a small spectral shift. With strong bases, however, deprotonation occurs, reflected by a strong bathochromic shift and fluorescence quenching which can be easily visualized under the UV-lamp (**Picture 14.1**) as well as traced through spectroscopy (**Fig. 14.1**).

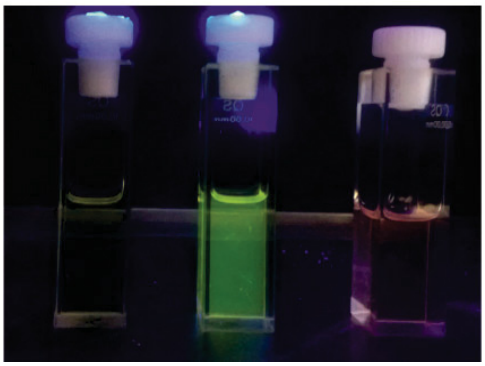

Picture 14.1 M7 in free (left), H-bonding (middle) and deprotonation state (right)

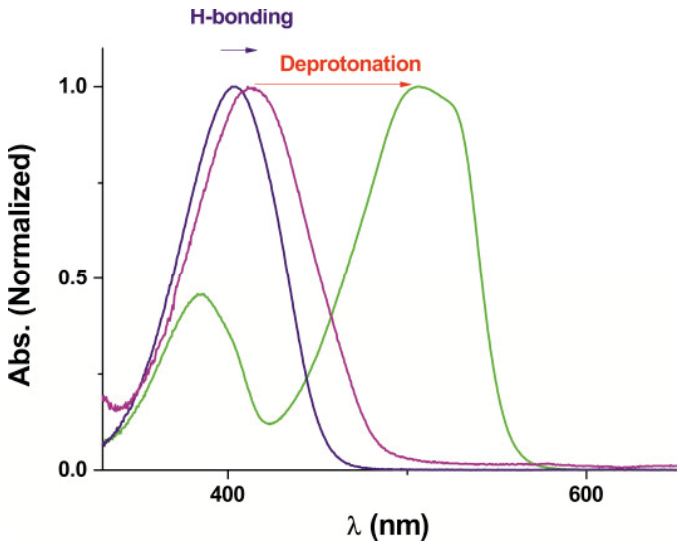

Fig. 14.2 Corresponding spectra to **Picture 14.1**: free (blue), H-bonding (maganta) and deprotonated (green) state.

Both benzoate and acetate seem to be too strong bases for **M7**, so that even in less polar solvents like chloroform, deprotonation instead of H-bonding complex formation was observed. This is easily determined through the change of the colour to red.

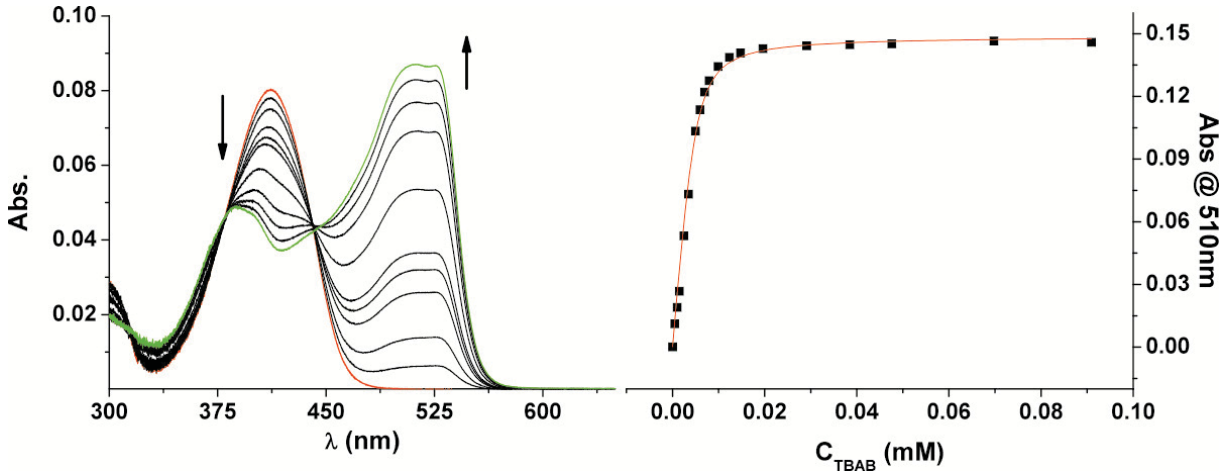

Fig. 14.3 Absorption titration spectra (left) of **M7** (5 µM) with TBAB in $CHCl_3$ (C_{TBAB}=2-500 µM starting point spectra in red, end point spectra in green) and the binding curve (right) by absorption at 510 nm.

In a UV/vis titration, deprotonation is manifested by a decrease of the absorption band at 403 nm and a corresponding increase of the absorption band at over 500 nm. A clear isosbestic point stresses the acid-base reaction (**Fig. 14.3**). When fitting this titration data with Hyp Spec software, two species with different absorption bands are resolved. The free species decreases along the titration process and the deprotonated species increases steadily until conversion is reached (**Fig. 14.4**).

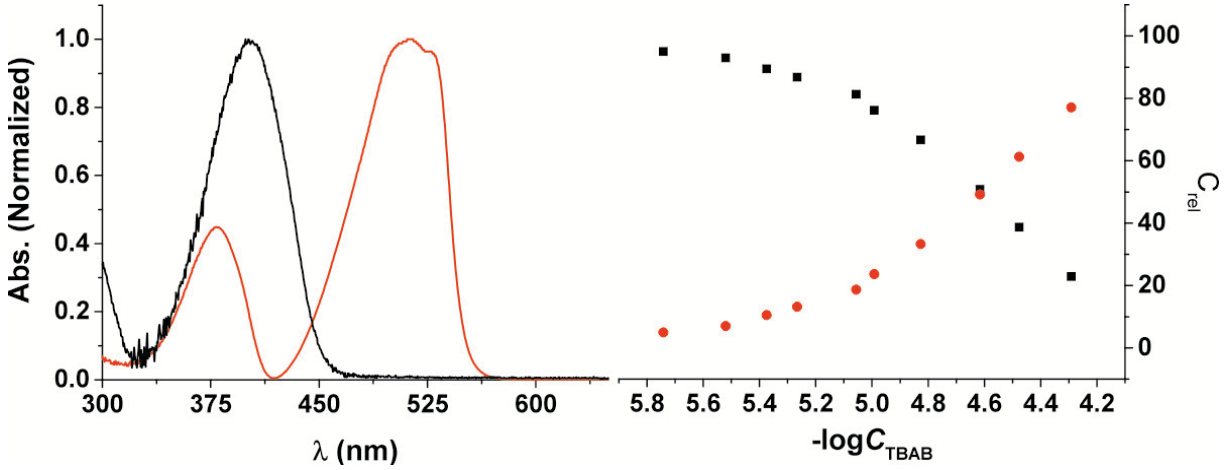

Fig. 14.4 Fitting results for the titrations shown in **Fig. 14.3**. Species spectra (left) and relative concentrations during the course of the titration (right) of free **M7** (black) and deprotonated **M7** (red)

H-bond formation is characterized by a slight shift of the absorption spectra and a fluorescence enhancement. Unlike the case of pure deprotonation by TBAB, for TBA-Z-L-Phe no clear isosbestic point is observed during a titration in $CHCl_3$. However, if the titration spectra are analysed for three species, i.e., is separated into two processes, an isosbestic point can be found for the complex formation before the deprotonation begins (**Fig. 14.5**). These results are further supported by 3D fluorescence scans. From **Fig. 14.6** it is evident that **M7** shows a single excitation-emission pattern in $CHCl_3$, although the emission is comparatively weak. When TBA-Z-L-Phe is added, a slight shift of the pattern is observed with an enhanced intensity. In accordance with the very low fluorescence QY of the deprotonated species, no traces of this species are found in the 3D matrix with the monochromator and detector settings used to record the strong fluorescence of the H-bonded complex.

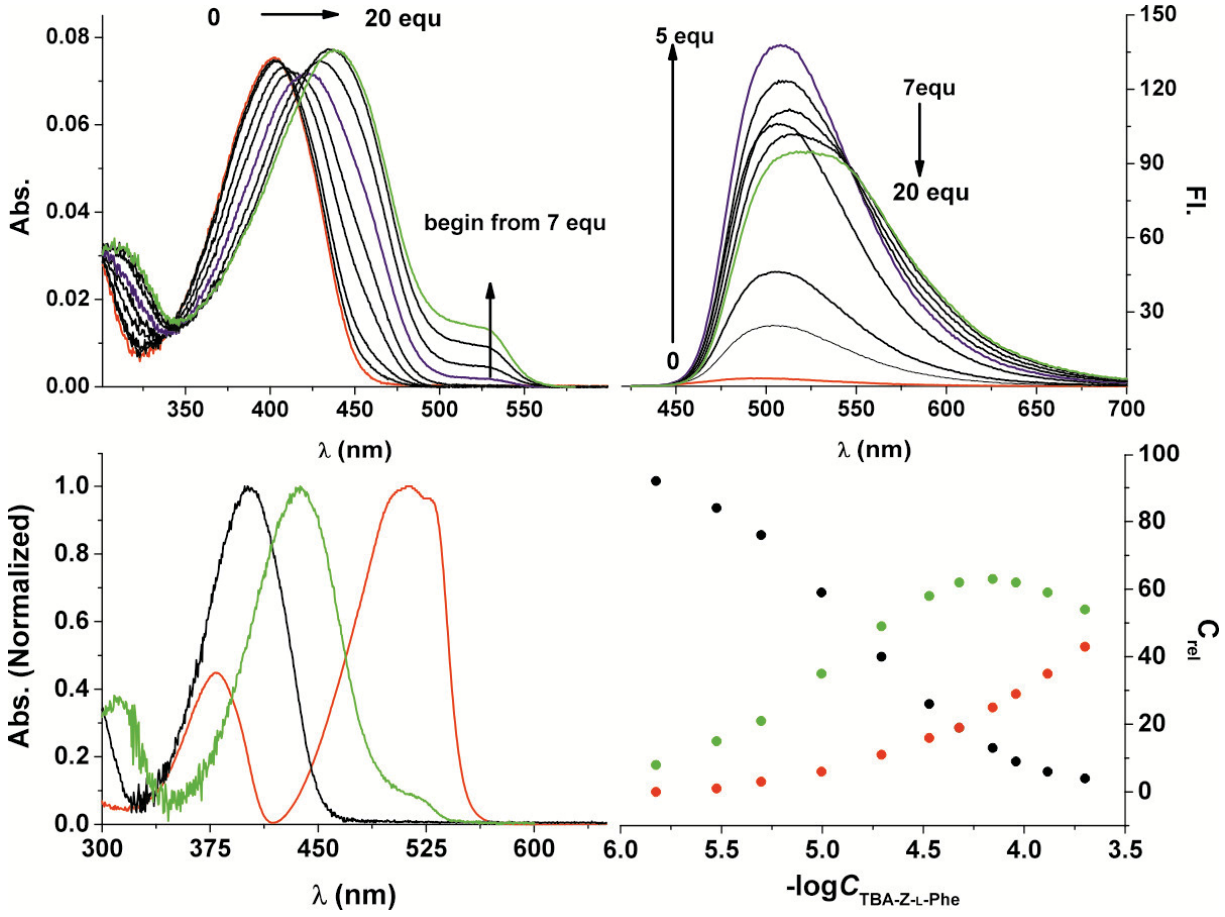

Fig.14.5 Absorption (top left) and fluorescence (top right) titration spectra of **M7** (5 μM) with TBA-Z-L-Phe in $CHCl_3$ ($C_{TBA\text{-}Z\text{-}L\text{-}Phe}$ = 2.5-700 μM, starting point spectra in red, end point spectra in green) and the fitting results with species spectra (bottom left) and the species distribution (bottom right) free **M7** (black), **M7**⊂Z-L-Phe$^-$ (blue) and deprotonated **M7** (red)

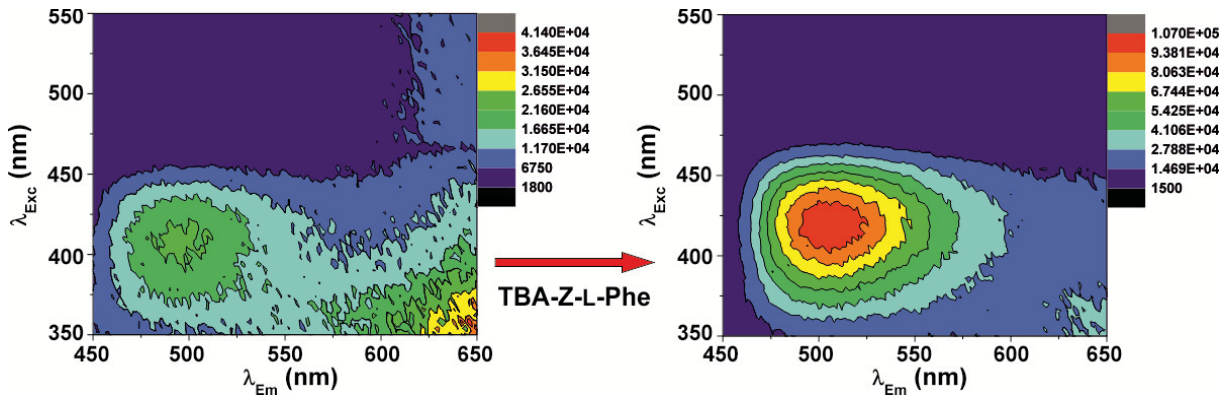

Fig.14.6 3D fluorescence plot of **M7** and its complex with TBA-Z-L-Phe

Both **M8** and **M9** show a quenching mode, however due to their low QY, they are not suitable as chromogenic monomer to be integrated into MIP matrices.

Although **M7** is not suitable for imprinting of benzoate and acetate due to the monomer's high acidity and the induced deprotonation, the affinity to weak bases such as TBA-Z-L-Phe (binding constant log*K*=4.88 ± 0.02) is significantly enhanced as compared with for instance **M6**.

14.4 Counter-ion Effect

As already shown before, for a given urea-type probe or monomer the strength of H-bonding relies on the basicity of the H-bond acceptor (anion). This basicity depends on the anion itself, but is also influenced by the solvent and the counter-ion. Pentamethylpiperidine (PMP) was widely used for in-situ deprotonation of for instance carboxylic acids in anion imprinting. However, it was found to be not effective in our case. The anions deprotonated in-situ with PMP always showed a low affinity, e.g., only log*K*=2.55±0.01 for TBA-Z-L-Phe in $CHCl_3$. In more polar MeCN the affinity is slightly increased to log*K*= 3.62±0.02. This low binding constant may be due to ternary complex formation of the protonated PMP, the carboxylate anion and the urea monomer as shown in **Fig. 14.7**. The closer it can approach the negatively charged carboxylate and the higher the electrostatic attraction, e.g., because of a high charge density, the more the counter-ion reduces the electron density of the anion, thus diminishing the effective basicity of the anion. Another disadvantage of using PMP for deprotonation lies with the gradual re-protonation of the anion, especially under the elevated temperature in the polymerization procedure. Due to these two disadvantages, the preparation of anions in form of TBA salts seems to be a better approach for anion imprinting here.

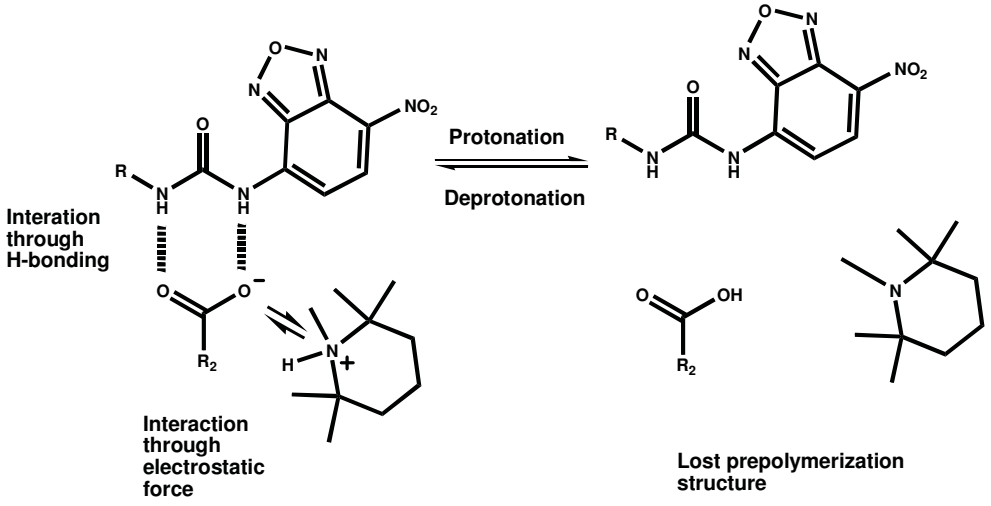

Fig. 14.7 Ternary complex of **M7** with carboxylate in the presence of $HPMP^+$ counter-ion

To ascertain this assumption, benzoate deprotonated in-situ with PMP (PMPB) was used to complex compound **M7**. Unlike in the case of the titration with TBAB, no deprotonation was observed for PMPB. As a control, an anion with a stronger tendency to coordinate with PMP, bromide, was subsequently introduced. Br^- ion-pairs with protonated PMP and dislocates it from the ternary complex leaving a bare benzoate center, which in turn led to the deprotonation of **M7** visible by the appearance of the characteristic absorption band at 520 nm (**Fig. 14.8**). This experiment impressively stresses the importance of the counter-ion and ternary complex formation in such complexes that involve hydrogen bonding and electrostatic forces.

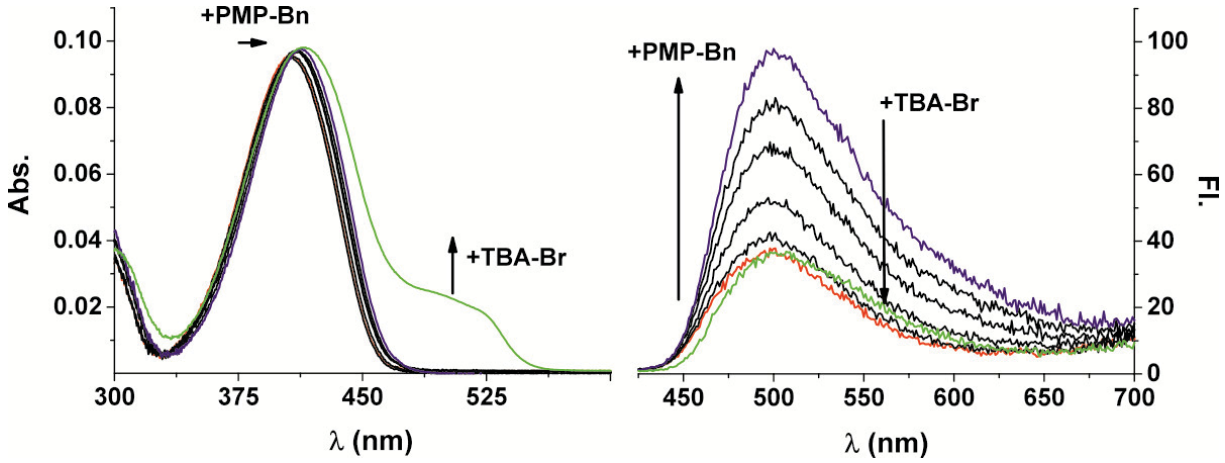

Fig. 14.8 Absorption (left) and emission (right) titration spectra of **M7** (5 µM) with PMP-benzoate in $CHCl_3$ (C_{Bn}-= 2.5-500 µM starting point spectra in red, end point spectra in blue), and added 500 µM TBA-Br thereafter (green)

To further study the counter-ion effect, a series of tetraalkylammonium Z-L-phenylalanine salts with alkyl varying from tetramethylammonium (TMA) to tetraoctylammonium (TOA) were used. These tetraalkyl counter-ions are all well solvated in organic solvents. The binding constant for **M7**⊂Z-L-Phe was found to increase steadily from the TMA to the TOA salt as listed in **Table 14.3**. On the other hand, the deprotonation tendency also increases. Especially in the case of TOA, deprotonation of **M7** already began at the addition of the first equivalent (**Fig. 14.9**). If we invoke the ternary complex model proposed above, the reason for the present behavior can again be attributed to the distance between the cation and the anion center. The charge density is higher in TMA and TEA than

in TBA and TOA and the small size allows TMA and TEA to approach the anion center better, as shown in **Scheme 14.2**. Both effects help to decrease the effective basicity of the anion, yet also enhance H-bond complex formation and hence the magnitude of the spectroscopic response.

Table 14.3 Binding constant of **M7**-Z-L-Phe for different TXA-Z-L-Phe salts in $CHCl_3$

Z-L-Phe salts	TMA	TEA	TBA	TOA	PMP
log*K*	4.09±0.01	4.67±0.02	4.88±0.03	5.21±0.03	2.55±0.02

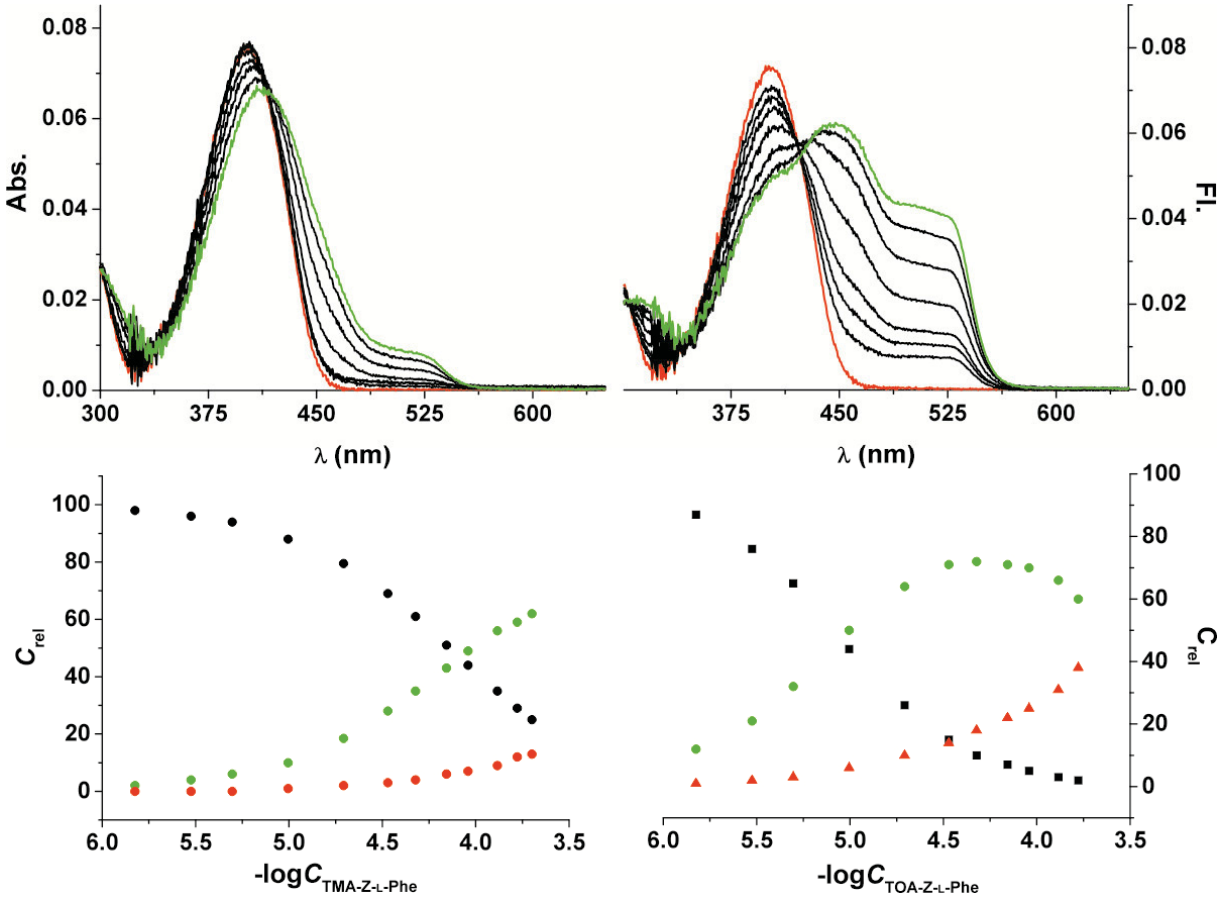

Fig. 14.9 Absorption titration spectra of **M7** (5μM) with TMA-Z-L-Phe (top left) and TOA-Z-L-Phe (top right) in $CHCl_3$ ($C_{TBA\text{-}Z\text{-}L\text{-}Phe}$ =2.5-700 μM starting point spectra in red, end point spectra in green, begin of deprotonation spectra in blue) and the species distribution (bottom left and right) during the titration (free **M7** in black, **M7**⊂Z-L-Phe$^-$ in blue and deprotonated **M7** in red)

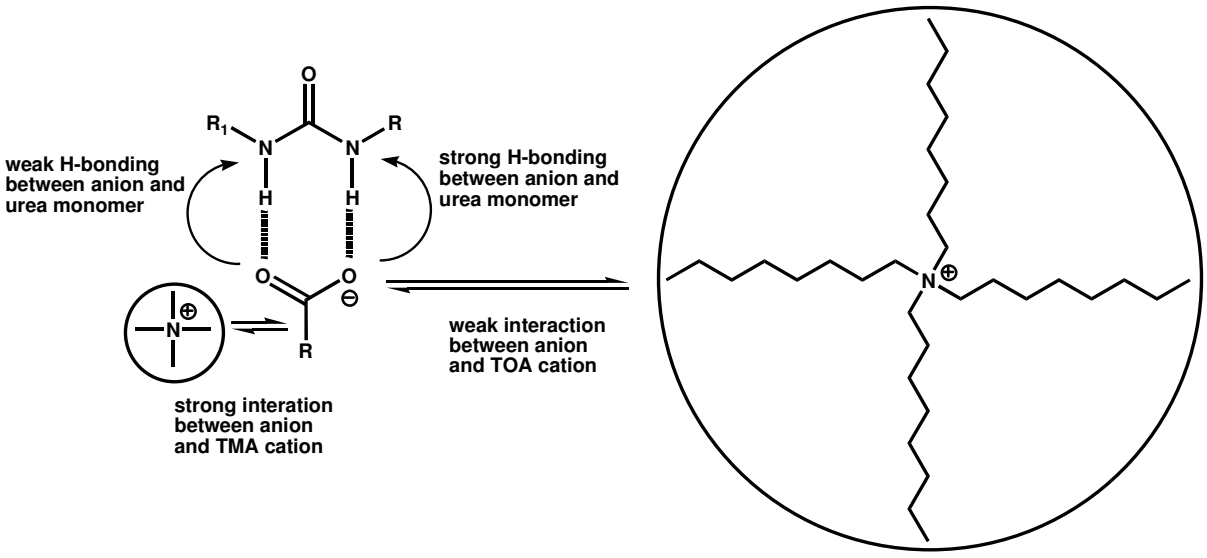

Scheme 14.2 Size influence of counter-ion in receptor affinity towards anion

The deprotonation of **M7** by the anion was observed in all four cases, yet for the small counter-ion as TMA, a considerable deprotonation was only observed after addition of a high excess of anion, the binding constant for the H-bonding process is also low. On the other hand, for large counter-ion as TOA, consideratble deprotonation was observed even below 1:1 stoichiometry. In the case of TBA-Z-L-Phe, the deprotonation begins after the addition of 7 equivalents of anion (**Fig. 14.6**). Thus the use of TBA-Z-L-Phe as template ensures the dominant presence of the H-bonding complex when attempting stoichiometric MIP synthesis. In all the cases, the deprotonation is characterized by the development of the new absorption band at over 500 nm and the decrease of the fluorescence intensity.

14.5 Pre-polymerization studies

Because of the considerations mentioned above in the naphthalimide section and the possibility that deprotonation might interfere at elevated concentrations, monomer **M7** was also studied under pre-polymerization conditions in three solvents that are suitable for polymerization. As shown in **Fig. 14.10**, **M7** forms mainly the H-bonding species at equimolar ratios of TBA-Z-L-Phe in $CHCl_3$, however, sizeable deprotonation already occurred at such concentrations in MeCN and THF. The addition of co-monomer and crosslinker to **M7** Z-L-Phe solution in $CHCl_3$ showed again little interference. The stability of the complex at the elevated temperature required for polymerization was also studied through

heating the pre-polymerization mixture to 80 °C. Even under such conditions, only a very minor blue shift in the absorption spectrum was observed. This indicates that the complex is considerably stable and negligible decomplexation will most likely occur under the real polymerization conditions at 50 °C.

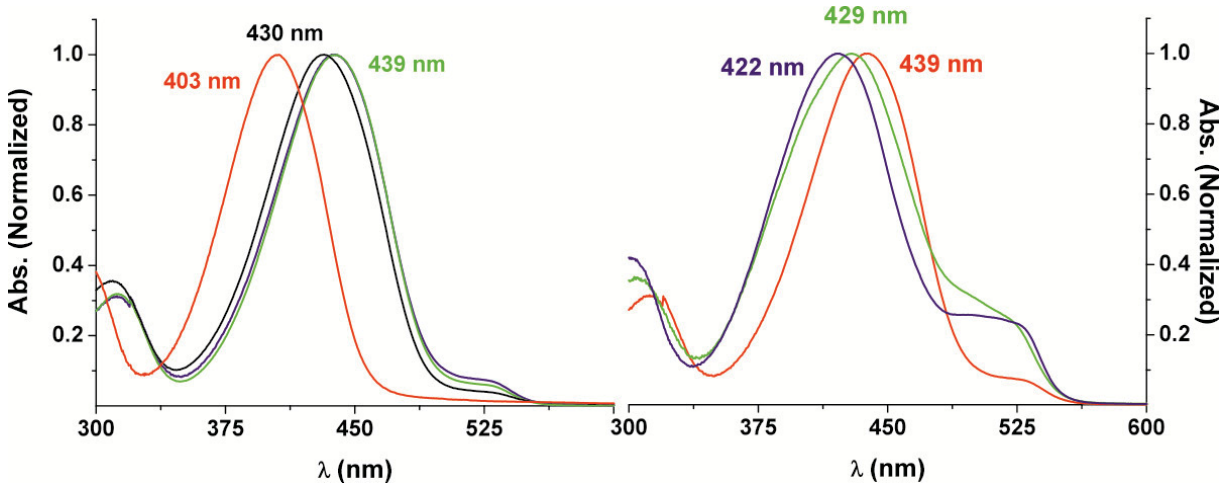

Fig. 14.10 Left: Normalized absorption spectra of **M7** (1 mM) in $CHCl_3$ (red), the complex with TBA-Z-L-Phe (blue), after addition of co-monomer and cross-linker (green) at room temperature and after heating at 80 °C (black). Right: Normalized absorption of **M7**:TBA-Z-L-Phe complex (1 mM) in $CHCl_3$ (red), in MeCN (green) and in THF (blue).

14.6 NMR titration

The H-bonding/deprotonation dualism was further investigated by NMR titrations. **M7** was mixed with 0.25, 1 and 4 equivalents of TBAA and TBA-Z-L-Phe respectively in $CDCl_3$ and the NMR spectra were registered.

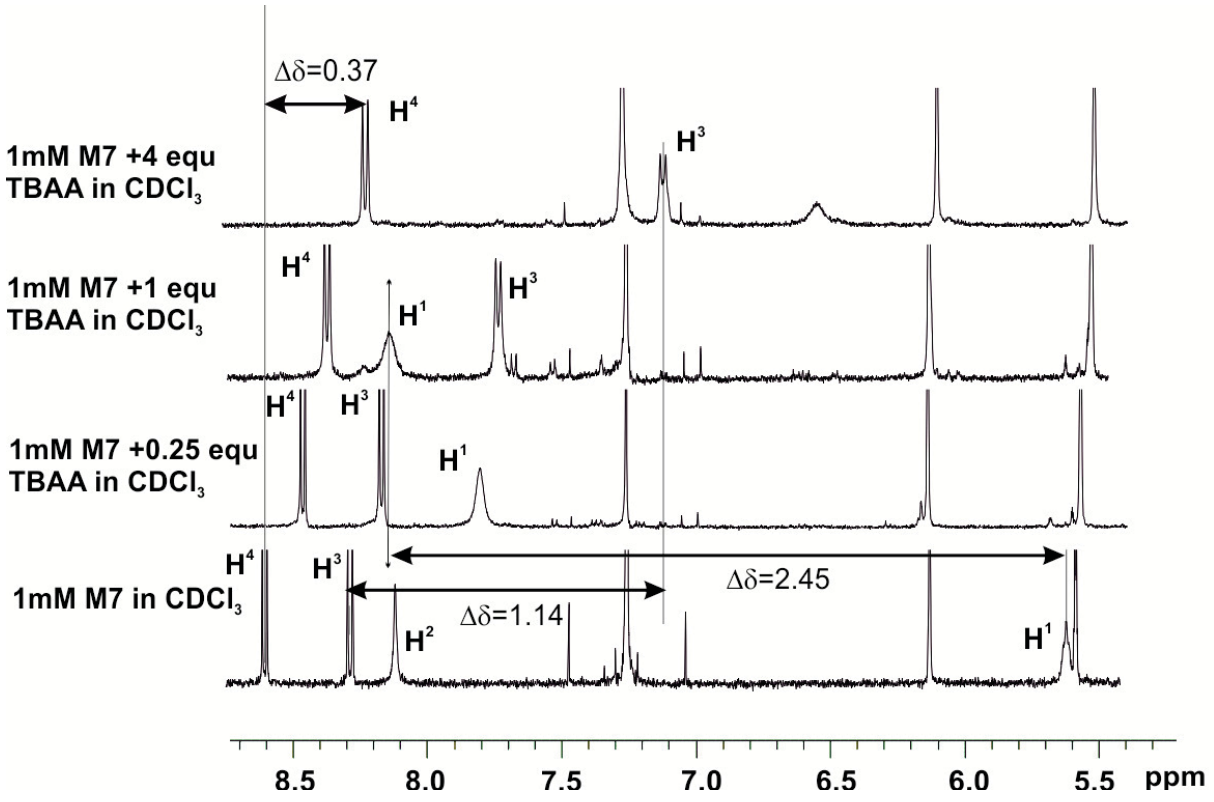

Fig. 14.11 NMR titration spectra of **M7** with TBAA in $CDCl_3$. The titration was carried out in steps of 0.25, 1, and 4 equivalents from bottom to top

As shown in **Fig. 14.11**, in the case of interaction with tetrabutylammonium acetate (TBAA), one of the urea protons $\mathbf{H^1}$ (red) shifted steadily down-field. The other urea proton $\mathbf{H^2}$ is invisible due to the deprotonation. The two protons at the benzene ring $\mathbf{H^3}$ and $\mathbf{H^4}$ steadily shifted up-field. At the last step M:T=1:4, the signal for the urea proton $\mathbf{H^1}$ also disappeared.

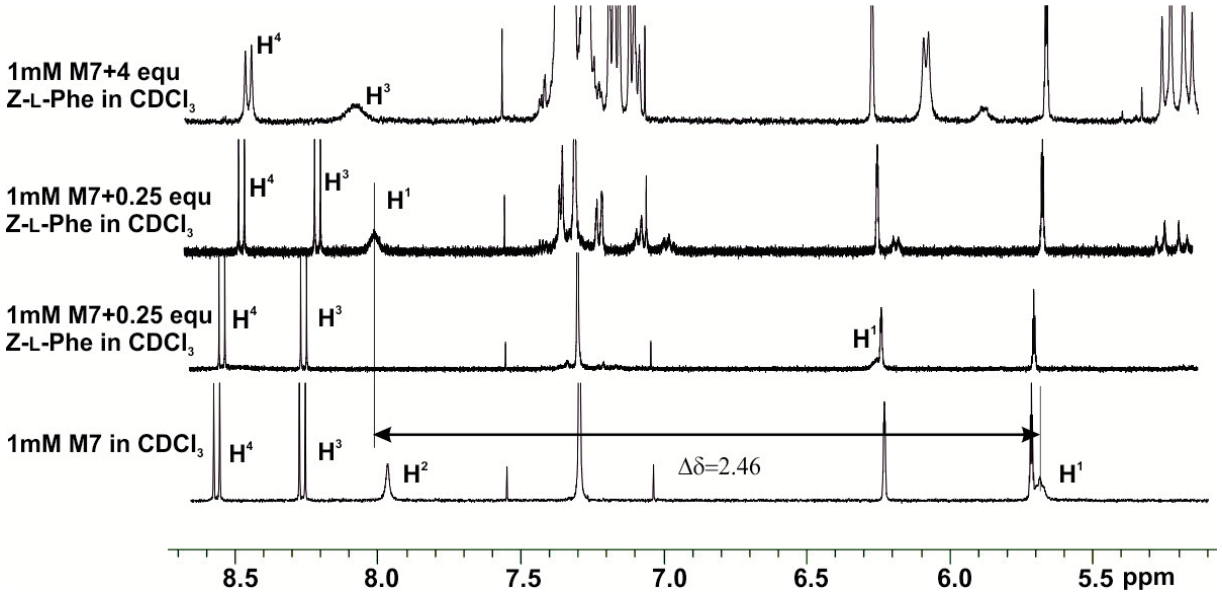

Fig. 14.12 NMR titration spectra of **M7** with TBA-Z-L-Phe in $CDCl_3$. The titration was carried out in steps of 0.25, 1, and 4 from bottom to top

In the case of H-bonding formation with TBA-Z-L-Phe shown in **Fig. 14.12**, the two protons on the benzene ring $\mathbf{H^3}$ and $\mathbf{H^4}$ remain unaltered, only at the last step, they shifted slightly up-field, which might be due to minor deprotonation at the high concentration. Referring to the fluorescence titration spectra, the deprotonation is also observed at high excess of anion (see Section 14.4). The urea proton $\mathbf{H^1}$ shifted steadily down-field, at the last step, the signal becomes broad which can also be attributed to the partial deprotonation. However, the other urea proton $\mathbf{H^2}$ is invisible at the beginning of anion addition.

In conclusion, **M7** shows a considerably high affinity to carboxylate anions. Although its high acidity gives rise to a H-bonding/deprotonation dualism for several combinations of target anion, counter-ion and solvent, deprotonation is negligible under imprinting conditions for our model amino acid template Z-L-Phe when used as TBA salt in $CHCl_3$ as the porogen. The clear advantage of **M7** is that it shows an obvious fluorescence enhancement upon formation of the H-bonding complex. This promises that upon successful preparation of a fluorescent MIP sensor, a turn-on response might be obtained (see Section 18.8).

15 Phenazine-based Monomers

The last fluorogenic monomer investigated in this thesis is a phenazine-type dye containing two urea binding sites per dye unit. The monomer was prepared through a single step condensation reaction from commercially available 2,3-diaminophenazine with an isocyanate precursor of the polymerizable unit following a route recently established by a project partner.[185] This monomer has two polymerizable urea arms which can play a role both as recognition site and for the integration into the polymer matrix.

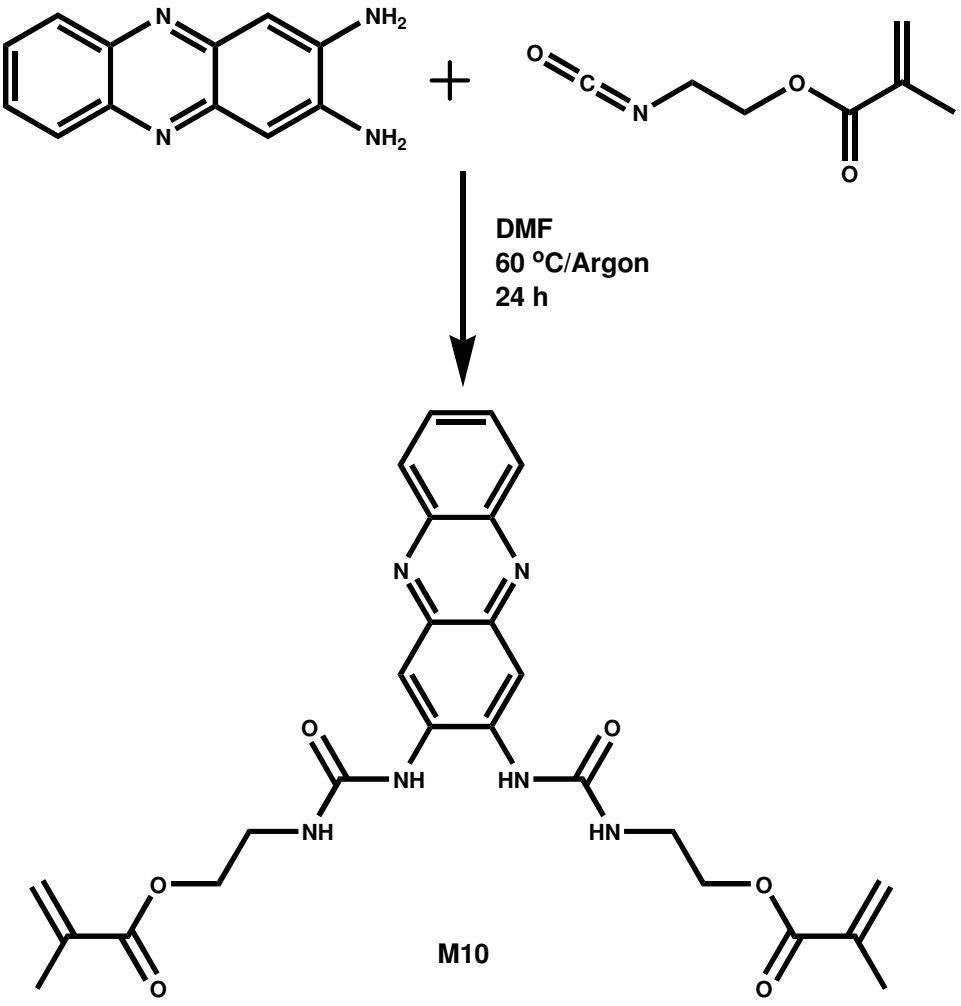

Scheme 15.1 Synthesis route of **M10**

15.1 Spectroscopic properties

In MeCN, the absorption maximum of **M10** lies at 403 nm with a considerable absorption coefficient of 17800 (L $mol^{-1}cm^{-1}$) and the emission maximum at 494 nm. It is a solvatochromic dye and the spectra are bathochromically displaced when increasing the solvent polarity, the data are listed in **Table 15.1**. Similar to the other urea-based fluorogenic monomers, **M10** shows also only a limited solubility in most relevant solvents except for DMSO and DMF. However, the solubility is greatly enhanced in the presence of anion species that can be bound by the probe monomer. The complexation of an anion always introduced a red shift in both absorption and emission, accompanied by an enhanced absorption coefficient and fluorescence QY.

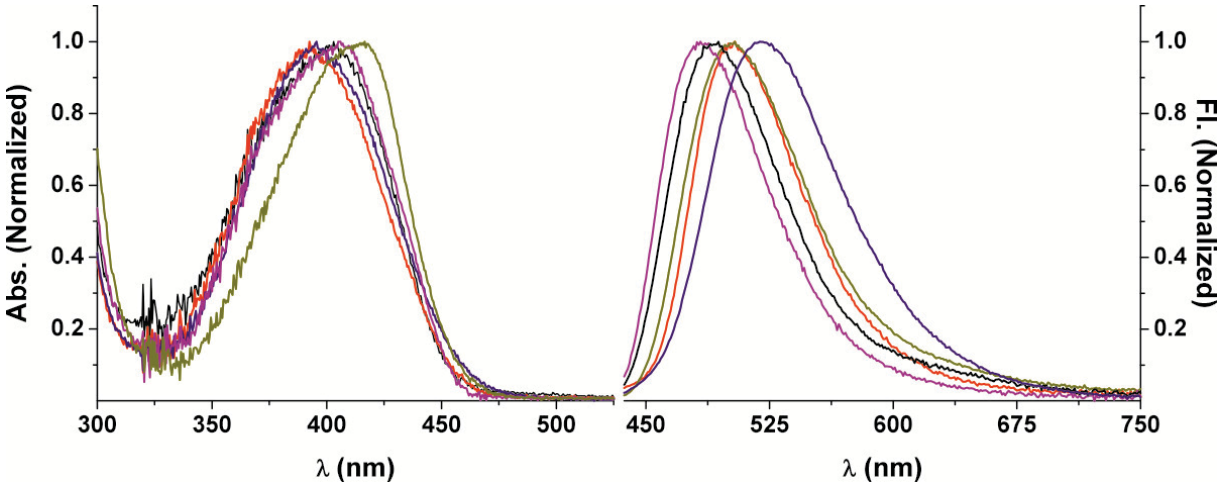

Fig. 15.1 Normalized absorption (left) and fluorescence (right) spectra of **M10** in selected solvents, MeCN (black), $CHCl_3$ (red), MeOH (blue), THF (magenta) and DMSO (dark yellow)

Table 15.1 Spectroscopic properties of **M10** in selected solvents

	λ_{abs}/ nm	λ_{em}/ nm	Φ_f
$CHCl_3$	392	504	0.027
THF	405	483	0.019
MeCN	403	494	0.028
MeOH	395	519	0.124
DMSO	416	504	0.055

15.1.1 Excited State Proton Transfer

As will be seen in the subsequent Sections and in 18.9, different to most other fluorogenic monomers and probes, **M10** has another promising signal transduction mechanism: Excited State Proton Transfer (ESPT). This mechanism is based on the different acidity of the fluorophore in the ground and excited state (**Fig. 15.2**). Amino groups in a fluorophore, especially if a CT process plays a role upon excitation, are commonly more acidic in the excited state than in the ground state (**Scheme 15.2**). In a tightly bound H-bonding complex the possibility thus exists that a proton will transfer from the excited fluorophore to the anion within the complex on a very fast time scale (usually a few picoseconds). Due to the fast relaxation of fluorescence and if the complex stability is high enough in the excited state, the ESPT complex remains associated during its lifetime and can emit the excitation energy by means of a strongly red-shifted, so-called ESPT fluorescence, which is followed by the back proton transfer and restoration of the fluorophore within the complex again in the ground state. Throughout the whole excitation/relaxation cycle the complex stays intact and only the proton shuttles, i.e., strong dipole moment changes occur. The latter results in a strong shift between the two emission bands. Compared to the other transduction mechanisms, the ESPT is very interesting because of its exceptionally large Stokes shift between complex absorption and ESPT complex fluorescence. Since also the LE fluorescence is especially significant, this behavior can be exploited for ratiometric measurements.

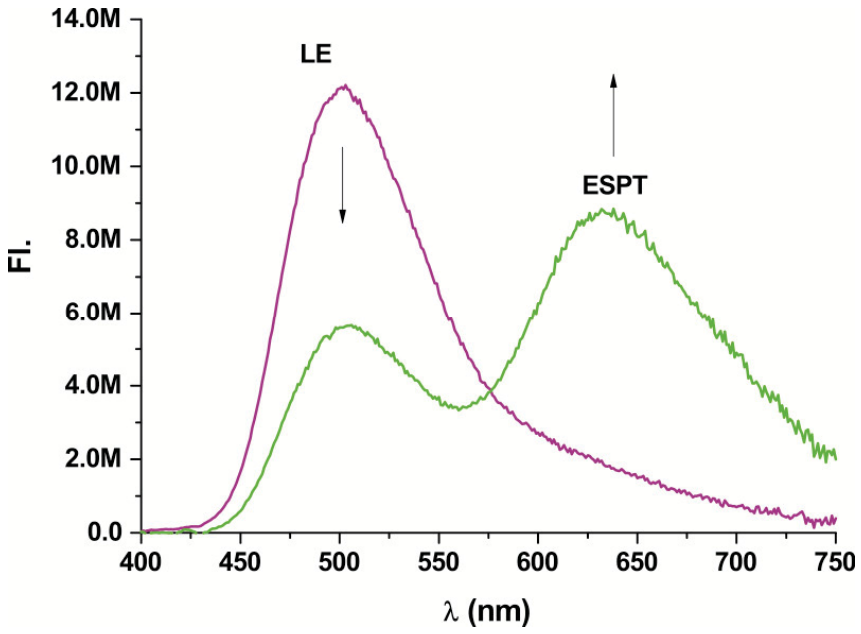

Fig. 15.2 Fluorescence of a dye in LE and ESPT state

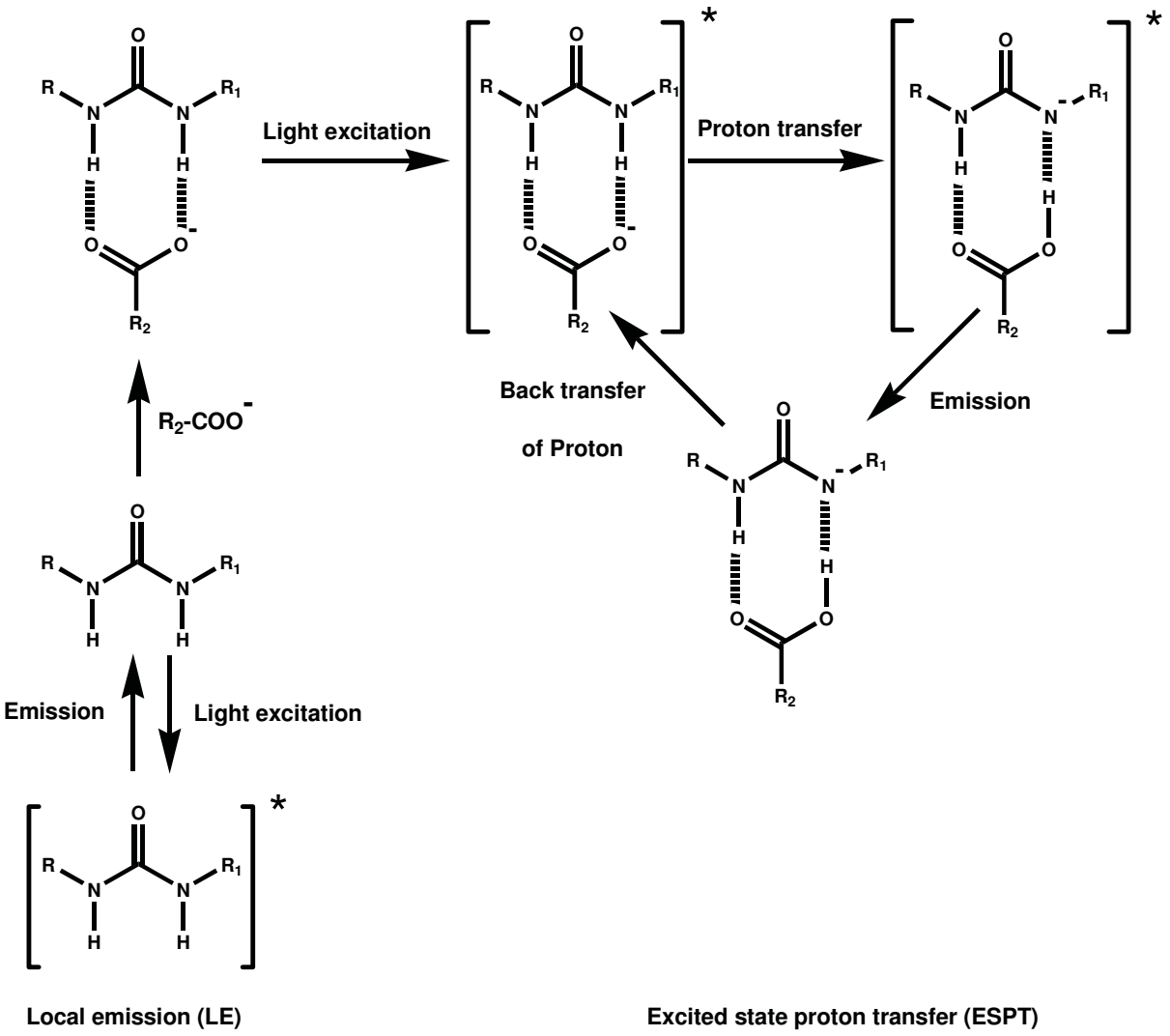

Scheme 15.2 Transduction mechanism of ESPT

There are only few fluorophores which show an intramolecular ESPT emission.[186, 187] Moreover, even less examples of excited host-guest complexes that show intermolecular ESPT fluorescence have been reported.[188, 189] The latter is particularly attractive when both the free probe and the ESPT state are emissive because two well-separated emission bands, which are also distinctly Stokes shifted with regard to the probe's and the complex's absorption, should arise and enable ratiometric signal assessment. Another important criterion of the ensemble is that the corresponding acid of the anion should have a pK_a that lies between the pK_a of the fluorophore in the ground and the excited state (pK_a*). As will be discussed in the following, the phenazine derivative **M10** can undergo ESPT when bound to

phosphate anions. Because phosphates play a key role in protein biochemistry, see also Section 12.3, only this type of analyte was studied with the phenazine monomer.

15.2 Binding studies

The binding studies were performed with phenylphosphate (PPA). With weak bases such as mono-deprotonated TBA-PPA, i.e., $[N(C_4H_9)_4^+]$ $C_6H_5OPO_3H^-$, the monomer shows a red shift of the absorption band from 402 nm to 421 nm with an increase of the absorption coefficient. An isobestic point is observed at 386 nm. The fluorescence shows firstly an enhancement with a slight spectral shift from 488 nm to 502 nm. Subsequently, an ESPT band at 633 nm developed with the concomitant decrease of the locally excited (LE) band at 502 nm (**Fig. 15.3**). The binding constant for the ESPT process was determined to log$K$ = 5.22±0.02.

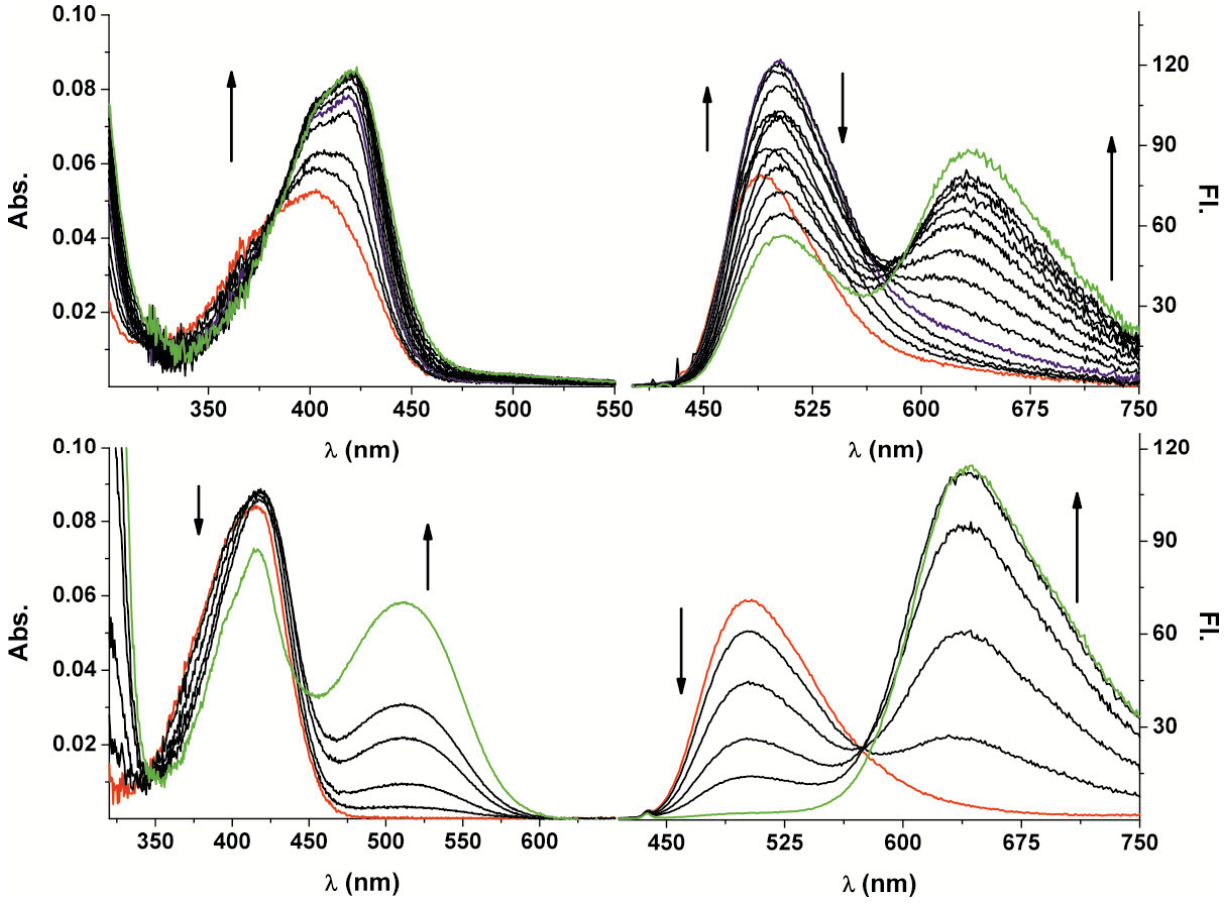

Fig. 15.3 Absorption titration (top left) and fluorescence titration (top right) spectra of **M10** (5 µM) with TBA-PPA in MeCN ($C_{TBA\text{-}PPA}$=2-700 µM) and the absorption titration (bottom left) and fluorescence titration (bottom right) spectra of **M10** (5 µM) with $(TBA)_2$-PPA in MeCN ($C_{(TBA)2\text{-}PPA}$=2-300 µM), (starting point spectra in red, end point spectra in green)

With the more basic anion (TBA)$_2$-PPA, i.e., $[N(C_4H_9)_4^+]_2$ $C_6H_5OPO_3^{2-}$, **M10** undergoes deprotonation in the ground state (**Fig. 15.3** bottom). This deprotonation is certified by the development of a new absorption band shifted for over 100 nm to longer wavelengths. In the emission spectra, a new band at 643 nm is developed and the LE band at 502 nm only decreases. Different to the case of TBA-PPA, there is no intermediate increase in the LE band and at saturation, the LE band has totally disappeared. This spectral similarity of the newly developed bands in both cases indicates that the emitting state of the ESPT is similar to that of the deprotonated state. Intermolecular ESPT fluorescence arising from dye-acid [190, 191] or dye-solvent [192, 193] contact pairs is known, further strengthening the conclusion that **M10** is a potent ESPT-active probe, which is especially valuable in the case of TBA-PPA.

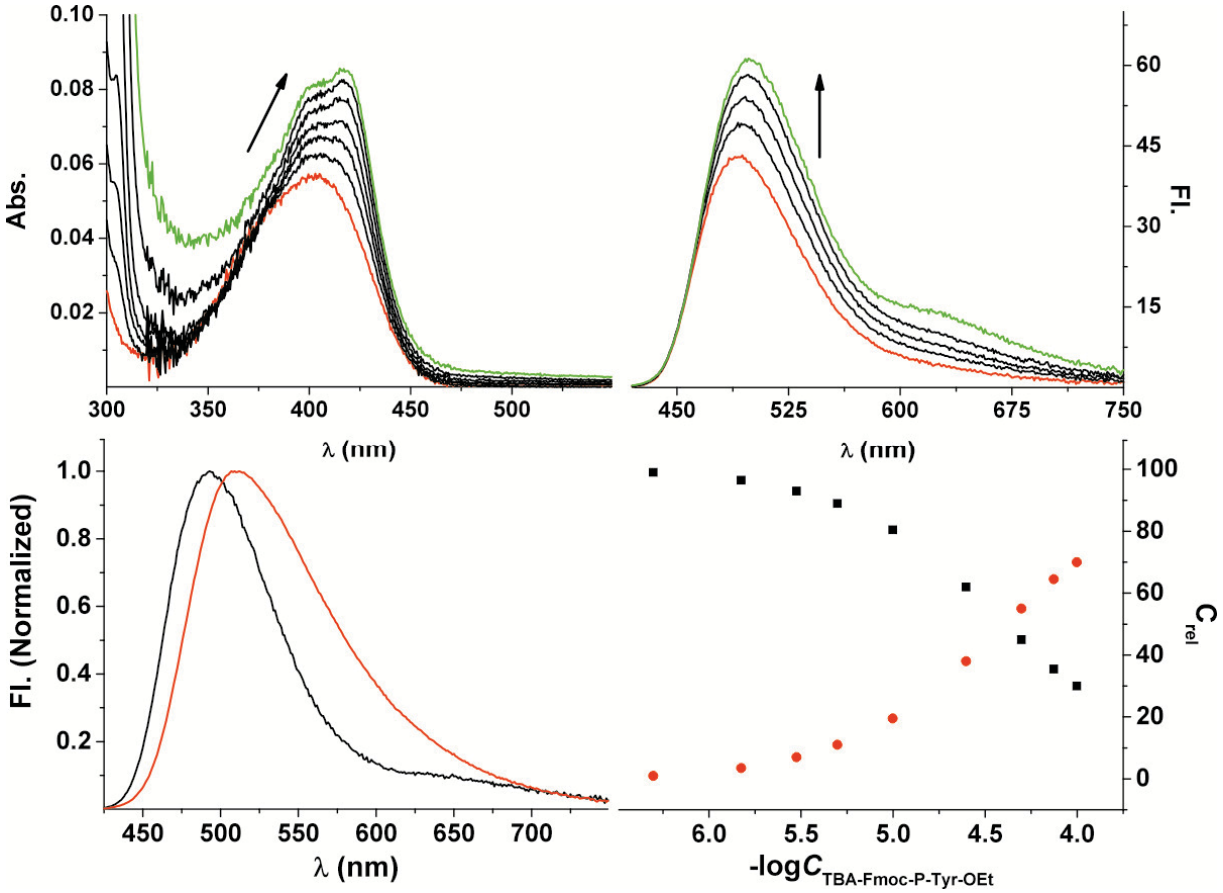

Fig. 15.4 Absorption (top left) and fluorescence (top right) titration spectra of **M10** (5 µM) with TBA-Fmoc-P-Tyr-OEt in $CHCl_3$ ($C_{TBA\text{-}Fmoc\text{-}P\text{-}Tyr\text{-}OEt}$=1.5-600 µM) (starting point spectra in red, end point spectra in red). Fitted results species spectra (bottom left) and relative concentrations during the course of the titration (bottom right), **M10** (black), **M10**⊂TBA-Fmoc-P-Tyr-OEt (red)

Fmoc-P-Tyr-OEt is a phosphorylated amino acid. Its anion has a lower basicity than PPA. The complexation was also studied with the mono and bi-deprotonated form. In case of the mono-deprotonated phosphate, only spectral shifts in both absorption and emission spectra were observed. However, the ESPT band was absent (**Fig. 15.4** top). This indicates that the anion's basicity is low and even in the excited state not strong enough to induce the proton transfer. When fitting the fluorescence titration data with Hyp Spec, two colored species with fluorescence maxima at 494 nm and 519 nm can be resolved (**Fig. 15.4** bottom), the binding constant can be calculated as log*K*=4.6±0.003. The H-bonding complex increased with the decrease of the free **M10.**

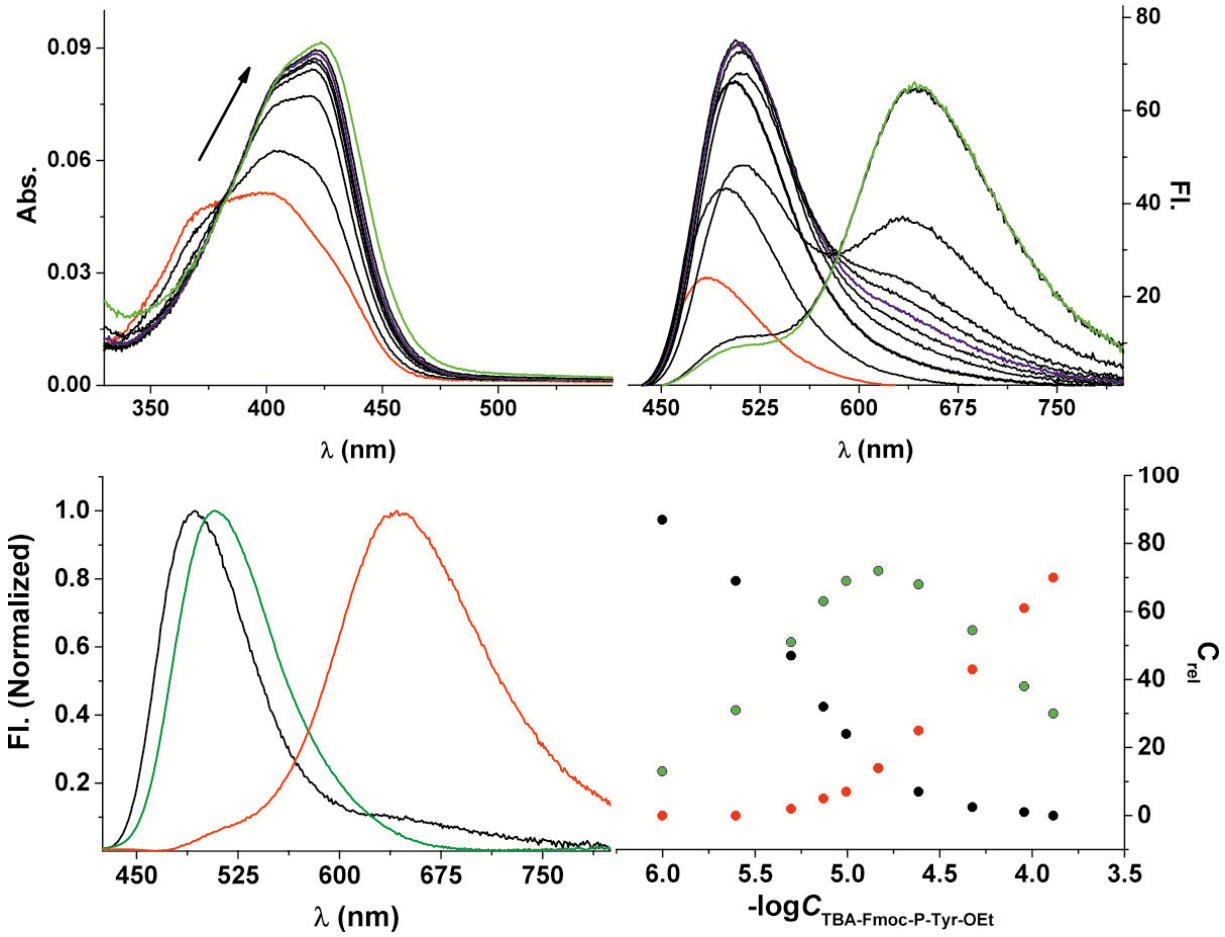

Fig. 15.5 Absorption (top left) and fluorescence (top right) titration spectra of **M10** (5 µM) with $(TBA)_2$-Fmoc-P-Tyr-OEt in CHCl3 ($_{CFmoc\text{-}P\text{-}Tyr\text{-}OEt}$=1.5-750 µM, starting point spectra in red, end point spectra in green). Fitting results with species spectra (bottom left) and relative concentrations during the course of the titration (bottom right) of free **M10** in black, local emission of **M10**⊂$(TBA)_2$Fmoc-P-Tyr-OEt in blue and ESPT emission in red.

The bi-deprotonated phosphate $(TBA)_2$-Fmoc-P-Tyr-OEt has a higher basicity. This species now shows a similar behavior as mono-deprotonated PPA. At first, the absorption and emission spectra show minor red shifts and an increase in intensity. Then an ESPT band develops with a concomitant decrease of the LE band (**Fig. 15.5**). During the entire experiment, no deprotonation was observed.

When fitting the fluorescence titration data with Hyp Spec, three species with fluorescence maxima at 494 nm, 518 nm and 649 nm can be resolved. They belong to the free probe, the simple H-bonding species and the ESPT species, respectively. The free probe decreases with the addition of $(TBA)_2$-Fmoc-P-Tyr-OEt, the H-bonding species first increases and later on decreases and the ESPT species increases until saturation (**Fig. 15.5**). The first process has a binding constant of $\log K$=6.7±0.003 and the second with $\log K$=4.5±0.002.

15.3 Pre-polymerization studies

In Section 18.9, it will be shown how **M10** is used to assemble SiO_2@MIP sensor particles for the detection of phosphorylated tyrosines. As already described for the monomers discussed above, pre-polymerization studies are an important step toward the successful preparation of such sensors. Such studies were carried out here for the mono- as well as di-deprotonated form of the template anion. Both anions form stable H-bonding complexes with **M10** and no deprotonation was observed in the pre-polymerization mixtures. In both cases, the bonding with analyte induces prominent red shifts in absorption spectra and no deprotonation was observed. The addition of co-monomer and crosslinker has less interference towards the H-bonding complex (**Fig. 15.6** left). However, the ESPT band is only observed in case of **M10** with $(TBA)_2$-Fmoc-P-Tyr-OEt (**Fig. 15.6** top right).

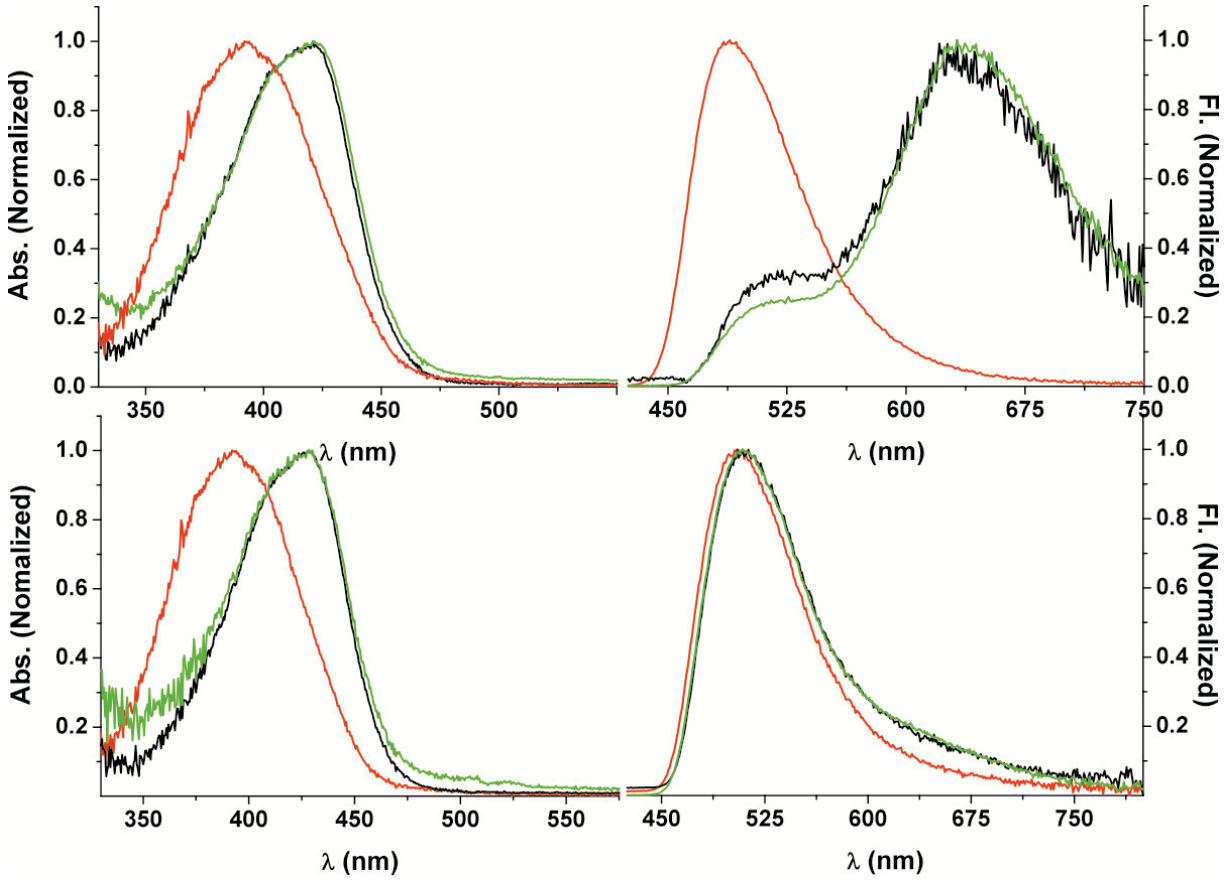

Fig. 15.6 Absorption (top left) and fluorescence (top right) spectra of **M10** with $(TBA)_2$-Fmoc-P-Tyr-OEt at pre-polymerization condition and absorption (bottom left) and emission (bottom right) of **M10** with TBA-Fmoc-P-Tyr-OEt at pre-polymerization conditions.

However, according to the pilot polymerization studies, the grafted polymer is influenced by the charge of the template. The imprinting effect is amended when directly using bi-deprotonated phosphate as template. Thus, mono-deprotonated phosphate has to be used as a kind of dummy template for MIP preparation.

15.4 NMR titration

The intermolecular H-bonding between **M10** and the phosphates was also examined by NMR titration. The formation of H-bonding complex is indicated by the down-field shift of the urea protons. Upon addition of mono-deprotonated PPA, both urea protons $\mathbf{H^1}$ and $\mathbf{H^2}$ shifted downfield by 1.49 and 1.23 ppm, respectively. $\mathbf{H^3}$ also shifted slightly downfield. $\mathbf{H^4}$ and $\mathbf{H^5}$ shifted slightly upfield. The shift ended after the addition of 2 equivalents of PPA which corresponds to a 1:2 stoichiometry (**Fig. 15.7**). This is further supported by the absorption and fluorescence spectra under pre-polymerization conditions. At high concentrations of 1 mM, the spectral shift due to complexation stops at a ratio of 1:2 of **M10** and phosphate anion.

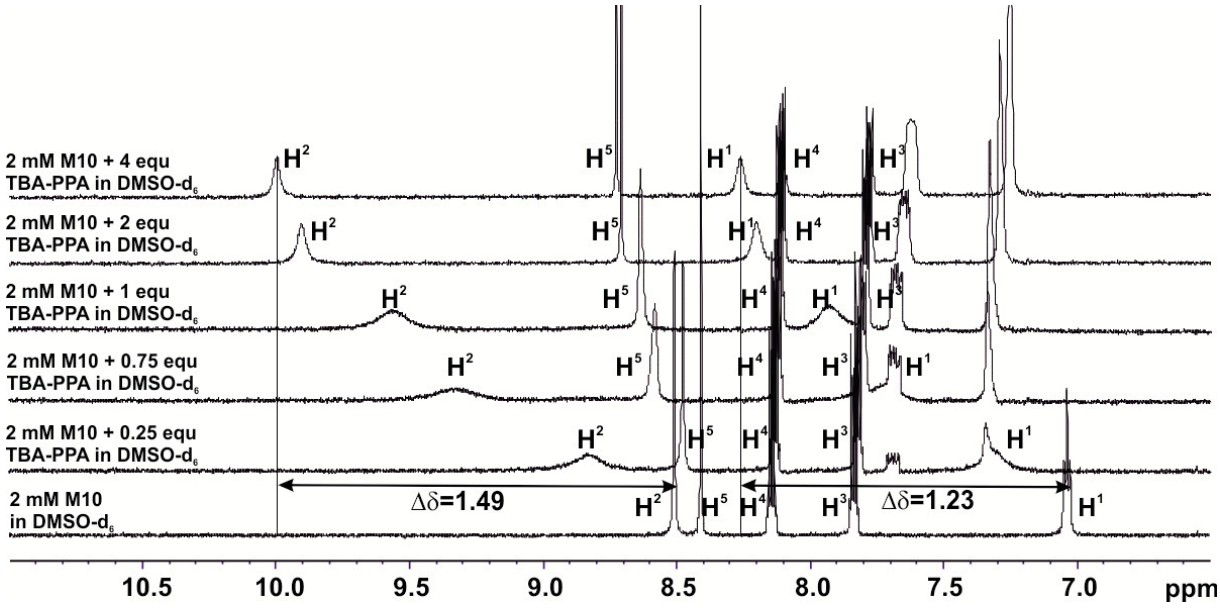

Fig. 15.7 NMR titration of **M10** with TBA-PPA in DMSO-d_6,

A further NMR-titration experiment was made using Fmoc-P-Tyr-OEt in the form of mono and bi-TBA salts (**Fig. 15.8**). This anion is later used as template for MIP preparation. In case of the titration in deuterated DMSO, both urea NH protons become broadened and difficult to resolve. In agreement with the UV/vis absorption spectra, which show the typical deprotonation band already at the first titration step, this signal broadening of the NH protons is also assigned to deprotonation. We thus transferred the experiment to less polar CD_3CN. In this case, both the urea NHs show downfield shifts and the aromatic protons shift slightly upfield. As shown in **Fig. 15.9** right and **Table 15.2**, in the titration of **M10** with $(TBA)_2$-Fmoc-P-Tyr-OEt, only the two NH protons $\mathbf{H^1}$ and $\mathbf{H^2}$ shifted down-field with 2.82 and 3.24 ppm respectively; $\mathbf{H^3}$ shifted slightly downfield. $\mathbf{H^4}$ and $\mathbf{H^5}$ shifted slightly upfield.

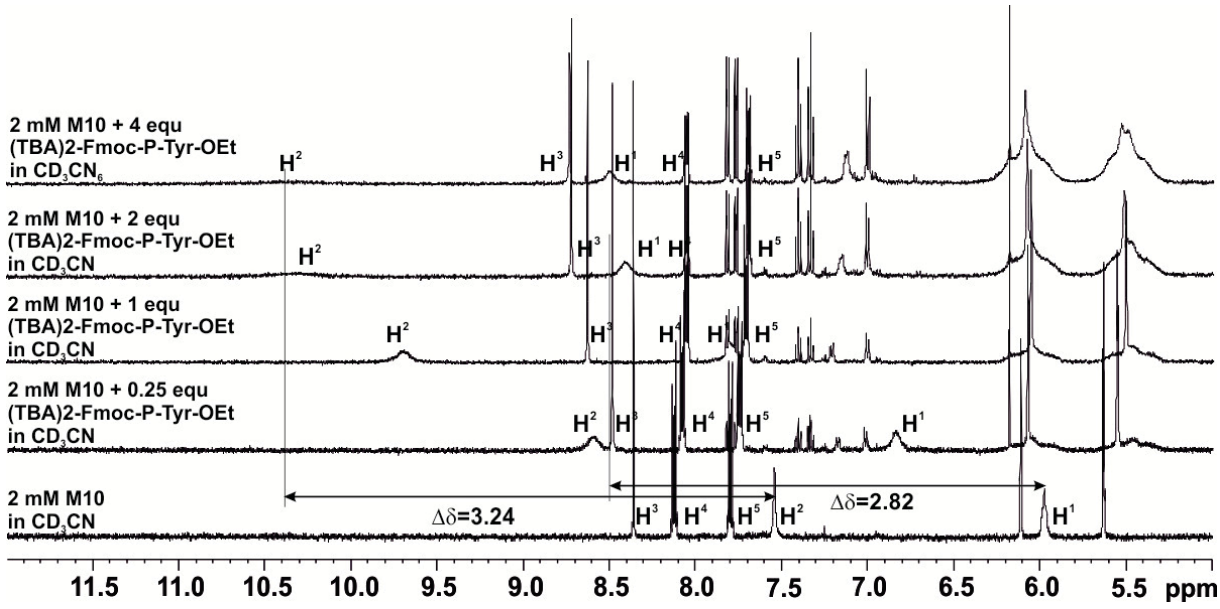

Fig. 15.8 NMR titration of **M10** with $(TBA)_2$-Fmoc-P-Tyr-OEt

When the titration was conducted with a less basic anion with similar geometry (mono-deprotonated phosphate salts), a similar chemical shift was observed, 2.77 and 3.24 for mono- as well as bi-deprotonated Fmoc-P-Tyr-OEt for $\mathbf{H^2}$ e.g. and the titration ended at a 1:2 equilibrium ratio in case of the mono-deprotonated species (**Fig. 15.9** left).

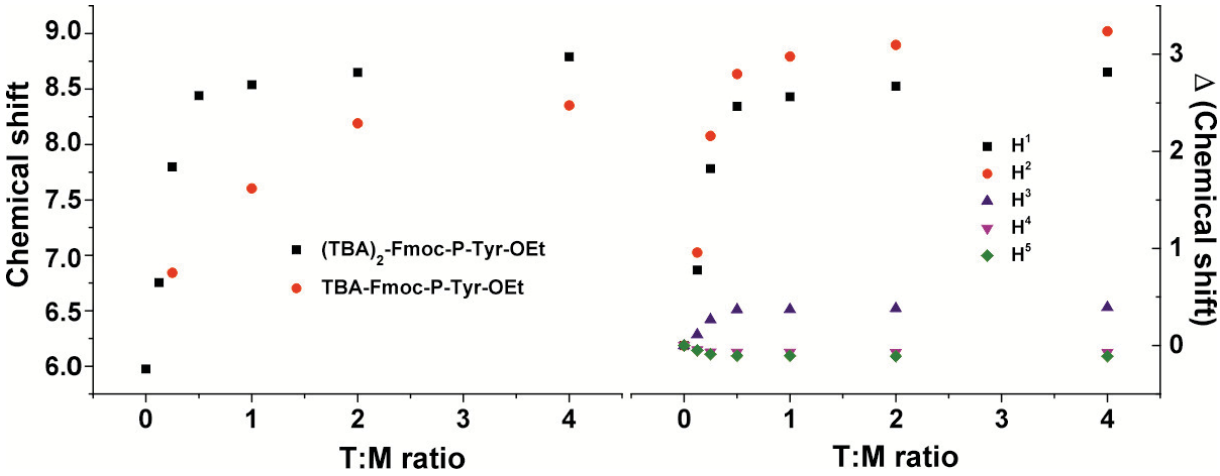

Fig. 15.9 Plot of chemical shift of $\mathbf{H^2}$ during titration of **M10** with TBA-Fmoc-P-Tyr-OEt (red) and $(TBA)_2$-Fmoc-P-Tyr-OEt (black) in MeCN (left) and chemical shift of all protons in $(TBA)_2$-Fmoc-P-Tyr-OEt in MeCN (right)

Table 15.2 Chemical shifts of **M10** titration with $(TBA)_2$-Fmoc-P-Tyr-OEt

Proton	1	2	3	4	5
M10	5.976	7.542	8.361	8.127	7.801
M10:T 8:1	6.754	8.500	8.472	8.082	7.750
M10:T 4:1	7.798	9.701	8.627	8.057	7.710
M10:T 2:1	8.440	10.34	8.730	8.055	7.694
M10:T 1:1	8.539	10.52	8.733	8.055	7.694
M10:T 1:2	8.649	10.64	8.743	8.054	7.690
M10:T 1:4	8.791	10.78	8.754	8.054	7.690

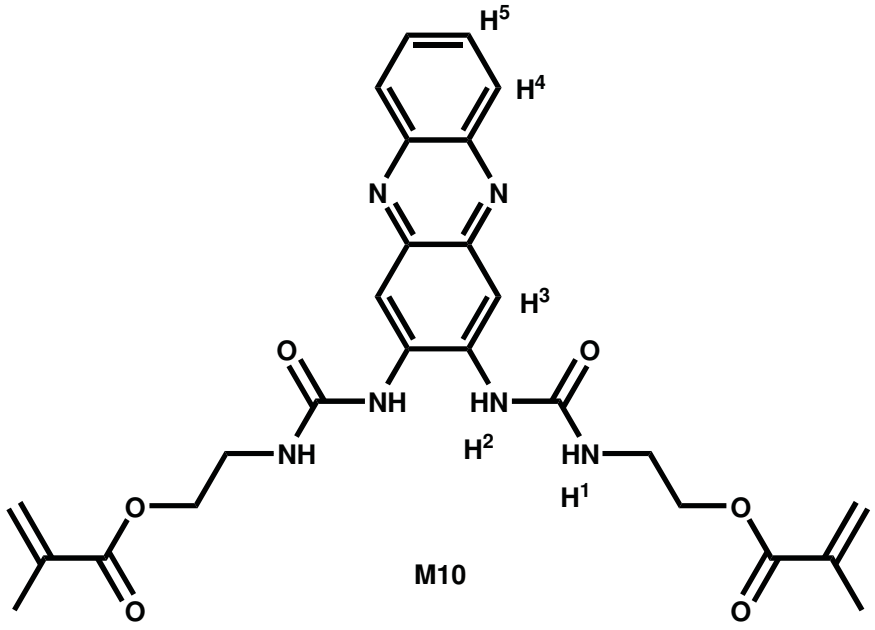

In conclusion, similar to the other urea monomers, **M10** also shows a considerably high affinity to oxy-anions. It has also convenient excitation and emission windows above 400 nm with fluorescence enhancing properties which is suitable for the preparation of fluorescence sensors. Besides and more interesting, this monomer shows an ESPT behavior which is sensitive to the basicity of the anion. After embedding this monomer into MIP matrices, a potential ratiometric sensor can be prepared.

16 Fluorescent MIP Monoliths

The conventional format of MIPs is a bulk polymer or monolith, which is commonly grounded into smaller particles for use in separation applications.[69] The advantage of this format is its simplicity: mix the precursors, polymerize the bulk, grind it into the desired particle size and employ it in the application.

A ubiquitous protocol is to mix all components (monomer, crosslinker, template, initiator, porogen) in a sealed glass tube and initiate the polymerization through either temperature or UV light. After polymerization, the tube is crashed and the bulk polymer is grinded and sieved to different sizes for further application.[194] However, bulk polymers have several drawbacks. First, the grinded particles always have irregular shapes. The binding sites are also heterogeneously distributed, with some of them even being buried deep in the matrix and thus being difficult to reach for both template extraction and rebinding.[195] The particles prepared through this method are always considerably large (5-100 μm).

Regarding the monomers used in this thesis, the preparation and performance testing of fluorescent MIP monoliths was attempted primarily for reference purposes, to get a better overview of the pros and cons of the different formats principally available for the development of sensors. Thus, only two of the monomers, **M6** and **M7**, were employed for MIP monolith preparation.

16.1 Monoliths from naphthalimide monomer

MIP monoliths containing the naphthalimide monomer **M6** were prepared in the Sellergren group with several templates by radical polymerization.[61] The imprinting performance was first examined with HPLC in classical terms of retention time and binding capacity. In these studies, the monolith MIPs showed longer retention times than the monolith non imprinted polymers (NIPs), revealing better binding ability. The MIPs displayed also a remarkable enantio-selectivity when prepared with Z-L-Glu as well as Z-L-Phe as template. The imprinting effect can further be controlled through adapting the mobile phase. However, as can be seen in **Picture 16.1**, only the NIP shows the typical orange colour of unperturbed **M6** and the MIP against penicillin G (PenG) on the right shows the red colour of the imprinted, H-bonding complex. The two MIPs against amino acids in the middle are brown and green respectively thus indicating that the majority of the contained **M6** probe monomers has been

deprotonated during the processing. The latter hampers the performance and led to divergent results for HPLC and optical spectroscopic rebinding.[61, 196] In this thesis, these monolith MIPs have only be investigated by time-resolved fluorescence spectroscopy to possibly derive further mechanistic insight. The results however were not too conclusive and will not be detailed here. In conclusion, **M6**-based monolith MIPs do not present a useful fluorogenic sensor format.

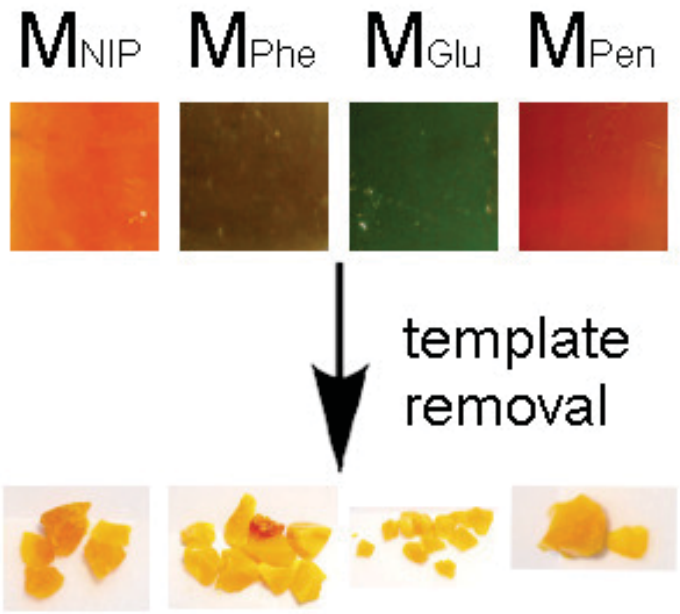

Picture 16.1 Colours of monolith MIPs prepared from **M6** and templates Z-L-Phe (second from the left), Z-L-Glu (second from the right) and PenG (right) prior to (top row) and after (bottom row) extraction; a representative NIP is shown on the left.

16.2 Monoliths from nitrobenzoxadiazole monomer

To verify the adequacy or inadequacy of the monolith format for fluorescent sensor MIPs, a second monomer was tested. Preparation proceeded in a similar fashion and was also carried out in the Sellergren group. The spectral properties (**Fig. 16.1**) of the grinded particles were then examined here. Due to the strong scattering signal from the sieved, irregular and rather large particles, the absorption spectra was registered through a reflectance mode and fluorescence spectra was measured using a front-face geometry. The maxima of fluorescence excitation and emission spectra were determined to 415 and 495 nm.

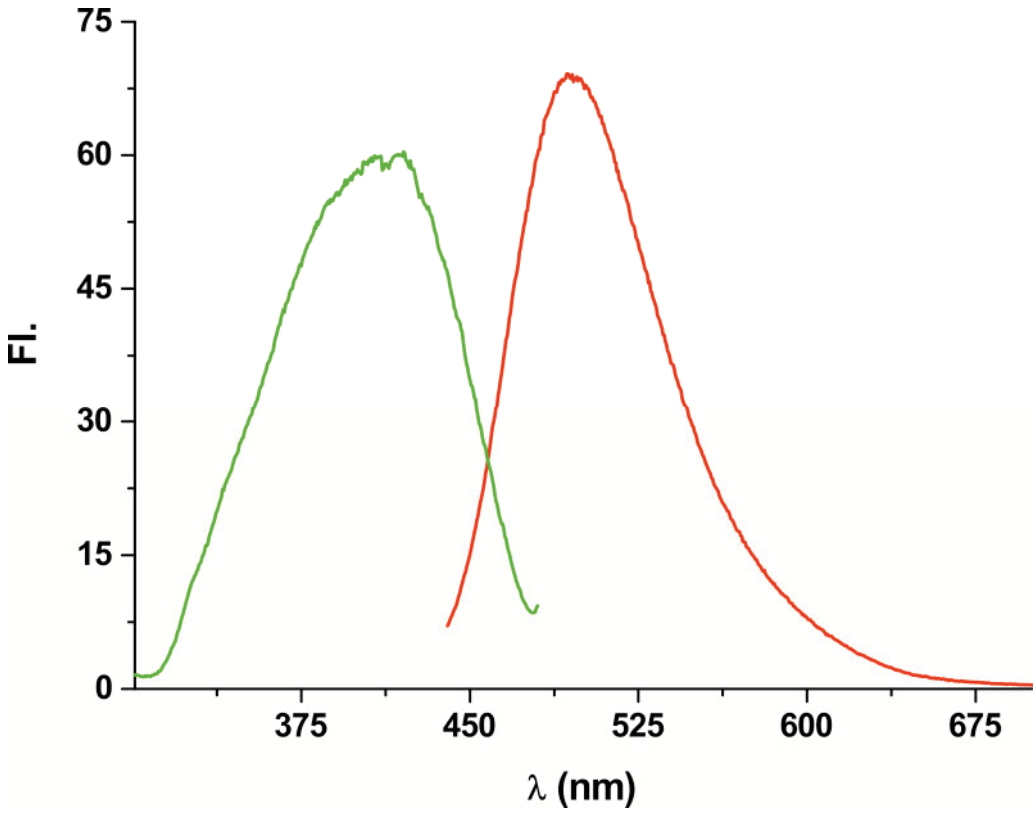

Fig. 16.1 Excitation (green) and emission (red) spectra of grinded **M7**-MIP monoliths

The sensing response was examined by incubation of the MIP/NIP particles in a solution containing the template and measurement of the fluorescence signal. No significant spectroscopic responses were observed. The irregular particle shape and considerably large particle size also made the acquisition of a stable measurement signal difficult. These findings indicate that the monolith is not a suitable format for an optical sensor. Monoliths were thus not further pursued in this work.

17 Fluorescent MIP Thin Films

Technically, thin films as such are a much more promising MIP format for optical sensor applications because such films, especially if they are optically transparent, can be coated on flat glass supports[74] or optical fibres[197]. Commonly, the thickness of thin films ranges from several nm to several µm.[61, 196] When coated on solid supports, thin films can also be prepared in the free-standing state for specific applications as membranes.[198]

In our studies, the MIP thin films were prepared according to **Scheme 17.1** directly on surface-activated cover slips. These slips were first washed with diluted HCl to remove residual metal ions, followed by a further activation step using piranha solution (3:1 H_2SO_4: H_2O_2). The slips were suspended in acidic piranha solution for 30 minutes. These freshly activated slips were further modified with methacrylate functional groups by suspending the supports in methacryloxy propyltriethoxysilane (MPTES) solution. These activated glass surfaces are thus covered with methacrylate groups for subsequent covalent anchoring of the MIPs.

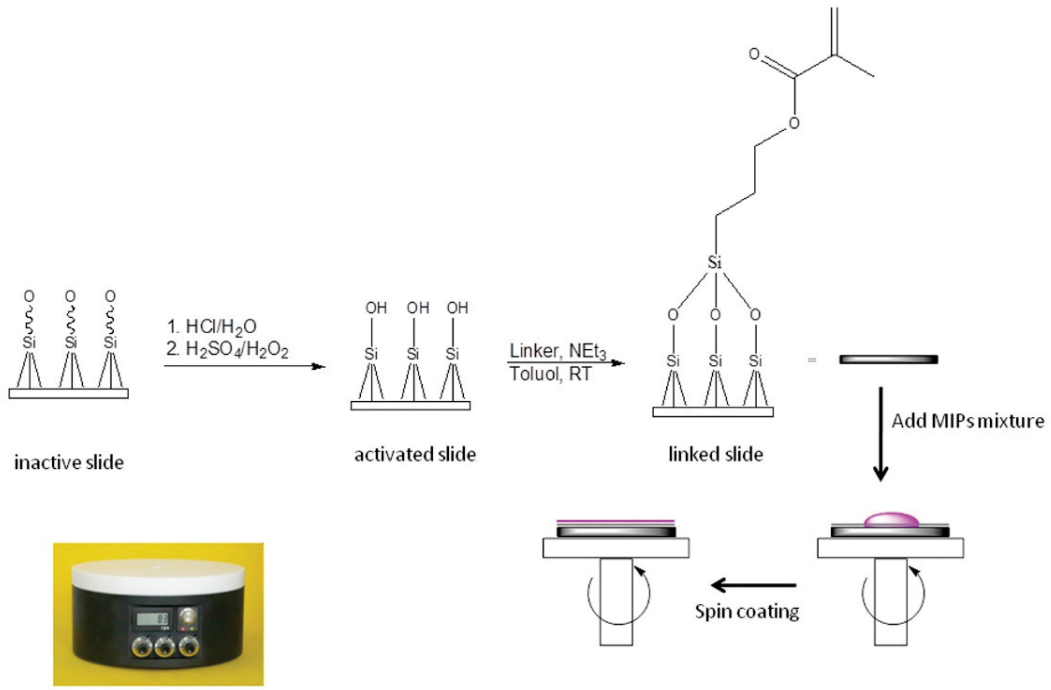

Fig. 17.1 Preparation procedure of MIP film

17.1 Thin films from naphthalimide monomer

M6 was the first monomer employed for this format and Z-L-Phe was used as primary template. The pre-polymerization mixture was prepared with methyl methacrylate (MMA) or benzyl methacrylate (BMA) as co-monomer and EDMA as crosslinker. The performance is quantified by impriniting factor α, which is defined as the ratio of fluorescence enhancement factor of MIP and NIP $\Delta F_{MIP}/\Delta F_{NIP}$ after addition of template molecule. In the case of the MMA/EDMA recipe, an imprinting factor of 3.4 was observed at 0.5 mM template stock solution (**Fig. 17.2**). The enantio-discrimination factor $\beta=\Delta F_{Z\text{-}L\text{-}Phe}/\Delta F_{Z\text{-}D\text{-}Phe}$ was determined to 1.7. Both values are rather promising results compared to previous work.[58]

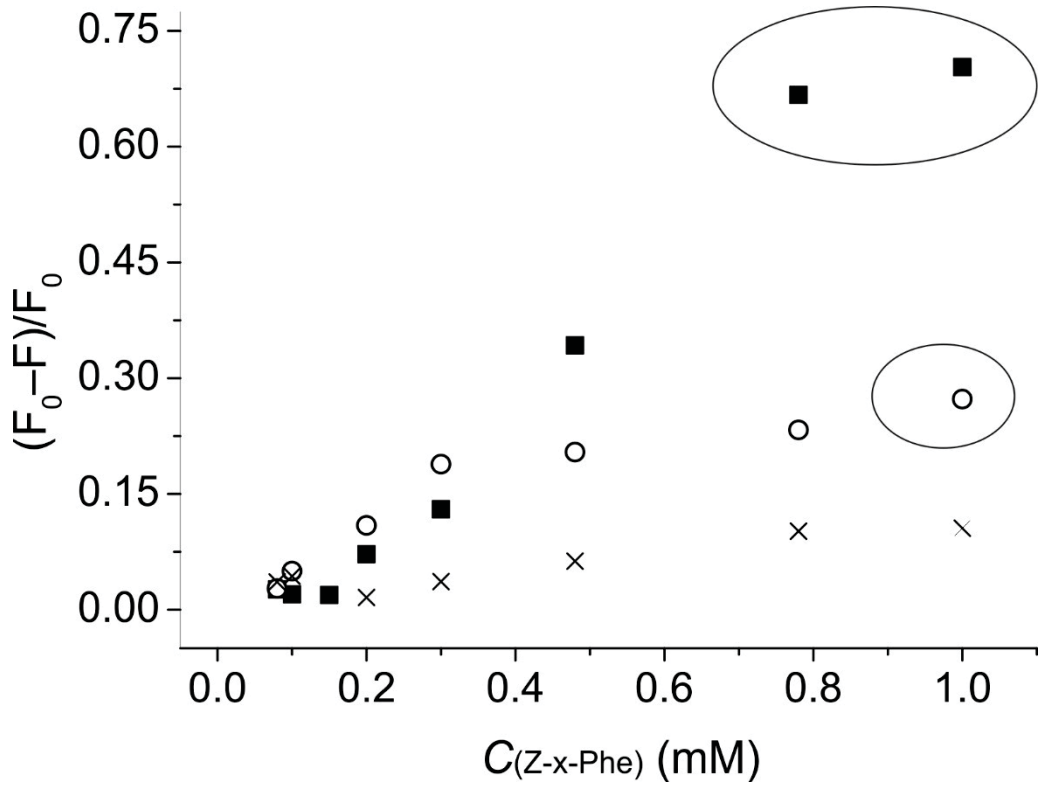

Fig. 17.2 Titration curves of MIP film prepared with MMA and EDMA in the presence of Z-L-Phe (squares) and Z-D-Phe (circles) as well as NIP film in the presence of Z-L-Phe (crosses) in acetonitrile; encircled data points at higher concentrations belong to spectra that show already contributions of deprotonation, i.e., the quenching recorded for these points is disproportionally large.

After changing the co-monomer from MMA to BMA, the imprinting factor α is even further increased to 18.6 and the enantio-discrimination factor β rises to 2.8 (**Fig. 17.3**). This

improved performance can be attributed to the additional π-π stacking interaction from the BMA co-monomer which enables multi-point recognition.

Although the preparation and application of MIP thin films was reported by many research groups,[61, 196] their use in real sensing applications is still limited.[199] The difficulty lies in the control of the polymer layer, both in thickness as such and in homogeneity. Film thickness is most crucial in terms of film stability, e.g. for repetitive use, and response times for achieving fast equilibration both in the presence and absence of the analyte for continuous sensing applications. In addition, swelling phenomena have to be taken into account. For instance, although very thin MIP films can be synthesized through electro-polymerization, the stability of these thin films is poor and reversible use is difficult,[74] which would greatly increase the assay costs in a real application.

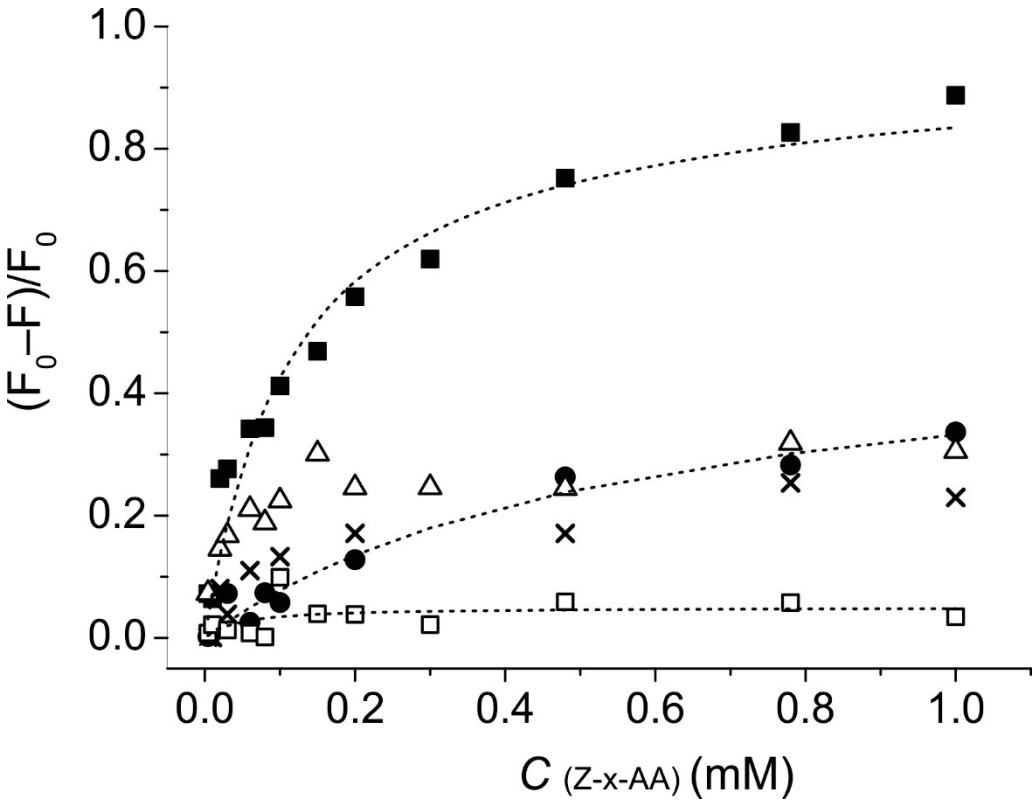

Fig. 17.3 Titration curves of MIP film in the presence of Z-L-Phe (squares), Z-D-Phe (circles), Z-L-Glu (crosses) and Z-L-Tyr (triangles) as well as NIP film in the presence of Z-D-Phe (squares) in acetonitrile; lines are only guides to the eye for MIP with Z-L-Phe, MIP with Z-D-Phe and NIP with Z-D-Phe; AA = amino acid.

17.2 Thin films from nitrobenzoxadiazole monomer

Besides the fluorescence turn-off thin films incorporating **M6**, the most promising nitrobenzoxadiazole monomer **M7** was also employed for film preparation to potentially obtain turn-on MIP sensor layers. For this purpose, the MIP synthesis mixture was first pre-polymerized at 50 ^{o}C to form a viscous solution. The viscous solution was then carried onto the glass slide by spin coating and sealed in a home designed reactor (**Picture 17.2**) for complete polymerization. The total polymerization succeeds in 18 h at 50 ^{o}C and maturation was achieved at 70 ^{o}C for 2 h. The prepared thin film-coated slips were Soxhlet-extracted with MeOH for 24 h to remove the template.

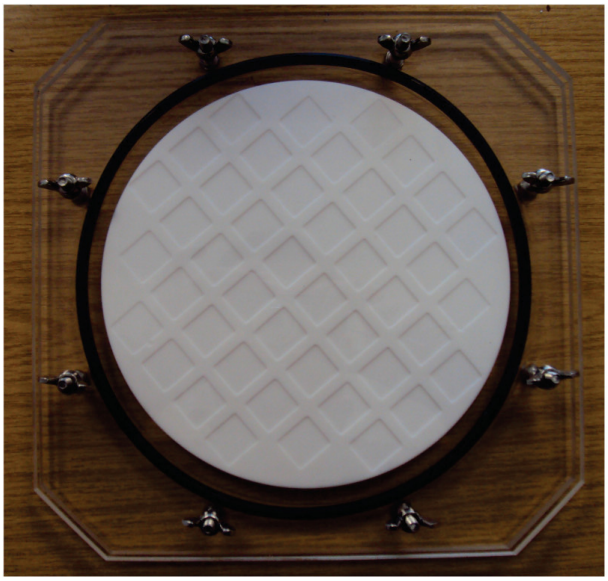

Picture 17.2 Home-designed MIP film preparation device

The imprinting effect was examined through template rebinding experiments. This rebinding is carried out by dipping the slide into a stock solution of the template molecule and measuring the fluorescence with a fluorometer using a front-face set-up.

As can be seen in **Fig. 17.4**, the MIP film shows a red-shifted emission maximum compared to the NIP film after synthesis, i.e., before extraction. After extraction with MeOH, the MIP film shows blue shifted spectra, and rebinding of the template leads again to a bathochromic shift. These changes are in accordance with the expected template extraction and rebinding cycle. However, the NIP film shows a red shift after subjecting it to a similar

extraction procedure with MeOH; incubation in template solution then does not induce any noticeable changes in emission. The bathochromic shift of the fluorescence of the NIP film after extraction is attributed to a change of the polarity in the microenvironment around the embedded probe molecules. The unchanged spectra after incubation of the NIP films in template solution indicate that these microenvironmental effects are most likely not due to the formation of (sizeable) cavities in the NIP, because no response toward the template and hence no unspecific binding is observed, but due to swelling of the polymer film as such.

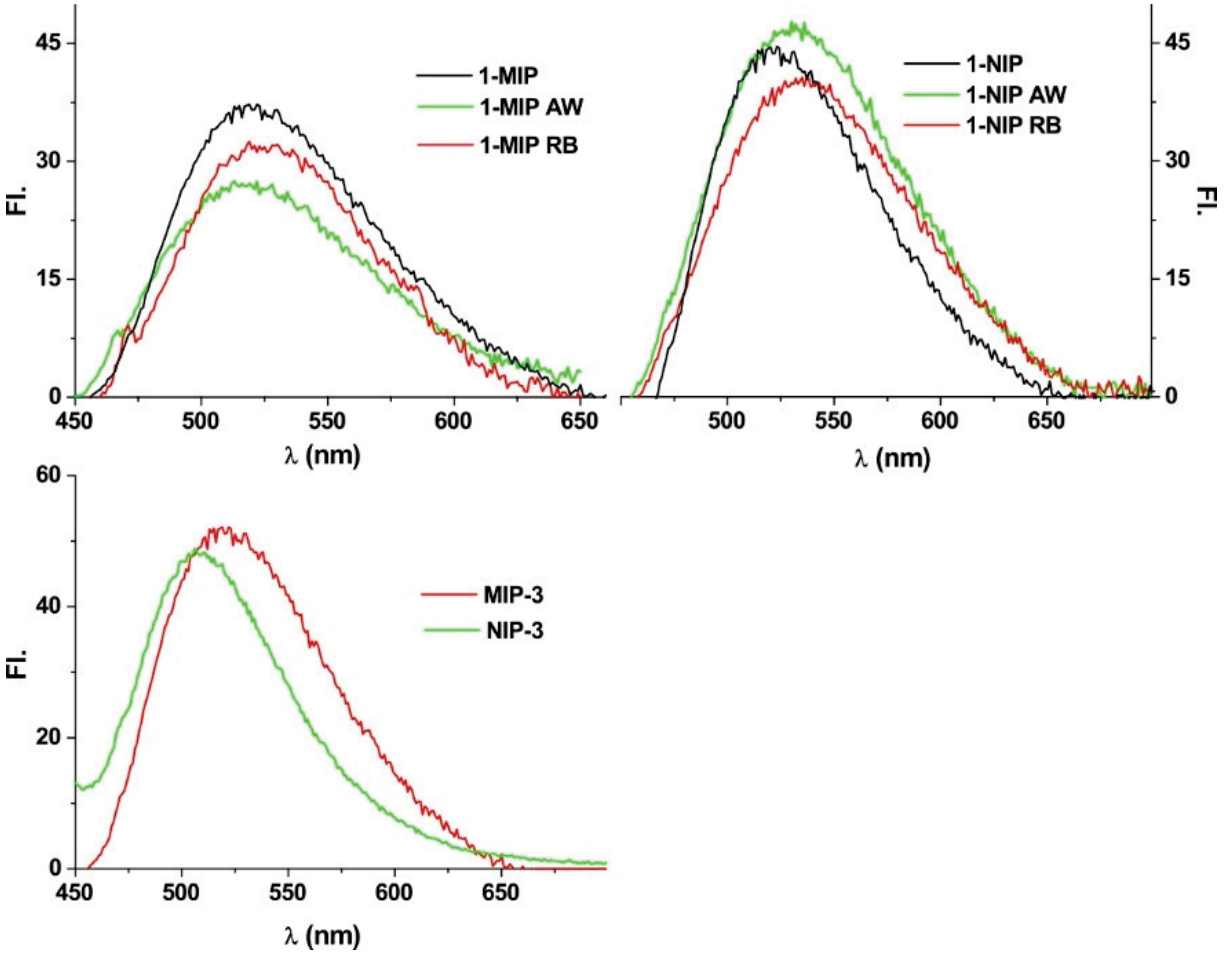

Fig. 17.4 Fluorescence spectra comparison (bottom) of **M7** film, MIP (red) and NIP (green), spectra response of MIP (bottom left) and NIP (top right) towards template (TBA-Z-L-Phe), after synthesis (black), after extraction (green) and after dipping into 5 mM template stock solution in $CHCl_3$ (red).

Although the qualitative response of the system looks promising, these swelling effects make a quantitative analysis very difficult. Intensity changes would not only be due to the presence of a certain amount of analyte, but would also depend on the degree of swelling in the medium of application and possibly also on spectral shifts as a consequence of changes in polarity or ionic strength of the sample medium. Although the prepared films are only ca. 2 µm thin as determined by SEM shown in **Fig. 17.5**, this layer is still considerably thick to undergo sizeable swelling. In addition, the polymer surface is also not smooth, which can introduce additional positioning or focus errors during measurement, especially when such films are used in dipping and not in continuous monitoring analysis. Thus the quantification becomes inherently difficult.

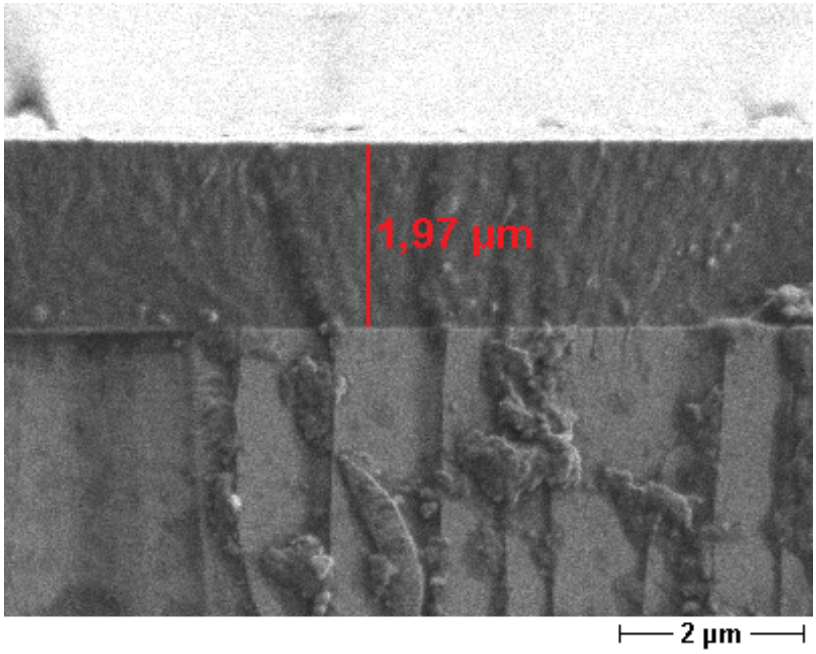

Fig. 17.5 Image of a representitaive MIP film (ca. 2 µm thick) coated on a glass slip.

18 Fluorescent Silica Core-MIP Shell Particles

Chapters 16 and 17 revealed that neither MIP monoliths nor MIP thin films are an ideal format for sensor applications. Whereas the first shows generally inferior features when considering optical sensing applications, the second shows significant drawbacks with regard to reliability and quantification. The final quest in this thesis thus was to develop a format with improved features.

Recently, core-shell particles have been intensively studied in many groups.[200, 201] They can be prepared by grafting a thin organic/inorganic polymer shell onto an organic/inorganic particle core. Core-shell particles have also been employed in the context of MIPs, i.e., the MIP here generally represents the shell domain. A further advantage of core-shell particles is that they are usually homogeneous in shape and size, which improves batch-to-batch reproducibility. The commonly smaller particle sizes, smaller than grounded monoliths, increase greatly the surface area and hence the amount of accessible binding sites. The thin shell also decreases the average diffusion path length, which makes rebinding much faster than in a bulk polymer. This also reduces the amount of non-accessible binding sites. With regard to sensor applications, this reduces the background signal and permits to reach a better sensitivity.

18.1 Preparation of core particle

SiO_2 is a good candidate as the core material. It can be easily prepared in the lab through sol-gel chemistry and silica particles are also commercially available in various sizes. A great variety of surface modification agents is available to provide plenty of grafting strategies. The high density of SiO_2 facilitates handling and especially washing procedures.

The so-called Stöber method, developed by Stöber in 1968,[202] has become a ubiquitous method to prepare monodisperse SiO_2 particles. In this method, tetraalkoxysilanes such as tetraethyloxysilane (TEOS) are added to an alcohol-water mixture under basic condition. The result is the hydrolysis of TEOS groups to silanol groups, followed by condensation reactions. The size of the particles is influenced by the silane reagent and/or the amine concentration. The size can be conveniently monitored through dynamic light scattering (DLS) and confirmation through transmission electron microscopy (TEM) is readily achieved.

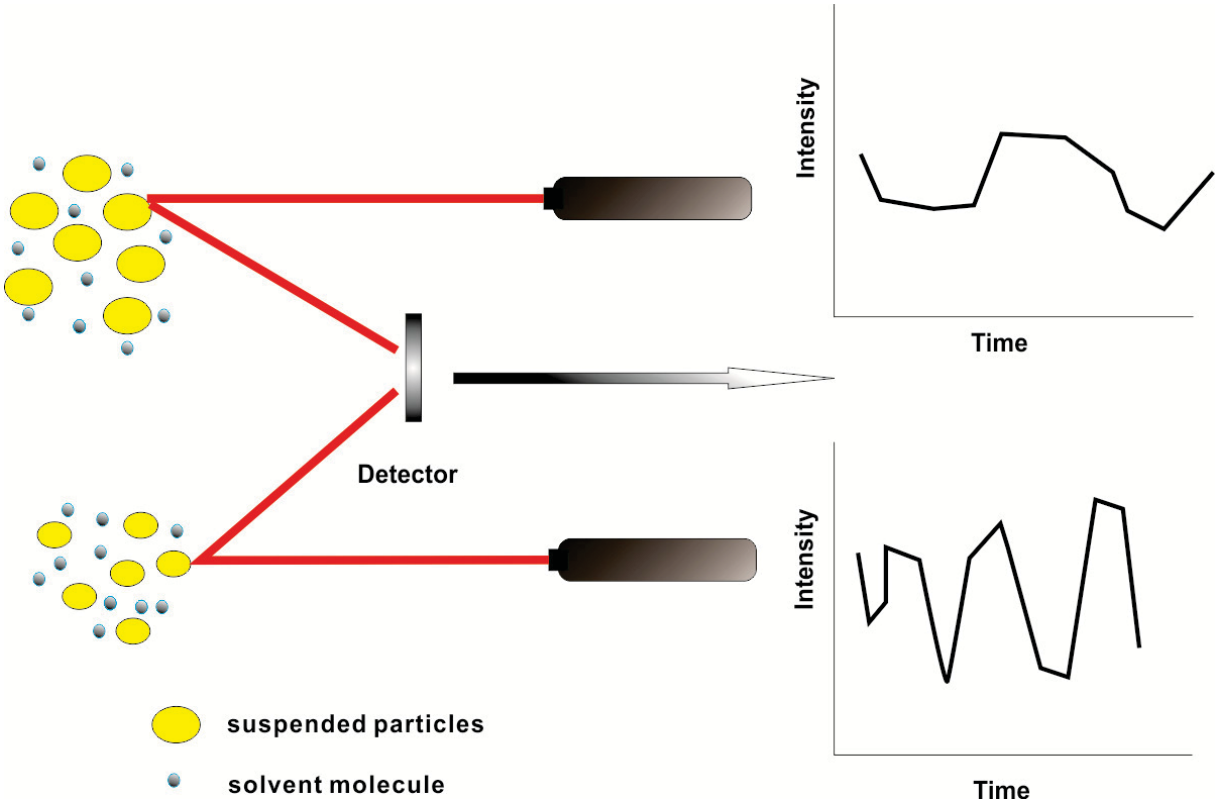

Fig. 18.1 Particle size measurement using DLS

18.2 Size distribution

DLS is perhaps the most relevant method for measuring the size distribution of small particles in solution at any desired point in time during synthesis and handling. The measurement is based on the time-dependent fluctuation in the scattering intensity as shown in **Fig. 18.1**. The fluctuation is a result of the Brownian motion of the particles in suspension. The larger the particle is the weaker is the fluctuation. DLS operates well for bare particles, however, the determination of the particle size for core-shell structures is more difficult. This is due to the different refractive indices of the shell and the core material. Moreover, coloured and fluorescent compounds embedded in either core or shell can also influence the results of this optical analysis technique. Thus, to precisely evaluate the size distribution of the core-shell structures, we relied mainly on TEM measurements. It has to be kept in mind however that the sizes obtained by TEM can vary from the actual sizes in solution due to the fact that samples are measured under vacuum in conventional TEM.

The concentration of the base and the silane are decisive parameters for the size of the formed SiO_2 particle. Thus control experiments were carried out to study the influence of the base concentration. The concentration of the silane was fixed in this series and particles were prepared with varying ammonia concentrations. The resulting sizes were determined by DLS with polydispersity index (PDI) small as 0.05 and listed in **Table 18.1**. We found that the particle size increases with increasing base concentration up to a certain point, and then drops again. It turns out that the Stöber method is suitable for the preparation of particles with a diameter below 500 nm. Larger particles would have to be prepared through multi-step growth procedures.[203]

Tab 18.1 Influence of base concentration on SiO_2 particle size

	Size/ nm	TEOS/ mL	Ethanol/ mL	H_2O/ mL	$NH_3.H_2O$/ mL
WW-BS-01	280	4.5	65.75	24.75	5
WW-BS-02	360	4.5	61.75	24.75	9
WW-BS-03	400	4.5	59.75	24.75	11
WW-BS-04	500	4.5	57.75	24.75	13
WW-BS-05	560	4.5	55.75	24.75	15
WW-BS-06	400	4.5	53.75	24.75	17
WW-BS-07	300	4.5	50.75	24.75	20

18.3 Surface modification by RAFT polymerization

The grafting of the polymer onto the particle surface can be accomplished through direct growth onto the surface of the silica particle, which is called the "grafting to"-strategy (**Fig. 18.2**).[204] This is achieved by a first modification of the surface with a polymerizable group, for instance, with a silane reagent such as methacrylate-propyltriethoxylsilane. The polymer chain is formed first in the solvent and successively adsorbed onto the particle surface through hydrophobic or H-bonding effects. In a final step, the polymer forms a stable covalent bond with the surface polymerizable group.

Another approach is termed "grafting from"-strategy. In this method, an initiator is first covalently immobilized onto the particle surface.[205] The radicals are generated directly at the particle surface. The polymer chain grows then directly from the particle surface. This method allows for a more homogeneous surface layer than the "grafting to"-strategy, and a possible introduction of block co-polymer morphologies is possible.[206]

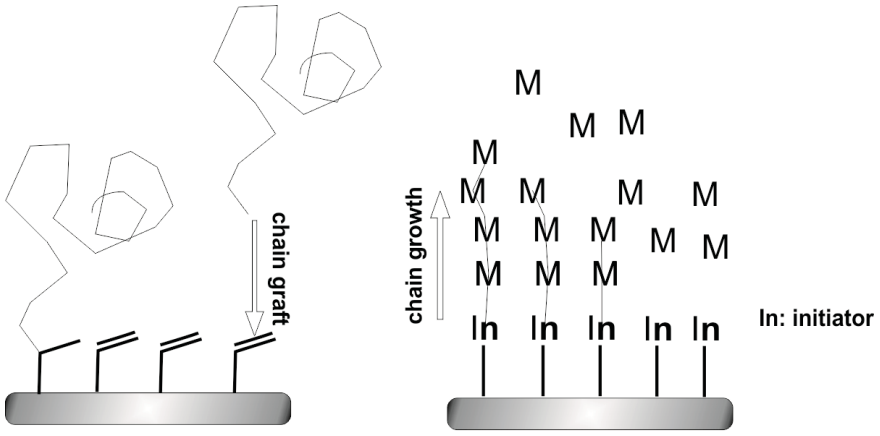

Fig. 18.2 "grafting to"- and "grafting from"-strategy

Instead of an initiator, a RAFT agent can also been immobilized onto the particle surface. As already discussed before (Sect. 4.1), the RAFT polymerization can provide a more homogeneous polymer layer due to its living profile (**Scheme 18.1**).[201] The RAFT agent is coupled onto the particle surface through covalent coupling such as an amide bond in our case. The radical is generated through thermal or photo dissociation of the initiator in bulk solvent. The radical is then transferred to the particle surface through a semi-substitution reaction. The polymer chain is then grown from the surface. Due to the living polymerization character, the grafted polymer chains have similar lengths. The growth of the chain is terminated when two radicals recombine.[207] In addition, residual RAFT agent remains on the surface and can be further re-initiated and enable layer by layer polymerization.

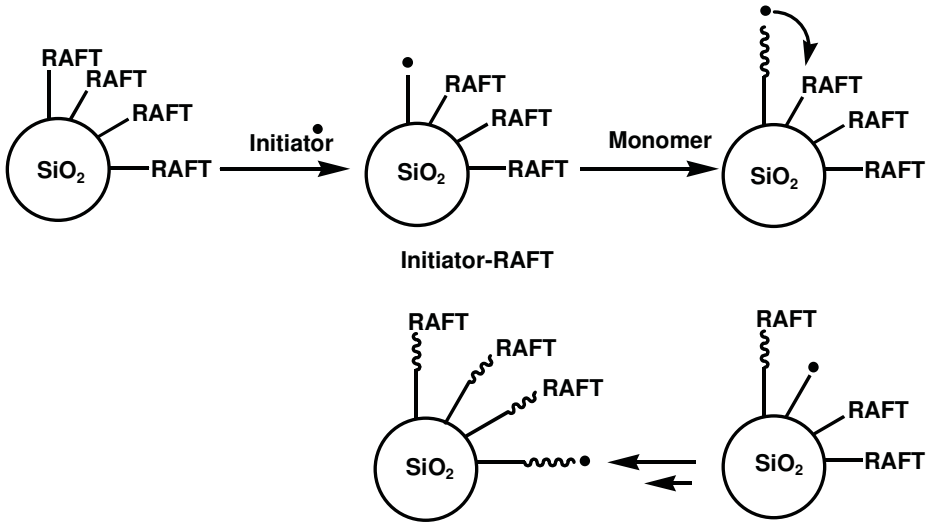

Scheme 18.1 RAFT polymerization on the particle surface

The RAFT agent-coated SiO_2 particles are prepared according to **Fig. 18.3**. First, SiO_2 cores were prepared by a modified Stöber method. The surface was then coated with amino groups using (3-aminopropyl)triethoxysilane (APTES). The RAFT agent was then covalently coupled onto the particle surface with amide chemistry. As we know that the surface available OH group lose their activity due to dehydration and to reduce the batch-to-batch difference, surface modification with APTES and coupling with 4-cyano-4(phenylcarbonothioylthio) pentanoic acid (CPDB) was carried out directly after preparation of the SiO_2 cores without any storage step. The prepared RAFT-functionalized particles were stored under –20 ^{o}C and are stable for over 1 year.

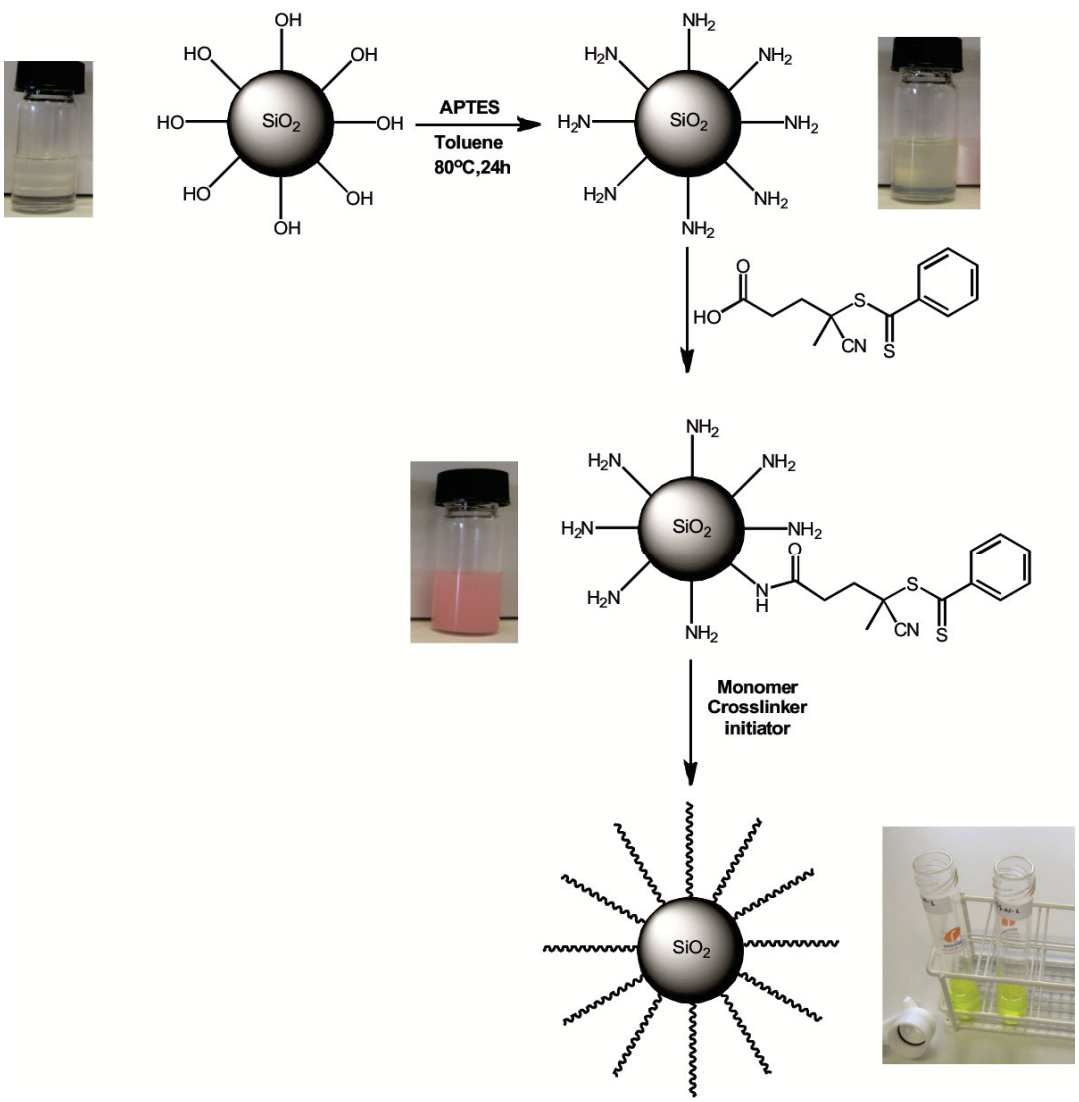

Fig. 18.3 Preparation of RAFT agent-coated particles

The surface functionalization of the SiO_2 microparticles can be tracked by FTIR measurements (**Fig. 18.4**). The broad band in the 3250-3500 cm^{-1} region belongs to the NH stretching. After coupling with CPDB, this broad band is weakened and two new bands develop at 2497 and 2602 cm^{-1}. After polymerization, these bands disappear.

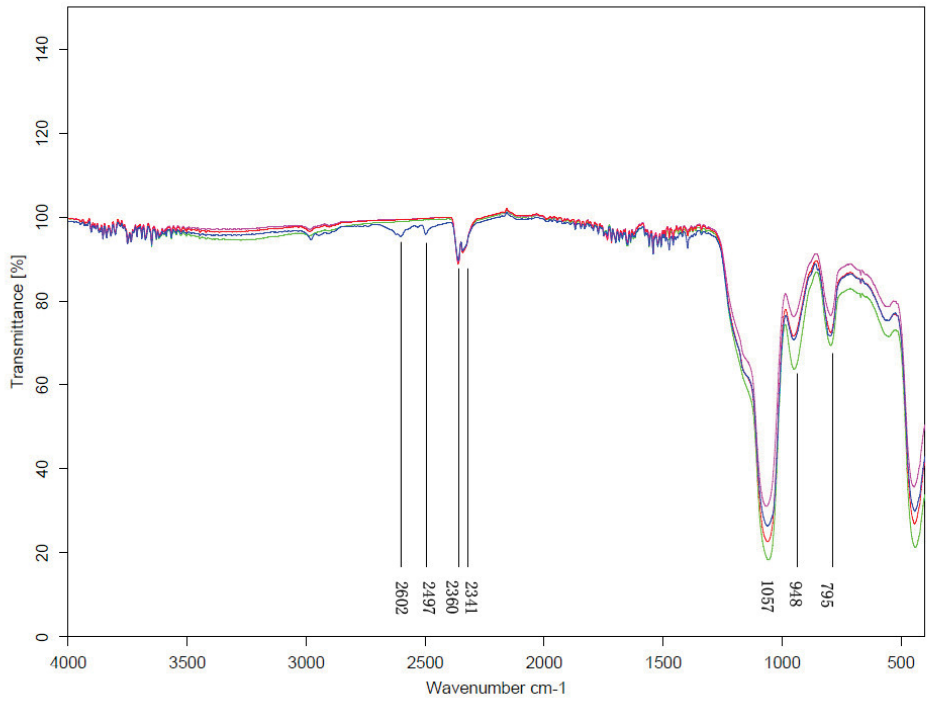

Fig. 18.4 FTIR spectra of APTES-SiO_2 (green), CPDB-SiO_2 (blue), **CSM75**-MIP (red) and **CSM75**-NIP (pink)

The coupling of CPDB is also verified by EDX (**Fig. 18.5**) by the presence of chlorine and sulfur peaks. The surface-immobilized RAFT agents enable the formation of a thin polymer layer under high control on the SiO_2 surface. The size distribution was examined by DLS and TEM. The low PDI (< 0.05) measured by DLS indicates a high monodispersity of these particles. This was further confirmed by TEM images in **Fig 18.5**.

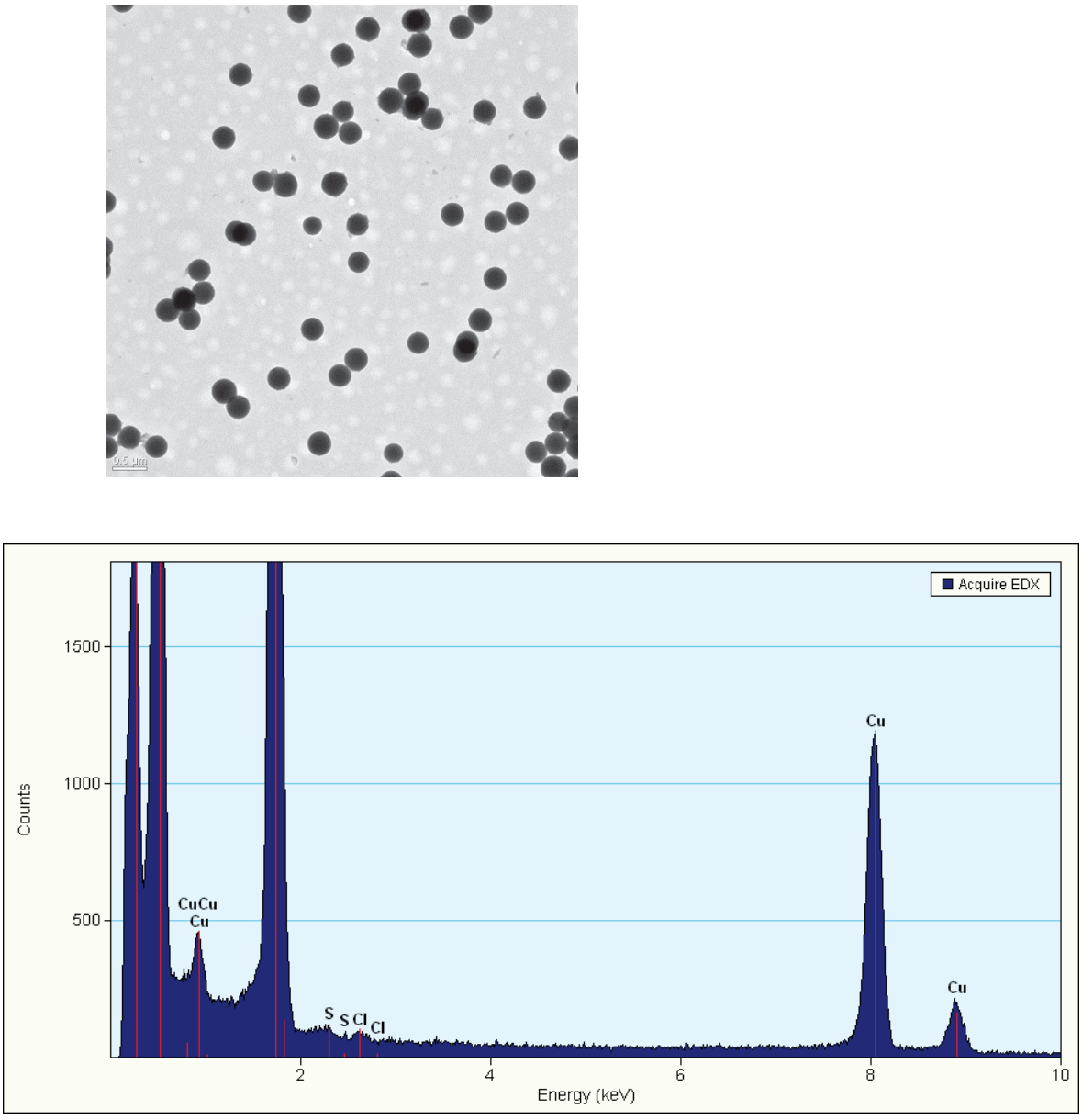

Fig. 18.5 TEM image of the RAFT-coated SiO_2 cores (top) and corresponding EDX measurement (bottom)

The surface coverage with RAFT agent was calculated from TGA and elemental analysis (**Fig. 18.6**). The weight loss before 100 °C is due to the evaporation of the surface-adsorbed water. A further weight loss from 200 °C to 600 °C is due to the burning of surface organic components such as APTES. For CPDB-coupled particles, a first exothermic differential scanning calorimetry (DSC) peak was observed at 190 °C, then a second one at 500 °C. Both MIPs and NIPs shows similar weight losses and DSC peaks, which means that the polymer components are similar. From these data, a surface coverage of 300 μmol g^{-1} was derived for CPDB on the SiO_2 cores.

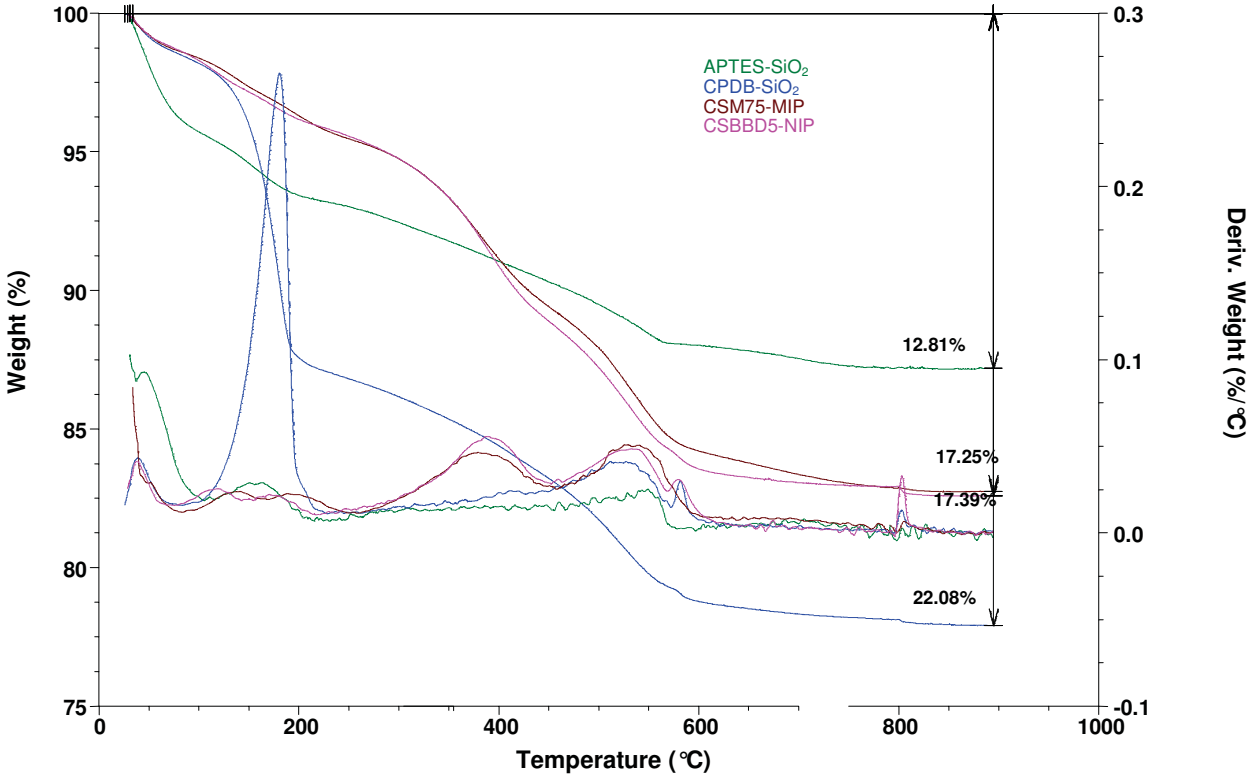

Fig. 18.6 TGA thermograms of APTES-SiO_2 (green), CPDB-SiO_2 (blue), **CSM75-MIP** (brown) and **CSM75-NIP** (pink)

18.4 Inference of the shell thickness

In the preparation of the core-shell particles, we also found that the presence of the chromogenic monomer and anion template can influence the shell thickness (**Fig. 18.7**). In the absence of the chromogenic monomer and template, the shell can infinitely grow if co-monomer and crosslinker are present in sufficient amount; co-monomer and crosslinker can be quantitatively grafted onto the particle surface. In the presence of the chromogenic monomer and the template, the grafting terminates after some time. Only a part of co-monomer and crosslinker are grafted onto the particle surface. This can be simply determined through comparing the shell thickness in TEM images. In the case of anion imprinted core-shell particles, the polymer layer is much thinner, about 10 nm, however the polymer layer growth to 15 nm when the anion is absent. The reason is ascribed to the accumulation of charges onto the particle surface which prevents the additional grafting of the polymer onto the surface. This observation is further supported by the Elemental analysis, the NIP has more organic component than the MIP prepared in the presence of anion (**Table 18.2**).

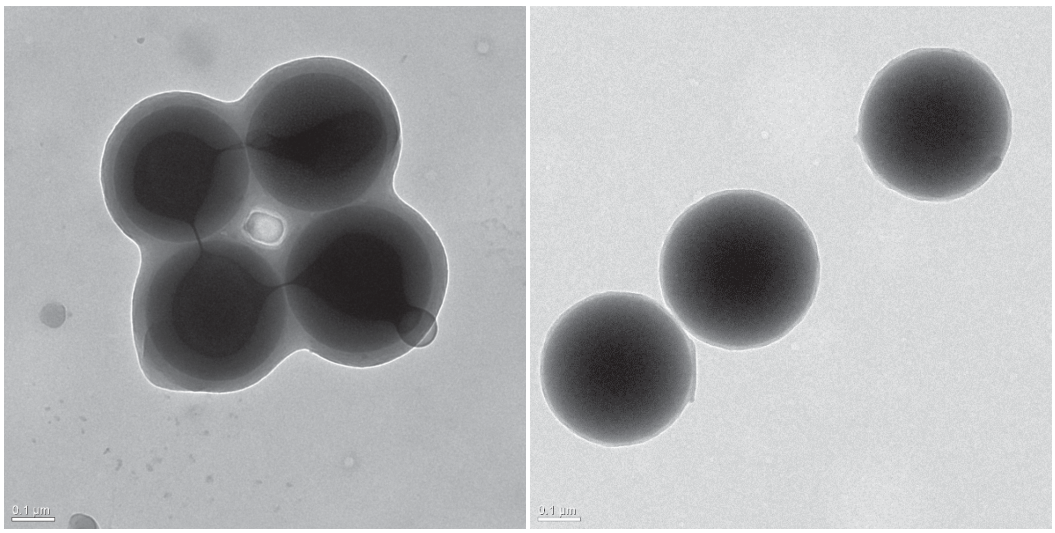

Fig. 18.7 TEM images of core-shell particles prepared without anionic template (left) and with anionic template (right), the scale bar for the image is 0.1 μm

Table 18.2 Elemental analysis of RAFT coated SiO_2, MIP and NIP particles

	N %	C %	H %	S %
RAFT@SiO_2	0.911	9.27	2.321	0.134
CSM75-MIP@SiO_2	0.582	6.918	1.696	0.050
CSM75-NIP@SiO_2	0.645	8.516	1.834	0.052

18.5 Assessment of sensing performance

A suspension assay was developed for evaluating the sensing performance of the sensor particles. MIP/NIP particles were suspended in an organic solvent, analytes were gradually added into the suspension and the fluorescence signal was registered. Since the analyte and the sensor particles were in the same solvent, the change of polarity in the binding cavity can be neglected. Thus the sole parameter to induce the fluorescence intensity change ΔF is the formation of the H-bonding complex in the binding cavity. In addition, the measurements were carried out in the same solvent as used for the synthesis process, to avoid any swelling effects. The imprinting effect is assessed through a comparison of the fluorescence intensity change $\Delta F/F_0$ of the MIP and NIP particles after addition of the template molecule. The selectivity is evaluated by the fluorescence intensity change of the sensor particle towards addition of analyte as well as competitor.

18.6 Core-shell particles from BODIPY monomer

The BODIPY-based fluorogenic monomer **M4** was used to prepare MIP-sensor particles for phosphorylated tyrosine. The template used was $(TBA)_2$-Fmoc-P-Tyr-OEt. Methacrylamid (MAAM) was used as co-monomer and EDMA as crosslinker (**Fig. 18.8**). The polymerization was carried out in $CHCl_3$ to achieve better monomer-to-template binding. Because the monomer has sufficient solubility in $CHCl_3$, the NIP particles were prepared only with the fluorogenic monomer instead of using a dummy template. Similar to the binding response of the monomer with the anion, the addition of the template anion leads to the fluorescence quenching of the sensor particles.

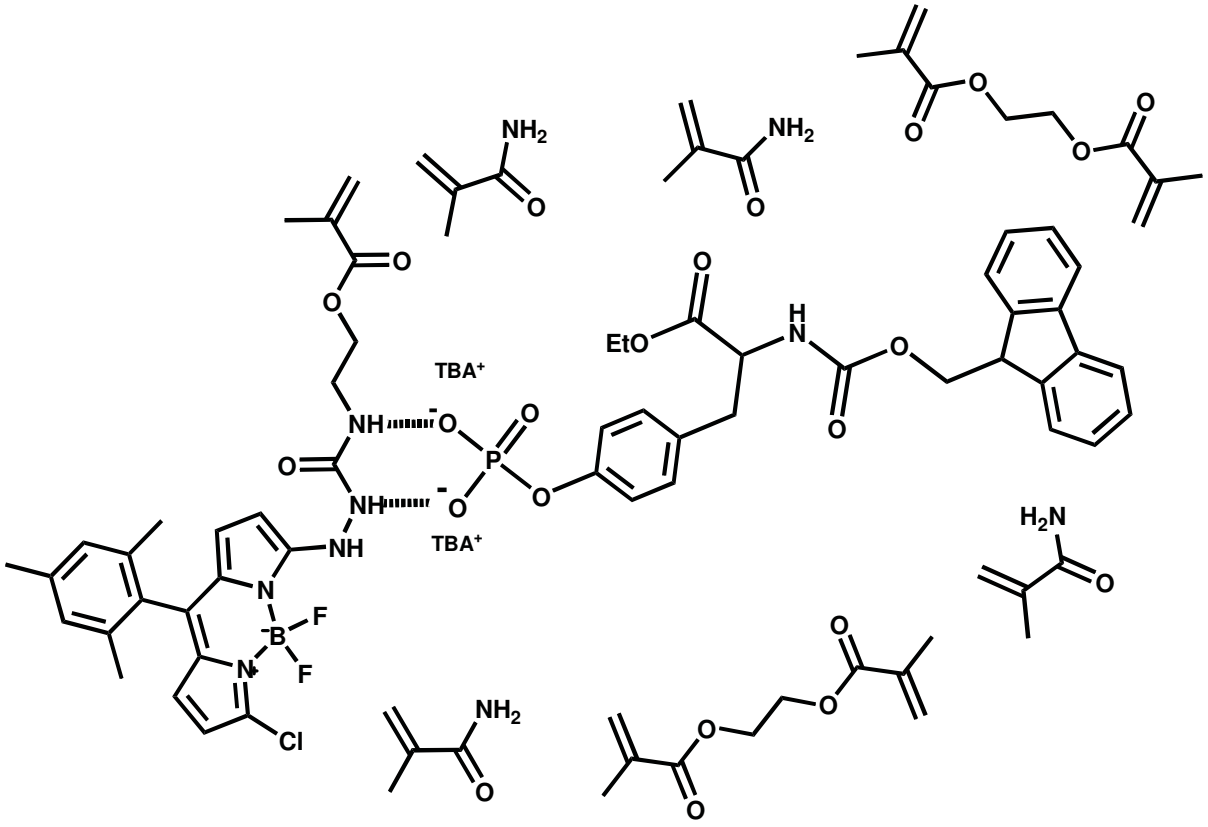

Fig. 18.8 Pre-polymerization system of **CSM4-1**

However, after synthesis and extraction, the fluorescence maximum of the MIP core-shell particle **CSM4-1** was found at 566 nm, 46 nm red shifted compared to the bare monomer **M4** in $CHCl_3$. This is readily to be observed under the UV lamp through a colour change from green to orange. The addition of the template molecule shows a steady decrease of the fluorescence intensity in both MIP and NIP particles with the quenching being stronger in the

MIP case, i.e., the maximum signal is >80% quenching for the MIP and 20 % for the NIP (Fig. 18.9). This difference should be due to the lack of the binding cavities in the non-imprinted polymer matrix, reflecting the extent of non-specific binding.

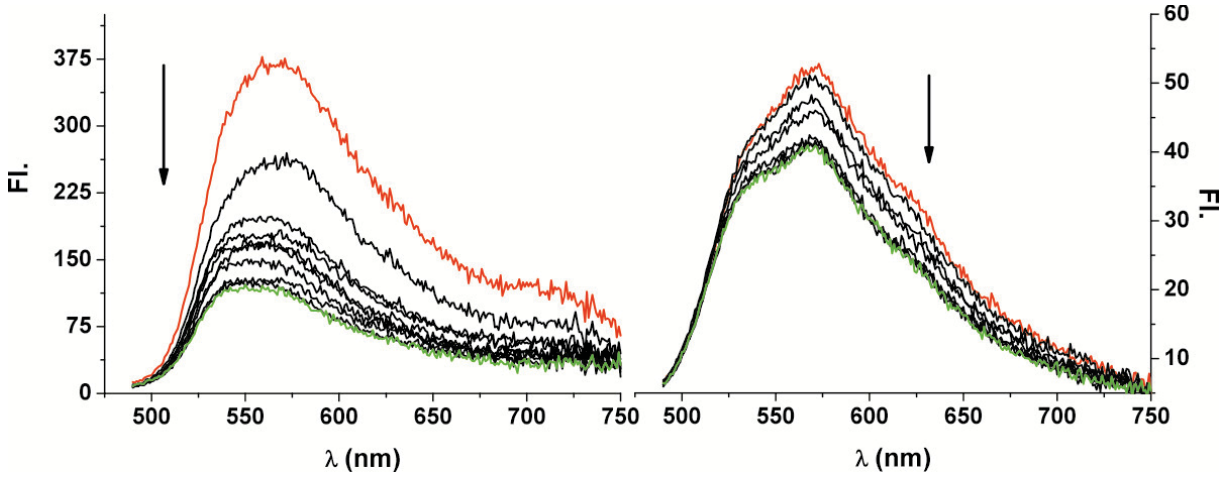

Fig. 18.9 Fluorescence titration of 1 mg/mL **CSM4-1-MIP** (top left) and **CSM4-1-NIP** (top right) with $(TBA)_2$-Fmoc-P-Tyr-OEt in $CHCl_3$ ($C_{analyte}$=2-500 µM, starting point spectra in red, end point spectra in green) and the fluorescence response towards selected analyte (bottom)

Moreover, the fluorescence measurements suggest that less polymer is coated on the surface of the MIPs compared with the NIPs. At the same particle concentration, the NIP shows stronger fluorescence than the MIP. Because TEM images provide further support, a simple environmental polarity effect in the polymer matrix around the BODIPY residues can be excluded. This has been a general observation during the thesis that the NIPs prepared without a dummy template always possess a thicker polymer shell than the MIPs (see Section 18.4). However, this higher content of fluorogenic monomer in NIPs does not contribute to a stronger response, showing that even under such conditions non-specific binding is not enhanced.

Although we observed this favourable sensing performance of the system, the selectivity of the MIP particles is rather low. The selectivity was examined by using non-phosphorylated tyrosine including TBA-Fmoc-Tyr-OEt, $(TBA)_2$-Fmoc-Tyr-OH and $(TBA)_2$-Z-L-Tyr-OH as potential interferences (**Fig. 18.10**), for chemical structures of species, see **Fig 18.24**. Disappointedly, the particles show very little discrimination to all these interferences.

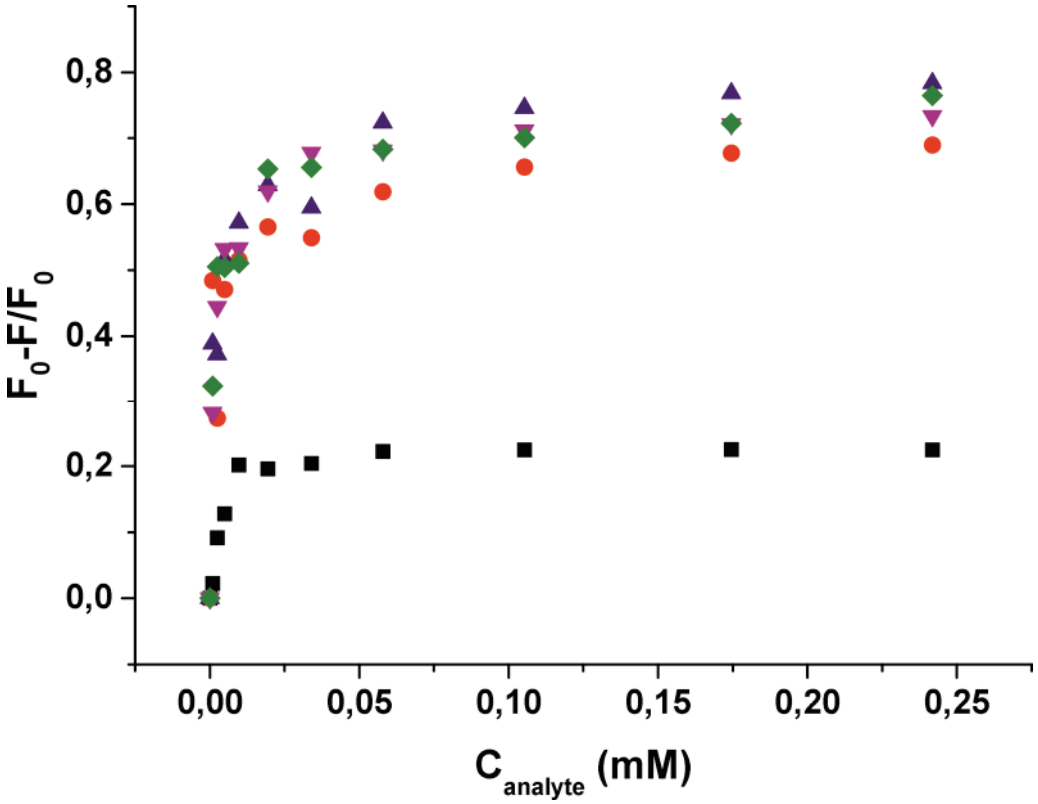

Fig. 18.10 Fluorescence response of **CSM4-1-MIP** with $(TBA)_2$-Fmoc-P-Tyr-OEt (red sphere), with TBA-Fmoc-Tyr-OEt (blue triangle), with $(TBA)_2$-Fmoc-Tyr-OH (magenta triangle), $(TBA)_2$-z-L-Tyr-OH (green diamond) and **CSM4-1-NIP** with $(TBA)_2$-Fmoc-P-Tyr-OEt (black square)

A possible explanation for these findings is that the fluorogenic monomer itself is rather large, the bulky size leading to expanded cavities. Moreover, since the MIP shell is considerably thin larger cavities close to the shell surface might become more open and provide for instance only single-point instead of multi-point recognition. The latter would greatly reduce the selectivity of the sensor.

18.7 Core-shell particles from phenoxazinone monomer

The fluorogenic monomer **M5** shows an outstanding sensing potential in the molecular solvent studies. After complexation with an anion, an over ten-fold fluorescence enhancement can be achieved. Thus, several templates were used to prepare MIP sensor particles from **M5**. These templates include Z-L-Phe, penicillin G, and phenylphosphate as a model for the phosphorylated amino acids (**Fig. 18.11**). The preparation of the MIP particles was similar to the protocol used in the **CSM5-1**.

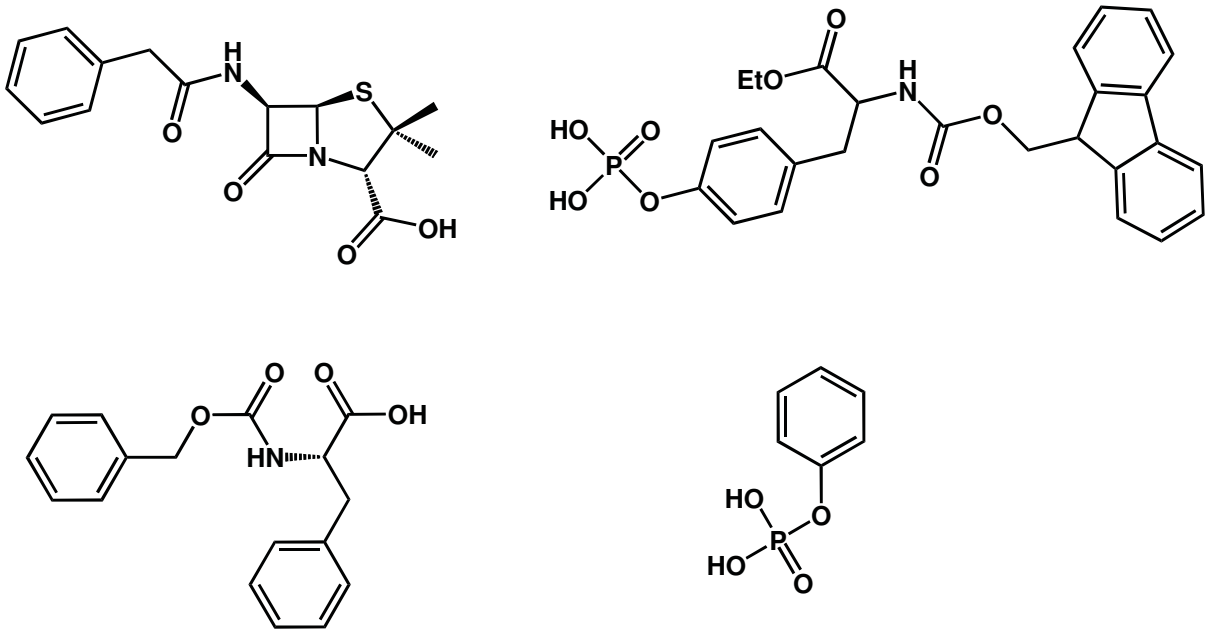

Fig. 18.11 Templates used for preparation of **M5**-based MIP particles

CSM5-1 was prepared with using Z-L-Phe as the template, BMA as co-monomer and EDMA as crosslinker. A considerable fluorescence enhancement of 2.2 is observed after rebinding of the template molecule (**Fig. 18.12**).

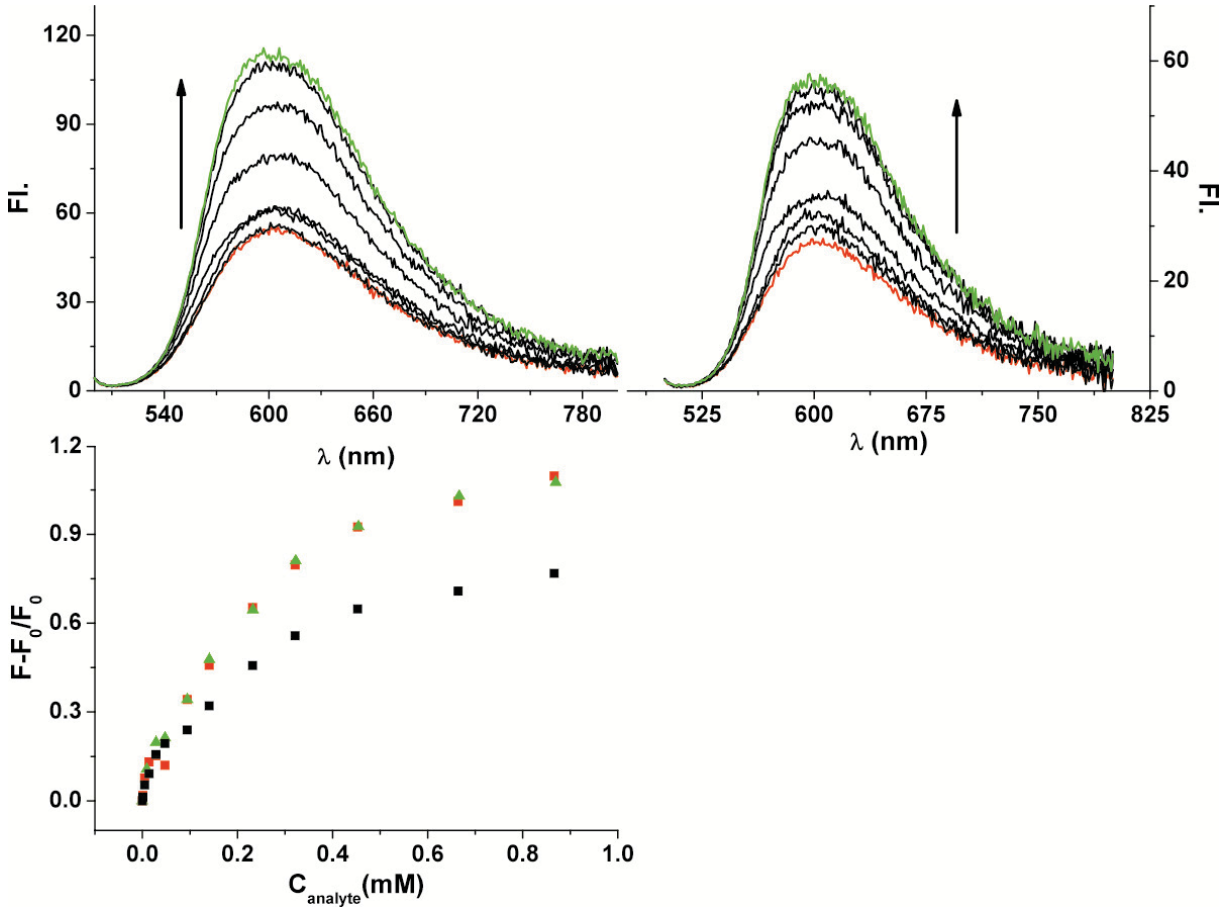

Fig. 18.12 Sensing response of **CSM5-1** MIP (top-left) and **CSM5-1** NIP (top-right) towards template and the binding curve (bottom) of **CSM5-1** MIP with Z-L-Phe (red square) and Z-D-Phe (green triangel) as well as **CSM5-1** NIP with Z-L-Phe (black square)

However, the difference between MIP and NIP is much smaller here than for the BODIPY system. Furthermore, enantiomeric discrimination is virtually absent.

CSM5-2 was prepared with TBA-PenG as template, BMA as co-monomer and EDMA as crosslinker. The result was similar to the **CSM5-1** case. Although the MIP particles show high fluorescence enhancement, the difference between MIP and NIP is also small (**Fig. 18.13**).

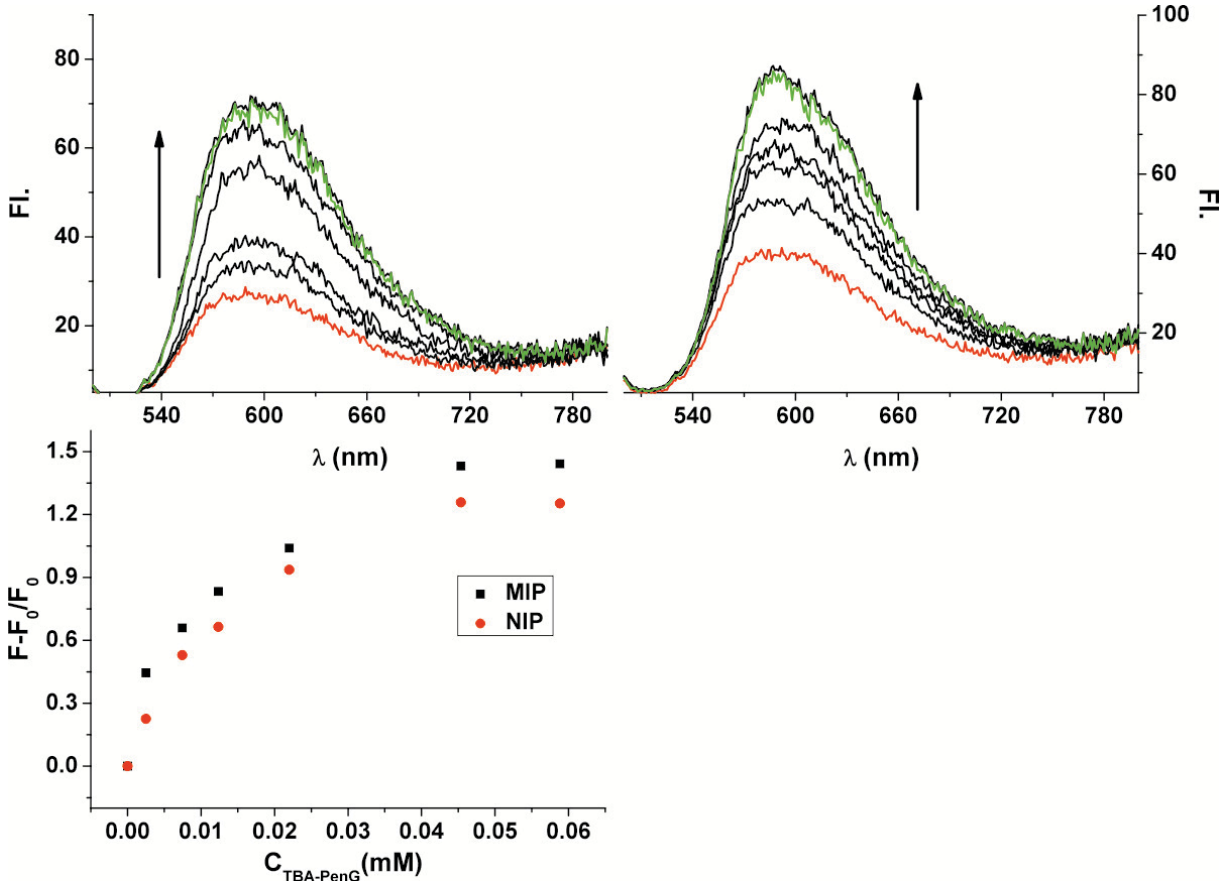

Fig. 18.13 Fluorescence response of **CSM5-2** MIP (top-left) and **CSM5-2** NIP (top-right) with PenG/TBA and the corresponding binding curve (bottom) of **CSM5-1** MIP (black square) and **CSM5-1** (red sphere)

Finally, the imprinting with the phosphate anion templates TBA-PPA and TBA-Fmoc-P-Tyr-OEt also did not improve the performance significantly. We assume that the elongated form of the fluorescent monomer along with the rather large aromatic three-ring system leads to the formation of too large cavities. Referring to **Scheme 18.2**, although target binding can occur close to the anchor point of the monomer into the covalent polymer network, the fluorophore moiety stretches out considerably into the cavity, expanding it. The lack of interaction between the aromatic ring with other components might also make the pore much larger than the material prepared for instance with fluorogenic monomer **M7**. Like in the BODIPY case, such rather larger cavities close to the shell's surface do not seem to be optimal. With multi-point interaction being also amended in this case, enantioselectivity is lost.

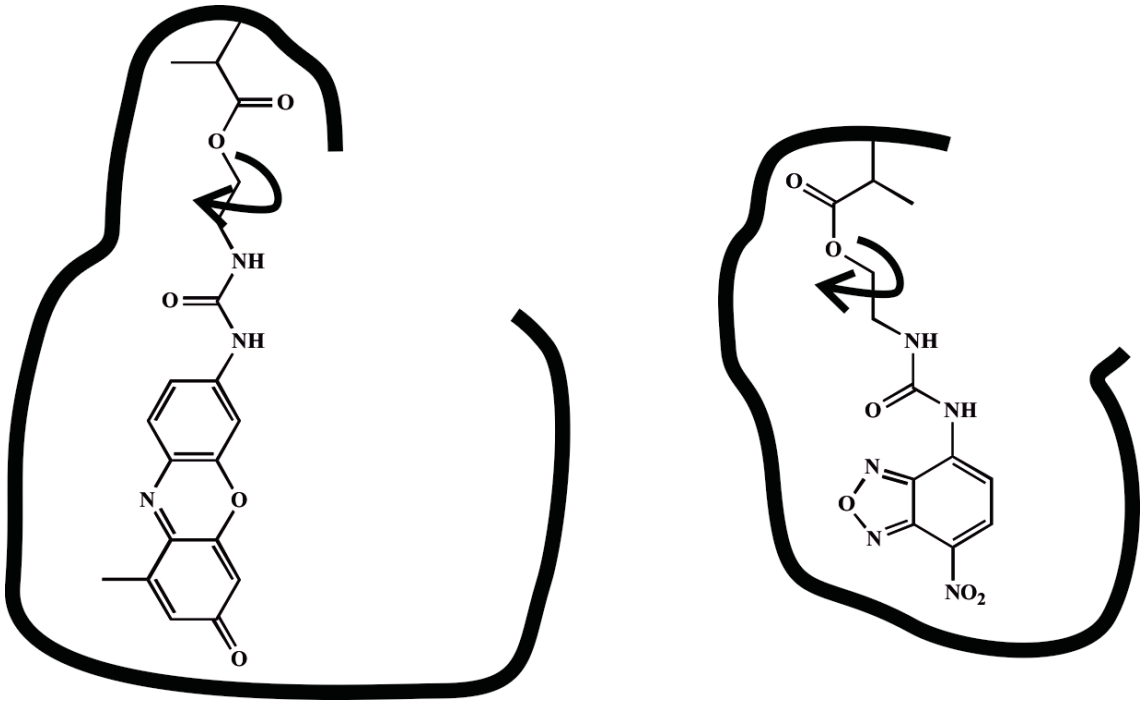

Scheme. 18.2 Influence of the chromophore size on the MIP cavity

18.8 Core-shell particles from nitrobenzoxadiazole monomer

The benzoxadiazole monomer **M7** is one of the most successful fluorogenic monomers developed for the preparation of MIP sensor particles in this thesis. Because of the high affinity toward carboxylates, TBA-Z-L-Phe was used as the model template and various co-monomers, crosslinkers and porogens were screened to refine the imprinting performance.

The size and core-shell morphology of the particles were examined by TEM and T-SEM (**Fig. 18.14**). From these images, a homogeneous particle size distribution of 360 ± 20 nm can be determined. The shell thickness is about 10 nm. This layer can also be resolved by T-SEM as the rough structure on the particle surface.

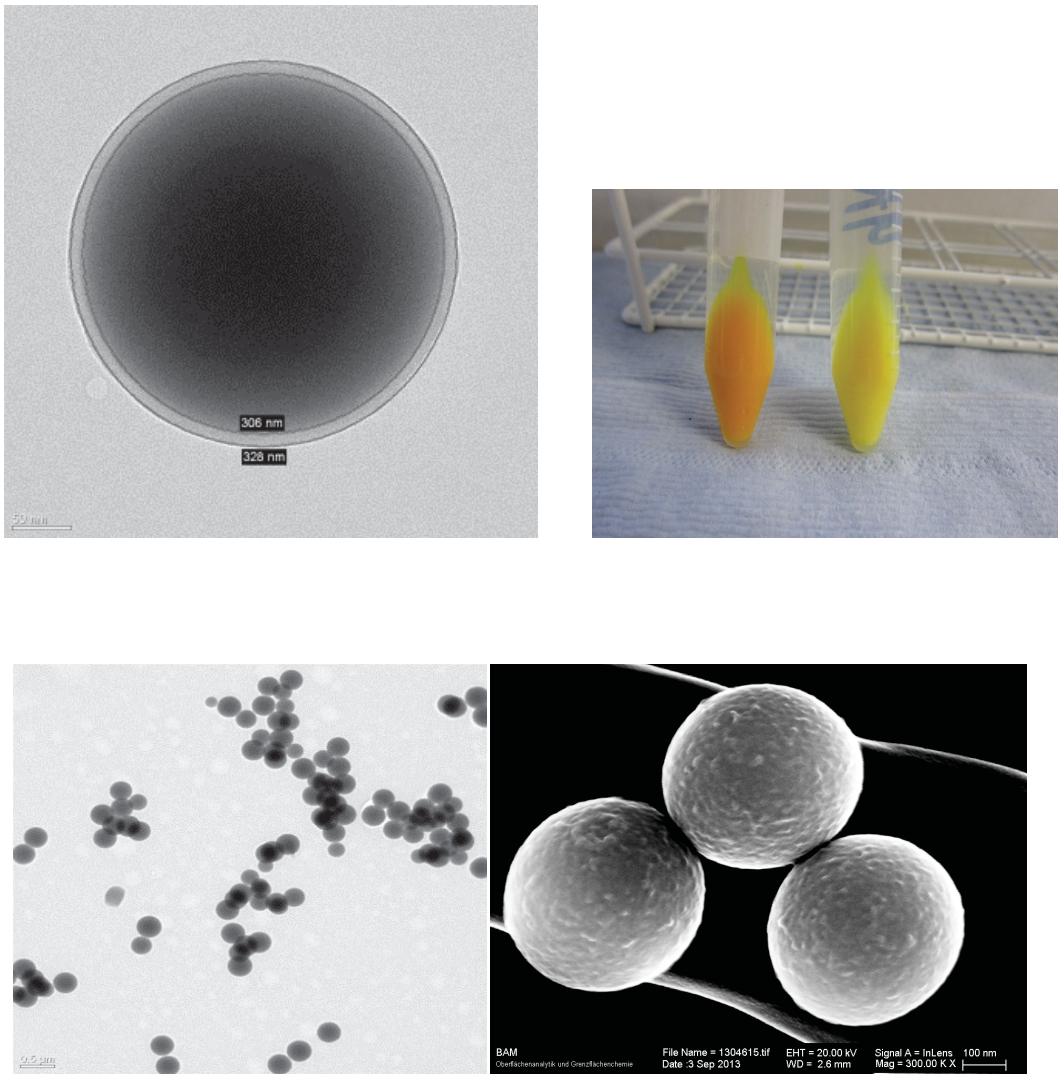

Fig. 18.14 TEM (top left and bottom left) and T-SEM (bottom right) images of **CSM7-5-MIP** particles and picture of as-synthesized MIP (left) and NIP (right) particle (top right)

The prepared sensor particles fluoresce at 494 nm and the band is gradually shifted to 510 nm upon addition and rebinding of the template TBA-Z-L-Phe. The fluorescence is also enhanced by a factor of 1.5. The response is similar to the case of the monomer in solvent which was disccussed above. Although the particles have a similar sensing response as the neat monomer, they still show some differences. The MIP particles show a weaker fluorescence enhancement factor than the neat monomer in solution. This may result from two facts. First, although the polymer preparation proceeds under best possible control, there are most likely still some "dead" binding sites buried in the matrix, which are non-accessible to an added template. These "dead" binding sites can lead to higher background fluorescence and would not contribute to fluorescence enhancement. Second, the polymer matrix provides a more polar environment as neat $CHCl_3$. Through comparison of the absorption spectrum of

the MIP particles (411 nm), the polarity in the MIP shell is more similar to that of neat **M7** in MeCN (410 nm). The higher polarity of the microenvironment leads to different QYs of the free and the complexed form of the dye monomer in the MIP particles and thus to an altered fluorescence modulation, in this case a lower enhancement due to the increased local polarity.

When template molecules are added to the monomer solution, the fluorescence enhancement ΔF is proportional to the concentration of template before saturation. After saturation, a decrease was observed due to the deprotonation of **M7**. In the case of the MIP particles, however, a plateau was formed at the titration end without the intensity decrease. This suggests a reduced susceptibility of **M7** for deprotonation in the MIP matrix. This effect might be due to the steric restriction in the binding cavity, since the deprotonation always results from the participation of a second anion. The small cavity does not provide enough space for the second anion. The plot of $\Delta F/F_0$ of the MIP particles against the concentration of the target molecule does not strictly follow a straight line as that in case of the neat monomer, which can result from a heterogeneous distribution of the binding sites in the polymer matrices.

18.8.1 Sensing performance

To assess the sensing performance, a parameter $\Delta F/F_0$ as the reduced fluorescence instead of the simple change in fluorescence ΔF is introduced; here ΔF is the fluorescence enhancement and F_0 is the fluorescence of the sensor particle in the absence of an analyte. This quotient removes the influence of different amount of sensor particles in different assays because of weighing errors and the different amounts of dye due to the different coating thicknesses (see section 18.4).

The imprinting factor IF_{fL} is defined as the ratio of $\Delta F/F_0$ by MIP and NIP towards the template molecule. The selectivity factor SF_{fL} is the ratio of fluorescence enhancement of MIP particle towards template and different competitors. From **Fig. 18.15**, the MIP shows a large $\Delta F/F_0$ than the NIP particle.

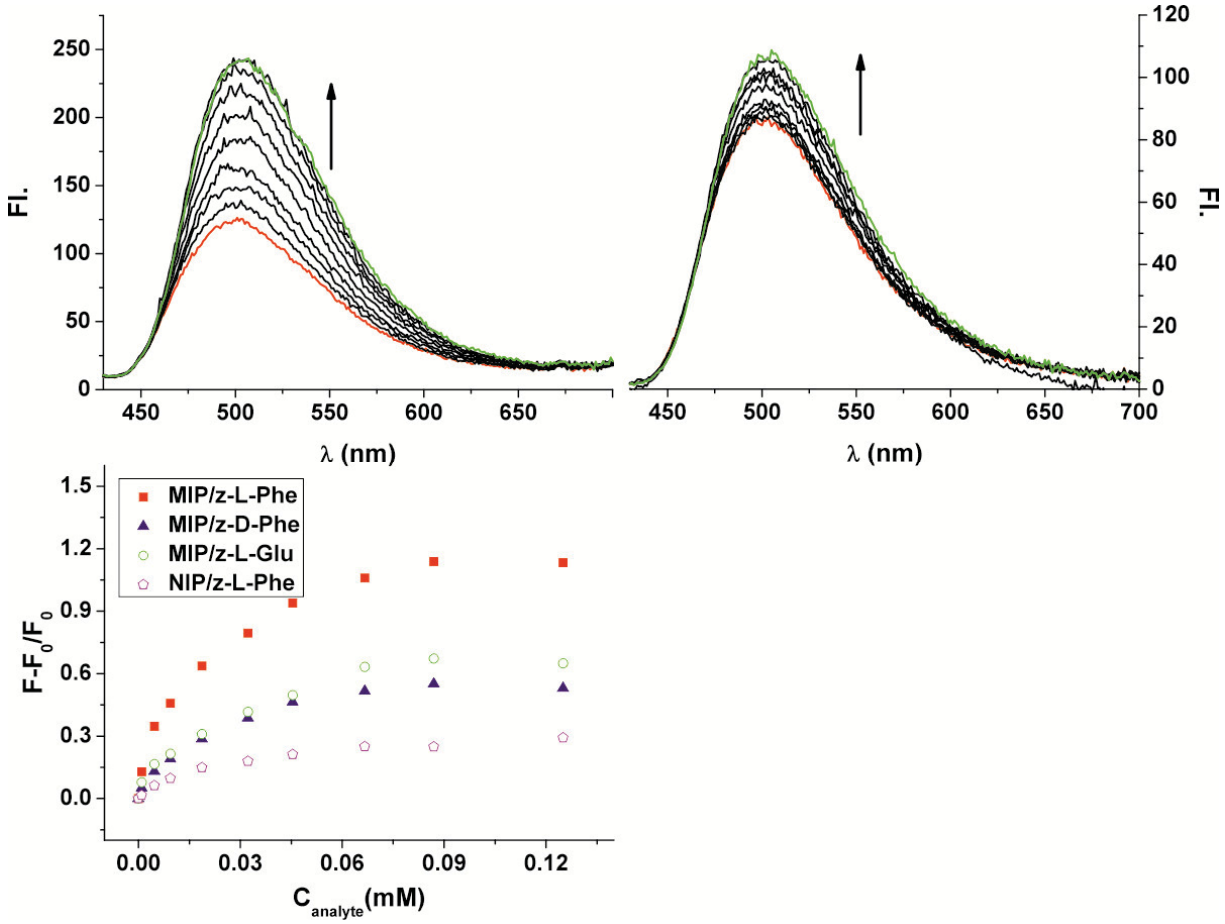

Fig. 18.15 Fluorescence response of 1mg/L **CSM7-5-** MIP (top) and NIP particles (bottom) towards a template in $CHCl_3$

For Z-L-Phe, the selectivity is examined with its enantiomer Z-D-Phe and with Z-L-Glu, a related amino acid carrying an additional potentially interfering carboxylic acid group (**Fig. 18.16**). We found that the NIPs show the lowest fluorescence enhancement. The imprinting factor was determined to be 3.6 The enantiomer Z-D-Phe and the interference Z-L-Glu show also less fluorescence enhancement than Z-L-Phe does, but still a higher response than the NIPs. The enantioselectivity was calculated as 1.9.

18.8.2 Modification of MIP preparation

For sensor applications, the most important parameters are the sensitivity and selectivity. To achieve a better performance, the MIP matrix should be modified in terms of co-monomer, crosslinker and porogen. Under this guidance, we prepared a series of sensor particles using **M7** as chromogenic monomer, the result is listed in **Table 18.3**.

Table 18.3 Modification of **M7**-based MIP particle, TBA-Z-L-Phe used as template in all cases

a: The ratio of fluorescence enhancement factor of MIP to NIP

b: The ratio of fluorescence enhancement factor of MIP particle to Z-D/L-Phe

No.	Monomer	Crosslinker	Porogen	MIP/NIP[a]	D/L[b]
CSM7-1	20 MMA	100 EDMA	$CHCl_3$	2.8	1.2
CSM7-2	20 VP	80 EDMA	$CHCl_3$	no discrimination	
CSM7-3	100 MMA	500 EDMA	$CHCl_3$	no discrimination	
CSM7-4	10 Sty 10 MMA	100 EDMA	$CHCl_3$	2.2	1.5
CSM7-5	20 BMA	100 EDMA	$CHCl_3$	3.6	1.9
CSM7-6	20 MAM	100 EDMA	$CHCl_3$	gelation	
CSM7-7	20 BMA	100 EDMA	3:7 Heptane:$CHCl_3$	3.1	1.2
CSM7-8	20 BMA	100 EDMA	3:7 Toluene:$CHCl_3$	2.4	1.3

The best result was achieved for **CSM7-5** by polymerization in $CHCl_3$, using BMA as co-monomer and EDMA as crosslinker. The MMA:EDMA pair (**CSM7-1**) shows less discrimination between the enantiomers. This enhanced effect could be attributed to the additional π-π stacking interaction of the BMA to the Z-L-Phe anion. The polymerization in the solvent mixture of heptane/$CHCl_3$ (**CSM7-7**) and toluene/$CHCl_3$ (**CSM7-8**) did not show an increased imprinting effect and enantiomeric discrimination, however, the performance is better than **CSM7-1**. This further strengthened the previous proposal that the co-monomer and crosslinker are more prominent parameters for a better selectivity. The decrease of imprinting effect may be due to the slight interruption of the solubility of the polymer components. In case of **CSM7-2** where vinyl pyridine (VP) is used as co-monomer, there are no optical changes after addition of the analyte, this is due to the high local polarity in the polymer cavity where the QY of the fluorogenic monomer is preset to a high level.

18.8.3 Fluorescence lifetime measurements

The fluorescence lifetime is also a good parameter to get more information on species interactions such as a binding event. For **M7** in $CHCl_3$, the lifetime measurements show a biexponential decay of 580 and 90 ps. After complexation with Z-L-Phe, a longer lifetime component of ca. 1480 ps appears accompanied by a decrease of the amplitude of the short

lifetime species. The deprotonated species on the other hand has a very weak fluorescence and distinctly shorter lifetime of 90 ps.

The situation is somewhat changed in the polymer matrix. The complex has a prolonged lifetime up to 2.4 ns, which might be due to the restricted environment in the polymer matrix that greatly reduced the dispersion of the excited state through molecular vibrations or rotations. On the other hand, an increase of the long lifetime species with a decrease of the native state was observed only in the MIP not in the NIP.

Table 18.4 Fluorescence lifetimes of **M7** in different solvents and protonation states and MIP/NIP particle before and after analyte rebinding

	τ_1 (ps)	a_{rel} (1)	τ_2 (ps)	a_{rel} (2)	τ_3 (ps)	a_{rel} (3)
M7 in $CHCl_3$	580	0.64	90	0.36		
M7:Z-L-Phe in $CHCl_3$	580	0.37	90	0.26	1480	0.38
deprotonated **M7**	580	0.14	90	0.86		
CSM7-5-MIP	520	0.31	100	0.62	2400	0.07
CSM7-5-MIP rebinding	520	0.45	100	0.41	2400	0.14
CSM7-5-NIP	520	0.18	100	0.80	2400	0.02
CSM7-5-NIP rebinding	520	0.19	100	0.78	2400	0.03

18.8.4 Binding isotherms

Binding isotherms are essential to describe the affinity of the binding site. Scatchard plots, were made here to analyze the binding data. The MIP particles were incubated in TBA-Z-L-Phe solution and the free Z-L-Phe was quantified by measuring the absorption of the filtered supernatant. The MIP particles show two different binding constants of log$K$=2.4±0.01 and log$K$=3.45±0.01 while the NIP particles show only a single binding constant of log$K$=2.5±0.01 calculated from **Fig 18.16**. The small binding constant is thus ascribed to the non-specific adsorption onto the polymer, while the higher binding constant reflects the specific binding of the MIP cavities. The plot of the fluorescence enhancement factor versus the quantity of adsorbed Z-L-Phe shows a plateau after 352 µmol of analyte have been adsorbed onto the particle. Compared to the Scatchard plot, the inflection point corresponds to an adsorption of 198 µmol. A reasonable binding capacity is thus calculated to 19.8 µmol mg^{-1}.

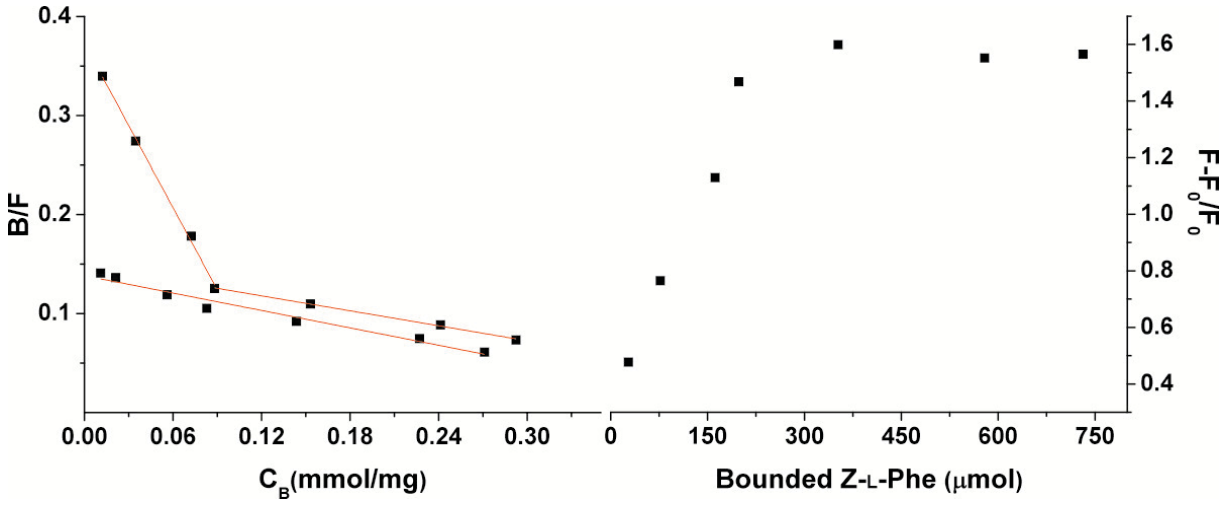

Fig. 18.16 Scatchard plot of **CSM7-5-**MIP/NIP particles and TBA-Z-L-Phe in $CHCl_3$ (left) and the corresponding fluorescence response (right)

18.8.5 Binding kinetics

The response time of a sensor is an important parameter in terms of sensor performance. In our case, the signal transduction process is relatively fast, i.e., on a picosecond time scale. Thus, the speed-determining step is the diffusion of the analyte to the binding cavity. The thickness of the polymer layer and the pore size determine the diffusion speed. The latter can be measured by screening the fluorescence enhancement with time; signal saturation was achieved in about 20 seconds (**Fig. 18.17**). This extraordinary sensing kinetic for a MIP layer is the result of the thin sensing shell of 10 nm grafted onto the silica cores, which greatly reduces the analyte diffusion time.

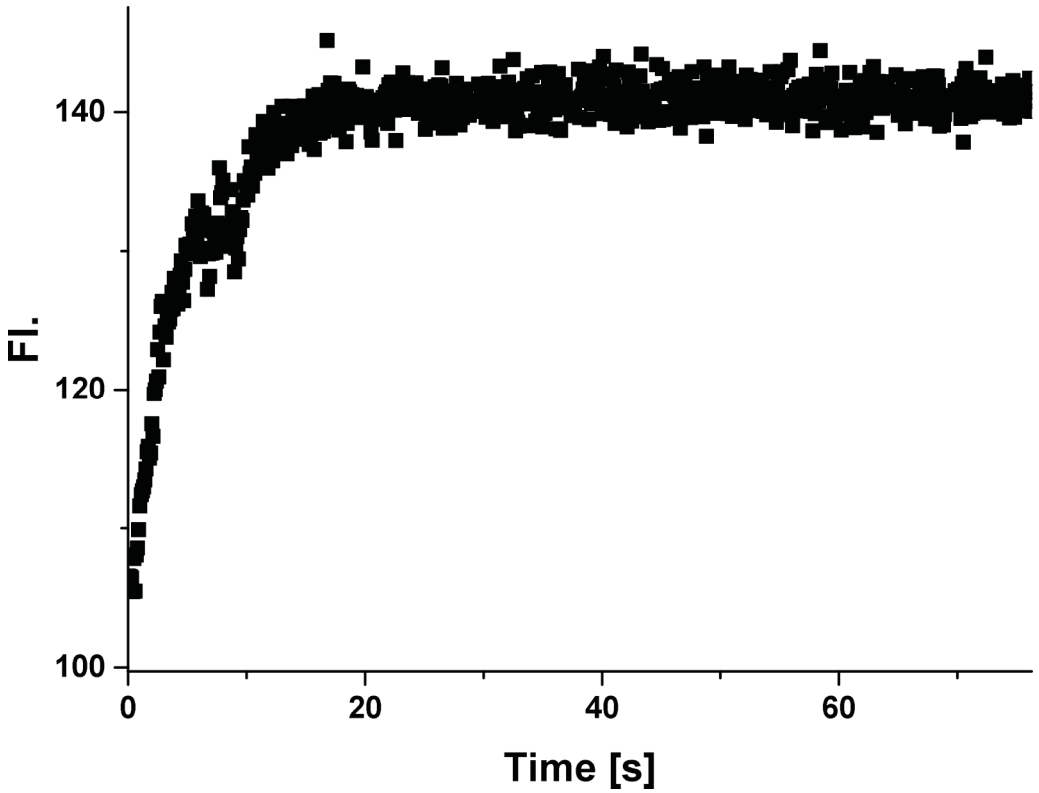

Fig. 18.17 Time course of the rebinding kinetics of **CSM7-5-MIP** and Z-L-Phe/TBA in $CHCl_3$

18.8.6 Sensing in aqueous system

The sensor particles show prominent sensitivity and enantiomeric selectivity in $CHCl_3$. However, the question of how the system performs under more relevant aqueous assay conditions remains to be elucidated. Some strategies are adopted to address this problem. We have first examined the sensing performance of the sensor particles in pure water as well as in MeCN/H_2O mixtures at different ratios. Unfortunately, as the selected example in **Fig. 18.18** shows, only quenching of the fluorescence is observed.

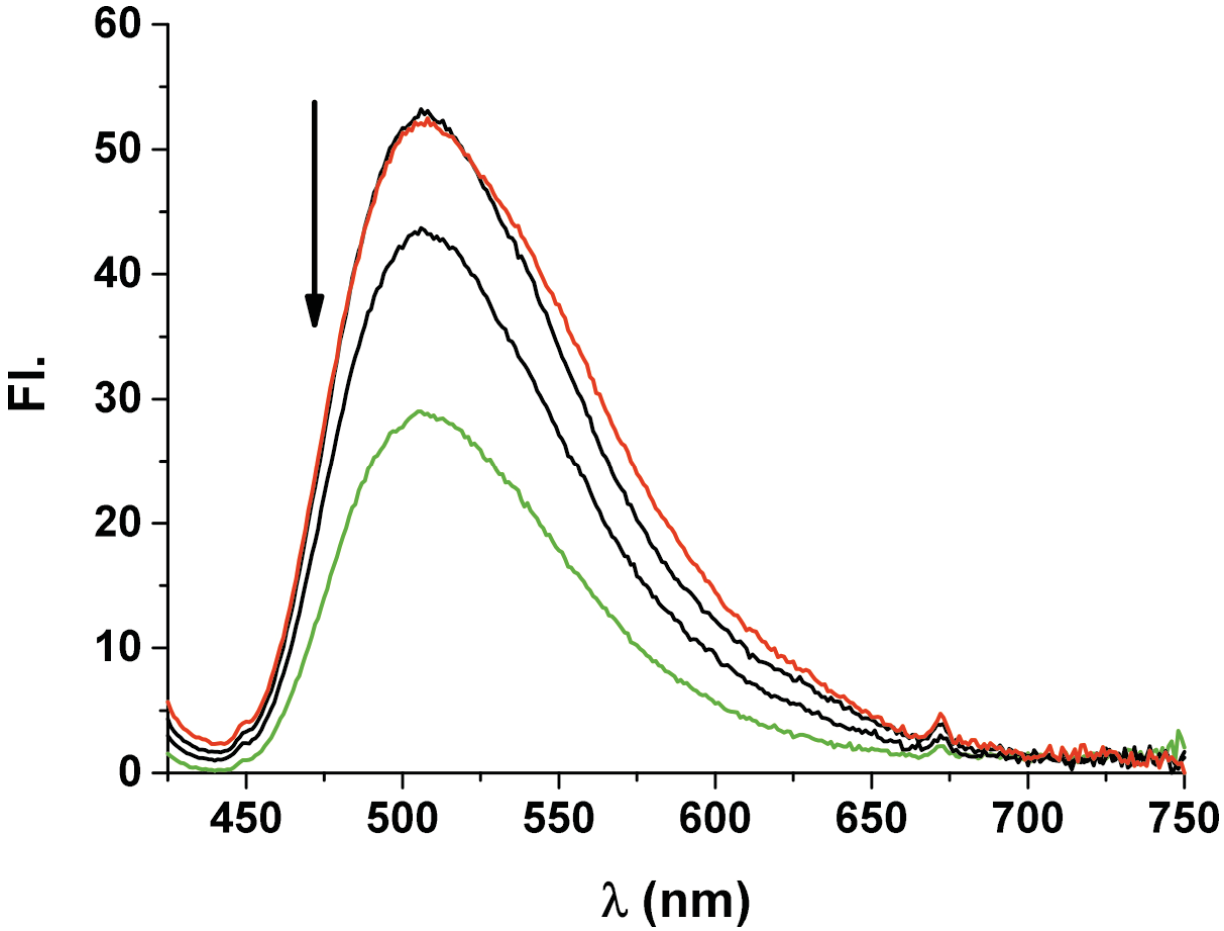

Fig. 18.18 1 mg/mL **CSM7-5-MIP** particles with (0-20 µM Z-L-Phe/TBA) in MeCN/H_2O (1:1), from red to green at different steps.

Instead of a fluorescence enhancement observed in $CHCl_3$, no spectral changes were observed and the fluorescence was even quenched. This result is again due to the comparatively thin shell which only poorly shields the matrix from water. Water on the other

hand can easily interfere with H-bonding between the fluorogenic monomer and the template molecule.

18.8.7 Embedding particles in hydrogel

There are different ways of how to improve the response of probes or sensory nano-objects in aqueous solution by shielding. In a first approach, **CSM7-5-MIP** particles were suspended in $CHCl_3$ and spin-coated onto a macroporos thin film slip. Afterwards, the slip was coated with a hydrogel which is prepared in a mixture of MeCN and H_2O. The slip was dipped into template stock solution to trace the fluorescence changes. Again, the addition of template only shows fluorescence quenching instead of enhancement (**Fig. 18.19**), so only a rather similar inferior performance like in neat water.

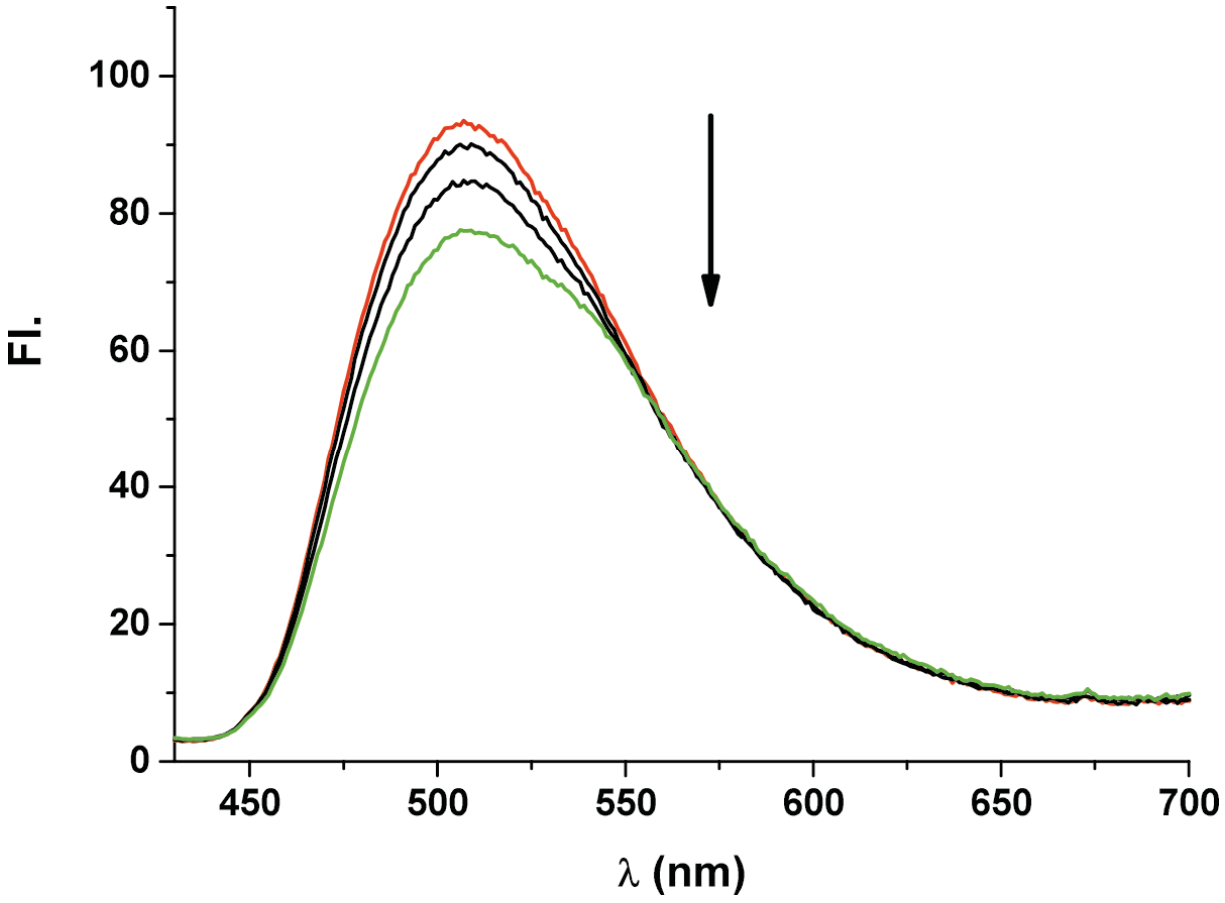

Fig. 18.19 Sensing response for **CSM7-5-MIP** particles embedded in a hydrogel, treated with (0-200 µM Z-L-Phe/K) aqueous solution, from green to red in different steps.

18.8.8 Two-phase extraction/detection protocols

Apparently, a hydrogel matrix still does not provide a suitable environment to allow for an application in realistic media. For **M7**, only the response in an organic solvent is promising, the performance in water is poor. The reason is again ascribed to the thin polymer layer and insufficient shielding against competing water in the binding cavity. Unfortunately, the use of a more hydrophobic co-monomer/crosslinker combination (styrene/divinylbenzene) did also not show any prominent improvement. Thus, a two phase extraction assay was developed. The sensor particles were first suspended in 2 mL $CHCl_3$ and 1 mL deionised water or buffer was added. Under continuous stirring, 0.1-1.4 µmol template molecule, TBA-Z-L-Phe, was carefully added to the aqueous phase (**Picture 18.3**). The system was equilibrated for 5 minutes and then the fluorescence of the suspension was registered. The remaining TBA-Z-L-Phe in the aqueous phase was quantified by HPLC for validation. With this assay, a better imprinting effect of 6.8 as shown in **Fig. 18.20** was achieved.

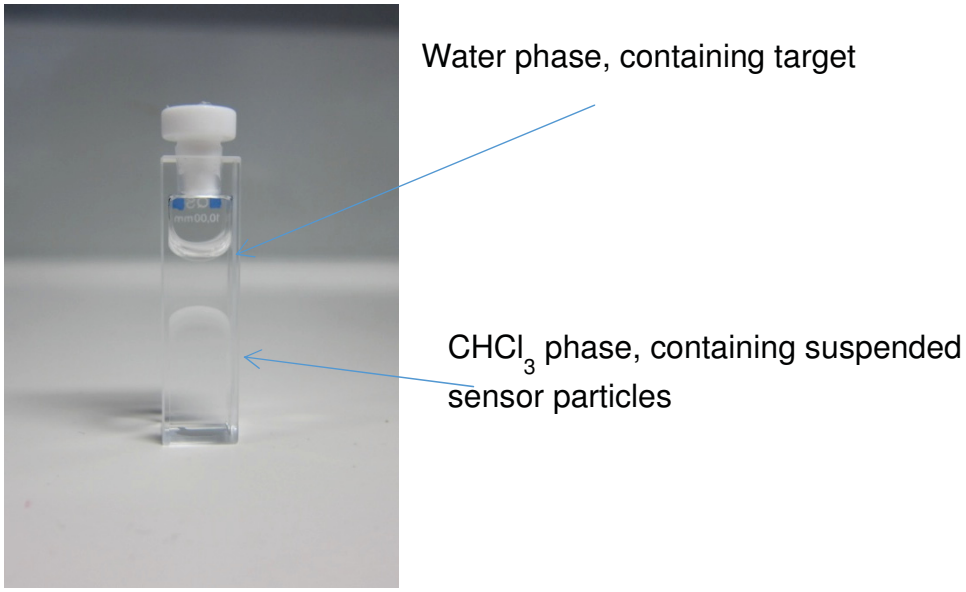

Picture 18.3 Sensing design of two phase system

This improvement regarding the imprinting effect is most likely due to a more effective suppression of the non-specific binding, since the fluorescence response of the NIP is significantly reduced compared to the case in $CHCl_3$ (**Fig. 18.20**).

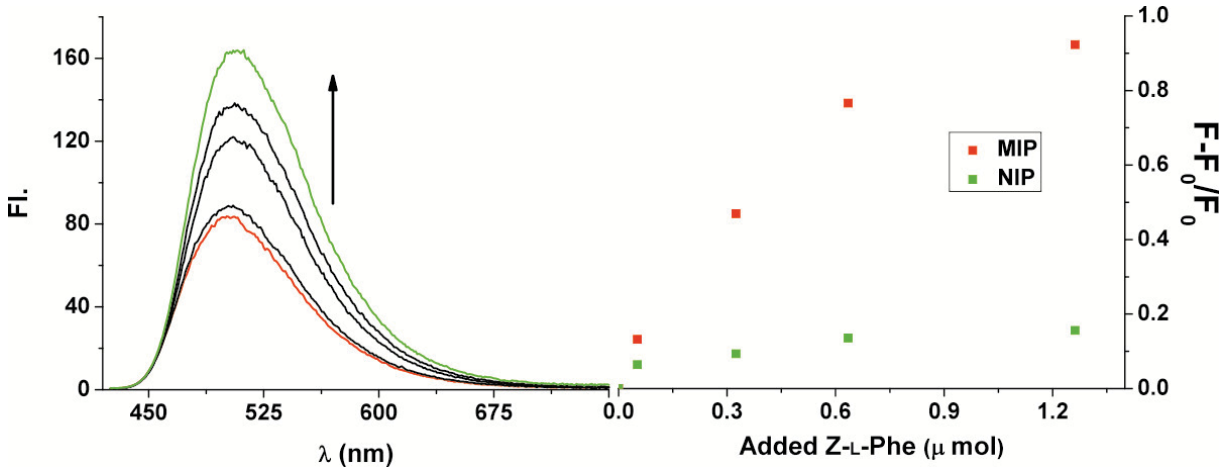

Fig. 18.20 Fluorescence response of **CSM7-5-** MIP/NIP particles towards TBA-Z-L-Phe in two-phase extraction assay, fluorescence spectrum of **CSM7-5-MIP** $CHCl_3$ phase without (red) and with Z-L-Phe/TBA of different concentration in the aqueous phase

To summarize this section, a fluorogenic sensor monomer based on the benzoxadiazole skeleton has been successfully imprinted in a polymer shell. With this monomer we have further developed a sensitive optical MIP sensor in the core-shell particle format for carboxylate-containing species. The introduction of RAFT-immobilized particles provides a versatile protocol for assembling SiO_2@MIP sensor particles with a thin layer of 10 nm. This thin layer does not only yield a low limit of detection (LOD) (determined by 3σ of the blank signal) of 60 nM with a good enantioselectivity factor of 2 but also a fast sensing response of less than 1 min. A favorable imprinting factor of 3.6 is achieved in a normal suspension assay, while in a phase-transfer assay this factor can be further enhanced to ca. 6. This system holds a lot of prospects for many applications of fluorogenic MIP particles in the future.

18.9 Core-shell particles from phenazine monomer

The final approach toward silica core-MIP shell sensory particles was made with the fluorogenic **M10** monomer. Having established the extraordinary ESPT-type signaling behavior in the molecular form, the key question was whether this favorable ratiometric indication scheme could be installed in a real sensor format. A series of phosphate anions was used as template, and co-monomer, crosslinker and porogen were adjusted to modify and optimize the sensing performance.

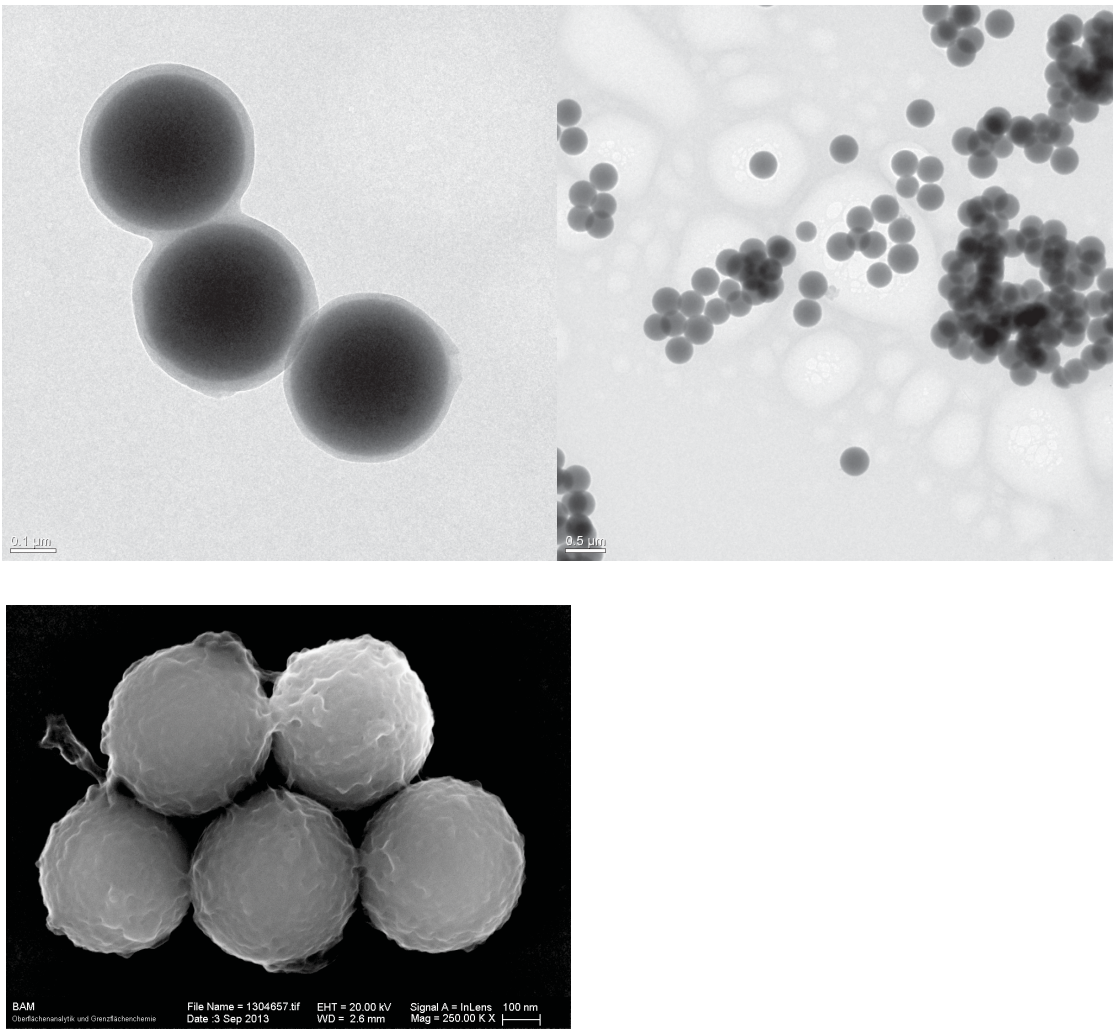

Fig. 18.21 TEM (top) and SEM (bottom) image of **CSM10-8**-MIP

The particles were also prepared using RAFT agent-modified SiO_2 particles. Due to the low solubility of **M10** in the polymerization solvent, TBAA is used as dummy template for the NIP preparation. The size and surface profile were examined by TEM, SEM and T-

SEM. Also in this case, a thin MIP layer of 10 nm was coated onto the core particles according to TEM and T-SEM imaging techniques (**Fig. 18.21**).

18.9.1 MIP for TBA-PPA

TBA-PPA was the first template used. BMA and EDMA were employed as co-monomer and crosslinker. The prepared particles have a yellow colour and can be well dispersed in MeCN. However, as shown in **Fig. 18.22**, the MIP and NIP show very similar spectral changes upon the addition of the analyte. First, a fluorescence enhancement with slight spectral shift in the local emission (LE) band was observed. Second, the ESPT band developed at 591 nm, accompanied by a decrease of the LE band. The lack of discrimination between MIP and NIP is attributed to the small size of the template molecule. Apparently, even the NIP can generate large enough pores to receive the template molecule.

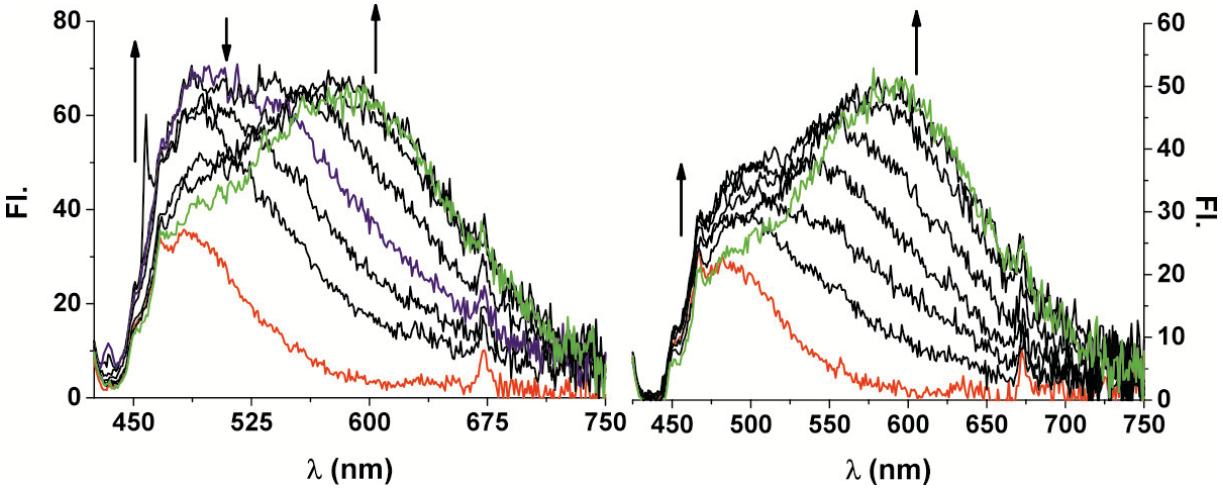

Fig. 18.22 Emission of MIP (top) and NIP (bottom) of **M10** particles with TBA-PPA (10-600 µM) in different steps in MeCN.

Although the small model template was not successfully been imprinted, a further test with a larger template molecule, Fmoc-P-Tyr-OEt, shows better performance.

18.9.2 MIP for Fmoc-P-Tyr-OEt

For imprinting Fmoc-P-Tyr-OEt, both mono- and bi-deprotonated anions can be used as template since the mono-deprotonated phosphate has a similar structure as the di-deprotonated one. As shown in **Table 18.5**, the particles prepared with di-deprotonated Fmoc-P-Tyr-OEt

show a worse imprinting effect, in some cases, the NIP even gives better response. This is due to the thin layer prepared with the dianion (less than 3 nm), so that a selective cavity was not formed, as discussed in the previous section. Thus the MIP particles were further prepared only using mono anionic Fmoc-P-Tyr-OEt as a template. The sensing is done, however, using the dianionic species to promote the ESPT when evaluating the imprinting effect. The synthesis recipe was also modified by the type of the co-monomer, crosslinker, porogen and template molecules used. The result is listed in **Table 18.5**.

Table 18.5 Modification of **M10**-based MIP particles, MAA: Methacylic acid, MMA: Methyl methacrylate, BMA: Bezyl methacrylate, MAAM: Methacrylamide, DMAA: N´N dimethyl methacrylamide, EDMA: Ethylenglycoldimethacrylate, TRIM: Trimethacrylate and NOBE: N, O-bismethacrylethanolamine

No.	Template	CM	CL	Porogen	MIP/NIP
CSM10-1	$(TBA)_2$-Fmoc-P-Tyr-OEt	MAA	EDMA	MeCN	0.9
CSM10-2	$(TBA)_2$-Fmoc-P-Tyr-OEt	MMA	EDMA	MeCN	0.8
CSM10-3	$(TBA)_2$-Fmoc-P-Tyr-OEt	BMA	EDMA	MeCN	0.8
CSM10-4	$(TBA)_2$-Fmoc-P-Tyr-OEt	NOBE		MeCN	1.0
CSM10-5	TBA-Fmoc-P-Tyr-OEt	BMA	EDMA	MeCN	1.2
CSM10-6	TBA-Fmoc-P-Tyr-OEt	BMA	EDMA	$CHCl_3$	1.9
CSM10-7	TBA-Fmoc-P-Tyr-OEt	MAAM	TRIM	$CHCl_3$	1.3
CSM10-8	TBA-Fmoc-P-Tyr-OEt	MAAM	EDMA	$CHCl_3$	3.7
CSM10-9	TBA-Fmoc-P-Tyr-OEt	DMAA	EDMA	$CHCl_3$	1.3
CSM10-10	TBA-Fmoc-P-Tyr-OEt	DMAA	TRIM	$CHCl_3$	1.1

As shown in this table, the particles prepared in $CHCl_3$ (**CSM10-6)** have a better imprinting effect than in MeCN (**CSM10-5)**, this is in accordance with our previous results. The change of EDMA (**CSM10-8**) to TRIM (**CSM10-7**) did not improve the imprinting effect, although in the TRIM case, both MIP and NIP shows strong fluorescence enhancement, as more polymer is grafted onto the particle surface. Particles prepared with MAAM (**CSM10-8**) show a better performance than the particles prepared with other co-monomers such as BMA

(**CSM10-6**) and DMAA (**CSM10-9**). In conclusion, **CSM10-8** shows the best imprinting performance. Accordingly, they were subjected to more detailed tests of cross selectivity.

The **CSM10-8** MIPs show a fluorescence enhancement of the local emission band at 494 nm with a slight red-shift to 510 nm at low analyte concentrations. Upon further addition of the template molecule, the ESPT band develops with a concomitant decrease of the LE band (**Fig. 18.23**). In case of the NIP particles, the addition of the template molecule also leads to a certain fluorescence enhancement of the LE band, however, only at much higher concentrations than for the MIPs. The ESPT band was not observed in case of the NIP particles.

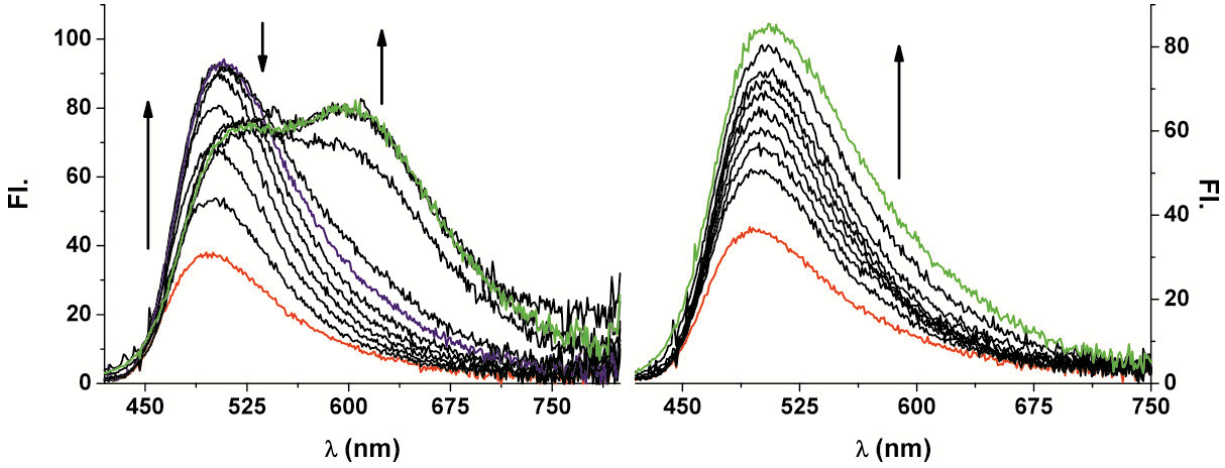

Fig. 18.23 Emission of 1 mg/mL **CSM10-8** MIP (top) and **CSM10-8** NIP (bottom) with $(TBA)_2$-Fmoc-P-Tyr-OEt (2-150 µM) in $CHCl_3$

The cross selectivity was examined with TBA-Fmoc-Tyr-OEt, $(TBA)_2$-Fmoc-Tyr-OH, Z-L-Tyr-OH and $(TBA)_2$-Fmoc-P-Ser (**Fig. 18.24**). TBA-Z-L-Phe shows less fluorescence enhancement compared to the template molecule, which can be due to the large difference of the protecting group or the weaker binding strength of the carboxylate group. $(TBA)_2$-Fmoc-P-Ser also shows less fluorescence enhancement due to its structural difference. The NIP particles also show a weaker fluorescence modulation with a slow signal development.

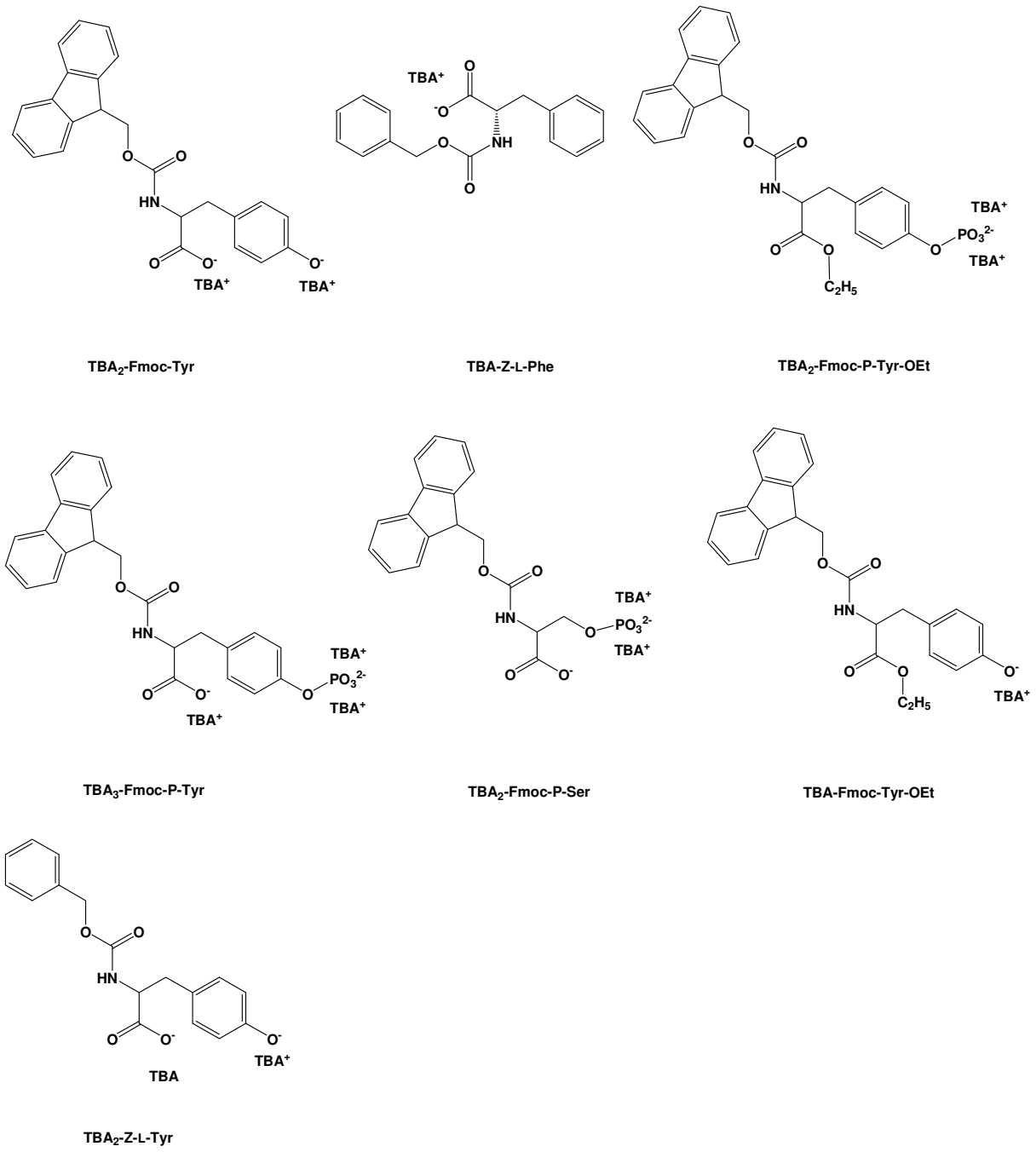

Fig. 18.24 Compounds used for cross-selectivity assessment

The discrimination of the phosphorylated and non-phosphorylated species is difficult in $CHCl_3$. This is due to the small differences in structure and charge distribution. As discussed in Section 11.2, the binding affinity of the anion towards the urea functional group is depending to the charge density of the anion or, in other words, the basicity of the anion. The tyrosine anion is more basic than the phosphate, and has thus a higher affinity to the

binding site. Since these binding cavities are considerably large, the discrimination ability is rather low (**Fig. 18.25**).

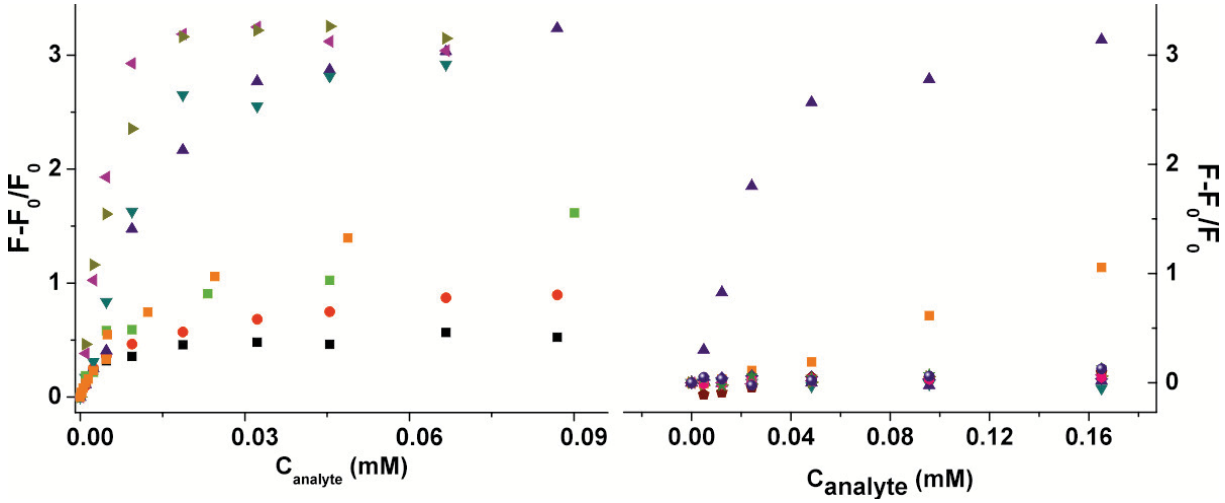

Fig. 18.25 Cross-selectivity of sensor particles examined with structural analogues in $CHCl_3$: **CSM10-8** MIP with $(TBA)_3$-Fmoc-P-Ser (black square), TBA-Fmoc-Tyr (red sphere), Fmoc-P-Tyr-OEt (blue triangle), Fmoc-Tyr-OEt (green triangle), $(TBA)_2$-Fmoc-P-Tyr-OH (brown triangle), $(TBA)_2$-Fmoc-Tyr-OH (violet triangle), TBA-Z-L-Phe (green square), **CSM10-8** NIP with $(TBA)_2$-Fmoc-P-Tyr-OEt (orange square) (left) and in bi-phase (Mes-Tris buffer (pH 7.5):$CHCl_3$ 2:3): **CSM10-8** MIP with Fmoc-P-Tyr-OEt (blue triangle), Fmoc-Tyr-OEt (green triangle), $(TBA)_2$-Fmoc-P-Tyr-OH (brown triangle), $(TBA)_2$-Fmoc-Tyr-OH (violet triangle), **CSM10-8** NIP with Fmoc-P-Tyr-OEt (blue sphere), Fmoc-Tyr-OEt (brown petagon), $(TBA)_2$-Fmoc-P-Tyr-OH (blue star), $(TBA)_2$-Fmoc-Tyr-OH (pink square)

We also observed that unlike **CSM4-1 MIP,** where the cavity has poor selectivity, **CSM10-8 MIP** still has a high discrimination between Z-L-Tyr-OH and Fmoc-P-Tyr-OEt. This indicates that the selective cavity formed by **M10** is better than **M4**. To improve the selectivity we again adopt the two phase strategy.

The desired sensing response for this system was also obtained when taking the step to the two-phase experiment. Here, the sensor particles were suspended in $CHCl_3$ and a MES-Tris buffer of pH 7.5 was added as the second phase. The system was stirred to reach a fast equilibrium. A small aliquot of an analyte stock solution was then added into the buffer phase and allowed to reach equilibrium within 3 minutes before registering the fluorescence spectra after each step of addition. From **Fig. 18.25**, it is obvious that a better discrimination is now achieved and that the interference from the non-phosphorylated tyrosine is diminished, because of the protonation of Tyr under the present buffering conditions.

18.9.3 Sensing of a short peptide

The prepared particles showed also a high affinity towards a phosphorylated tri-peptide. Two candidates, Fmoc-T(P)-T-G-OMe (P1) and Fmoc-T-T(P)-G-OMe (P2) in the form of di-deprotonated TBA salts were used to assess the recognition ability. Both peptides showed a similarly high affinity to the sensor particles (**Fig. 18.26**). The binding is characterized through the enhanced LE fluorescence. The ESPT band was not observed in either of the two cases, even at much higher excess. This can be due to the large size of the tri-peptide which hinders a further penetration into the MIP matrix to achieve optimum binding for ESPT to occur. Most likely, only the binding sites near the surface were involved in target binding. The steric hindrance also increases the distance between the two components, reducing the proton transfer efficiency.

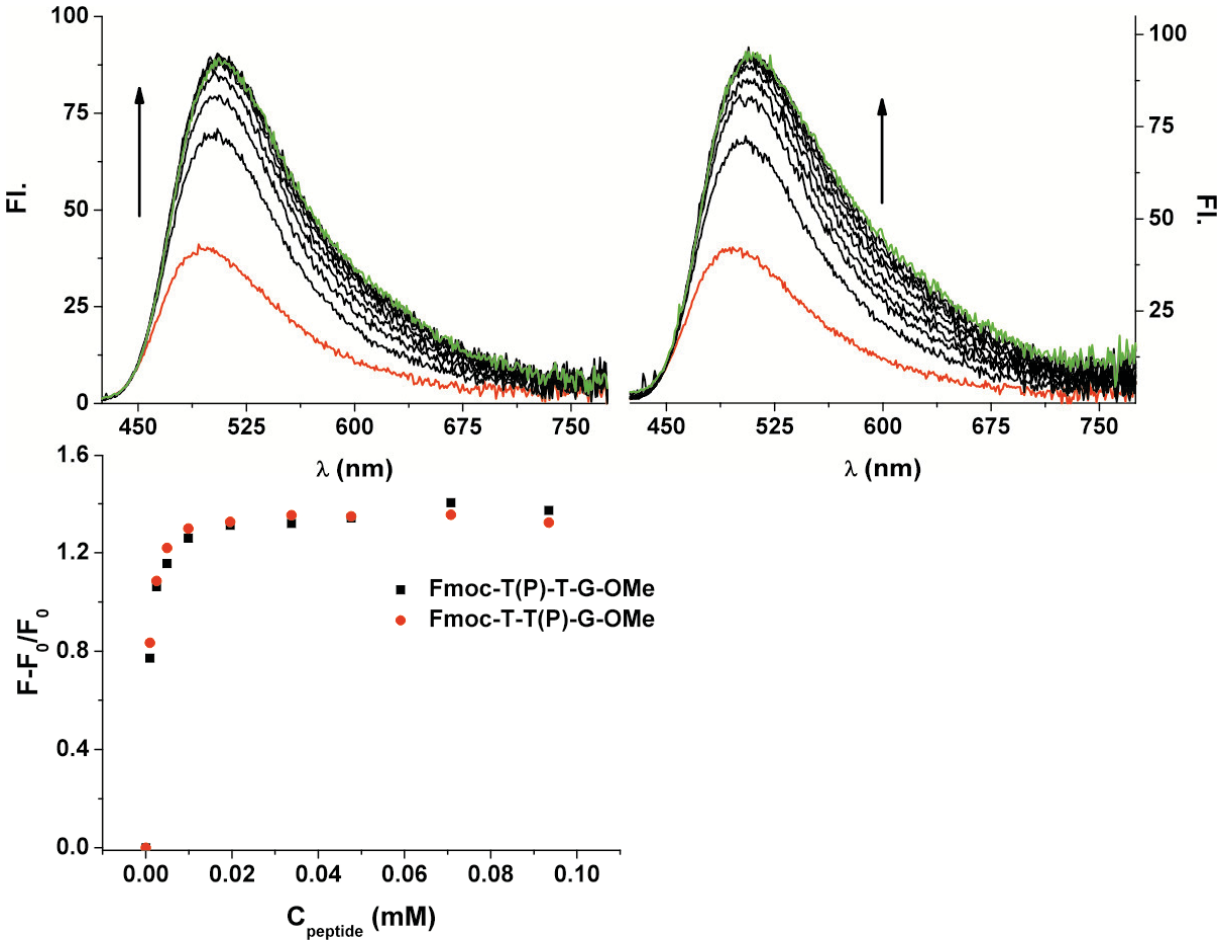

Fig. 18.26 Fluorescence response of 1 mg/mL **CSM10-8** MIP towards 3mer peptide Fmoc-T(P)-T-G-OMe (top left) and Fmoc-T-T(P)-G-OMe (top right) in $CHCl_3$, ($C_{peptide}$=2-500 µM, starting point spectra in red, end point spectra in green) and the binding curve measured by fluorescence at 525 nm), Fmoc-T(P)-T-G-OMe in red and and Fmoc-T-T(P)-G-OMe in black

In conclusion, **M10** is a promising fluorogenic monomer which possesses a high affinity to carboxylate as well as to phosphate. The ESPT band provides a potential two-channel ratiometric signaling scheme, which is very promising in terms of real sensor design. This ESPT band is sensitive to the effective basicity of the anion and the distance as well orientation of the respective partners. The successful embedding of the monomer into the MIP matrix enabled a good discrimination of a phosphorylated tyrosine to the non-phosphorylated one. Using a two-phase extraction assay format, the discrimination could be further enhanced rendering the system a promising fluorescence sensor. The sensor particles can also recognize short phosphorylated peptides, however, the ESPT band was not formed and the discrimination between different peptides still has to be improved. In future work, the binding sites still have to be improved for satisfying peptide recognition

19 Comparison of MIP Formats

MIPs can be prepared in different formats. Monoliths are the most common and popular ones. They can be prepared by mixing all the components such as monomer, crosslinker, initiator, template and porogen in a sealed glass tube. After polymerization, the glass tube is broken and the prepared monolith can be grinded and sieved into small particle for further application. Although they are widely applied in separation, their disadvantage regarding sensing applications has been demonstrated here. This is primarily due to the fact that the particles are polydisperse and show a heterogeneity of the binding sites.

Thin MIP films or membranes are also an established and relevant format. They vary from very thin films of few nanometers thickness, such as self-assembled monolayers, to very thick films of up to a few 100 µm. But their stability is quite often an issue, toward macroscopic (external) forces as well as swelling or local inhomogeneities. To circumvent these problems at least to some degree, they are often grafted onto a stable substrate such as a glass slide. However, certain stability issues like swelling also remain on a rigid support, which limits their broad application.

Small particles, especially core-shell particles, are a very promising format especially for optical chemical sensors. Their very thin polymer layer is remarkably stable. Moreover, such coatings generally show a greatly reduced heterogeneity and fast analyte diffusion times. The use of such materials is especially relevant in case of imprinting expensive templates. The synthesis of particles does not suffer from thermal dissipation problems, potentially rendering upscaling for industrial purposes facile. In addition, since today's nanoparticle research activities allow for an almost limitless combination of materials and integration of functionalities, the cores of such C/S beads can be made magnetic, can be equipped with a code or can be a multi-functional entity in itself.

In conclusion, core-shell particles have turned to be a promising MIP format in various fields.

20 Conclusion and Outlook

The fluorogenic monomer is the most important building block in this project. Various fluorophores including indole, BODIPY, naphthalimide, benzoxadiazole, phenoxazinone and phenazine were used to design the functional monomers. Indole was abandoned due to the unsuitable spectral windows. The other classes can be excited above 400 nm and emit below 700 nm which is compatible with economical light sources and detectors. Various sensing behaviors such as fluorescence quenching (**M6** and **M4**), fluorescence enhancement (**M5** and **M7**) with small spectral shifts and ESPT (**M10**) have been achieved.

The affinity of the monomer to the template is a decisive parameter. It increased with increasing acidity of the urea N-H, but with the risk of deprotonation. The increase of acidity can be achieved through substitution of the urea with electron withdrawing moieties. Affinity is also influenced by the solvent polarity and the counter-ion. Nevertheless, all prepared monomers have proven to have high binding constants towards the templates as shown by spectrophotometric and NMR titration. Thus, they can be used in stoichiometric noncovalent imprinting.

In conclusion we have developed a series of urea based fluorogenic monomers covering various chromogenic groups. These functional monomers show different sensing responses as fluorescence enhancement, fluorescence quenching and ESPT. Except for **M10,** operating through an ESPT transduction mechanism, the other fluorogenic monomers are based on a charge transfer mechanism. Most monomers show prominent affinity and sensing response towards the target molecules. Upon introduction into the MIP matrix, some monomers such as BODIPY and phenoxazinone based monomers show prominent sensing responses, yet a low selectivity. This was attributed to a larger cavity formed during polymerization. This large cavity cannot provide enough discrimination towards different analytes. Fortunately, some monomers such as benzoxodiazole, naphathalimide and **M10** show prominent imprinting effects as well as selectivity towards competitors and enantiomers. Especially the MIPs prepared in the format of core-shell particles greatly decrease the sensing time, favorable signal saturation within 20 seconds being achieved which is very promising for fast detection. These successful results are encouraging to further refine this sensor system towards real applications.

Firstly, there is still space for functional monomer modification. As discussed in the previous Section, sensor particles prepared from **M5** show poor discrimination in all cases. We suppose that the orientation of the fluorogenic monomer in the MIP matrix might be the reason. However, due to the limited time of this project, this could not systematically be studied. It would be an interesting research topic for the future, for instance, by modifying the point of integration into the network or introduction of a second polymerizable group, to assess the potential of fluorescent probe crosslinkers which will not only introduce more fluorogenic monomer into the MIP matrix but also promote the sensing response of the already succeed monomers.

Secondly, in these studies, most transduction mechanisms are based on charge transfer. The other commonly employed transduction mechanisms such as electron transfer based on PET and energy transfer such as FRET have not been investigated here. However, it would be interesting to introduce them into optical MIP sensors in the future. Especially the FRET process can provide a two channel ratiometric sensing scheme which might be a very sensitive and robust technique for signaling MIPs. This can either be achieved through co-doping a fluorescent counter-ion as FRET donor/acceptor. By recognition, the ternary system would trigger a FRET signal. Another strategy might be to design a displacement assay with a FRET active partner where the FRET signal is switched off in the analytical (displacement) reaction.

Thirdly, additional functional shells can be introduced to enable additional gating functions. These can be photo-switchable layers or lower/upper critical solution temperature (LCST/UCST) layers to enable photo- or thermal switching of the protecting layer to control access of the analyte to the MIP shell. In natural systems such as an enzyme, the hydrophobic binding site is protected by the protein backbone. Nature uses a complicated coding system to synthesize a long peptide chain and then fold it into the right ternary structure. However, this is impossible for us to realize within the structure of a polymer. Although we have more monomers at hand than nature, a systematic polymerization is difficult. To simplify this problem we can initially only mimic the effective position with a limited monomer system and introduce a protective shell in a later step through post-grafting.

Fourthly, the application format can be elaborated. In a sensing system, a sensor array can provide more information about the sample under invesitgation. Regarding high sample throughput, fast and reliable measuring array sensors can greatly improve performance. Array systems can be realized on a slide by depositing different sensor particles in spots onto glass slides and assessing them through an array scanner.[208] Another array format can be realized in

liquid phase and processed through flow cytometer or microfluidic chip. Here for example different barcoded sensor particles can be suspended in solution and mixed with analytes. These particles will pass the detection area and the sensing response will be registered.

Array system cannot only provide multi-target detection but also increase the dynamic range. In our studies, the dynamic range is relatively narrow. The array format can, however, greatly expand the dynamic range and simplify the sensing process.

Microfluidic chips are potentially a very promising sensing system for the future. This miniaturized flow system can be easily coupled to portable detection units. With the help of advanced and miniaturized camera system (e.g., webcams, smartphones), true handheld optical sensors can be assembled. Raw data registered by such systems can be directly transmitted through wireless connections and for instance, they can automatically be delivered to a medical centre for further diagnosis and advice. Especially coupled to the nowadays highly developed cloud storage and high-speed internet systems, a remote diagnostic and medical treatment system can be build in the near future. This would be very exciting not only for the patient but also for those people doing daily health monitoring.

21 Experimental Section:

21.1 Materials and instruments. Acetonitrile, chloroform, toluene (all anhydrous), all other solvents (UV-Vis grade), 3-aminopropyltriethoxysilane (APTES), 1,5-dianiline, 2,2'-azobis(2,4-dimethylvaleronitril) (ABDV), benzylmethylacrylate (BMA), boron trifluoride diethyl etherate (>46%), 4-chloro-7-nitrobenzofurazan (NBD-Cl), 4-cyano-4-(thiobenzoylthio)pentanoic acid (CPDB), 2,3-diamonophenazine, N,N'-dicyclohexyl-carbodiimide (DCC), N, N'-dicyclohexylurea (DCU), 4-(dimethylamino)-pyridine (DMAP), 2,6-di-tert-butyl-4-methyl-phenol (BHT), ethanolamine, hydrazine monohydrate (66-68%), hydrogen peroxide solution (30%), methylacryamide (MAAM), methylmethacrylate (MMA), mesitaldehyde, methyacrylic acid-2-isocyanatoethylester, palladium acetate, silicagel 60 (70-230 mesh), styrene, tetrabutylammonium hydroxide 30 hydrate, 3,5-bis trifluomethyl benzyl isocyanate, triethyl amine and triphenyl phosphin, were purchased from Sigma Aldrich, aluminum oxide (150 mesh) and ethylchloroformate from Fluka, tetraethylorthosilicat (TEOS) from Merck, trifluoroacetic acid and ammonium hydroide solution (32%) from Applichem, Z-D-phenyalanine, Z-L-phenylalanine, Z-L-glutamicacid were purchased from ABCR. 1,2,2,6,6-pentamethylpiperidine (PMP) was purchased from Alfa Aesar (karlsruhe). Fmoc-T(P)-T-G-OMe and Fmoc-T-T(P)-G-OMe were received from Dr. Shinde. Cover Glasses with a diameter of 5 mm and nominal thickness of 0.145 mm were purchased from Thermo Scientific, Menzel GmbH & Co. KG.

BMA, MMA and EDMA were distillated to remove the inhibitor before use.

M1 and **M6** were received from Dr. Wagner, BODIPY based monomers were received from Dr. Biyikal.

TGA spectra were measured with SETARAM TAG24 from SETARAM Instrumentation. ^{1}H- and ^{13}C-NMR was recorded on a Bruker AV-400 spectrometer. Mass spectra were measured with CT Premier XE - TOF Mass Spectrometer. Absorption spectra and UV/vis-spectrophotometric titrations were recorded on a Specord 210 Plus absorption spectrometer (Analytik Jena) and fluorescence spectra and titrations were measured with a FluoroMax 4 spectrofluorometer (Horiba Jobin Yvon) at 298 ± 1 K. TEM images were registered with Tecnai Transmission Electron Microscope. SEM and T-SEM images were registered with REM Zeiss SUPRA 40 (Carl Zeiss). DLS was mearsured with Zetasizer Nano ZS (Malvern).

21.2 Preparation of monomer

21.2.1 7-chloro-5,5-difluoro-3-((3-(3-(2-(methacryloyloxy)ethyl)ureido)phenyl)amino)-10-(p-tolyl)-5H-dipyrrolo[1,2-c:2',1'-f][1,3,2]diazaborinin-4-ium-5-uide (M2)

20 mg (0.06 mmol) 3,5-dichloro-4,4-difluoro-8-(4-tolyl)-4-bora-3a,4a-diaza-*s*-indacene (prepared following Rohand et al. procedure [209]) and 20 mg (0.13 mmol) 2-(3-(3-aminophenyl)ureido)ethyl methacrylate were dissolved in 6 mL DMF, the mixture was stirred at 55 ^{o}C for 16 h. The solvent was removed in vacuum. The raw product was purified by column chromatography on silica gel with DCM : MeOH (5:0.1) to obtain 35 mg (90 %) product as red oil. ^{1}H-NMR (500 MHz, DMSO-d_6) δ: 1.88 (s, 3H), 2.39 (s, 3H), 4.12 (t, *J* = 5.5, 2H), 5.68 (t, *J* = 1.5, 1H), 6.06 (s, 1H), 6.30 (q, *J* = 5.0, 2H), 6.43 (d, *J* = 5.0, 1H), 6.91 (d, *J* = 8.5, 1H), 6.99 (d, *J* = 5, 2H), 7.33 (m, 6H), 7.76 (s, 1H), 8.75 (s, 1H), 10.11 (s, 1H). ^{13}C-NMR (DMSO-d_6) δ: 18.30, 21.4, 39.7, 63.9, 112.0, 113.4, 116.5, 116.7, 121.8, 126.3, 129.1, 129.2, 130.3, 130.7, 131.2, 132.1, 132.9, 134.0, 135.7, 135.9, 138.0, 139.7, 140.1, 155.0, 158.5, 167.7. **CHN-Analysis** ($C_{29}H_{27}BClF_2N_5O_3$): Cal. C 60.28, H 4.71, N 12.12; found. C 60.506, H 4.981, N 11.154. MS: *m/z* 578.18 ($(M+H)^+$)

21.2.2 (E)-7-chloro-5,5-difluoro-3-(4-(3-(2-(methacryloyloxy)ethyl)ureido)styryl)-10-(p-tolyl)-5H-dipyrrolo[1,2-c:2',1'-f][1,3,2]diazaborinin-4-ium-5-uide (M3)

23 mg (0.07 mmol) 3,5-dichloro-4,4-difluoro-8-(4-tolyl)-4-bora-3a,4a-diaza-*s*-indacene and 50 mg (0.18 mmol) 2-(3-(4-vinylphenyl)ureido)ethyl methacrylate were dissolved in 1.1 mL MeCN, 4 mg palladium acetate, 4 mg phenyl phosphine and 50 uL TEA as catalyst were added into the solution. The mixture was stirred at 80 ^{o}C for 16 h. Solvent was removed and the raw product was purified by column chromatography on silica gel with $CHCl_3$: MeOH (5:0.1) to obtain 22 mg (53%) product as violet powder. mp: 245-247 ^{o}C. ^{1}H-NMR (500 MHz, DMSO-d_6) δ: 1.84 (s, 3H), 3.47 (q, *J* = 5, 2H), 4.17 (t, *J* = 5, 2H), 5.10 (d, *J* = 10, 1H), 5.37 (t, *J* = 5, 1H), 5.49 (t, *J* = 1.5, 1H), 5.57 (d, *J* = 17.5 1H), 6.57 (dxd, J_1 = 15, J_2=10 1H), 6.95 (s, 1H), 7.22 (m, 4H). **CHN-Analysis** ($C_{31}H_{28}BClF_2N_4O_3$): Cal. C 63.23, H 4.79, N 9.51; found. C 67.290, H 6.553, N 8.410. MS: *m/z* 589.79 ($(M+H)^+$)

21.2.3 3-chloro-5,5-difluoro-10-mesityl-7-(2-((2(methacryloyloxy)ethyl)carbamoyl)-hydrazinyl)-5H-dipyrrolo[1,2-c:2',1'-f][1,3,2]diazaborinin-4-ium-5-uide(M4)

20 mg (0.05 mmol) 3-chloro-5,5-difluoro-7-hydrazinyl-10-mesityl-5H-dipyrrolo[1,2-c:2',1'-f][1,3,2]diazaborinin-4-ium-5-uide (prepared following Dilek´s procedure [210]) and 20 uL methyacrylic acid-2-isocyanato ethyl ester were dissolved in 3 mL DCM, 5 mg DMAP as

catalyst and 5 mg BHT as inhibitor were added into the solution. The mixture was stirred at 55 ^{o}C for 24 h. Solvent was removed in vacuum and the raw product was purified by column chromatography on silica gel with DCM : MeOH (5:0.1) to obtain 13 mg (50%) product as black powder. mp: 221-223 ^{o}C. ^{1}H-NMR (500 MHz, $CDCl_3$) δ: 1.90 (s, 3H), 2.08 (s, 6H), 2.34 (s, 3H), 3.58 (s, 2H), 4.25 (t, *J* = 5, 2H), 5.54 (t, *J* = 1.5, 1H), 5.87 (s, 1H), 6.10 (s, 1H), 6.17 (d, *J*=3, 1H), 6.22 (d, *J*=3, 1H), 6.30 (d, *J*=4, 1H), 6.66 (d, *J*=4, 1H), 6.79 (s, 1H), 6.92 (s, 2H), 7.79 (s, 1H). ^{13}C-NMR ($CDCl_3$) δ:14.10, 19.23, 19.86, 21.09, 29.69, 34.00, 38.73, 39.47, 109.87, 114.28, 122.79, 126.25, 128.17, 128.80, 132.01, 133.37, 134.33, 135.85, 139.95, 138.61 **CHN-Analysis** ($C_{25}H_{27}BClF_2N_5O_3$): Cal. C 56.68, H 5.14, N 13.22; found. C 58.42, H 6.28, N 15.76. MS: *m/z* 530.6 ($(M+H)^+$)

21.2.4 2-(3-(1-methyl-3-oxo-3H-phenoxazin-7-yl)ureido)ethyl 3-methylbut-3-enoate (M5)

754 mg 7-amino-1-methyl-3H-phenoxazin-3-one (prepared following the procedure of Descalzo et. al.[164]) and 8mL methyacrylic acid-2-isocyanato ethyl ester were dissolved in 18 mL pyridine, 470 mg DMAP was added into the solution, the mixture was stirred at 85 ^{o}C for 7 h. After cooling to RT, 50 mL hexane was added into the solution and a black solid as raw product was precipitated out. Raw product was purified by column chromatography on Alox (neutral Al_2O_3) with DCM: ethanol (5:0.05) to obtain 500 mg (39%) black powder. mp: 230-232 ^{o}C. ^{1}H-NMR (500 MHz, DMSO-d_6) δ: 1.90 (s, 3H,), 2.34 (s, 3H,), 3.43 (q, *J* = 9, 2H), 4.15 (t, *J* = 4,5, 2H), 5.71 (t, *J* = 2.5, 1H), 6.09 (m, 1H,), 6.17 (d, *J* = 3.5, 1H), 6.63 (m, 2H), 7.28 (dxd, J_1=4, J_2= 18.5, 1H), 7.688 (s, 1H,), 7.73 (t, *J*=3.5, 1H), 9.47 (s, 1H). ^{13}C-NMR (DMSO-d_6) δ: 16.80, 18.47, 64.14, 94.38, 103.10, 105.39, 115.62, 126.49, 127.86, 131.33, 131.83, 136.25, 143.31, 145.32, 145.72, 150.65, 155.07, 167.00, 185.31, 215.68. **CHN-Analysis** ($C_{20}H_{19}N_3O_5$): Cal. C 63.79, H 5.35, N 10.63; found. C 66.45, H 7.40, N 12.56. MS: *m/z* 396.28 ($(M+H)^+$)

21.2.5 2-(3-(4-Nitrobenzo[c][1,2,5]oxadiazol-7-yl)ureido)ethyl methacrylate (M7).

200 mg (1.1 mmol) 4-amino-7-nitrobenzo[c][1,2,5]oxadiazole (prepared following the protocol from Uchiyama et al.[181]) were dissolved in 10 mL dry pyridine. After the addition of 122 mg DMAP, 20 mg BHT as stabilizer and 257 mg (1.7 mmol) methyacrylic acid-2-isocyanatoethylester, the mixture was further stirred at RT for 12 h. The solid was precipitated after addition of 50 mL hexane. The raw product was purified by column chromatography on silica gel with ethyl acetate-hexane (2:3) and re-crystallized from ethyl acetate to obtain 294.8

mg (80%) yellow powder. mp: 186-188 °C. ^{1}H NMR (400 MHz, $CDCl_3$): δ: 1.90 (s, 3H), 3.63 (q, *J* = 5.0, 2H), 4.32 (t, *J* = 5.0, 2H), 5.58 (t, 1H), 5.65 (t, 1H), 6.11 (t, 1H), 8.13 (s, 1H), 8.18 (d, *J* = 8.5, 1H), 8.49 (d, *J* = 8.5, 1H). ^{13}C-NMR($CDCl_3$) δ: 49.86, 52.25, 64.95, 123.85, 125.40, 146.27, 161.66, 175.28, 204.82, 208.22, 214.37, 217.32. CHN-Analysis ($C_{13}H_{13}N_5O_6$): Cal. C 46.57, H 3.91, N 20.89; found. C 48.98, H 5.88, N 22.25. MS: *m/z* 336.19 ($(M+H)^+$)

21.2.6 1-(4-nitrobenzo[c][1,2,5]oxadiazol-7-yl)-3-(4-vinylphenyl)urea (M8).

100 mg (0.6 mmol) 4-amino-7-nitrobenzo[c][1,2,5]oxadiazole were dissolved in 10 mL dry pyridine. After the addition of 61 mg DMAP, 10 mg BHT as stabilizer and 257 mg (3 mmol) vinyl-benzyl isocyanate (prepared following a procedure from Wagner et al.[61]), the mixture was further stirred at RT for 24 h. The solid was precipitated after addition of 50 mL hexane. The raw product was purified by column chromatography on silica gel with ethyl acetate-hexane (2:3) and re-crystallized from methanol to obtain 294.8 mg (50%) red powder. mp: 186-188 °C. ^{1}H NMR (400 MHz, $CDCl_3$): δ: 5.35 (d, J=11, 1H), 5.81 (q, *J* = 16.5, 1H), 6.75 (q, *J* = 10.0, 2H),7.36 (d, J = 8.5, 2H), 7.36 (d, J = 8.5, 2H), 7.55 (d, J = 8.5, 2H), 7.73 (s, 1H), 8.47 (d, *J* = 9, 1H). ^{13}C-NMR($CDCl_3$) δ: 86.06, 101.14, 101.86, 115.20, 123.20, 124.06, 127.87, 135.79, 135.30, 136.70, 139.61, 150.49, 152.86, 156.29, 175.79. CHN-Analysis ($C_{13}H_{13}N_5O_6$): Cal. C 55.39, H 3.41, N 21.53; found. C 56.55, H 4.58, N 23.66. MS: *m/z* 326.28 ($(M+H)^+$)

21.2.7 2-(2-(7-nitrobenzo[c][1,2,5]oxadiazol-4-yl)hydrazinecarboxamido)ethyl methacrylate (M9)

200 mg, (1.1 mmol) 4-hydrazino-7-nitro-2,1,3-benzoxadiazole was were dissolved in 10 mL dry pyridine, after the addition of 122 mg DMAP, 20 mg BHT as stabilisator and 250 mg (1.7 mmol) methyacrylacid-2-isocyanatoethylester were added into the solution, the mixture was further stirred for 24 hours. The solid was precipitated and washed with 50 mL hexane, it was further purified with silica gel with AcOEt-Hexane (2:3) and re-crystalized with MeOH. 294.8 mg green powder is obtained with a yield of 60%. ^{1}H NMR (500 MHz, $CDCl_3$): δ: 1.82 (s, 3H), 3.51 (t, *J* = 5.5, 2H), 4.17 (t, *J* = 5.5, 2H), 5.52(s, 1H), 6.02 (s, 1H), 6.15 (d, J = 10.5, 1H), 7.26 (d, J = 10.5, 1H). CHN-Analysis ($C_{13}H_{14}N_6O_6$): Cal. C 44.57, H 4.03, N 23.99; found. C 47.21, H 5.02, N 24.56. MS: *m/z* 351.22 ($(M+H)^+$)

21.2.8 (((phenazine-2,3-diylbis(azanediyl))bis(carbonyl))bis(azanediyl))bis(ethane-2,1-diyl) bis(2-methylacrylate) (M10)

300 mg (1.43 mmol) of 2,3-diamonophenazine and 445 mL (3.15 mmol) of the methyacrylacid-2-isocyanatoethylester were dissolved under Ar in 10 mL of anhydrous DMF, 10 mg BTH was added to prevent the polymerization. The mixture was stirred at 60 ºC. After 3 h, 445 mL (3.15 mmol) additional methyacrylacid-2-isocyanatoethylester were added to the solution and the reaction was left at 60 ºC for 20 h. The solvent was removed in vacuum, and the orange-brown solid residue obtained was further purified by column chromatography on silica gel with DCM : MeOH (10:1) to obtain 204 mg (65 %) brown powder. mp: 223-225 ^{o}C. ^{1}H NMR (400 MHz, DMSO-d_6): δ: 1.92 (s, 6H), 3.49 (d, *J* = 7, 4H), 4.21 (t, *J* = 6.5, 4H), 5.71(t, J = 2, 2H), 6.11 (s, 2H), 7.01(t, J = 6.5, 2H), 7.82 (q, J = 8.5, 2H), 8.12 (q, J = 4.5, 2H), 8.40 (s, 2H), 8.48 (s, 2H). ^{13}C NMR (500 MHz, $CDCl_3$) δ:17.8, 38.1, 63.5, 116.3, 125.8, 128.7, 129.3, 135.6, 136.1, 140.9, 141.9, 166.2. CHN-Analysis ($C_{26}H_{28}N_6O_6$): Cal. C 59.99, H 5.42, N 16.14; found. C 61.88, H 6.87, N 17.98. MS: *m/z* 521.42 ($(M+H)^+$)

21.2.9 7-((3-(3-(3,5-bis(trifluoromethyl)phenyl)thioureido)phenyl)amino)-3-chloro-5,5-difluoro-10-(p-tolyl)-5H-dipyrrolo[1,2-c:2',1'-f][1,3,2]diazaborinin-4-ium-5-uide (C1)

26 mg (0.06 mmol) 3,5-dichloro-4,4-difluoro-8-(4-mesityl)-4-bora-3a,4a-diaza-*s*-indacene and 50 uL 1-(3,5-bis(trifluoromethyl)phenyl)-3-(4-aminophenyl)thiourea were dissolved in 2 mL THF, 5 mg DMAP were added to the solution and the mixture was stirred at RT for 16 h. After removing the solvent, the raw product was further purified by column chromatography on silica gel with ethyl acetate: cyclohexane (1:3) to obtain 45 mg (95 %) red powder. mp: 201-203 ^{o}C.^{1}H-NMR (500 MHz, $CDCl_3$) δ: 2.04 (s, 6H,), 2.28 (s, 3H,), 6.13 (q, *J* = 4.5, 2H), 6.33 (d, *J* = 4,5, 1H), 6.64 (d, *J* = 4.5, 1H), 6.87 (s, 2H,), 7.27 (d, *J* = 9, 2H), 7.36 (d, *J* = 9, 2H), 7.64 (s, 1H,), 7.93 (s, 2H,), 8,09 (br.s, 1H). **CHN-Analysis** ($C_{33}H_{25}BClF_8N_5S$): Cal. C 54.90, H 3.49, N 9.70, S 4.44; found. C 58.522, H 4.872, N 7.443, S 3.476. MS: *m/z* 694.22 ($(M+H)^+$)

21.2.10 7-((3-(3-(3,5-bis(trifluoromethyl)phenyl)ureido)phenyl)amino)-3-chloro-5,5-difluoro-10-(p-tolyl)-5H-dipyrrolo[1,2-c:2',1'-f][1,3,2]diazaborinin-4-ium-5-uide (C3)

26 mg (0.07 mmol) 3,5-dichloro-4,4-difluoro-8-(4-toluyl)-4-bora-3a,4a-diaza-*s*-indacene and 30 mg (0.08 mmol) 1-(3,5-bis(trifluoromethyl)phenyl)-3-(4-aminophenyl)urea were dissolved in 1 mL DMF, 50 uL TEA were added to the solution and the mixture was stirred at 100 ^{o}C for 2 h. The product was washed with 50 mL 1M HCl and saturated $NaHCO_3$ solution and extracted with ethyl acetate. After removing the solvent, the raw product was further purified

by column chromatography on silica gel with ethyl acetate: cyclohexane (1:3) to obtain 47 mg (95 %) red powder. mp: 211-213 °C. ^{1}H-NMR (500 MHz, DMSO-d_6) δ: 2.39 (s, 3H,), 6.31 (q, J=4, 2H), 6.47 (d, *J* = 5 Hz, 1H), 7.61 (m, 2H), 7.35 (m, 6H), 7.64 (d, J=8, 2H,), 8.12 (s, 2H), 9.18 (s, 1H), 9.44 (s, 1H,), 10.18 (s, 1H,), 10.52 (br.s, 1H). ^{13}C-NMR (DMSO-d_6) δ: 20.94, 112.52, 114.62, 115.03, 116.82, 118.14, 118.17, 118.90, 119.00, 124.68, 129.18, 129.29, 129.66, 130.15, 130.32, 130.62, 130.91, 133.35, 138.34, 139.21, 139.95, 141.73, 152.44, 159.72 **CHN-Analysis** ($C_{31}H_{21}BClF_8N_5O$): Cal. C 54.93, H 3.12, N 10.33; found. C 54,704, H 3.912, N 9.204. MS: *m/z* 678.30 ($(M+H)^+$)

21.2.11 (E)-7-(4-(3-(3,5-bis(trifluoromethyl)phenyl)ureido)styryl)-3-chloro-5,5-difluoro-10-(p-tolyl)-5H-dipyrrolo[1,2-c:2',1'-f][1,3,2]diazaborinin-4-ium-5-uide (C4)

29 mg (0.08 mmol) 3,5-dichloro-4,4-difluoro-8-(4-mesityl)-4-bora-3a,4a-diaza-*s*-indacene and 33 mg (0.1 mmol) 1-(3,5-bis(trifluoromethyl)phenyl)-3-(4-vinylphenyl)urea were dissolved in 1.2 mL dry DMF, 5mg palladium acetate, 6 mg triphenyl phosphine and 40 uL TEA were added as catalyst into the solution. The mixture was stirred at 45 °C for 72 h. After removing the solvent, the raw product was further purified by column chromatography on silica gel with ethyl acetate and cyclohexane (1:3) to obtain 24 mg (41 %) violet powder. mp: 224-226 °C. ^{1}H-NMR (500 MHz, $CDCl_3$) δ: 2.40 (s, 3H), 4.30 (t, J=7, 1H), 5.01 (d, J=5, 1H), 6.29 (d, *J* = 4.5, 1H), 6.66 (d, *J* = 4.5, 1H), 6.88 (dxd, *J1=20, J2= 4.5,* 2H), 7.27 (m, 6H), 7.39 (d, *J*=3.5, 6H), 7.54 (d, *J* = 16.5, 1H), 7.78 (s, 1H), 7.83 (s, 2H), 7.93 (s, 1H), 8.58 (s, 1H), 9.69 (s, 1H). ^{13}C-NMR ($CDCl_3$) δ: 22.68,23.46, 23.85, 23.93, 29.15, 32.31, 41.10, 51.00, 58.35, 59.23, 59.33, 60.06, 103.84, 108.00, 129.02, 129.20, 130.47, 139.56, 139.68, 144.46, 146.46, 202.53. MS: *m/z* 689.79 ($(M+H)^+$)

21.2.12 7-((3-(3-(3,5-bis(trifluoromethyl)phenyl)ureido)phenyl)amino)-3-chloro-5,5-difluoro-10-mesityl-5H-dipyrrolo[1,2-c:2',1'-f][1,3,2]diazaborinin-4-ium-5-uide (C5)

114 mg (0.3 mmol) 3,5-dichloro-4,4-difluoro-8-(4-mesityl)-4-bora-3a,4a-diaza-*s*-indacene and 125 mg (0.34 mmol) 1-(3,5-bis(trifluoromethyl)phenyl)-3-(3-aminophenyl)urea were dissolved in 1 mL DMF, 100 uL TEA were added to the solution and the mixture was stirred at 100 °C for 2 h. The product was washed with 50 mL 1M HCl and saturated $NaHCO_3$ solution and extracted with ethyl acetate. After removing the solvent, the raw product was further purified by column chromatography on silica gel with ethyl acetate: cyclohexane (1:3) to obtain 214 mg (90%) red powder. mp: 204-206 °C. ^{1}H-NMR (500 MHz, DMSO-d_6) δ: 2.03 (s, 6H), 5.93 (d, J=5, 1H), 6.22 (d, J=4, 1H), 6.41 (d, *J* = 5.0, 1H), 6.71 (d, *J* = 5, 1H), 7.00 (s, 2H), 7.07 (t, *J* = 2.0, 2H), 7.36 (d, *J*=2, 2H), 7.64 (d, *J* = 19, 2H), 8.13 (s, 2H), 9.20 (s, 2H),

9.46 (s, 1H), 10.30 (s, 1H). ^{13}C-NMR (DMSO-d_6) δ: 19.79, 21.00, 23.71, 26.58, 29.88, 115.44, 118.39, 118.42, 128.39, 129.41, 129.89, 136.78, 141.98, 152.70. **CHN-Analysis** ($C_{33}H_{25}BClF_8N_5O$): Cal. C 56.15, H 3.57, N 9.92; found. C 56.927, H 3.803, N 9.684. MS: *m/z* 706.22 ($(M+H)^+$)

21.2.13 7-((4-(3-(3,5-bis(trifluoromethyl)phenyl)ureido)phenyl)amino)-3-chloro-5,5-difluoro-10-mesityl-5H-dipyrrolo[1,2-c:2',1'-f][1,3,2]diazaborinin-4-ium-5-uide (C6)

52 mg (0.15 mmol) 3,5-dichloro-4,4-difluoro-8-(4-mesityl)-4-bora-3a,4a-diaza-*s*-indacene and 65 mg (0.17 mmol) 1-(3,5-bis(trifluoromethyl)phenyl)-3-(4-aminophenyl)urea were dissolved in 1 mL DMF, 100 uL TEA was added to the solution and the mixture was stirred at 100 ^{o}C for 2 h. The product was washed with 50 mL 1M HCl and saturated $NaHCO_3$ solution and extracted with ethyl acetate. After removing the solvent, the raw product was further purified by column chromatography on silica gel with ethyl acetate: cyclohexane (1:3) to obtain 103 mg (91%) red powder. mp: 214-215 ^{o}C. ^{1}H-NMR (500 MHz, DMSO-d_6) δ: 2.03 (s, 6H), 2.29 (s, 3H), 5.90 (d, *J* = 4.0, 1H), 6.20 (d, *J* = 3.5, 1H), 6.32 (d, *J* = 5.0, 1H), 6.67 (d, *J* = 5.0, 1H), 6.99 (s, 2H), 7.32 (d, *J* = 8.5, 2H), 7.53 (d, *J* = 8.5, 2H), 7.65 (s, 1H), 8.13 (s, 2H), 9.16 (s, 1H), 9.46 (s, 1H), 10.2 (br. s, 1H). ^{13}C-NMR ($CDCl_3$) δ: 19.9, 21.1, 112.3, 114.5, 115.3, 116.9, 118.1, 119.5, 122.3, 124.4, 125.8, 125.9, 126.4, 128.1, 129.2, 130.4, 130.6, 130.9, 131.0, 131.2, 132.3, 134.1, 134.6, 136.6, 137.6, 137.7, 141.8, 152.5, 160.1. **CHN-Analysis** ($C_{33}H_{25}BClF_8N_5O$): Cal. C 56.15, H 3.57, N 9.92; found. C 56.919, H 3.675, N 8.933. MS: *m/z* 706.31 ($(M+H)^+$)

21.2.14 7-((2-(3-(3,5-bis(trifluoromethyl)phenyl)ureido)phenyl)amino)-3-chloro-5,5-difluoro-10-mesityl-5H-dipyrrolo[1,2-c:2',1'-f][1,3,2]diazaborinin-4-ium-5-uide (C7)

43 mg (0.11 mmol) 3,5-dichloro-4,4-difluoro-8-(4-mesityl)-4-bora-3a,4a-diaza-*s*-indacene and 50 mg (0.14 mmol) 1-(3,5-bis(trifluoromethyl)phenyl)-3-(2-aminophenyl)urea were dissolved in 1 mL DMF, 100 uL TEA was added into the solution and the mixture was stirred at 100 ^{o}C for 2 h. The product was washed with 50 mL 1M HCl and saturated $NaHCO_3$ solution and extracted with ethyl acetate. After removing the solvent, the raw product was further purified by column chromatography on silica gel with ethyl acetate: cyclohexane (1:3) to obtain 66 mg (85 %) red powder. mp: 198-199 ^{o}C. ^{1}H-NMR (500 MHz, DMSO-d_6) δ: 2.00 (s, 3H,), 2.29 (s, 3H), 5.93 (d, *J* = 3.5 Hz, 1H), 6.19 (t, J=5.5, 2H), 7.29 (t, J=8, 1H), 7.38 (t, J=8.5, 1H,), 7.52 (q, J=3, 1H), 7.67 (s, 1H), 8.19(s, 1H,), 8.90 (s, 1H,), 9.68 (s, 1H), 9.81 (s, 1H), 9.81 (s, 1H). ^{13}C-NMR (DMSO-d_6) δ: 19.50, 20.72, 32.38, 57.21, 65.28, 73.13, 79.18, 85.61, 114.42, 118.67, 126.97, 127.90, 128.12, 129.05, 130.97, 136.46, 153.18.

CHN-Analysis ($C_{33}H_{25}BClF_8N_5O$): Cal. C 56.15, H 3.57, N 9.92; found. C 57.154, H 3.979, N 9.157. MS: *m/z* 706.11 ($(M+H)^+$)

21.2.15 1-(3,5-bis(trifluoromethyl)phenyl)-3-(3-aminophenyl)thiourea

160 mg (1.5 mmol) 1,5-dianiline and 200 uL 3,5-bis trifluomethyl benzyl isocyanate were dissolved in 6 mL THF. The mixture was stirred at RT for 16h. The solvent was removed in vacumm. The raw product was purified by column chromatography on silica gel with ethyl acetate:cyclohexane (1:1) to obtain 185 mg (32%) yellow powder. mp:145-147 ^oC. ^1H-NMR (500 MHz, CDCl3) δ: 2.04 (s, 6H), 2.27 (s, 3H), 3.68 (s, 1H), 6.06 (q, J=4, 2H), 6.32 (d, *J* = 5, 1H), 6.52 (m, 4H), 6.86 (s, 2H), 7.09 (t, *J*=8, 1H), 7.98 (s, 1H). ^{13}C-NMR ($CDCl_3$) δ: 19.93, 21.12, 26.93, 108.92, 109.12, 112.41, 112.67, 112.86, 112.98, 113.19, 120.14, 128.10, 129.39, 130.57, 131.88, 132.32, 133.36, 134.21, 136.97, 137.29, 138.25, 147.84, 159.03. MS: *m/z* 380.17 ($(M+H)^+$)

21.2.16 1-(3,5-bis(trifluoromethyl)phenyl)-3-(3-aminophenyl)urea

500 mg (4.6 mmol) 1,3-dianiline and 200 uL isocyanate were dissolved in 5 mL CHCl3. The mixture was stirred at RT for 16 h. After removing the solvent, the raw product was purified by column chromatography on silica gel with ethyl acetate and cyclo hexane (1:1) to obtain 320 mg (20 %) white powder. mp: 176-177 ^oC.

21.2.17 1-(3,5-bis(trifluoromethyl)phenyl)-3-(4-aminophenyl)thiourea

500 mg (4.6 mmol) 1,4-dianiline and 200 uL isocyanate were dissolved in 5 mL CHCl3. The mixture was stirred at RT for 16h. After removing the solvent, the raw product was purified by column chromatography on silica gel with ethyl acetate and cyclohexane (1:1) to obtain 473 mg (27 %) white powder. mp: 188-189 ^oC.

21.2.18 N, O-bismethacrylethanolamine (NOBE)

Synthesis of NOBE was modified from a previously published report in Spivak´s group.[37] 4 g (65.49 mmol) ethanolamine was dissolved in 250 mL DCM. The mixture was then cooled to 0 ºC, (13.1 mmol) DMAP and 1.59 g (183.4 mmol) methacrylic acid were added to the mixture at 0 ^oC. 27 g (131 mmol) N,N'-dicyclohexylcarbodiimide (DCC) was added slowly (2 g per minute) to the mixture and stirred under argon protection at RT for 48h. The resulting solution was filtered to remove the N,N'-dicyclohexylurea (DCU) and washed with (4 x 15 mL 1M

HCl (aq) and 8 x 15 mL saturated $NaHCO_3$ solution). The organic layer is then filtered and dried over $MgSO_4$. The resulting solution is concentrated by half and purified by column chromatography on silica gel with (50/50 hexane/ethyl acetate) to obtain 10 g (77%) colorless oil. ^{1}H-NMR (500 MHz, $CDCl_3$) δ: 1.94 (s, 3H), 1.95 (s, 3H), 3.61 (q, *J* = 5.5, 2H), 4.29 (t, *J* = 5, 2H), 5.59 (t, *J* = 1.5, 1H), 5.69 (s, 1H), 6.11(s, 1H), 6.24 (bs, 1H). ^{13}C-NMR ($CDCl_3$) δ:. **CHN-Analysis** ($C_{10}H_{14}NO_3$): Cal. C 61.21, H 7.19, N 7.14; found. C 63.44, H 9.88, N 9.24. MS: *m/z* 197.22 ($(M+H)^+$)

21.2.19 TBA salts

TBA salts of all used templates were prepared by mixing the TBA-OH stock solution at desired ratio with the acid in MeCN. After stirring at room temperature for half an hour, the solution was dried in a vacuum concentrator for 16 h and stored at -20 ^{o}C.

21.3 Preparation of thin film MIP

Cover slips were pre-cleaned for 12 h with 1M KOH solution and subsequently carefully rinsed with deionized water. To activate the surface, the cover slips were left in piranha solution (3:1 concentrated sulfuric acid to 30% hydrogen peroxide) overnight and rinsed with water, acetone and toluene, and dried in vacuum. The linker 3-methacryloxy-propyltrimethoxysilane was immobilized by stirring the cover slips in a solution of the linker (20 mL) and TEA (7 mL) in toluene (150 mL) for 24 h. Subsequently, the cover slips were washed with toluene and methyl *tert*-butyl ether (MTBE) and dried in vacuum.

Polymer film formation by grafting-to strategy

0.06 mg (0.15 μmol) TBA Z-L-Phe and 1 equivalent chromogenic monomer, 20 equivalent MMA or BMA, and 80 equivalent EDMA were dissolved in 25 μL toluene. The pre-polymerization mixtures were flushed with nitrogen and the azo-initiator ABDV was added. Subsequently, 2 μL of the solutions were dropped onto a glass slide and covered with a 3-methacryloxypropyltrimethoxysilane-modified cover slip. Polymerization was initiated thermally by heating with a heat-gun 3 x 10 seconds and subsequently in the oven at 70 °C for 1 h. The obtained polymer films were extracted using a Soxhlet apparatus with MeOH for 24 h. The NIPs were prepared accordingly, without addition of the template.

21.3.2 RAFT system

Prior to usage the glass slides were washed with saturated KOH, 1.67 mM HCl and subsequently with 30 mL 30 % H_2O_2 and 90 mL H_2SO_4. The slides were then rinsed twice with copious amounts of water and with acetone and dried.

Aminolysation

2 g of the activated glass slides were rinsed with dry toluene and then refluxed in presence of APTES (2.267 g, 0.010 mM) in 250 mL of dry toluene for 24 h.

Immobilisation of the RAFT agent (4-cyanopentanoic acid dithiobenzoate)

Prior to usage the apparatus consisting of a three neck flask equipped with an overhead stirrer and a dropping funnel was heated and flushed extensively with argon. It was kept under argon for the whole reaction time.

The RAFT agent (321 mg, 1.149 mmol), 125 uL (1.149 mmol) ethylchloroformate and 116 uL (1.149 mmol) TEA were dissolved in 50 mL dry THF in a three neck flask equipped with an overhead stirrer and a dropping funnel. The reaction mixture was cooled to -78 °C using a liquid-nitrogen-ethanol bath and stirred for 30 min at this temperature. Subsequently the functionalized glass slides were added and the mixture was stirred another 3 h at -78 °C. The reaction mixture was then kept at RT overnight.

The glass slides were separated from the reaction mixture via filtration and washed extensively with THF and MeOH to remove the precipitate. Subsequently they were dried under vacuum at RT and stored under inert conditions at 8 °C.

21.4 Preparation and activation of SiO_2 nanoparticles.

320 nm SiO_2 nanoparticles were prepared following a modified Stöber method.[202] 32% ammonia solution (9 mL) and 99.9% pure ethanol (16.25 mL) and deionized water (24.75 mL) were mixed in a round flask and stirred at 1000 rpm. Subsequently, a mixture of TEOS (4.5 mL) and ethanol (45.5 mL) was added and further mixed at 500 rpm for 2 h. The product was washed with distilled water and ethanol and dried under vacuum overnight. 1g silica nanoparticles and 4 mL of APTES were added into anhydrous toluene to make 60 mL of mixture solution. The mixture was refluxed for 12 h under dry nitrogen. The resulting APTES-modified silica particles were separated by centrifugation, washed with toluene, and dried in vacuum.

21.5 Preparation of CPDB-coated SiO_2 nanoparticles.

822 mg CPDB (2.948 mmol), ethylchloroformate (282 µL, 2.948 mmol) and triethyl amine (411 uL, 2.948 mmol) were added into a three necked flask with anhydrous THF (60 mL). The mixture was purged with argon and cooled to –78 ^{o}C for 40 min. Then, 3.5 g APTES-modified SiO_2 nanoparticles were added at –10 ^{o}C and the mixture was stirred at ambient temperature overnight. The particles were precipitated in 200 mL hexane, washed with acetone and THF and dried under vacuum overnight.

21.6 Preparation of core/shell particles.

For the MIP particles, CPDB-functionalized SiO_2 nanoparticles (150 mg), benzyl-methacrylate (56 µL, 0.331 mmol), EDMA (314 µL, 1.667 mmol), monomer, e.g. M5 (5.54 mg, 16.55 µmol), template, e.g. TBA-Z-L-Phe (8.95 mg, 16.55 µmol) and ABDV (10.85 mg, 29.1 µmol) were suspended and mixed in 20 mL anhydrous $CHCl_3$ and the mixture was purged with argon at –78 ^{o}C. Subsequently, the mixture was polymerized at 50 ^{o}C for 18 h and further aged for 2 h at 70 ^{o}C. The synthesized particles were washed with MeCN and $CHCl_3$ and dried under vacuum overnight. The non-imprinted polymer (NIP) control particles were synthesized under identical conditions but without the template salt. The surface coverage of the SiO_2 nanoparticles with APTES as well as CPDB was assessed with thermogravimetric analysis (TGA). The size and core/shell structure of the nanoparticles was determined by transmission electron microscopy (TEM).

21.7 Spectroscopic studies:

21.7.1 Absorption coefficient

Absorption coefficient is obtained according to **equation 21-1**. The dye is dissolved in solution in a micromolar concentration. The solution is transferred into a 5cm quartz cell, the absorption is registered with Specord 210 Plus absorption spectrometer. Three independent samples were measured to form a mean as the result

$$\epsilon_\lambda = \frac{A}{c*l} \qquad \textbf{equation 21-1}$$

21.7.2 Fluorescence quantum yield measurement

Diluted solutions with an absorbance of less than 0.1 at the absorption maximum were used to determine the quantum yield. The fluorescence quantum yields (Φ_f) were determined relative to coumarin 153 in ethanol (Φ_f = 0.544) and Cresyl violet in ethanol (Φ_f = 0.58). The

uncertainties of measurement were determined to ± 5 % (for $\Phi_f > 0.2$), ± 10 % (for $0.2 > \Phi_f > 0.02$) and ± 20 % (for $0.02 > \Phi_f$).

21.7.3 Lifetime measurement

Fluorescence lifetimes (Φ_f) were determined by a unique customized laser impulse fluorometer with picosecond time resolution. The uncertainty of measurement amounted to ± 3 ps. The fluorescence lifetime profiles were analyzed with a PC using the software package Global Unlimited V2.2 (Laboratory for Fluorescence Dynamics, University of Illinois). The goodness of the fit of the single decays as judged by reduced chi-squared (χ_R^2) and the autocorrelation function *C(j)* of the residuals was always below $\chi_R^2 < 1.2$.

21.7.5 Prepolymerization condition assessment

Chromogenic monomer, template, co-monomer, and crosslinker were dissolved in the porogen under the same concentration as the polymerization. After vigorous mixture, 20 µL of the mixture are transferred to a round quartz cell with 100 µm optical path length. The spectra were recorded with a Specord 210 Plus. To assess the stability of the complex under elevated temperature, the prepolymerization mixture was heated up to 80 ^oC and the absorption spectra were quickly measured.

21.7.4 Counter-ion effect assessment

Z-L-Phenyalanine anion was prepared in form of TMA, TEA, TBA and TOA salts following Section 21.2.13. 5µM **M7** was titrated with TXA-Z-L-Phe stock solution in $CHCl_3$. the absorption and fluorescence data were registered using a Specord 210 Plus and a Fluoromax 4, respectively. The different binding constants due to the variation of the counterion were assessed using non-linear fitting.

21.7.5 Assay protocol for sensing.

1 mg core/shell particles were suspended in 2 mL chloroform in a 10 mm quartz cell. The suspension was titrated with 1 mM TBA salt of the template and competitors. After each step of addition, the suspension was allowed to equilibrate for 2 min before measuring the absorption and fluorescence spectra (while constantly stirring). Fluorescence spectra were obtained with excitation at 410 nm.

21.7.6 Two phase extraction assay protocol

1 mg particles were suspended in 1.5 mL $CHCl_3$, 1 mL deionized water or buffer was added on the top of $CHCl_3$ suspension. Analyte in stock solution is added into the aqeous phase steadily. The suspension was stirred for 5 minutes to reach the equilibrium before every measurement. Fluorescence was recorded and evaluated through Origin 8.0 as well as Hyper-Spec.

Literature:

[1] L. Trench, Materials and techniques in the decorative arts. An illustrated dictionary, John Murray Publishers, London, Editon edn., **2000**

[2] Polyakov, M., Adsorption properties and structure of silica gel. *Zhurnal Fizicheskoi Khimii* **1931**, 2, 799-805

[3] Pauling, L., A theory of the structure and process of formation of antibodies. *Journal of the American Chemical Society* **1940**, 62, (10), 2643-2657

[4] Dickey, F., The preparation of specific adsorbents. *Proceedings of the National Academy of Sciences* **1945**, 35, (5), 227-229

[5] Wulff, G., Macromolecular Colloquium. *Angewandte Chemie International Edition in English* **1972**, 11, (4), 334-342

[6] Wulff, G., Molecular Imprinting. *Annals of the New York Academy of Sciences* **1984**, 434, (1), 327-333

[7] Arshady, R.; Mosbach, K., Synthesis of substrate-selective polymers by host-guest polymerization. *Die Makromolekulare Chemie* **1981**, 182, (2), 687-692.

[8] Ye, L.; Mosbach, K., The Technique of Molecular Imprinting – Principle, State of the Art, and Future Aspects. *Journal of Inclusion Phenomena and Macrocyclic Chemistry* **2001**, 41, (1), 107-113.

[9] Chen, L.; Xu, S.; Li, J., Recent advances in molecular imprinting technology: current status, challenges and highlighted applications. *Chemical Society Reviews* **2011**, 40, (5), 2922-2942

[10] Kryscio, D. R.; Peppas, N. A., Critical review and perspective of macromolecularly imprinted polymers. *Acta Biomaterialia* **2012**, 8, (2), 461-473

[11] Spivak, D. A., Optimization, evaluation, and characterization of molecularly imprinted polymers. *Advanced Drug Delivery Reviews* **2005**, 57, (12), 1779-1794

[12] Mayes, A. G.; Whitcombe, M. J., Synthetic strategies for the generation of molecularly imprinted organic polymers. *Advanced Drug Delivery Reviews* **2005**, 57, (12), 1742-1778.

[13] Ye, L.; Mosbach, K., Molecular Imprinting: Synthetic Materials As Substitutes for Biological Antibodies and Receptors *Chemistry of Materials* **2008**, 20, (3), 859-868

[14] Yilmaz, E.; Mosbach, K.; Haupt, K., Influence of functional and cross-linking monomers and the amount of template on the performance of molecularly imprinted polymers in binding assays. *Analytical Communications* **1999**, 36, (5), 167-170

[15] Yoshizako, K.; Hosoya, K.; Iwakoshi, Y.; Kimata, K.; Tanaka, N., Porogen Imprinting Effects. *Analytical Chemistry* **1998**, 70, (2), 386-389

[16] Kugimiya, A.; Matsui, J.; Takeuchi, T.; Yano, K.; Muguruma, H.; Elgersma, A. V.; Karube, I., Recognition of Sialic Acid Using Molecularly Imprinted Polymer. *Analytical Letters* **1995**, 28, (13), 2317-2323

[17] Wulff, G., Enzyme-like Catalysis by Molecularly Imprinted Polymers. *Chemical Reviews* **2001**, 102, (1), 1-28

[18] Shea, K. J.; Sasaki, D. Y., On the control of microenvironment shape of functionalized network polymers prepared by template polymerization. *Journal of the American Chemical Society* **1989**, 111, (9), 3442-3444

[19] Shea, K. J.; Thompson, E., Template synthesis of macromolecules. Selective functionalization of an organic polymer. *The Journal of Organic Chemistry* **1978**, 43, (21), 4253-4255

[20] Cheong, S. H.; McNiven, S.; Rachkov, A.; Levi, R.; Yano, K.; Karube, I., Testosterone Receptor Binding Mimic Constructed Using Molecular Imprinting. *Macromolecules* **1997**, 30, (5), 1317-1322

[21] Whitcombe, M. J.; Rodriguez, M. E.; Villar, P.; Vulfson, E. N., A New Method for the Introduction of Recognition Site Functionality into Polymers Prepared by Molecular Imprinting: Synthesis and Characterization of Polymeric Receptors for Cholesterol. *Journal of the American Chemical Society* **1995**, 117, (27), 7105-7111

[22] Mosbach, K., Molecular imprinting. *Trends Biochem Sci* **1994**, 19, (1), 9-14

[23] Yan, M., *Moleuclarly imprinted materials science and technology*. Marcel Dekker: New York, **2005**, 29-30

[24] Wulff, G.; Knorr, K., Stoichiometric noncovalent interaction in molecular imprinting. *Bioseparation* **2001**, 10, (6), 257-276

[25] Tanabe, K.; Takeuchi, T.; Matsui, J.; Ikebukuro, K.; Yano, K.; Karube, I., Recognition of barbiturates in molecularly imprinted copolymers using multiple hydrogen bonding. *Journal of the Chemical Society, Chemical Communications* **1995**, (22), 2303-2304

[26] Matsui, J.; Doblhoff-Dier, O.; Takeuchi, T., 2-(Trifluoromethyl)acrylic acid: a novel functional monomer in non-covalent molecular imprinting. *Analytica Chimica Acta* **1997**, 343, (1–2), 1-4

[27] Scorrano, S.; Mergola, L.; Del Sole, R.; Vasapollo, G., Synthesis of Molecularly Imprinted Polymers for Amino Acid Derivates by Using Different Functional Monomers. *International Journal of Molecular Sciences* **2011**, 12, (3), 1735-1743

[28] Simon, R. L.; Spivak, D. A., Performance analysis of molecularly imprinted polymers for carboxylate and aminophosphate templates using commercially available basic functional monomers. *Journal of Chromatography B* **2004**, 804, (1), 203-209

[29] Kugimiya, A.; Takeuchi, T., Molecular recognition by indoleacetic acid-imprinted polymers - effects of 2-hydroxyethyl methacrylate content. *Analytical and Bioanalytical Chemistry* **2002**, 372, (2), 305-307

[30] Oral, E.; Peppas, N. A., Hydrophilic molecularly imprinted poly(hydroxyethyl-methacrylate) polymers. *Journal of Biomedical Materials Research Part A* **2006**, 78A, (1), 205-210

[31] Wulff, G.; Gross, T.; Schönfeld, R.; Schrader, T.; Kirsten, C., Molecular Imprinting for the Preparation of Enzyme-Analogous Polymers. In *Molecular and Ionic Recognition with Imprinted Polymers*, American Chemical Society: **1998**, Vol. 703, pp 10-28

[32] Hall, A. J.; Manesiotis, P.; Emgenbroich, M.; Quaglia, M.; De Lorenzi, E.; Sellergren, B., Urea Host Monomers for Stoichiometric Molecular Imprinting of Oxyanions. *The Journal of Organic Chemistry* **2005**, 70, (5), 1732-1736

[33] Rossi, C.; Haupt, K., Application of the Doehlert experimental design to molecularly imprinted polymers: surface response optimization of specific template recognition as a function of the type and degree of cross-linking. *Analytical and Bioanalytical Chemistry* **2007**, 389, (2), 455-460

[34] Wulff, G., Molecular Imprinting in Cross-Linked Materials with the Aid of Molecular Templates—A Way towards Artificial Antibodies. *Angewandte Chemie International Edition in English* **1995**, 34, (17), 1812-1832

[35] Kempe, M., Antibody-Mimicking Polymers as Chiral Stationary Phases in HPLC. *Analytical Chemistry* **1996**, 68, (11), 1948-1953

[36] Shea, K. J.; Stoddard, G. J.; Shavelle, D. M.; Wakui, F.; Choate, R. M., Synthesis and characterization of highly crosslinked poly(acrylamides) and poly(methacrylamides). A new class of macroporous polyamides. *Macromolecules* **1990**, 23, (21), 4497-4507

[37] LeJeune, J.; Spivak, D., Chiral effects of alkyl-substituted derivatives of N,O-bismethacryloyl ethanolamine on the performance of one monomer molecularly imprinted polymers (OMNiMIPs). *Analytical and Bioanalytical Chemistry* **2007**, 389, (2), 433-440

[38] Yoshimatsu, K.; LeJeune, J.; Spivak, D. A.; Ye, L., Peptide-imprinted polymer microspheres prepared by precipitation polymerization using a single bi-functional monomer. *Analyst* **2009**, 134, (4), 719-724

[39] Krzysztof Matyjaszewski, T. P. D., *Handbook of radical polymerization*. Wiley-Interscience: United States of America, **2002**, 118-131

[40] Fuchs, Y.; Soppera, O.; Haupt, K., Photopolymerization and photostructuring of molecularly imprinted polymers for sensor applications—A review. *Analytica Chimica Acta* **2012**, 717, 7-20

[41] O'Shannessy, D. J.; Ekberg, B.; Mosbach, K., Molecular imprinting of amino acid derivatives at low temperature (0°C) using photolytic homolysis of azobisnitriles. *Analytical Biochemistry* **1989**, 177, (1), 144-149

[42] He, J. f.; Zhu, Q. h.; Deng, Q. y., Investigation of imprinting parameters and their recognition nature for quinine-molecularly imprinted polymers. *Spectrochimica Acta Part A: Molecular and Biomolecular Spectroscopy* **2007**, 67, (5), 1297-1305

[43] Mayes, A. G.; Mosbach, K., Molecularly Imprinted Polymer Beads: Suspension Polymerization Using a Liquid Perfluorocarbon as the Dispersing Phase. *Analytical Chemistry* **1996**, 68, (21), 3769-3774

[44] Sellergren, B.; Shea, K. J., Influence of polymer morphology on the ability of imprinted network polymers to resolve enantiomers. *Journal of Chromatography A* **1993**, 635, (1), 31-49

[45] Reinholdsson, P.; Hargitai, T.; Isaksson, R.; Törnell, B., Preparation and properties of porous particles from trimethylolpropane trimethacrylate. *Die Angewandte Makromolekulare Chemie* **1991**, 192, (1), 113-132

[46] Noee, S.; Salimraftar, N.; Abdouss, M.; Riazi, G., Imprinted microspheres and nanoparticles with diclofenac sodium: effect of solvent on the morphology and recognition properties. *Polymer International* **2013**, 62, (12), 1711-1716

[47] Sellergren, B., *Molecularly imprinted polymers man-made mimics of antibodies and their applications in analytical chemistry* 2ed.; Elsevier: Amsterdam, 2003

[48] Joshi, V. P.; Karmalkar, R. N.; Kulkarni, M. G.; Mashelkar, R. A., Effect of Solvents on Selectivity in Separation Using Molecularly Imprinted Adsorbents: Separation of Phenol and Bisphenol A. *Industrial & Engineering Chemistry Research* **1999**, 38, (11), 4417-4423

[49] Dauwe, C.; Sellergren, B., Influence of template basicity and hydrophobicity on the molecular recognition properties of molecularly imprinted polymers. *Journal of Chromatography A* **1996**, 753, (2), 191-200

[50] Andersson, L. I., Application of Molecular Imprinting to the Development of Aqueous Buffer and Organic Solvent Based Radioligand Binding Assays for (S)-Propranolol. *Analytical Chemistry* **1996**, 68, (1), 111-117

[51] Williams, R. A.; Mamotte, C. D. S.; Burnett, J. R., Phenylketonuria: an inborn error of phenylalanine metabolism. *The Clinical biochemist. Reviews / Australian Association of Clinical Biochemists* **2008**, 29, (1), 31-41

[52] Lim, G. P.; Yang, F.; Chu, T.; Chen, P.; Beech, W.; Teter, B.; Tran, T.; Ubeda, O.; Ashe, K. H.; Frautschy, S. A.; Cole, G. M., Ibuprofen suppresses plaque pathology and inflammation in a mouse model for Alzheimer's disease. *Journal of Neuroscience,* **2000**, 20, (15), 5709-5714

[53] Schindle.Dw; Armstron.Fa; Brunskil.Gj; Holmgren, S. K., Eutrophication of lake-227, experimental lakes area, northwestern Ontario, by addition of phosphate and nitrate. *Journal of the Fisheries Research Board of Canada* **1971**, 28, (11), 1763-1782

[54] Leblond, J.; Petitjean, A., Molecular Tweezers: Concepts and Applications. *ChemPhysChem* **2011**, 12, (6), 1043-1051

[55] Jayasena, S. D., Aptamers: An emerging class of molecules that rival antibodies in diagnostics. *Clinical Chemistry,* **1999**, 45, (9), 1628-1650

[56] Goldman, E. R.; Medintz, I. L.; Whitley, J. L.; Hayhurst, A.; Clapp, A. R.; Uyeda, H. T.; Deschamps, J. R.; Lassman, M. E.; Mattoussi, H., A hybrid quantum dot-antibody fragment fluorescence resonance energy transfer-based TNT sensor. *Journal of the American Chemical Society* **2005**, 127, (18), 6744-6751

[57] Peng, H.; Zhang, Y.; Zhang, J.; Xie, Q.; Nie, L.; Yao, S., Development of a thickness shear mode acoustic sensor based on an electrosynthesized molecularly imprinted polymer using an underivatized amino acid as the template. *Analyst* **2001**, 126, (2), 189-194

[58] Hamase, K.; Iwashita, K.; Zaitsu, K., Enantio-Selective Derivatization of Amino Compounds in the Presence of a Molecular Imprint Polymer. *Analytical Sciences* **1999**, 15, (5), 411-412

[59] Benito-Peña, E.; Moreno-Bondi, M. C.; Aparicio, S.; Orellana, G.; Cederfur, J.; Kempe, M., Molecular Engineering of Fluorescent Penicillins for Molecularly Imprinted Polymer Assays. *Analytical Chemistry* **2006**, 78, (6), 2019-2027

[60] Urraca, J. L.; Hall, A. J.; Moreno-Bondi, M. C.; Sellergren, B., A Stoichiometric Molecularly Imprinted Polymer for the Class-Selective Recognition of Antibiotics in Aqueous Media. *Angewandte Chemie International Edition* **2006**, 45, (31), 5158-5161

[61] Wagner, R.; Wan, W.; Biyikal, M.; Benito- Peña, E.; Moreno-Bondi, M. C.; Lazraq, I.; Rurack, K.; Sellergren, B., Synthesis, Spectroscopic, and Analyte-Responsive Behavior of a Polymerizable Naphthalimide-Based Carboxylate Probe and Molecularly Imprinted Polymers Prepared Thereof. *The Journal of Organic Chemistry*, **2013**, 78, (4), 1377-1389

[62] Helling, S.; Shinde, S.; Brosseron, F.; Schnabel, A.; Müller, T.; Meyer, H. E.; Marcus, K.; Sellergren, B., Ultratrace Enrichment of Tyrosine Phosphorylated Peptides on an Imprinted Polymer. *Analytical Chemistry* **2011**, 83, (5), 1862-1865

[63] Xu, L.; Hu, Y.; Shen, F.; Li, Q.; Ren, X., Specific recognition of tyrosine-phosphorylated peptides by epitope imprinting of phenylphosphonic acid. *Journal of Chromatography A*, **2013**, 1293, 85-91

[64] Hans R. Kricheldorf, O. N., Graham Swift, *Handbook of Polymer Synthesis*. 2 ed.; Marcel Dekker: New York, **2005**

[65] Charles E. Carraher, J., *Polymer Chemistry*. 7 ed.; CRC Press: New York, **2006**

[66] J. Brandrup, E. H. I., E. A. Grulke, *Polymer Handbook*. **1998**

[67] Salian, V. D.; Byrne, M. E., Living Radical Polymerization and Molecular Imprinting: Improving Polymer Morphology in Imprinted Polymers. *Macromolecular Materials and Engineering,* **2013***,* 298, (4), 379-390

[68] Kowollik,C. B., *Handbook of Raft Polymerization*; Wiley-VCH Verlag: Darmstadt, 2008, 59-90

[69] Adbo, K.; Andersson, H. k. S.; Ankarloo, J.; Karlsson, J. G.; Norell, M. C.; Olofsson, L.; Svenson, J.; Ötegren, U.; Nicholls, I. A., Enantioselective Tröger's Base Synthetic Receptors. *Bioorganic Chemistry* **1999**, 27, (5), 363-371

[70] Piletska, E. V.; Guerreiro, A. R.; Romero-Guerra, M.; Chianella, I.; Turner, A. P. F.; Piletsky, S. A., Design of molecular imprinted polymers compatible with aqueous environment. *Analytica Chimica Acta* **2008**, 607, (1), 54-60

[71] Kugimiya, A.; Takeuchi, T.; Matsuib, J.; Ikebukuro, K.; Yano, K.; Karube, I., Recognition in Novel Molecularly Imprinted Polymer Sialic Acid Receptors in Aqueous Media. *Analytical Letters* **1996**, 29, (7), 1099-1107

[72] Renkecz, T.; Ceolin, G.; Horvath, V., Selective solid phase extraction of propranolol on multiwell membrane filter plates modified with molecularly imprinted polymer. *Analyst* **2011**, 136, (10), 2175-2182

[73] Bao, H.; Wei, T.; Li, X.; Zhao, Z.; Cui, H.; Zhang, P., Detection of TNT by a molecularly imprinted polymer film-based surface plasmon resonance sensor. *Chinese Science Bulletin* **2012**, 57, (17), 2102-2105

[74] Dechtrirat, D.; Jetzschmann, K. J.; Stöcklein, W. F. M.; Scheller, F. W.; Gajovic-Eichelmann, N., Protein Rebinding to a Surface-Confined Imprint. *Advanced Functional Materials* **2012**, 22, (24), 5231-5237

[75] Guo, T. y.; Zhang, L. y.; Hao, G. j.; Song, M. d.; Zhang, B. h., Preparation and Properties of Uniform-Sized Polymer Beads Imprinted with N-CBZ-L-Phenylalanine. *International Journal of Polymeric Materials* **2005**, 54, (8), 743-755

[76] Boonpangrak, S.; Prachayasittikul, V.; Bülow, L.; Ye, L., Molecularly imprinted polymer microspheres prepared by precipitation polymerization using a sacrificial covalent bond. *Journal of Applied Polymer Science* **2006**, 99, (4), 1390-1398

[77] Wang, J.; Cormack, P. A. G.; Sherrington, D. C.; Khoshdel, E., Monodisperse, Molecularly Imprinted Polymer Microspheres Prepared by Precipitation Polymerization for Affinity Separation Applications. *Angewandte Chemie International Edition* **2003**, 42, (43), 5336-5338

[78] Carter, S. R.; Rimmer, S., Surface Molecularly Imprinted Polymer Core–Shell Particles. *Advanced Functional Materials* **2004**, 14, (6), 553-561

[79] Liu, R.; Guan, G.; Wang, S.; Zhang, Z., Core-shell nanostructured molecular imprinting fluorescent chemosensor for selective detection of atrazine herbicide. *Analyst* **2011**, 136, (1), 184-190

[80] Descalzo, A. B.; Somoza, C.; Moreno-Bondi, M. C.; Orellana, G., Luminescent Core-Shell Imprinted Nanoparticles Engineered for Targeted Förster Resonance Energy Transfer-Based Sensing. *Analytical Chemistry* **2013**, 85, (11), 5316-5320

[81] Mehdinia, A.; Aziz-Zanjani, M. O.; Ahmadifar, M.; Jabbari, A., Design and synthesis of molecularly imprinted polypyrrole based on nanoreactor SBA-15 for recognition of ascorbic acid. *Biosensors and Bioelectronics* **2013**, 39, (1), 88-93

[82] Guo, W.; Chen, R.; Liu, Y.; Meng, M.; Meng, X.; Hu, Z.; Song, Z., Preparation of ion-imprinted mesoporous silica SBA-15 functionalized with triglycine for selective adsorption of Co(II). *Colloids and Surfaces A: Physicochemical and Engineering Aspects* **2013**, 436, (0), 693-703

[83] Kang, C.; Li, W.; Tan, L.; Li, H.; Wei, C.; Tang, Y., Highly ordered metal ion imprinted mesoporous silica particles exhibiting specific recognition and fast adsorption kinetics. *Journal of Materials Chemistry A* **2013**, 1, (24), 7147-7153

[84] Nematollahzadeh, A.; Shojaei, A.; Abdekhodaie, M. J.; Sellergren, B., Molecularly imprinted polydopamine nano-layer on the pore surface of porous particles for protein capture in HPLC column. *Journal of Colloid and Interface Science* **2013**, 404, (0), 117-126

[85] Wulff, G.; Chong, B.-O.; Kolb, U., Soluble Single-Molecule Nanogels of Controlled Structure as a Matrix for Efficient Artificial Enzymes. *Angewandte Chemie International Edition* **2006**, 45, (18), 2955-2958

[86] Carboni, D.; Flavin, K.; Servant, A.; Gouverneur, V.; Resmini, M., The First Example of Molecularly Imprinted Nanogels with Aldolase Type I Activity. *Chemistry – A European Journal* **2008**, 14, (23), 7059-7065

[87] Pan, G.; Guo, Q.; Cao, C.; Yang, H.; Li, B., Thermo-responsive molecularly imprinted nanogels for specific recognition and controlled release of proteins. *Soft Matter* **2013**, 9, (14), 3840-3850

[88] Ge, L.; Wang, S.; Yu, J.; Li, N.; Ge, S.; Yan, M., Molecularly Imprinted Polymer Grafted Porous Au-Paper Electrode for an Microfluidic Electro-Analytical Origami Device. *Advanced Functional Materials* **2013**, 23, (24), 3115-3123

[89] Bianchi, F.; Giannetto, M.; Mori, G.; D'Agostino, G.; Careri, M.; Mangia, A., Solid-phase microextraction of 2,4,6-trinitrotoluene using a molecularly imprinted-based fiber. *Analytical and Bioanalytical Chemistry* **2012**, 403, (8), 2411-2418

[90] Choong, C.-L.; Bendall, J. S.; Milne, W. I., Carbon nanotube array: A new MIP platform. *Biosensors and Bioelectronics* **2009**, 25, (3), 652-656

[91] Advincula, R., Engineering molecularly imprinted polymer (MIP) materials: Developments and challenges for sensing and separation technologies. *Korean Journal of Chemical Engineering* **2011**, 28, (6), 1313-1321

[92] Matsui, J.; Okada, M.; Tsuruoka, M.; Takeuchi, T., Solid-phase Extraction of a Triazine Herbicide Using a Molecularly Imprinted Synthetic Receptor. *Analytical Communications* **1997**, 34, (3), 85-87

[93] Gu, X. h.; Xu, R.; Yuan, G. l.; Lu, H.; Gu, B. r.; Xie, H. p., Preparation of chlorogenic acid surface-imprinted magnetic nanoparticles and their usage in separation of Traditional Chinese Medicine. *Analytica Chimica Acta* **2010**, 675, (1), 64-70

[94] Balamurugan, K.; Gokulakrishnan, K.; Prakasam, T., Preparation and evaluation of molecularly imprinted polymer liquid chromatography column for the separation of ephedrine enantiomers. *Arabian Journal of Chemistry* **2011**, DOI: 10.1016/j.arabjc.2011.06.024

[95] Bonomi, P.; Servant, A.; Resmini, M., Modulation of imprinting efficiency in nanogels with catalytic activity in the Kemp elimination. *Journal of Molecular Recognition* **2012**, 25, (6), 352-360

[96] Alvarez-Lorenzo, C.; Concheiro, A., Molecularly imprinted polymers for drug delivery. *Journal of Chromatography B* **2004**, 804, (1), 231-245

[97] Sellergren, B.; Allender, C. J., Molecularly imprinted polymers: A bridge to advanced drug delivery. *Advanced Drug Delivery Reviews* **2005**, 57, (12), 1733-1741

[98] Asadi, E.; Azodi-Deilami, S.; Abdouss, M.; Khaghani, S., Cyproterone Synthesis, Recognition and Controlled Release by Molecularly Imprinted Nanoparticle. *Applied Biochemistry and Biotechnology* **2012**, 167, (7), 2076-2087

[99] Yu, Y.; Ye, L.; Haupt, K.; Mosbach, K., Formation of a Class of Enzyme Inhibitors (Drugs), Including a Chiral Compound, by Using Imprinted Polymers or Biomolecules as Molecular-Scale Reaction Vessels. *Angewandte Chemie International Edition* **2002**, 41, (23), 4459-4463

[100] Zheng, C.; Zhang, X.-L.; Liu, W.; Liu, B.; Yang, H.-H.; Lin, Z.-A.; Chen, G.-N., A Selective Artificial Enzyme Inhibitor Based on Nanoparticle-Enzyme Interactions and Molecular Imprinting. *Advanced Materials* **2013**, 25, (41), 5922-5927

[101] Dickert, F. L.; Hayden, O., Molecular imprinting in chemical sensing. *TrAC Trends in Analytical Chemistry* **1999**, 18, (3), 192-199

[102] Askim, J. R.; Mahmoudi, M.; Suslick, K. S., Optical sensor arrays for chemical sensing: the optoelectronic nose. *Chemical Society Reviews* **2013**, 42, (22), 8649-8682

[103] Noworyta, K.; Kutner, W.; Wijesinghe, C. A.; Srour, S. G.; D´Souza, F., Nicotine, Cotinine, and Myosmine Determination Using Polymer Films of Tailor-Designed Zinc Porphyrins as Recognition Units for Piezoelectric Microgravimetry Chemosensors. *Analytical Chemistry* **2012**, 84, (5), 2154-2163

[104] Liu, F.; Liu, X.; Ng, S.-C.; Chan, H. S.-O., Enantioselective molecular imprinting polymer coated QCM for the recognition of l-tryptophan. *Sensors and Actuators B: Chemical* **2006**, 113, (1), 234-240

[105] Zhou, D.; Guo, T.; Yang, Y.; Zhang, Z., Surface imprinted macroporous film for high performance protein recognition in combination with quartz crystal microbalance. *Sensors and Actuators B: Chemical* **2011**, 153, (1), 96-102

[106] Stanley, S.; Percival, C. J.; Morel, T.; Braithwaite, A.; Newton, M. I.; McHale, G.; Hayes, W., Enantioselective detection of l-serine. *Sensors and Actuators B: Chemical* **2003**, 89, (1–2), 103-106

[107] Afkhami, A.; Ghaedi, H.; Madrakian, T.; Ahmadi, M.; Mahmood-Kashani, H., Fabrication of a new electrochemical sensor based on a new nano-molecularly imprinted polymer for highly selective and sensitive determination of tramadol in human urine samples. *Biosensors and Bioelectronics* **2013**, 44, 34-40

[108] Yang, Y.; Yi, C.; Luo, J.; Liu, R.; Liu, J.; Jiang, J.; Liu, X., Glucose sensors based on electrodeposition of molecularly imprinted polymeric micelles: A novel strategy for MIP sensors. *Biosensors and Bioelectronics* **2011**, 26, (5), 2607-2612

[109] Bompart, M.; Gheber, L. A.; De Wilde, Y.; Haupt, K., Direct detection of analyte binding to single molecularly imprinted polymer particles by confocal Raman spectroscopy. *Biosensors and Bioelectronics* **2009**, 25, (3), 568-571

[110] Sunayama, H.; Ooya, T.; Takeuchi, T., Fluorescent protein recognition polymer thin films capable of selective signal transduction of target binding events prepared by molecular imprinting with a post-imprinting treatment. *Biosensors and Bioelectronics* **2010**, 26, (2), 458-462

[111] Lotierzo, M.; Henry, O. Y. F.; Piletsky, S.; Tothill, I.; Cullen, D.; Kania, M.; Hock, B.; Turner, A. P. F., Surface plasmon resonance sensor for domoic acid based on grafted imprinted polymer. *Biosensors and Bioelectronics* **2004**, 20, (2), 145-152

[112] Manju, S.; Hari, P. R.; Sreenivasan, K., Fluorescent molecularly imprinted polymer film binds glucose with a concomitant changes in fluorescence. *Biosensors and Bioelectronics* **2010**, 26, (2), 894-897

[113] Pan, G.; Zhang, Y.; Guo, X.; Li, C.; Zhang, H., An efficient approach to obtaining water-compatible and stimuli-responsive molecularly imprinted polymers by the facile surface-grafting of functional polymer brushes via RAFT polymerization. *Biosensors and Bioelectronics* **2010**, 26, (3), 976-982

[114] Li, S.; Ge, Y.; Turner, A. P. F., A Catalytic and Positively Thermosensitive Molecularly Imprinted Polymer. *Advanced Functional Materials* **2011**, 21, (6), 1194-1200

[115] Li, S.; Ge, Y.; Piletsky, S. A.; Turner, A. P. F., A Zipper-Like On/Off-Switchable Molecularly Imprinted Polymer. *Advanced Functional Materials* 21, (17), 3344-3349

[116] Kanekiyo, Y.; Naganawa, R.; Tao, H., pH-Responsive Molecularly Imprinted Polymers. *Angewandte Chemie International Edition* **2003**, 42, (26), 3014-3016

[117] Zhao, W. F.; Fang, B. H.; Li, N.; Nie, S. Q.; Wei, Q.; Zhao, C. S., Fabrication of pH-responsive molecularly imprinted polyethersulfone particles for bisphenol-A uptake. *Journal of Applied Polymer Science* **2009**, 113, (2), 916-921

[118] Turkewitsch, P.; Wandelt, B.; Darling, G. D.; Powell, W. S., Fluorescent Functional Recognition Sites through Molecular Imprinting. A Polymer-Based Fluorescent Chemosensor for Aqueous cAMP. *Analytical Chemistry* **1998**, 70, (10), 2025-2030

[119] Jordan, L. M.; Boyle, P. D.; Sargent, A. L.; Allen, W. E., Binding of Carboxylic Acids by Fluorescent Pyridyl Ureas. *The Journal of Organic Chemistry* **2010**, 75, (24), 8450-8456

[120] Sánchez-Barragán, I.; Costa-Fernández, J. M.; Pereiro, R.; Sanz-Medel, A.; Salinas, A.; Segura, A.; Fernández-Gutiérrez, A.; Ballesteros, A.; González, J. M., Molecularly Imprinted Polymers Based on Iodinated Monomers for Selective Room-Temperature Phosphorescence Optosensing of Fluoranthene in Water. *Analytical Chemistry* **2005**, 77, (21), 7005-7011

[121] http://iupac.org/publications/pac/63/9/1247/.

[122] Wolfbeis, O. S., Editorial: Probes, Sensors, and Labels: Why is Real Progress Slow? *Angewandte Chemie International Edition* **2013**, 52, (38), 9864-9865

[123] Loudet, A.; Burgess, K., BODIPY Dyes and Their Derivatives: Syntheses and Spectroscopic Properties. *Chemical Reviews* **2007**, 107, (11), 4891-4932

[124] Dähne, S., Color and Constitution: One Hundred Years of Research. *Science* **1978**, 199, 1163-1167

[125] Wang, Y.-W.; Descalzo, A. B.; Shen, Z.; You, X.-Z.; Rurack, K., Dihydronaphthalene-Fused Boron–Dipyrromethene (BODIPY) Dyes: Insight into the Electronic and Conformational Tuning Modes of BODIPY Fluorophores. *Chemistry – A European Journal* **2010**, 16, (9), 2887-2903

[126] Descalzo, A. B.; Martínez-Máñez, R.; Radeglia, R.; Rurack, K.; Soto, J., Coupling Selectivity with Sensitivity in an Integrated Chemosensor Framework: Design of a Hg^{2+}-Responsive Probe, Operating above 500 nm. *Journal of the American Chemical Society* **2003**, 125, (12), 3418-3419

[127] Fabbrizzi, L.; Poggi, A., Sensors and switches from supramolecular chemistry. *Chemical Society Reviews* **1995**, 24, (3), 197-202

[128] Lakowicz, J. R.; Weber, G., Quenching of fluorescence by oxygen. Probe for structural fluctuations in macromolecules. *Biochemistry* **1973**, 12, (21), 4161-4170

[129] Eftink, M. R.; Ghiron, C. A., Exposure of tryptophanyl residues in proteins. Quantitative determination by fluorescence quenching studies. *Biochemistry* **1976**, 15, (3), 672-680

[130] Valeur, B.; Leray, I., Design principles of fluorescent molecular sensors for cation recognition. *Coordination Chemistry Reviews* **2000**, 205, (1), 3-40

[131] Matsui, J.; Kubo, H.; Takeuchi, T., Molecularly Imprinted Fluorescent-Shift Receptors Prepared with 2-(Trifluoromethyl)acrylic Acid. *Analytical Chemistry* **2000**, 72, (14), 3286-3290

[132] Suárez-Rodríguez, J. L.; Díaz-García, M. E., Flavonol fluorescent flow-through sensing based on a molecular imprinted polymer. *Analytica Chimica Acta* **2000**, 405, (1–2), 67-76

[133] Jones, P. F.; Siegel, S., Quenching of Naphthalene Luminescence by Oxygen and Nitric Oxide. *The Journal of Chemical Physics* **1971**, 54, (8), 3360-3366

[134] Abuin, E. B.; Lissi, E. A., Quenching rate constants in aqueous solution: influence of the hydrophobic effect. *Journal of Photochemistry and Photobiology A: Chemistry* **1993**, 71, (3), 263-267

[135] Martin, A.; Narayanaswamy, R., Studies on quenching of fluorescence of reagents in aqueous solution leading to an optical chloride-ion sensor. *Sensors and Actuators B: Chemical* **1997**, 39, (1–3), 330-333

[136] Hariharan, C.; Vijaysree, V.; Mishra, A. K., Quenching of 2,5-diphenyloxazole (PPO) fluorescence by metal ions. *Journal of Luminescence* **1997**, 75, (3), 205-211

[137] Goodpaster, J. V.; McGuffin, V. L., Fluorescence Quenching as an Indirect Detection Method for Nitrated Explosives. *Analytical Chemistry* **2001**, 73, (9), 2004-2011

[138] Razek, T. M. A.; Miller, M. J.; Hassan, S. S. M.; Arnold, M. A., Optical sensor for sulfur dioxide based on fluorescence quenching. *Talanta* **1999**, 50, (3), 491-498

[139] Descalzo, A.; Zhu, S.; Fischer, T.; Rurack, K., Optimization of the Coupling of Target Recognition and Signal Generation. In *Advanced Fluorescence Reporters in Chemistry and Biology II*, Demchenko, A. P., Ed. Springer Berlin Heidelberg: **2010**; Vol. 9, pp 41-106

[140] Mullett, W. M.; Lai, E. P. C., Determination of Theophylline in Serum by Molecularly Imprinted Solid-Phase Extraction with Pulsed Elution. *Analytical Chemistry* **1998**, 70, (17), 3636-3641

[141] Greene, N. T.; Shimizu, K. D., Colorimetric Molecularly Imprinted Polymer Sensor Array using Dye Displacement. *Journal of the American Chemical Society* **2005**, 127, (15), 5695-5700

[142] Rathbone, D. L.; Ge, Y., Selectivity of response in fluorescent polymers imprinted with N1-benzylidene pyridine-2-carboxamidrazones. *Analytica Chimica Acta* **2001**, 435, (1), 129-136

[143] Rachkov, A.; McNiven, S.; El'skaya, A.; Yano, K.; Karube, I., Fluorescence detection of β-estradiol using a molecularly imprinted polymer. *Analytica Chimica Acta* **2000**, 405, (1–2), 23-29

[144] Inoue, Y.; Kuwahara, A.; Ohmori, K.; Sunayama, H.; Ooya, T.; Takeuchi, T., Fluorescent molecularly imprinted polymer thin films for specific protein detection prepared with dansyl ethylenediamine-conjugated O-acryloyl l-hydroxyproline. *Biosensors and Bioelectronics* **2013**, 48, (0), 113-119

[145] Manesiotis, P.; Hall, A. J.; Emgenbroich, M.; Quaglia, M.; Lorenzi, E. D.; Sellergren, B., An enantioselective imprinted receptor for Z-glutamate exhibiting a binding induced color change. *Chemical Communications* **2004**, (20), 2278-2279

[146] Taki, M.; Watanabe, Y.; Yamamoto, Y., Development of ratiometric fluorescent probe for zinc ion based on indole fluorophore. *Tetrahedron Letters* **2009**, 50, (12), 1345-1347

[147] de Silva, A. P.; Gunaratne, H. Q. N.; Gunnlaugsson, T.; Huxley, A. J. M.; McCoy, C. P.; Rademacher, J. T.; Rice, T. E., Signaling Recognition Events with Fluorescent Sensors and Switches. *Chemical Reviews* **1997**, 97, (5), 1515-1566

[148] Bissell, R. A., E. Calle, et al. Luminescence and charge transfer. Part 2. Aminomethyl anthracene derivatives as fluorescent PET (photoinduced electron transfer) sensors for protons. *Journal of the Chemical Society, Perkin Transactions 2* **1992**, (9), 1559-1564

[149] Gunnlaugsson, T.; Ali, H.; Glynn, M.; Kruger, P.; Hussey, G.; Pfeffer, F.; dos Santos, C. G.; Tierney, J., Fluorescent Photoinduced Electron Transfer (PET) Sensors for Anions; From Design to Potential Application. *Journal of Fluorescence* **2005**, 15, (3), 287-299

[150] Ramachandram, B.; Samanta, A., Transition Metal Ion Induced Fluorescence Enhancement of 4-(N,N-Dimethylethylenediamino)-7-nitrobenz-2-oxa-1,3-diazole. *The Journal of Physical Chemistry A* **1998**, 102, (52), 10579-10587.

[151] Kollmannsberger, M.; Rurack, K., Ultrafast Charge Transfer in Amino-Substituted Boron Dipyrromethene Dyes and Its Inhibition by Cation Complexation: A New Design Concept for Highly Sensitive Fluorescent Probes. *The Journal of Physical Chemistry A* **1998**, 102, (50), 10211-10220

[152] Achelle, S.; Barsella, A.; Baudequin, C.; Caro, B.; Robin-le Guen, F., Synthesis and Photophysical Investigation of a Series of Push–Pull Arylvinyldiazine Chromophores. *The Journal of Organic Chemistry* **2012**, 77, (8), 4087-4096

[153] Upadhyay, K. K.; Mishra, R. K.; Kumar, V.; Chowdhury, P. K. R., A coumarin based ICT probe for fluoride in aqueous medium with its real application. *Talanta* **2010**, 82, (1), 312-318

[154] Wen, Z.-C.; Jiang, Y.-B., Ratiometric dual fluorescent receptors for anions under intramolecular charge transfer mechanism. *Tetrahedron* **2004,** 60, (49), 11109-11115

[155] Druzhinin, S. I.; Kovalenko, S. A.; Senyushkina, T. A.; Demeter, A.; Machinek, R.; Noltemeyer, M.; Zachariasse, K. A., Intramolecular Charge Transfer with the Planarized 4-Cyanofluorazene and Its Flexible Counterpart 4-Cyano-N-phenylpyrrole. Picosecond Fluorescence Decays and Femtosecond Excited-State Absorption. *The Journal of Physical Chemistry A* **2008**, 112, (36), 8238-8253

[156] Sapsford, K. E.; Berti, L.; Medintz, I. L., Materials for Fluorescence Resonance Energy Transfer Analysis: Beyond Traditional Donor–Acceptor Combinations. *Angewandte Chemie International Edition* **2006**, 45, (28), 4562-4589

[157] Stryer, L., Fluorescence energy-transfer as a spectroscopic ruler. *Annual Review of Biochemistry* **1978**, 47, 819-846

[158] Czímerová, A.; Bujdák, J.; Iyi, N., Fluorescence resonance energy transfer between laser dyes in saponite dispersions. *Journal of Photochemistry and Photobiology A: Chemistry* **2007**, 187, 160-166

[159] Fehr, M.; Frommer, W. B.; Lalonde, S., Visualization of maltose uptake in living yeast cells by fluorescent nanosensors. *Proceedings of the National Academy of Sciences* **2002**, 99, (15), 9846-9851

[160] Uchiyama, S.; Takehira, K.; Kohtani, S.; Imai, K.; Nakagaki, R.; Tobita, S.; Santa, T., Fluorescence on-off switching mechanism of benzofurazans. *Organic & Biomolecular Chemistry* **2003**, 1, (6), 1067-1072

[161] Gunnlaugsson, T.; Kruger, P. E.; Jensen, P.; Pfeffer, F. M.; Hussey, G. M., Simple naphthalimide based anion sensors: deprotonation induced colour changes and CO_2 fixation. *Tetrahedron Letters* **2003**, 44, (49), 8909-8913

[162] Boens, N.; Leen, V.; Dehaen, W., Fluorescent indicators based on BODIPY. *Chemical Society Reviews* **2012**, 41, (3), 1130-1172

[163] Shen, Z.; Röhr, H.; Rurack, K.; Uno, H.; Spieles, M.; Schulz, B.; Reck, G.; Ono, N., Boron–Diindomethene (BDI) Dyes and Their Tetrahydrobicyclo Precursors—en Route to a New Class of Highly Emissive Fluorophores for the Red Spectral Range. *Chemistry – A European Journal* **2004**, 10, (19), 4853-4871

[164] Descalzo, A. B.; Rurack, K.; Weisshoff, H.; Martínez-Mánez, R.; Marcos, M. D.; Amorós, P.; Hoffmann, K.; Soto, J., Rational Design of a Chromo- and Fluorogenic Hybrid Chemosensor Material for the Detection of Long-Chain Carboxylates. *Journal of the American Chemical Society* **2004**, 127, (1), 184-200

[165] Jose, J.; Burgess, K., Benzophenoxazine-based fluorescent dyes for labeling biomolecules. *Tetrahedron* **2006**, 62, (48), 11021-11037

[166] Bates, G. W.; Triyanti; Light, M. E.; Albrecht, M.; Gale, P. A., 2,7-Functionalized Indoles as Receptors for Anions. *The Journal of Organic Chemistry* **2007**, 72, (23), 8921-8927

[167] Vivian, J. T.; Callis, P. R., Mechanisms of Tryptophan Fluorescence Shifts in Proteins. *Biophysical Journal* **2001**, 80, (5), 2093-2109

[168] Chauhan, S. M. S.; Bisht, T.; Garg, B., Anion sensing by Phenazine-based urea/thiourea receptors. *Tetrahedron Letters* **2008**, 49, (47), 6646-6649

[169] Borisevich, N. A.; Raichenok, T. F., Absorption, fluorescence, and fluorescence excitation spectra of free molecules of indole and its derivatives. *Journal of Applied Spectroscopy* **2007**, 74, (2), 245-250

[170] Makuc, D.; Lenarcic, M.; Bates, G. W.; Gale, P. A.; Plavec, J., Anion-induced conformational changes in 2,7-disubstituted indole-based receptors. *Organic & Biomolecular Chemistry* **2009**, 7, (17), 3505-3511

[171] Chen, J.; Burghart, A.; Derecskei-Kovacs, A.; Burgess, K., 4,4-Difluoro-4-bora-3a,4a-diaza-s-indacene (BODIPY) Dyes Modified for Extended Conjugation and Restricted Bond Rotations. *The Journal of Organic Chemistry* **2000**, 65, (10), 2900-2906

[172] Gomez, D. E.; Fabbrizzi, L.; Licchelli, M.; Monzani, E., Urea vs. thiourea in anion recognition. *Organic & Biomolecular Chemistry* **2005**, 3, (8), 1495-1500

[173] Piggee, C., Phosphoproteomics: Miles To Go Before It´s Routine. *Analytical Chemistry* **2009**, 81, (7), 2418-2420

[174] Boiocchi, M.; Del Boca, L.; Esteban-Gómez, D.; Fabbrizzi, L.; Licchelli, M.; Monzani, E., Anion-Induced Urea Deprotonation. *Chemistry – A European Journal* **2005**, 11, (10), 3097-3104

[175] Amendola, V.; Boiocchi, M.; Fabbrizzi, L.; Palchetti, A., Anion Receptors Containing -NH Binding Sites: Hydrogen-Bond Formation or Neat Proton Transfer? *Chemistry – A European Journal* **2005**, 11, (1), 120-127.

[176] Esteban-Gómez, D.; Fabbrizzi, L.; Licchelli, M., Why, on Interaction of Urea-Based Receptors with Fluoride, Beautiful Colors Develop. *The Journal of Organic Chemistry* **2005**, 70, (14), 5717-5720

[177] Svenson, J.; Andersson, H. S.; Piletsky, S. A.; Nicholls, I. A., Spectroscopic studies of the molecular imprinting self-assembly process. *Journal of Molecular Recognition* **1998**, 11, (1-6), 83-86

[178] Fages, F. d. r.; Vögtle, F.; Žinic, M., Systematic Design of Amide- and Urea-Type Gelators with Tailored Properties. In *Low Molecular Mass Gelator*, Springer Berlin Heidelberg: **2005**; Vol. 256, pp 77-131

[179] Ali, H. D. P.; Kruger, P. E.; Gunnlaugsson, T., Colorimetric 'naked-eye' and fluorescent sensors for anions based on amidourea functionalised 1,8-naphthalimide structures: anion recognition via either deprotonation or hydrogen bonding in DMSO. *New Journal Of Chemistry* **2008**, 32, (7), 1153-1161

[180] Loving, G.; Imperiali, B., A Versatile Amino Acid Analogue of the Solvatochromic Fluorophore 4-N,N-Dimethylamino-1,8-naphthalimide: A Powerful Tool for the Study of Dynamic Protein Interactions. *Journal of the American Chemical Society* **2008**, 130, (41), 13630-13638

[181] Uchiyama, S.; Santa, T.; Fukushima, T.; Homma, H.; Imai, K., Effects of the substituent groups at the 4- and 7-positions on the fluorescence characteristics of benzofurazan compounds. *Journal of the Chemical Society, Perkin Transactions 2* **1998**, (10), 2165-2174

[182] Imai, K.; Watanabe, Y., Fluorimetric determination of secondary amino acids by 7-fluoro-4-nitrobenzo-2-oxa-1,3-diazole. *Analytica Chimica Acta* **1981**, 130, (2), 377-383

[183] Al-Dirbashi, O.; Kuroda, N.; Nakashima, K., Characterization of the fluorescence properties of 4-fluoro-7-nitrobenzo-2-oxa-1,3-diazole derivatives of some primary and secondary sympathomimetic amines. *Analytica Chimica Acta* **1998**, 365, 169-176

[184] Uchiyama, S.; Santa, T.; Imai, K., Fluorescence characteristics of six 4,7-disubstituted benzofurazan compounds: an experimental and semi-empirical MO study. *Journal of the Chemical Society, Perkin Transactions 2* **1999**, (11), 2525-2532

[185] Wan, W., Descalzo, A. B., Rurack, K., Sellergren, B., Phosphate sensing through ESPT using a molecular imprinted polymer receptor (manuscript under preparation)

[186] Klymchenko, A. S.; Ozturk, T.; Pivovarenko, V. G.; Demchenko, A. P., A 3-hydroxychromone with dramatically improved fluorescence properties. *Tetrahedron Letters* **2001**, 42, (45), 7967-7970

[187] Shynkar, V. V.; Mély, Y.; Duportail, G.; Piémont, E.; Klymchenko, A. S.; Demchenko, A. P., Picosecond Time-Resolved Fluorescence Studies Are Consistent with Reversible Excited-State Intramolecular Proton Transfer in 4-(Dialkylamino)-3-hydroxyflavones. *The Journal of Physical Chemistry A* **2003**, 107, (45), 9522-9529

[188] Choi, K.; Hamilton, A. D., A Dual Channel Fluorescence Chemosensor for Anions Involving Intermolecular Excited State Proton Transfer. *Angewandte Chemie International Edition* **2001**, 40, (20), 3912-3915

[189] Ghosh, K.; Kar, D.; Joardar, S.; Samadder, A.; Khuda-Bukhsh, A. R., Azaindole-1,2,3-triazole conjugate in a tripod for selective sensing of Cl^-, $H_2PO_4^-$ and ATP under different conditions. *RSC Advances* **2014**, 4, (23), 11590-11597

[190] Ucak-Astarlioglu, M. G.; Connors, R. E., Absorption and Fluorescence of 2,5-Diarylidenecyclopentanones in Acidic Media: Evidence for Excited-State Proton Transfer. *The Journal of Physical Chemistry A* **2005**, 109, (37), 8275-8279.

[191] Druzhinin, S. I.; Rodchenkov, G. M.; Uzhinov, B. M., Intermolecular excited state proton transfer reactions of diaryloxazoles. *Chemical Physics* **1988**, 128, 383-394

[192] Solntsev, K. M.; Poizat, O.; Dong, J.; Rehault, J.; Lou, Y.; Burda, C.; Tolbert, L. M., Meta and Para Effects in the Ultrafast Excited-State Dynamics of the Green Fluorescent Protein Chromophores1. *The Journal of Physical Chemistry B* **2008**, 112, (9), 2700-2711

[193] Kuchlyan, J.; Banik, D.; Kundu, N.; Ghosh, S.; Banerjee, C.; Sarkar, N., Effect of Confinement on Excited-State Proton Transfer of Firefly´s Chromophore d-Luciferin in AOT Reverse Micelles. *The Journal of Physical Chemistry B* **2014**, 118, (12), 3401-3408.

[194] Farrington, K.; Magner, E.; Regan, F., Predicting the performance of molecularly imprinted polymers: Selective extraction of caffeine by molecularly imprinted solid phase extraction. *Analytica Chimica Acta* **2006**, 566, (1), 60-68

[195] Yoshimatsu, K.; Reimhult, K.; Krozer, A.; Mosbach, K.; Sode, K.; Ye, L., Uniform molecularly imprinted microspheres and nanoparticles prepared by precipitation polymerization: The control of particle size suitable for different analytical applications. *Analytica Chimica Acta* **2008**, 584, (1), 112-121

[196] *Wagner, R.* Imprinted fluorogenic receptors composed of a polymerisable naphthalimide-based oxyanion probe Technische Universität Dortmund, Dortmund, **2013**

[197] Cennamo, N.; D'Agostino, G.; Galatus, R.; Bibbò, L.; Pesavento, M.; Zeni, L., Sensors based on surface plasmon resonance in a plastic optical fiber for the detection of trinitrotoluene. *Sensors and Actuators B: Chemical* **2013**, 188, 221-226

[198] Zhu, X.; Su, Q.; Cai, J.; Yang, J.; Gao, Y., Molecularly imprinted polymer membranes for substance-selective solid-phase extraction from aqueous solutions. *Journal of Applied Polymer Science* **2006**, 101, (6), 4468-4473

[199] Mustafa, G.; Lieberzeit, P. A., MIP Sensors on the Way to Real-World Applications. In Designing Receptors for the Next Generation of Biosensor **2012**; pp 1-21

[200] Burns, A.; Sengupta, P.; Zedayko, T.; Baird, B.; Wiesner, U., Core/Shell Fluorescent Silica Nanoparticles for Chemical Sensing: Towards Single-Particle Laboratories. *Small* **2006**, 2, (6), 723-726

[201] Li, C.; Han, J.; Ryu, C. Y.; Benicewicz, B. C., A Versatile Method To Prepare RAFT Agent Anchored Substrates and the Preparation of PMMA Grafted Nanoparticles. *Macromolecules* **2006**, 39, (9), 3175-3183

[202] Stöber, W.; Fink, A.; Bohn, E., Controlled growth of monodisperse silica spheres in the micron size range. *Journal of Colloid and Interface Science* **1968**, 26, (1), 62-69

[203] Zhang, Q.; Zhang, T.; Ge, J.; Yin, Y., Permeable Silica Shell through Surface-Protected Etching. *Nano Letters* **2008**, 8, (9), 2867-2871

[204] Gao, R.; Kong, X.; Su, F.; He, X.; Chen, L.; Zhang, Y., Synthesis and evaluation of molecularly imprinted core–shell carbon nanotubes for the determination of triclosan in environmental water samples. *Journal of Chromatography A* **2010**, 1217, (52), 8095-8102

[205] Sulitzky, C.; Rückert, B. r.; Hall, A. J.; Lanza, F.; Unger, K.; Sellergren, B., Grafting of Molecularly Imprinted Polymer Films on Silica Supports Containing Surface-Bound Free Radical Initiators. *Macromolecules* **2001**, 35, (1), 79-91

[206] Halhalli, M. R.; Aureliano, C. S. A.; Schillinger, E.; Sulitzky, C.; Titirici, M. M.; Sellergren, B., An improved grafting technique for producing imprinted thin film composite beads. *Polymer Chemistry* **2012**, 3, (4), 1033-1042

[207] Tsujii, Y.; Ejaz, M.; Sato, K.; Goto, A.; Fukuda, T., Mechanism and Kinetics of RAFT-Mediated Graft Polymerization of Styrene on a Solid Surface. 1. Experimental Evidence of Surface Radical Migration. *Macromolecules* **2001**, 34, (26), 8872-8878

[208] Loeffler, F.; Schirwitz, C.; Wagner, J.; Koenig, K.; Maerkle, F.; Torralba, G.; Hausmann, M.; Bischoff, F. R.; Nesterov-Mueller, A.; Breitling, F., Biomolecule Arrays Using Functional Combinatorial Particle Patterning on Microchips. *Advanced Functional Materials* **2012**, 22, (12), 2503-2508

[209] Rohand, T.; Qin, W.; Boens, N.; Dehaen, W., Palladium-Catalyzed Coupling Reactions for the Functionalization of BODIPY Dyes with Fluorescence Spanning the Visible Spectrum. *European Journal of Organic Chemistry* **2006**, 2006, (20), 4658-4663

[210] Dilek, Ö.; Bane, S. L., Synthesis of boron dipyrromethene fluorescent probes for bioorthogonal labeling. *Tetrahedron Letters* **2008**, 49, (8), 1413-1416

List of Abbreviations

ABDV	Azobisdimethylvaleronitrile
AIBN	Azobisisobutyronitrile
APD	Avalanche photodiode
ATRP	Atom transfer radical polymerisation
BMA	Benzyl methacrylate
BODIPY	Boron dipyrromethene
CIS	Complexiation induced shift
CRP	Controlled radical polymerization
CPDB	2-(2-Cyanopropyl) Dithiobenzoate
CT	Charge transfer
DAD	Diode-array Detector
DFG	Deutsche Forschungsgesellschaft
DLS	Dynamic light scattering
DVB	Divinyl benzene
EA	Elemental analysis
EDMA	Ethylene glycol dimethacrylate
EDG	Electron donating group
EDX	Energy-dispersive X-ray spectroscopy
ESPT	Excited state proton transfer
EWG	Electron withdrawing group

FRET	Förster resonance energy transfer
FTIR	Fourier transform infrared spectroscopy
HEMA	(Hydroxyethyl)methacrylate
HOMO	Highest occupied molecular orbital
HPLC	High performance liquid chromatography
IC	Internal conversion
ICT	Intramolecular charge transfer
IFQ	Imprinting factor calculated from fluorescence quenching
ISC	Intersystem crossing
IUPAC	International Union of Pure and Applied Chemistry
L-PA	L-Phenylalanine anilide
LASER	Light amplification by stimulated emission of radiation
LOD	Limit of detection
LUMO	Lowest unoccupied molecular orbital
MIP	Molecularly Imprinted Polymer
MMA	Methylmethacrylate
MPTES	Methacryloxypropyltriethoxysilane
NBD	Nitrobenzo-2-oxa-1,3-diazole
NIP	Non-Imprinted Polymer
NMR	Nuclear magnetic resonance
NMP	Nitroxide mediated polymerization
PD	Photodiode
PenG	Penicillin G

PET	Photoinduced electron transfer
PETEA	Pentaerythritol tetraacrylate
PETRA	Pentaerythritol triacrylate
PMP	1,2,2,6,6-Pentamethylpiperidine
PMT	Photomultiplier tube
PPA	Phenyl phosphate
PVB	Para-vinylbenzoic acid
QCM	Quartz crystal microbalance
QY	Quantum yield
RAFT	Reversible Addition-Fragmentation chain transfer
RTP	Room temperature phosphorescence
SPE	Solid phase extraction
SPR	Surface plasmon resonance
TBA	Tetra n-butyl ammonium
TEM	Transmission electron microscopy
TEOS	Tetraethyloxysilane
TGA	Thermogravimetric analysis
TRIM	Trimethylolpropane trimethacrylate
TSA	Transition state analogue

List of Functional monomers

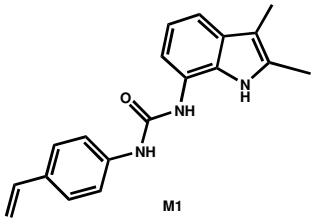

M1

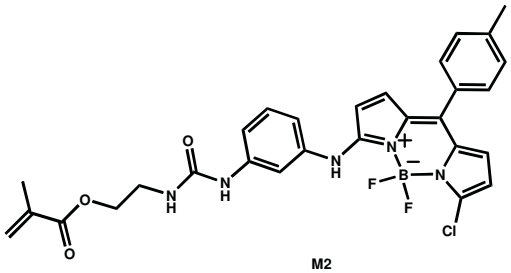

M2

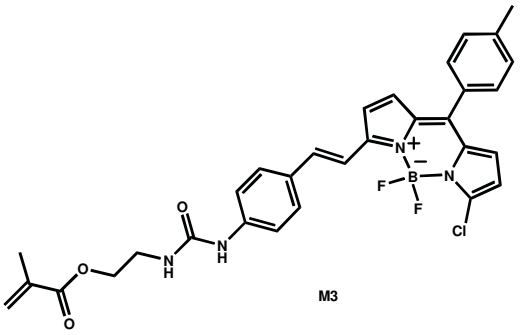

M3

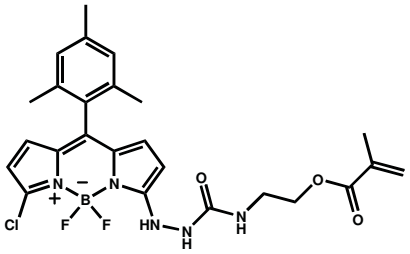

M4

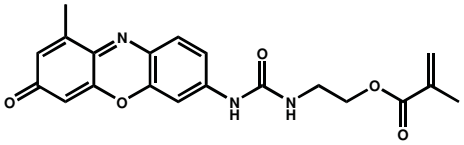

M5

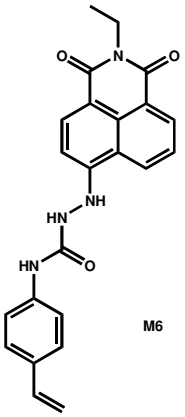

M6

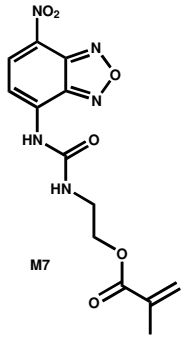

M7

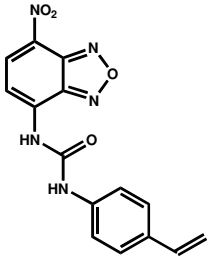

M8

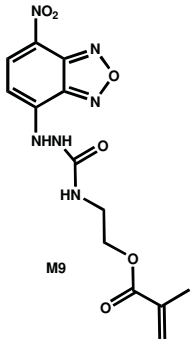

M9

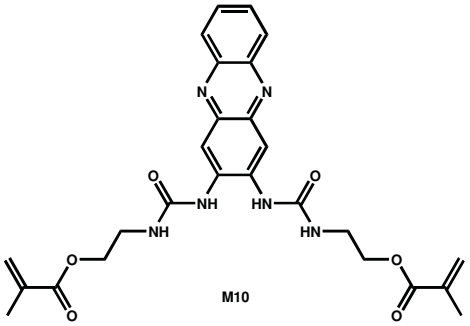

M10

List of Figures

List of Schemes

List of Tables

List of NMR spectra

M2

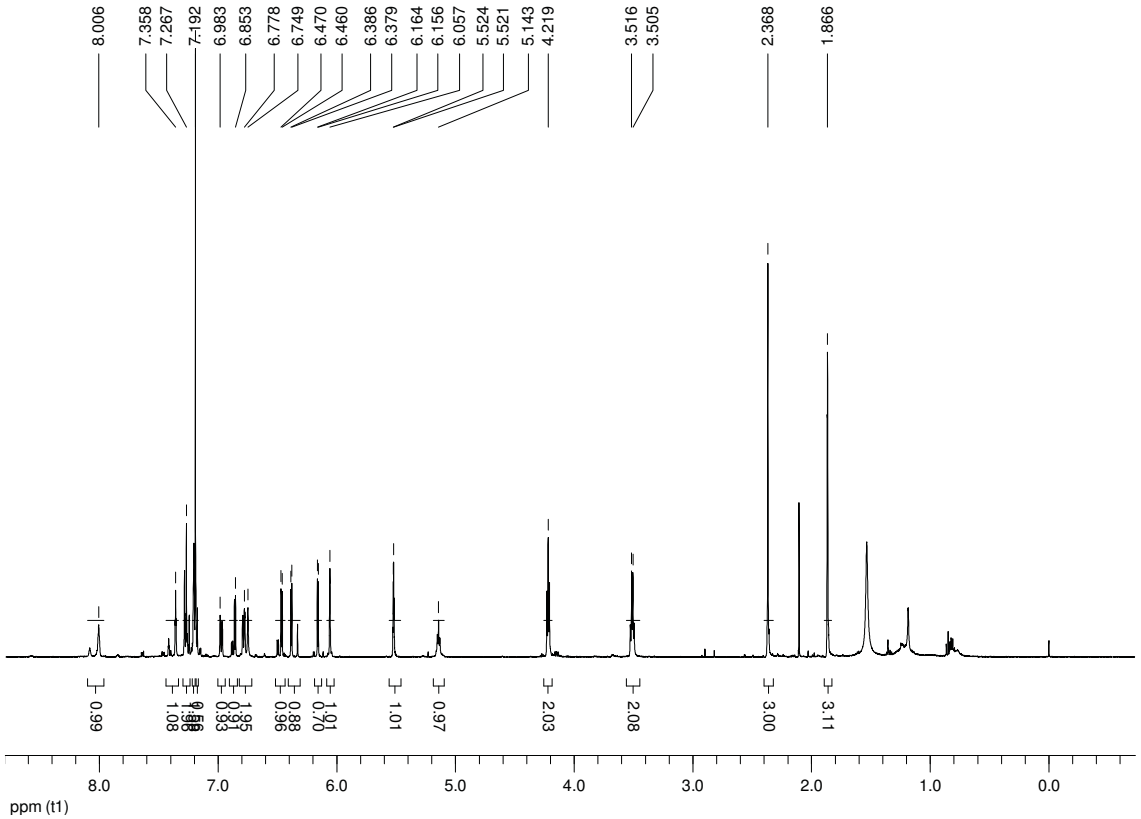

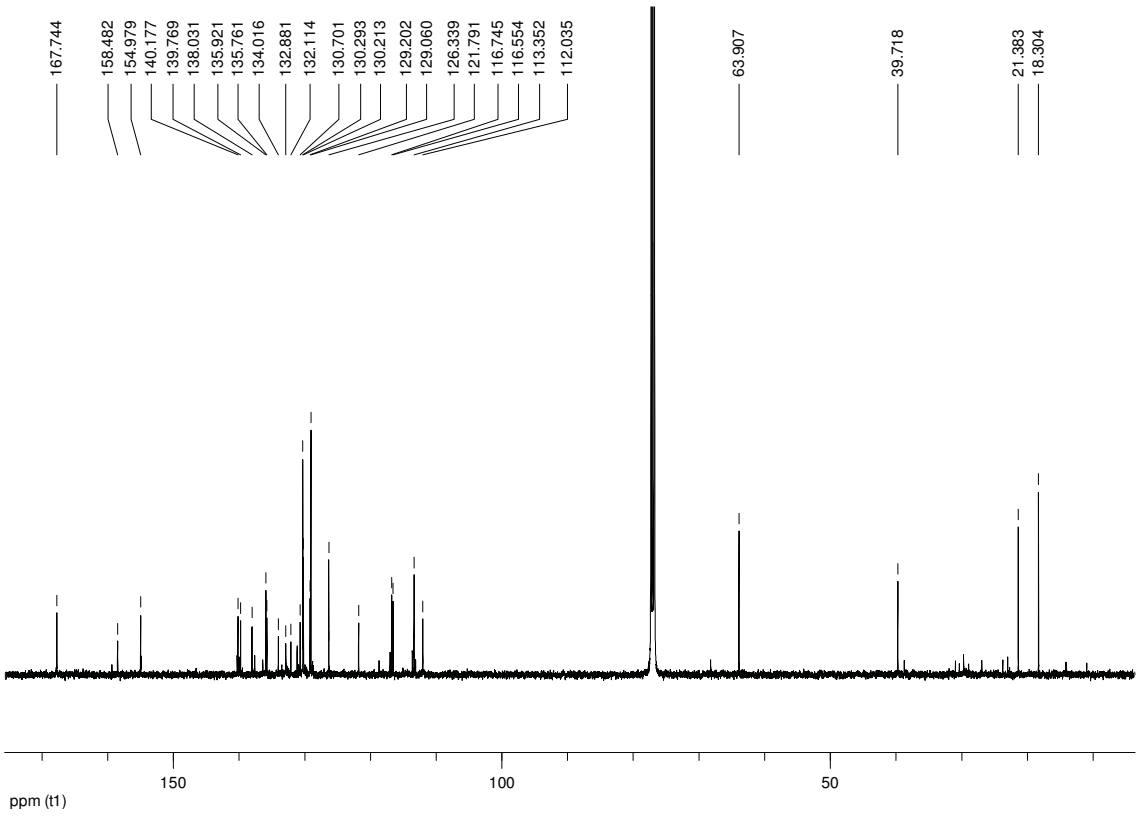

M3

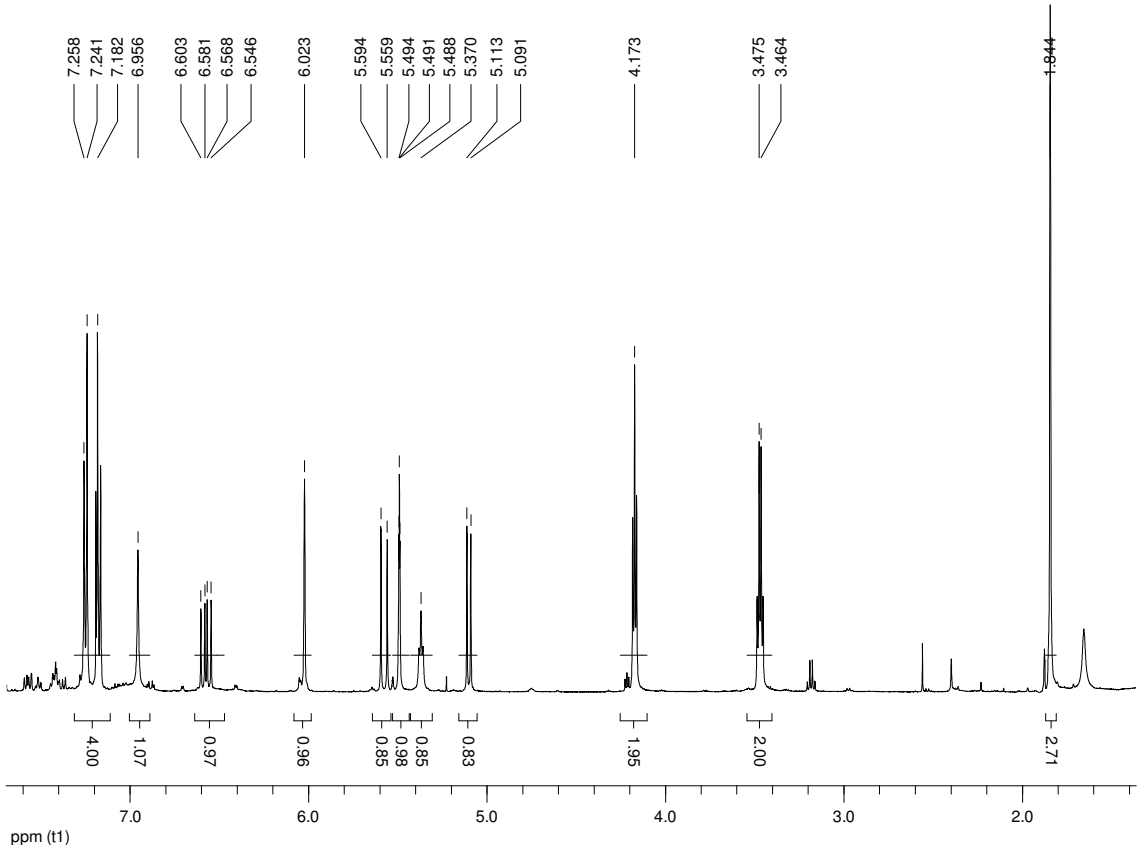
7.258
7.241
7.182
6.956
6.603
6.581
6.568
6.546
6.023
5.594
5.559
5.494
5.491
5.488
5.370
5.113
5.091
4.173
3.475
3.464
1.844
4.00
1.07
0.97
0.96
0.85
0.98
0.85
0.83
1.95
2.00
2.71
7.0
6.0
5.0
4.0
3.0
2.0
ppm (t1)

M4

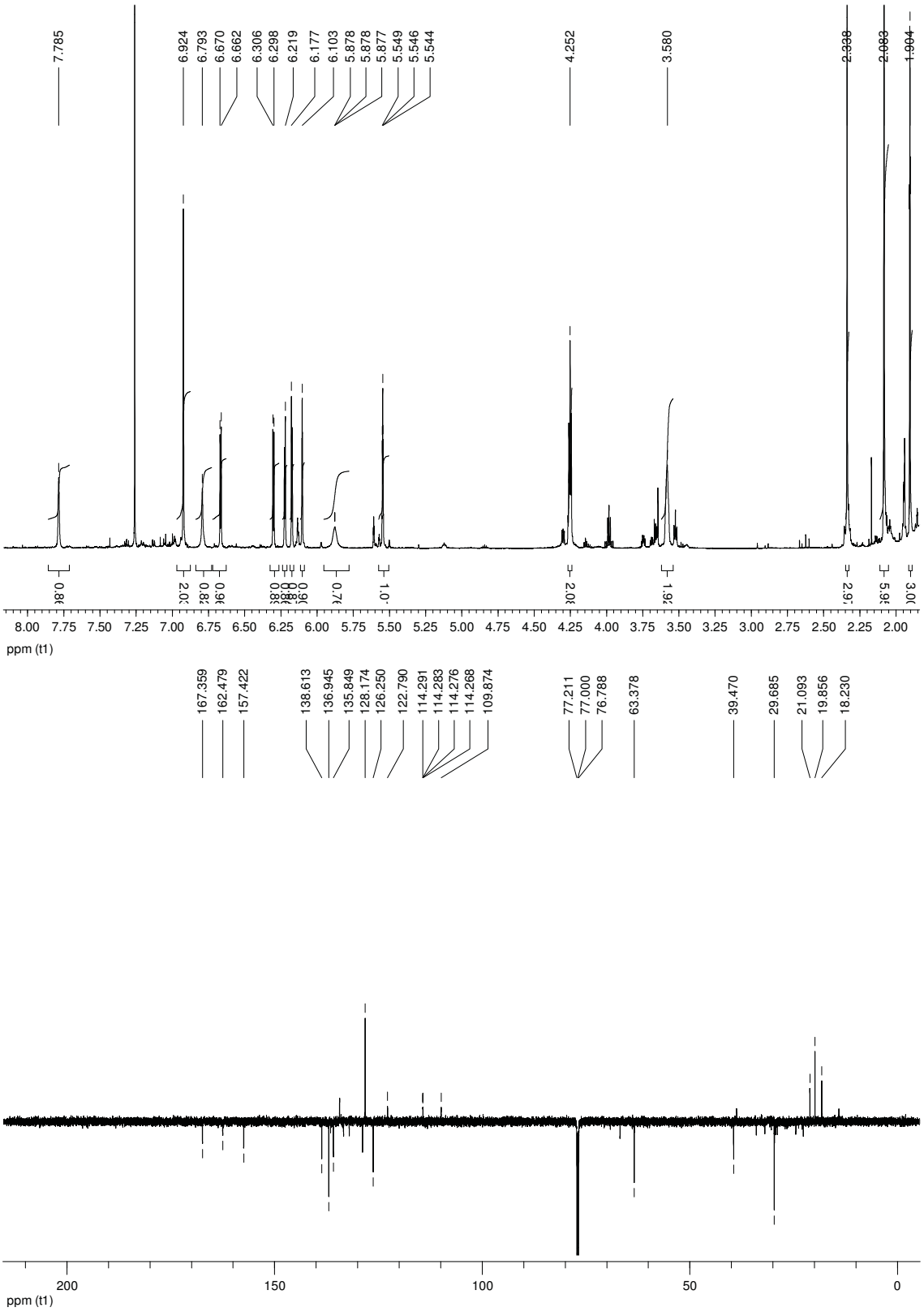
7.785
6.924
6.793
6.670
6.662
6.306
6.298
6.219
6.177
6.103
5.878
5.878
5.877
5.549
5.546
5.544
4.252
3.580
2.338
2.083
1.904
ppm (t1)
167.359
162.479
157.422
138.613
136.945
135.849
128.174
126.250
122.790
114.291
114.283
114.276
114.268
109.874
77.211
77.000
76.788
63.378
39.470
29.685
21.093
19.856
18.230
ppm (t1)

M5

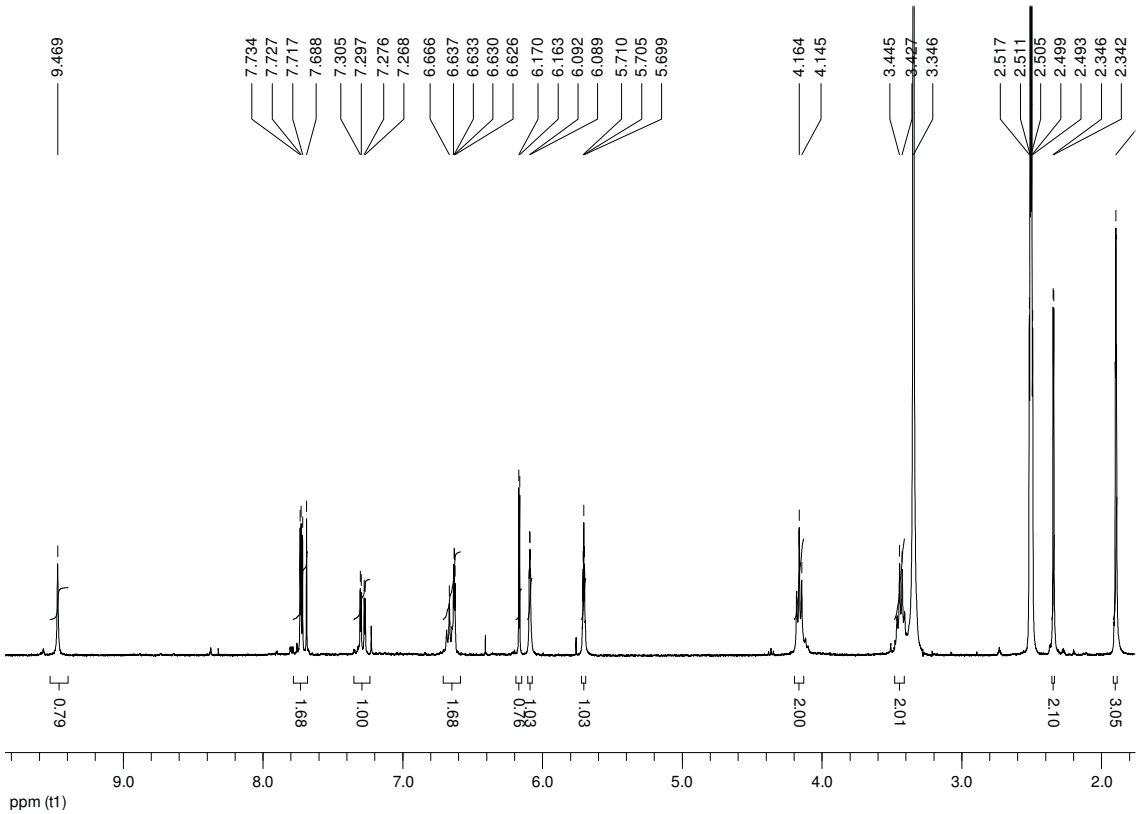
9.469
7.734
7.727
7.717
7.688
7.305
7.297
7.276
7.268
6.666
6.637
6.633
6.630
6.626
6.170
6.163
6.092
6.089
5.710
5.705
5.699
4.164
4.145
3.445
3.427
3.346
2.517
2.511
2.505
2.499
2.493
2.346
2.342
0.79
1.68
1.00
1.98
0.78
1.03
2.00
2.01
2.10
3.05
9.0
8.0
7.0
6.0
5.0
4.0
3.0
2.0
ppm (t1)

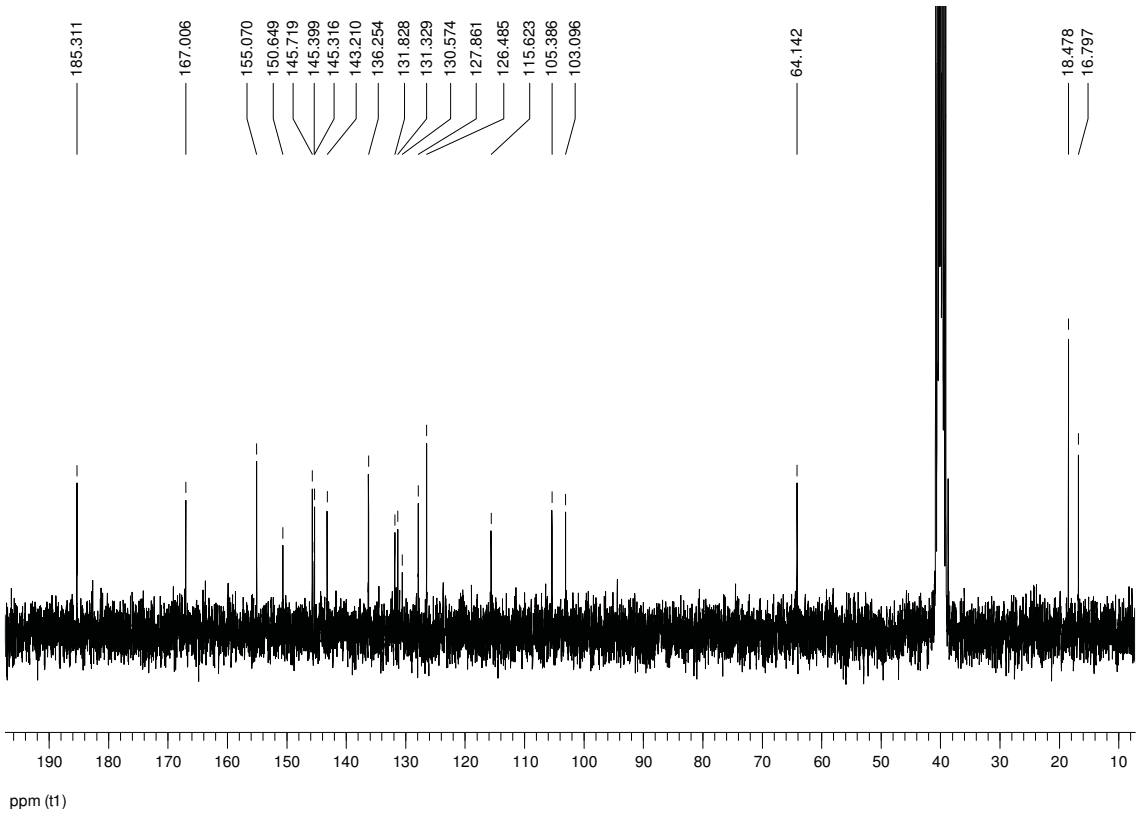
185.311
167.006
155.070
150.649
145.719
145.399
145.316
143.210
136.254
131.828
131.329
130.574
127.861
126.485
115.623
105.386
103.096
64.142
18.478
16.797
190
180
170
160
150
140
130
120
110
100
90
80
70
60
50
40
30
20
10
ppm (t1)

M7

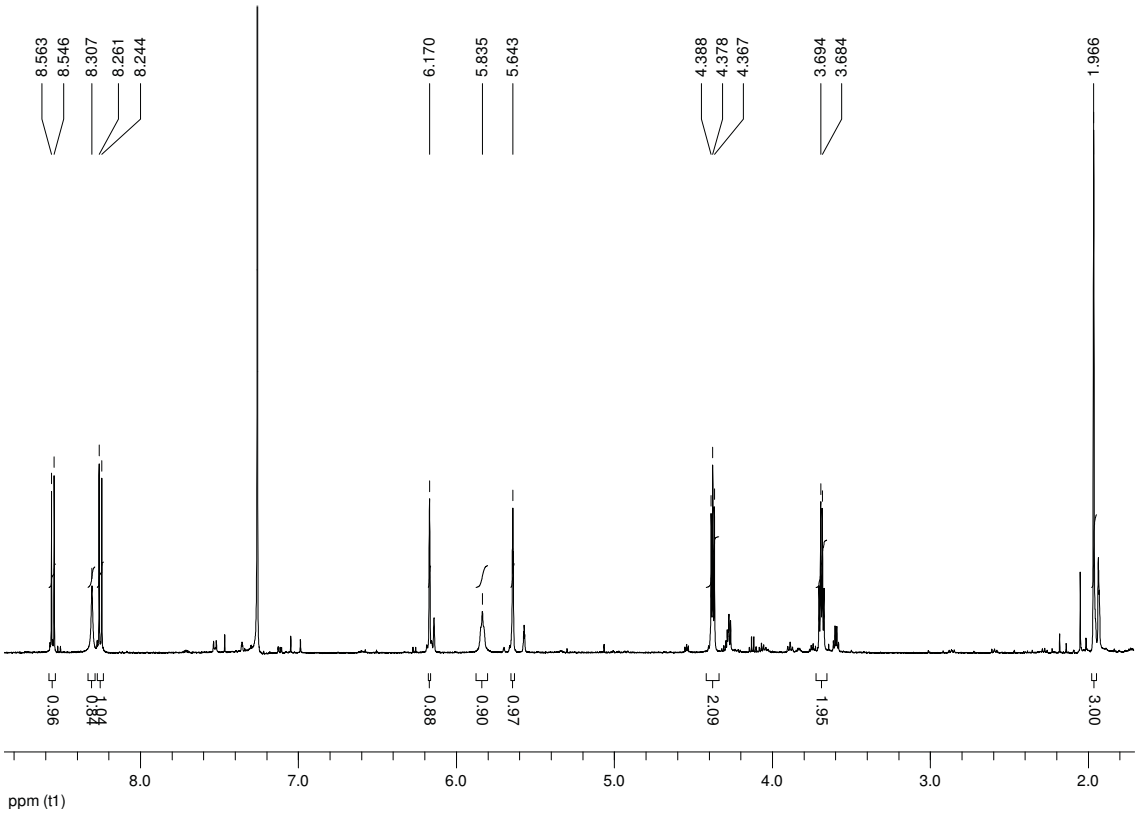
8.563
8.546
8.307
8.261
8.244
6.170
5.835
5.643
4.388
4.378
4.367
3.694
3.684
1.966
0.96
1.04
1.04
0.88
0.90
0.97
2.09
1.95
3.00
8.0
7.0
6.0
5.0
4.0
3.0
2.0
ppm (t1)

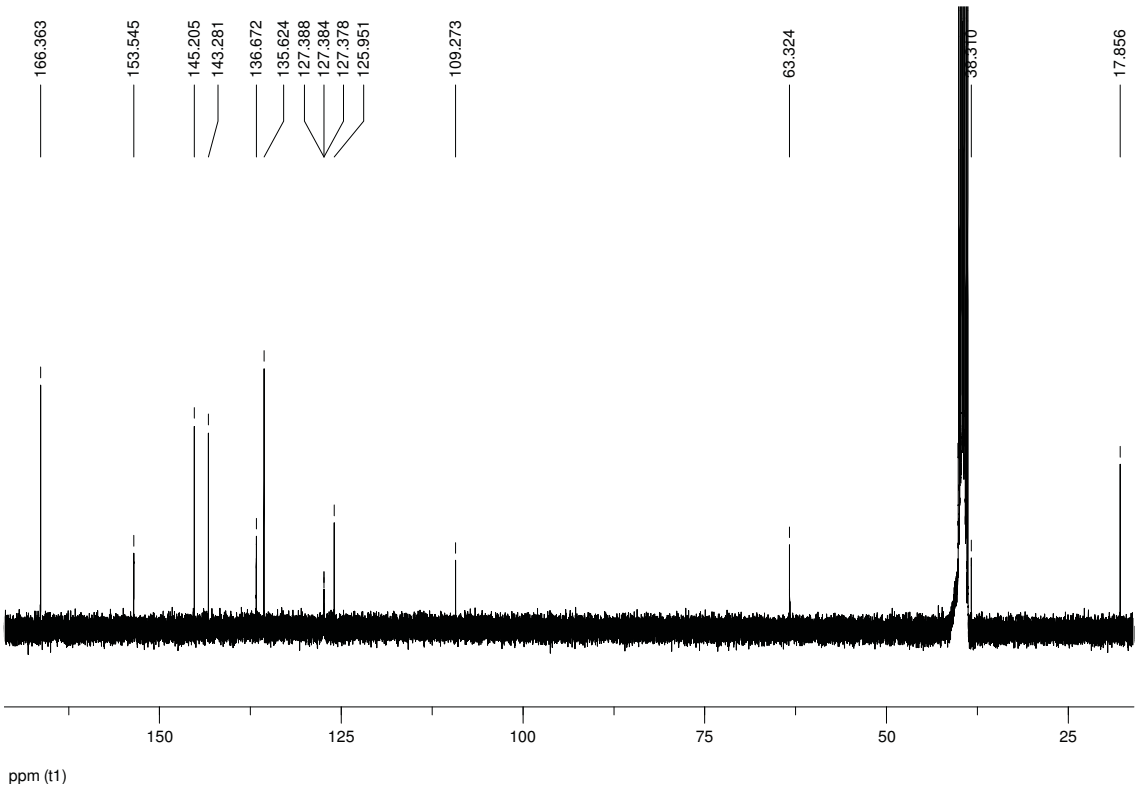
166.363
153.545
145.205
143.281
136.672
135.624
127.388
127.384
127.378
125.951
109.273
63.324
38.310
17.856
150
125
100
75
50
25
ppm (t1)

M8

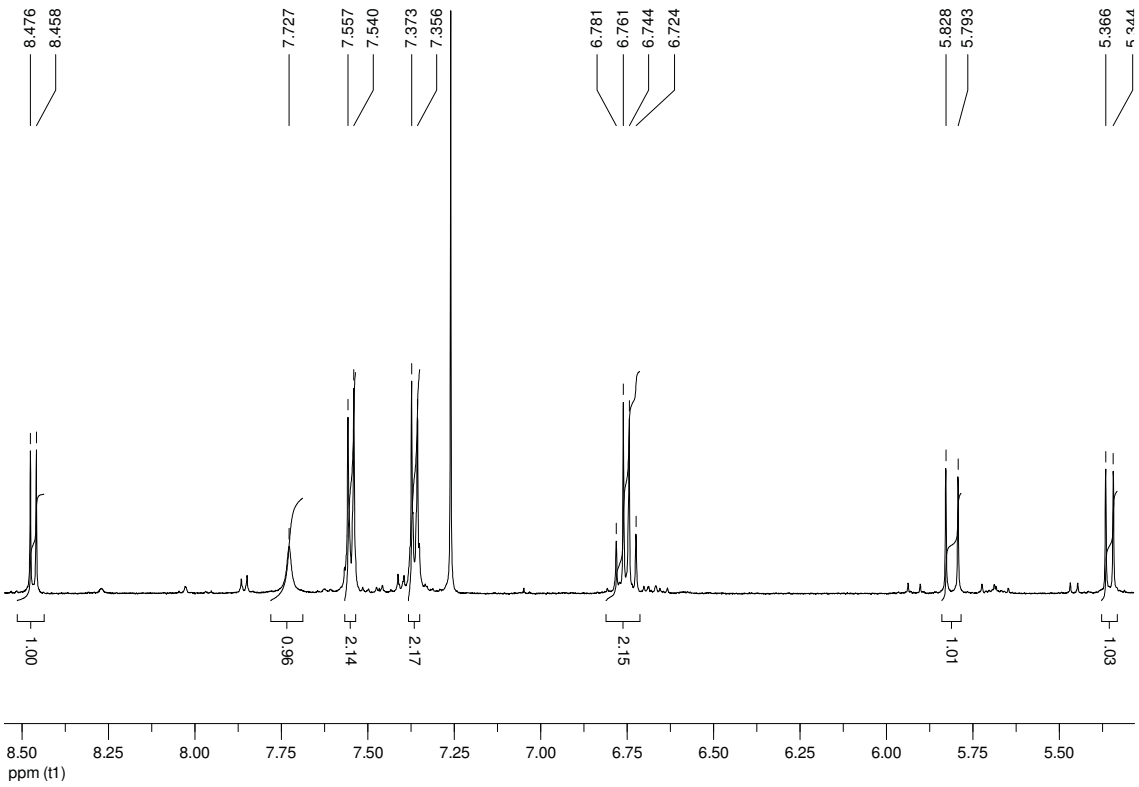
8.476
8.458
7.727
7.557
7.540
7.373
7.356
6.781
6.761
6.744
6.724
5.828
5.793
5.366
1.00
0.96
2.14
2.17
2.15
1.01
1.03
8.50
8.25
8.00
7.75
7.50
7.25
7.00
6.75
6.50
6.25
6.00
5.75
5.50
ppm (t1)

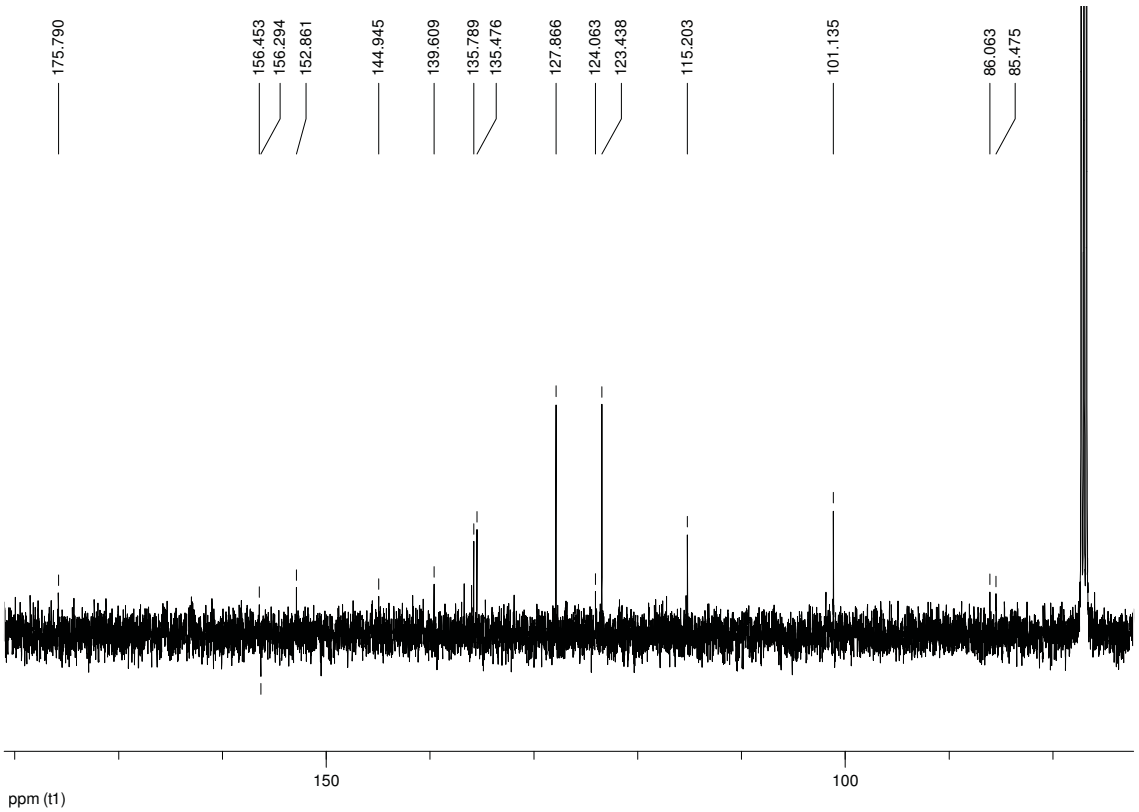
175.790
156.453
156.294
152.861
144.945
139.609
135.789
135.476
127.866
124.063
123.438
115.203
101.135
86.063
85.475
150
100
ppm (t1)

M9

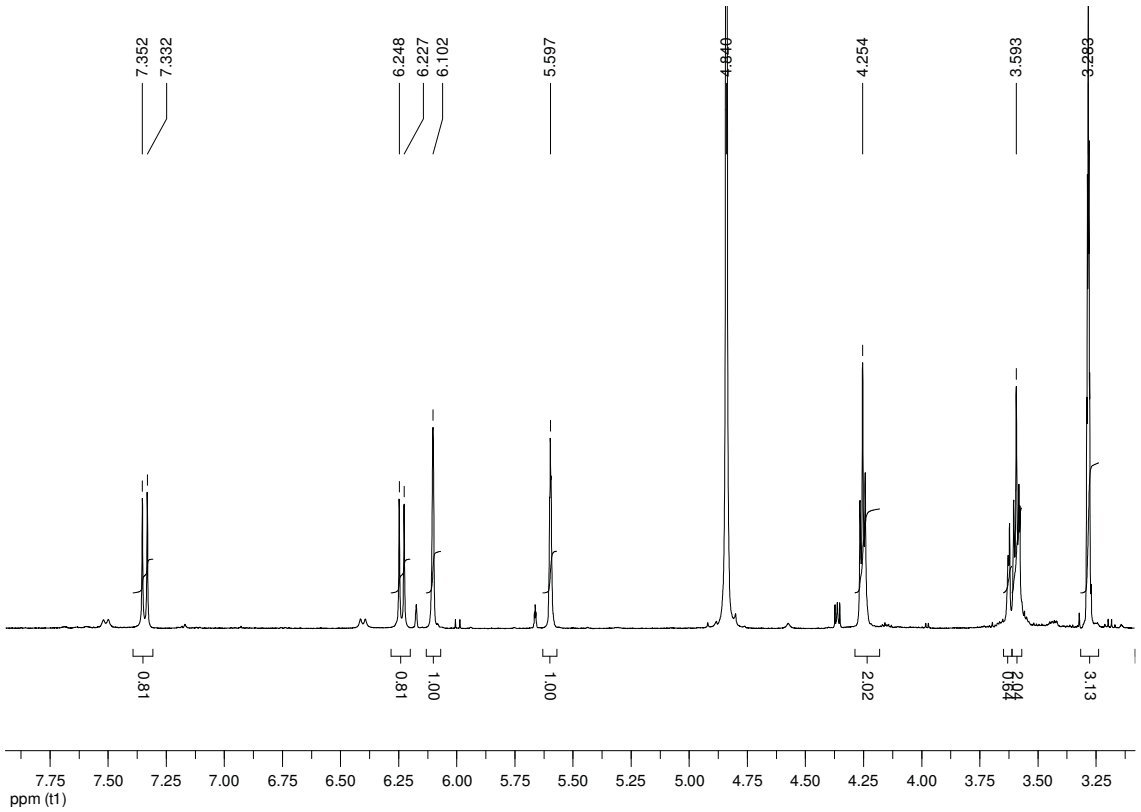
7.352
7.332
6.248
6.227
6.102
5.597
4.840
4.254
3.593
3.283
0.81
0.81
1.00
1.00
2.02
2.04
6.84
3.13
7.75 7.50 7.25 7.00 6.75 6.50 6.25 6.00 5.75 5.50 5.25 5.00 4.75 4.50 4.25 4.00 3.75 3.50 3.25
ppm (t1)

M10

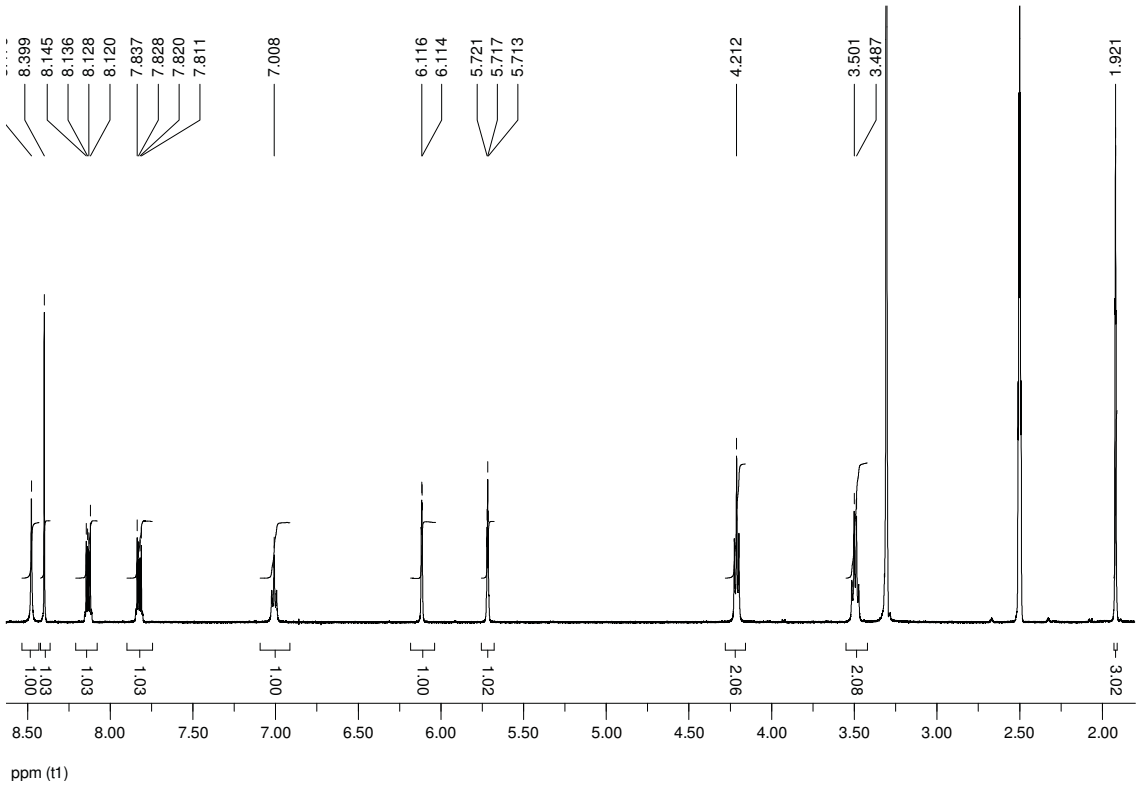
8.399
8.145
8.136
8.128
8.120
7.837
7.828
7.820
7.811
7.008
6.116
6.114
5.721
5.717
5.713
4.212
3.501
3.487
1.921
1.00
1.03
1.03
1.03
1.00
1.00
1.02
2.06
2.08
3.02
8.50 8.00 7.50 7.00 6.50 6.00 5.50 5.00 4.50 4.00 3.50 3.00 2.50 2.00
ppm (t1)

C1

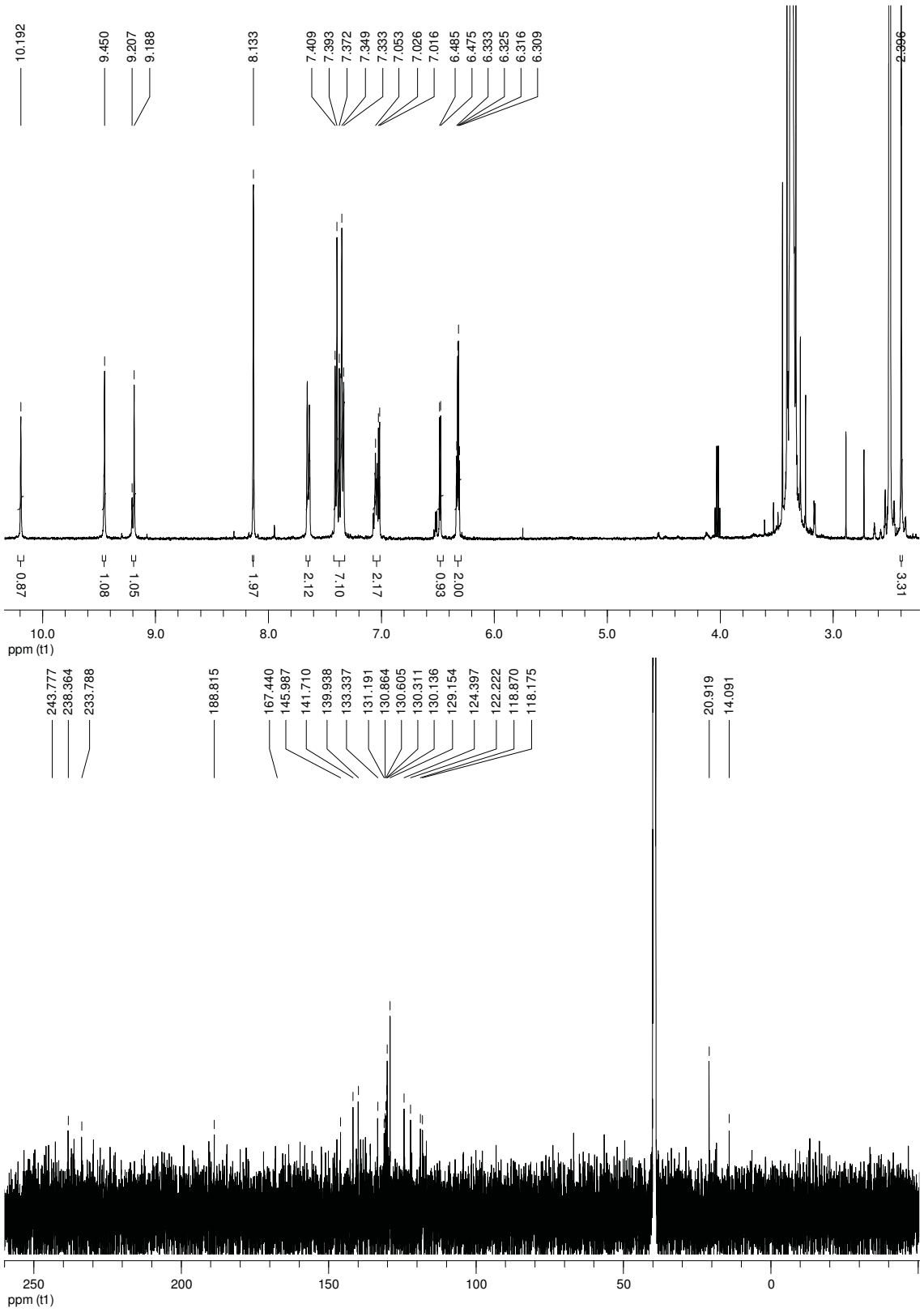
10.192
9.450
9.207
9.188
8.133
7.409
7.393
7.372
7.349
7.333
7.053
7.026
7.016
6.485
6.475
6.333
6.325
6.316
6.309
2.396
0.87
1.08
1.05
1.97
2.12
7.10
2.17
0.93
2.00
3.31
10.0
9.0
8.0
7.0
6.0
5.0
4.0
3.0
ppm (t1)
243.777
238.364
233.788
188.815
167.440
145.987
141.710
139.938
133.337
131.191
130.864
130.605
130.311
130.136
129.154
124.397
122.222
118.870
118.175
20.919
14.091
250
200
150
100
50
0
ppm (t1)

C3

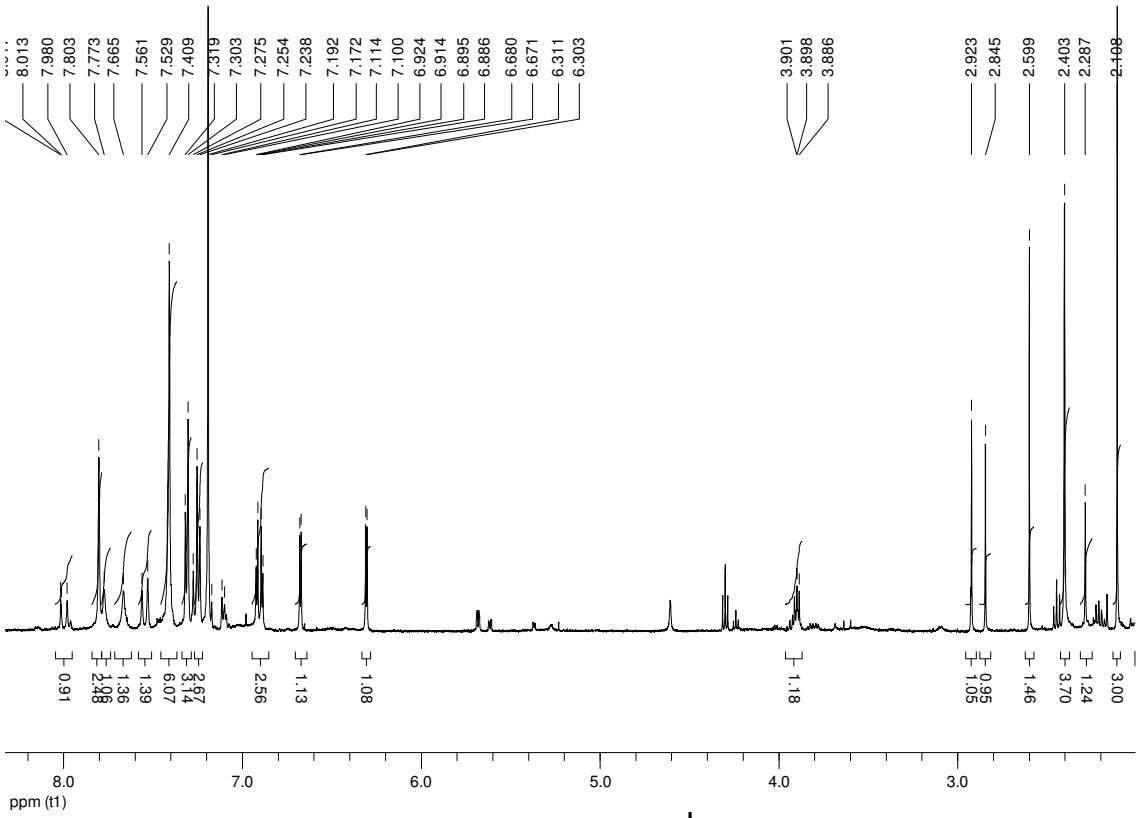
8.013
7.980
7.803
7.773
7.665
7.561
7.529
7.409
7.319
7.303
7.275
7.254
7.238
7.192
7.172
7.114
7.100
6.924
6.914
6.895
6.886
6.680
6.671
6.311
6.303
3.901
3.898
3.886
2.923
2.845
2.599
2.403
2.287
2.108
0.91
2.88
2.08
1.36
1.39
6.07
3.14
2.97
2.56
1.13
1.08
1.18
0.95
1.0
1.46
3.70
1.24
3.00
8.0
7.0
6.0
5.0
4.0
3.0
ppm (t1)

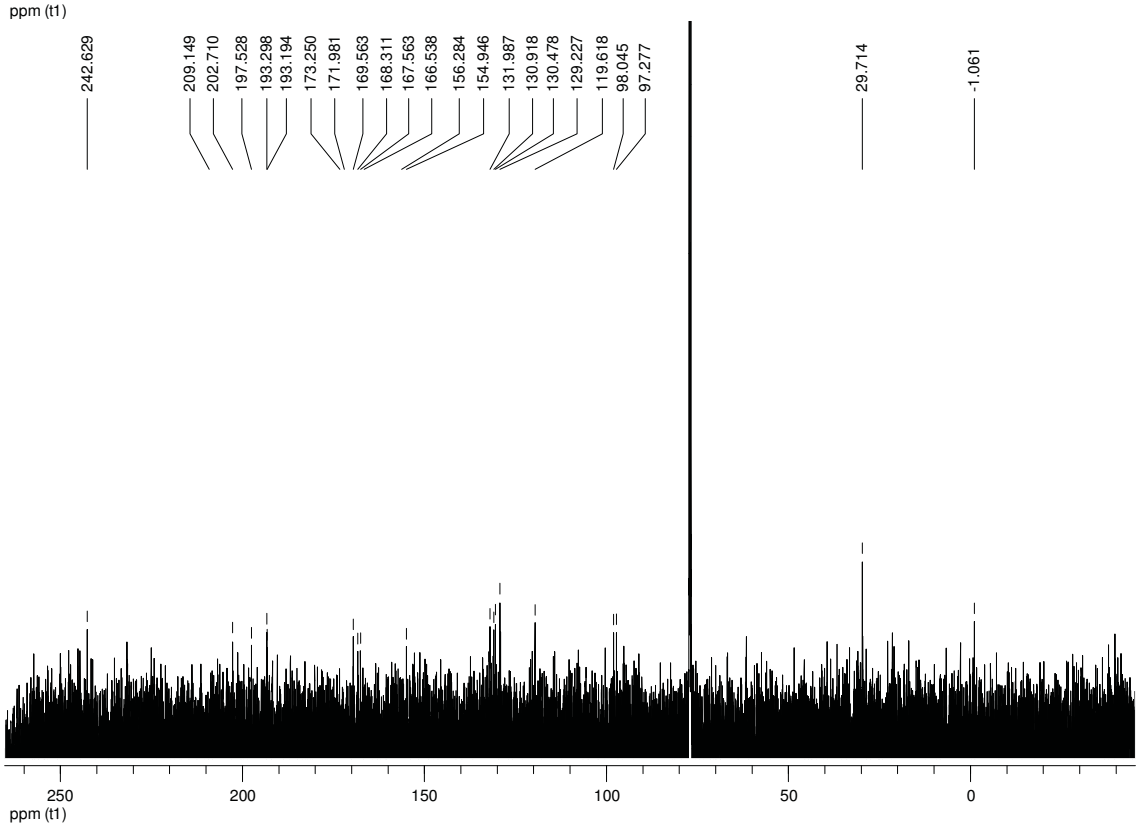
242.629
209.149
202.710
197.528
193.298
193.194
173.250
171.981
169.563
168.311
167.563
166.538
156.284
154.946
131.987
130.918
130.478
129.227
119.618
98.045
97.277
29.714
-1.061
250
200
150
100
50
0
ppm (t1)

C4

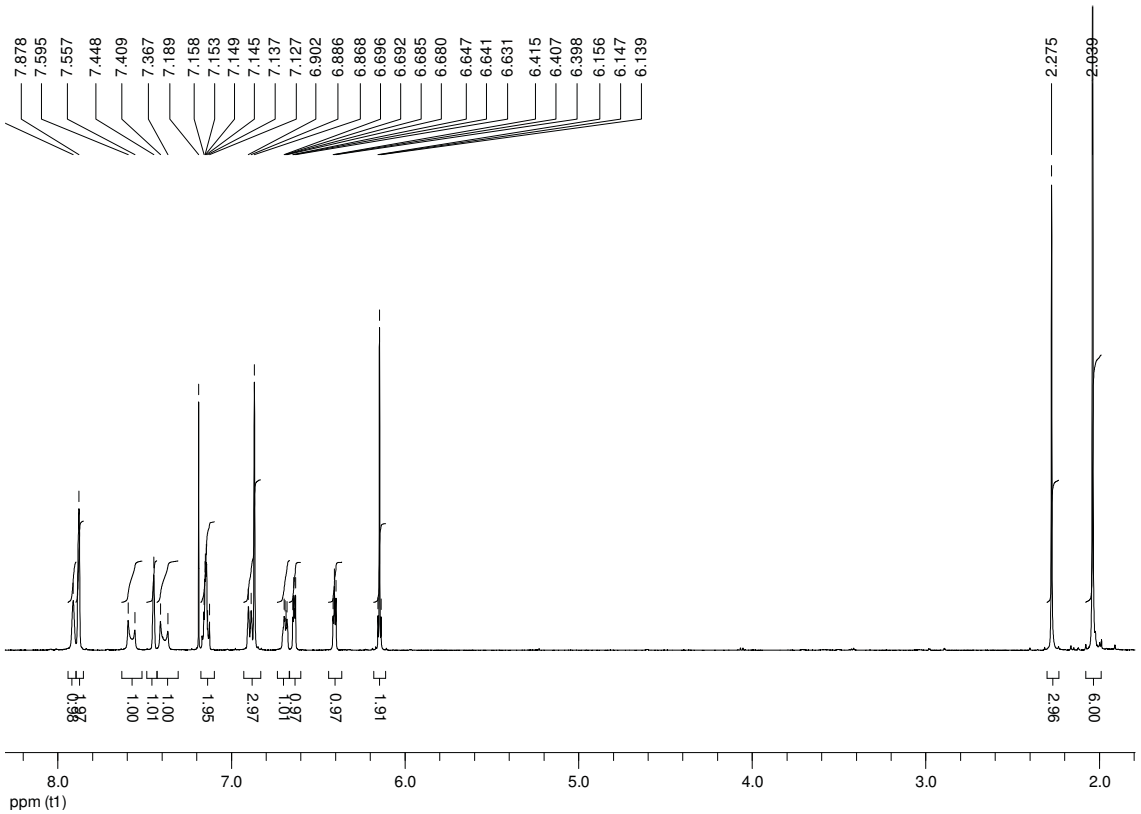
7.878
7.595
7.557
7.448
7.409
7.367
7.189
7.158
7.153
7.149
7.145
7.137
7.127
6.902
6.886
6.868
6.696
6.692
6.685
6.680
6.647
6.641
6.631
6.415
6.407
6.398
6.156
6.147
6.139
2.275
2.039
0.98
0.97
1.00
1.01
1.00
1.95
2.97
1.01
0.97
0.97
1.91
2.96
6.00
8.0
7.0
6.0
5.0
4.0
3.0
2.0
ppm (t1)

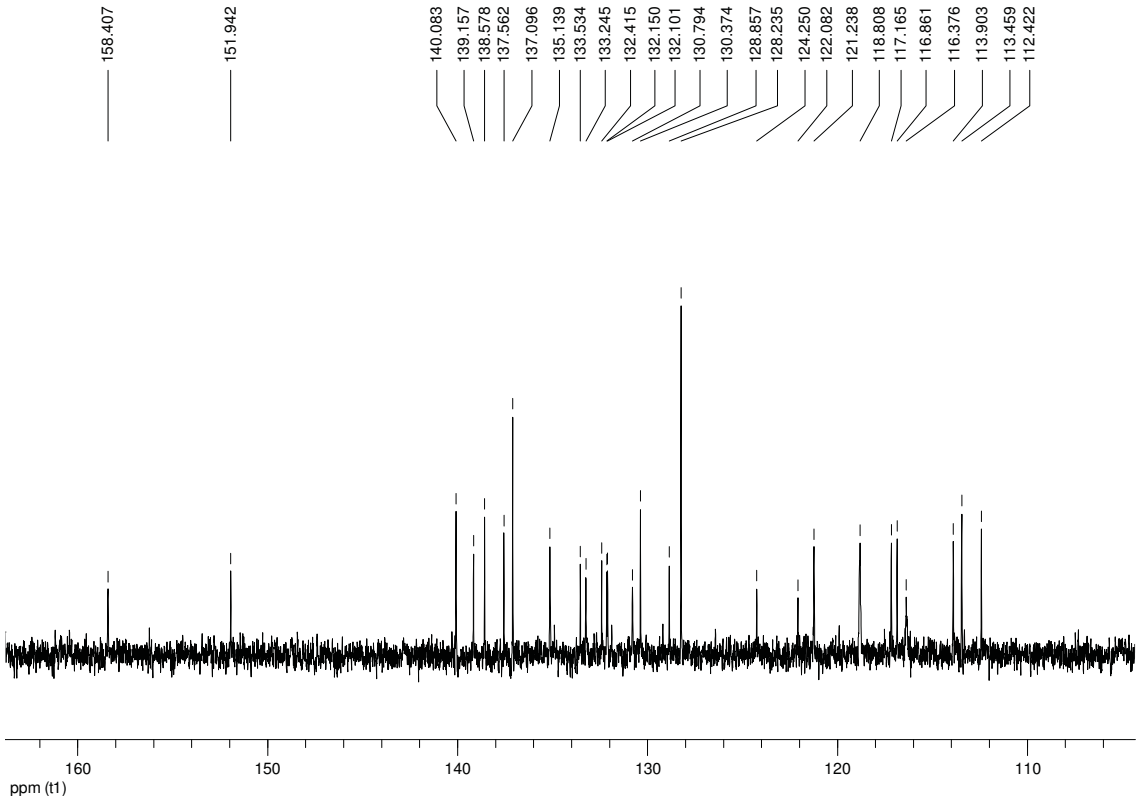
158.407
151.942
140.083
139.157
138.578
137.562
137.096
135.139
133.534
133.245
132.415
132.150
132.101
130.794
130.374
128.857
128.235
124.250
122.082
121.238
118.808
117.165
116.861
116.376
113.903
113.459
112.422
160
150
140
130
120
110
ppm (t1)

C5

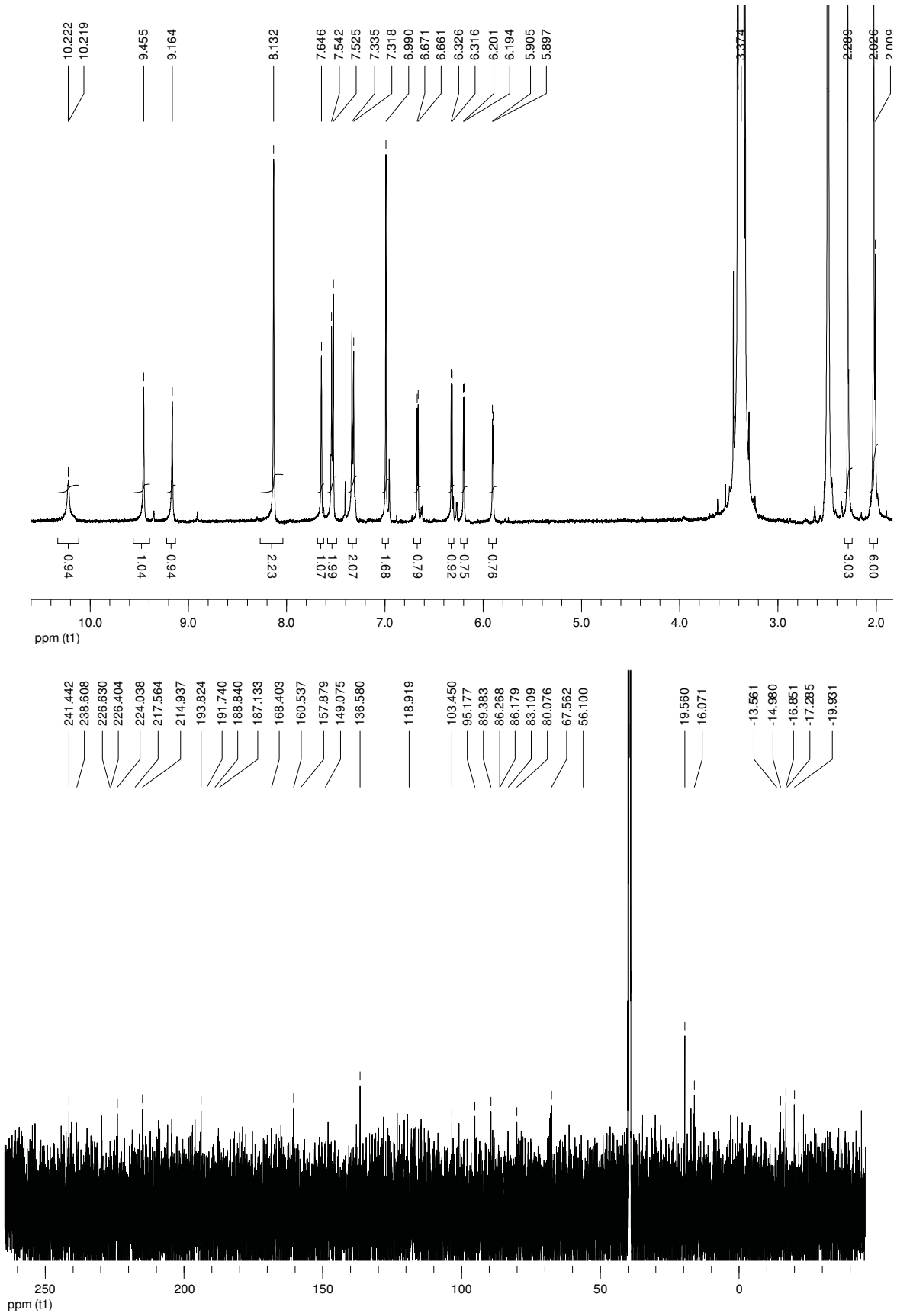
10.222
10.219
9.455
9.164
8.132
7.646
7.542
7.525
7.335
7.318
6.990
6.671
6.661
6.326
6.316
6.201
6.194
5.905
5.897
1.374
2.289
2.026
2.009
0.94
1.04
0.94
2.23
1.07
1.99
2.07
1.68
0.79
0.92
0.75
0.76
3.03
6.00
10.0
9.0
8.0
7.0
6.0
5.0
4.0
3.0
2.0
ppm (t1)
241.442
238.608
226.630
226.404
224.038
217.564
214.937
193.824
191.740
188.840
187.133
168.403
160.537
157.879
149.075
136.580
118.919
103.450
95.177
89.383
86.268
86.179
83.109
80.076
67.562
56.100
19.560
16.071
-13.561
-14.980
-16.851
-17.285
-19.931
250
200
150
100
50
0
ppm (t1)

C6

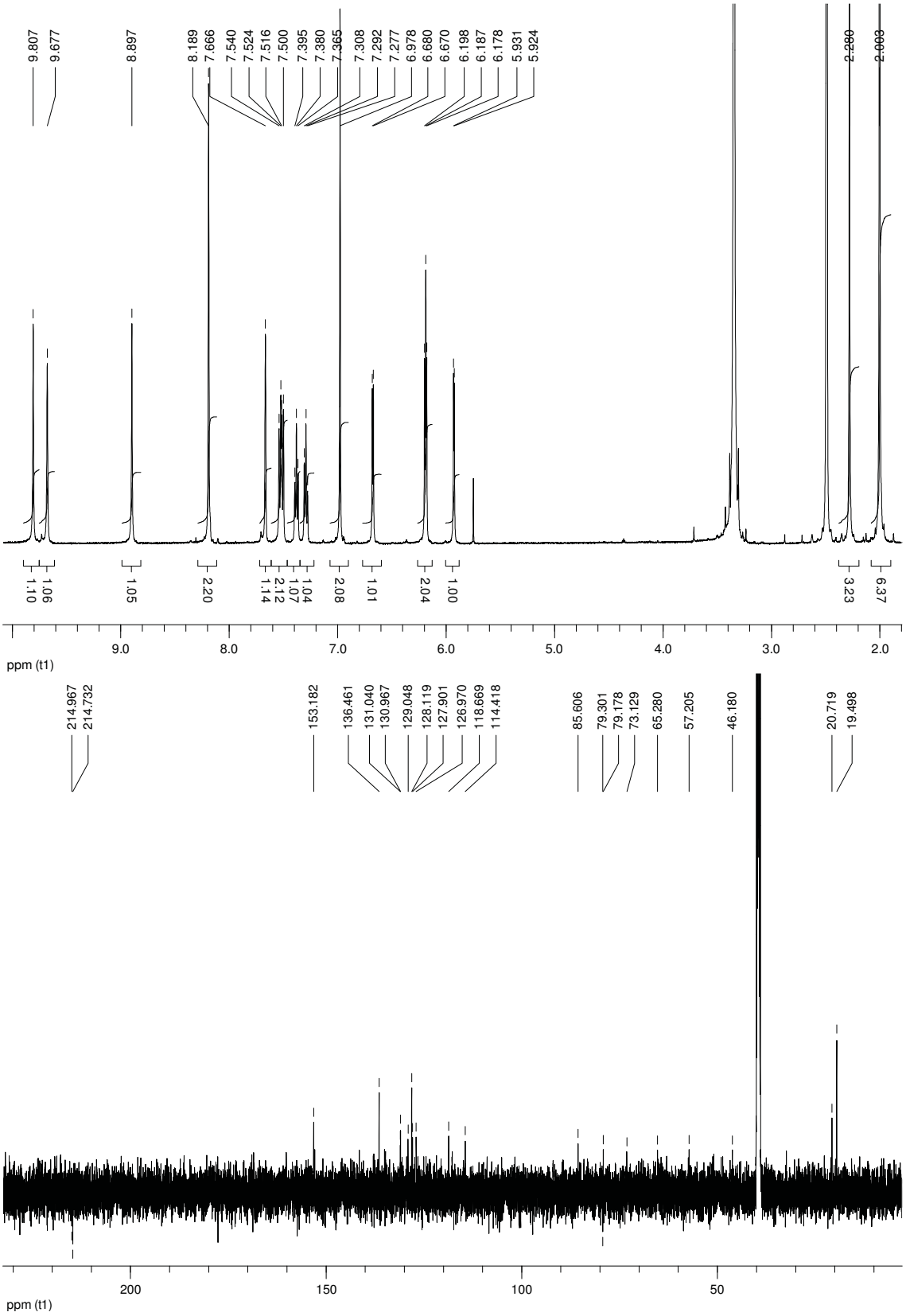
9.807
9.677
8.897
8.189
7.666
7.540
7.524
7.516
7.500
7.395
7.380
7.365
7.308
7.292
7.277
6.978
6.680
6.670
6.198
6.187
6.178
5.931
5.924
2.280
2.000
1.10
1.06
1.05
2.20
1.14
2.12
1.07
1.04
2.08
1.01
2.04
1.00
3.23
6.37
9.0
8.0
7.0
6.0
5.0
4.0
3.0
2.0
ppm (t1)
214.967
214.732
153.182
136.461
131.040
130.967
129.048
128.119
127.901
126.970
118.669
114.418
85.606
79.301
79.178
73.129
65.280
57.205
46.180
20.719
19.498
200
150
100
50
ppm (t1)

C7

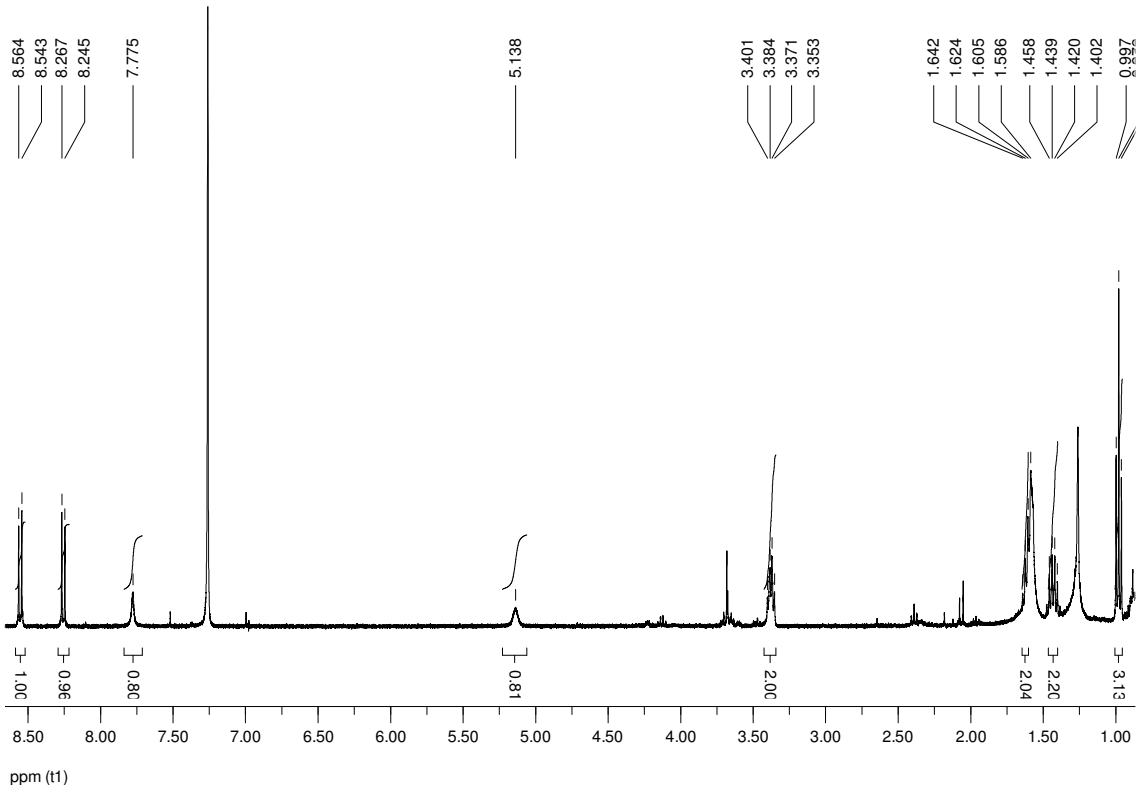
8.564
8.543
8.267
8.245
7.775
5.138
3.401
3.384
3.371
3.353
1.642
1.624
1.605
1.586
1.458
1.439
1.420
1.402
1.00
0.96
0.80
0.81
2.00
2.04
2.20
3.13
8.50
8.00
7.50
7.00
6.50
6.00
5.50
5.00
4.50
4.00
3.50
3.00
2.50
2.00
1.50
1.00
ppm (t1)

NOBE

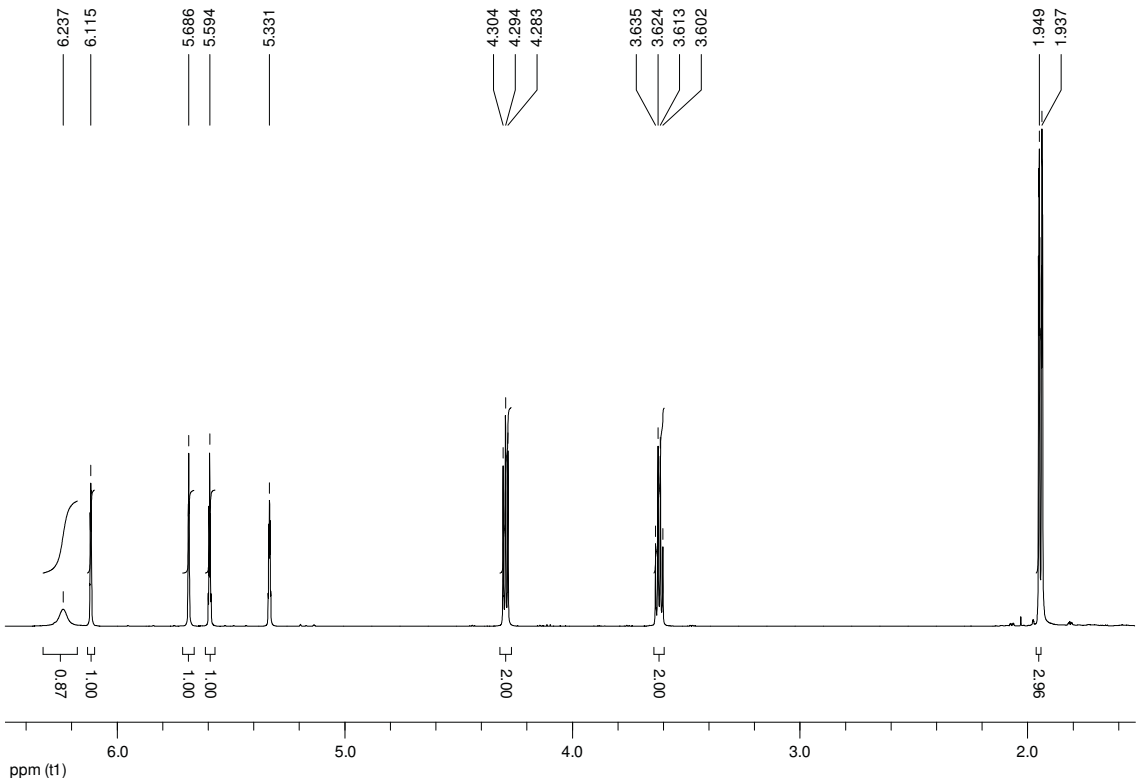
6.237
6.115
5.686
5.594
5.331
4.304
4.294
4.283
3.635
3.624
3.613
3.602
1.949
1.937
0.87
1.00
1.00
1.00
2.00
2.00
2.96
6.0
5.0
4.0
3.0
2.0
ppm (t1)

Erklärung

Hiermit erkläre ich, dass ich die vorliegende Dissertation selbstständig angefertigt sowie keine anderen als die angegebenen Quellen und Hilfsmittel verwendet habe. Alle wörtlich oder sinnentsprechend aus anderen Veröentlichungen übernommenen Stellen habe ich als solche gekennzeichnet. Diese Arbeit wurde in dieser oder ähnlicher Form bisher in keinem anderen Promotionsverfahren im In- oder Ausland vorgelegt.

Berlin, den_____

Wan Wei